

TECHNICAL REPORT SEMCA-2005-313

**A STATE-OF-THE-ART REVIEW
OF PAST PROGRAMS DEVOTED TO
FUEL BEHAVIOR UNDER LOCA CONDITIONS
Part One.**

**Clad Swelling and Rupture
Assembly Flow Blockage**

Author: Claude GRANDJEAN

DIRECTION DE LA PRÉVENTION DES ACCIDENTS MAJEURS

Service d'études et de modélisation du combustible en situations accidentelles

DIRECTION DE LA PRÉVENTION DES ACCIDENTS MAJEURS

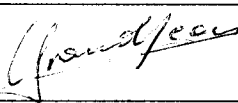
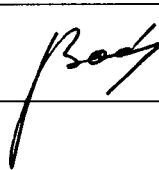
Service d'études et de modélisation du combustible en situations accidentelles

BP 3 13115 Saint-Paul-lez-Durance Cedex France tél. (33) 4 42 19 95 46 fax (33) 4 42 19 91 65

A State-Of-The-Art Review of Past Programs Devoted to Fuel Behavior Under LOCA Conditions. Part One. Clad Swelling and Rupture. Assembly Flow Blockage

DPAM/SEMCA

Note technique SEMCA-2005-313 - Décembre 2005

	Auteur	Vérificateur	Approbateur
Nom	Claude GRANDJEAN	Georges REPETTO	François BARRE
Date	19/12/2005	19/12/2005	31/1/2006
Visa			

La diffusion des informations contenues dans ce document auprès d'un tiers extérieur à l'IRSN est soumise à l'accord de l'unité émettrice.

This document, which contains proprietary or other confidential or privileged information, and any reproduction in whole or in part, shall not be disseminated outside the organization of the recipient without prior approval of the IRSN

DIRECTION DE LA PRÉVENTION DES ACCIDENTS MAJEURS

Service d'études et de modélisation du combustible en situations accidentelles

BP 3 13115 Saint-Paul-lez-Durance Cedex France tél. (33) 4 42 19 95 46 fax (33) 4 42 19 91 65

A State-Of-The-Art Review of Past Programs Devoted to Fuel Behavior Under LOCA Conditions. Part One. Clad Swelling and Rupture. Assembly Flow Blockage

Claude GRANDJEAN

Note technique SEMCA-2005-313 - December 2005

Abstract :

This report reviews the main experimental LOCA programs performed in the 70s and 80s devoted to the aspects of clad ballooning and burst as well as resulting flow blockage. For out-of-pile experimental programs, focus has been put on bundle experiments, essentially the REBEKA, ORNL and JAERI tests. For in-pile programs, single rod tests with irradiated fuel from FR2 and PBF programs have mainly been examined, with particular attention paid to the PHEBUS-LOCA bundle experiments, which are the only tests with a fully integral character.

Among the main lessons drawn from the results of these programs that were performed under various experimental conditions, it is worth pointing out the importance of thermal and mechanical interactions between rods as observed on bundle tests on the one hand, and the significant influence of rod pre-irradiation, as observed on PBF tests with single rods on the other hand. The superposition of these two aspects reveals the complete lack of results related to the bundle behavior of irradiated fuel rods, as was already pointed out in a previous recommendation raised in 1983.

A review of analytical work associated with these test results has been limited to a selection of summary reports, namely 1) the NUREG-630 report that recommended a set of correlations for clad rupture, burst strain and the flow blockage ratio, 2) the final comparison reports of the International Standard Problems on REBEKA and PHEBUS and 3) the summary report of LOCA studies related to the EDGAR and PHEBUS programs provided by IPSN. This review highlights the need to both revise the NUREG-630 correlations still used in most of current codes and further develop these LOCA calculation tools so as to take into account the two-dimensional aspects related to fuel-clad eccentricity and thermal & mechanical interactions between neighboring rods.

Key-words : LOCA, Clad Ballooning, Burst, Flow blockage

CONTENTS

1	INTRODUCTION	5
2	THE PROBLEM OF CLAD BALLOONING AND FLOW BLOCKAGE IN A LOCA	6
3	REVIEW OF OUT-OF-PILE TEST PROGRAMS	7
3.1	OUT-OF-PILE SINGLE ROD EXPERIMENTS	7
3.1.1	<i>The EDGAR Experiments</i>	7
3.1.1.1	Test Series	7
3.1.1.2	Burst Strain and Burst Criterion	8
3.1.2	<i>The REBEKA Single-rod Experiments</i>	10
3.1.3	<i>The ORNL Single-rod Experiments</i>	15
3.1.4	<i>Main lessons from single-rod test results</i>	16
3.2	MULTI-ROD OUT-OF-PILE TESTS.....	17
3.2.1	<i>The REBEKA multi-rod tests</i>	17
3.2.1.1	5x5 rods bundle tests.....	17
3.2.1.2	7x7 rods bundle tests.....	22
3.2.1.3	Conclusions on REBEKA multi-rod tests.....	24
3.2.2	<i>The ORNL-MRBT multi-rod tests</i>	25
3.2.2.1	4x4 rods bundle tests.....	25
3.2.2.2	8x8 rods bundle tests.....	28
3.2.2.3	Conclusions on ORNL multi-rod tests	31
3.2.3	<i>The JAERI multi-rod tests</i>	32
3.2.3.1	Unheated shroud tests	33
3.2.3.2	Tests with a guard ring of unpressurized heaters.....	34
3.2.3.3	Tests with a shroud backed by guard heaters	38
3.2.3.4	Conclusions on JAERI multi-rod tests	40
4	REVIEW OF IN-PILE TESTS PROGRAMS	41
4.1	SINGLE ROD TESTS	41
4.1.1	<i>PBF-LOC tests</i>	41
4.1.1.1	Common Characteristics	41
4.1.1.2	Deformation and rupture behavior	44
4.1.1.2.1	Deformations of irradiated rods compared with deformations of fresh rods	44
4.1.1.2.2	Analysis of deformation on rod LOC-6/11	46
4.1.1.2.3	Comparison with ORNL-MRBT results.....	47
4.1.1.3	Fuel behavior	49
4.1.2	<i>FR2 tests</i>	51
4.1.2.1	Common Characteristics	51
4.1.2.2	Deformation and rupture behavior	52
4.1.2.3	Fuel behavior	56
4.1.3	<i>Main findings from the PBF-LOC and FR2 test results</i>	60
4.1.4	<i>ESSOR Tests</i>	60
4.1.4.1	Experimental conditions	60
4.1.4.2	Results	61
4.1.5	<i>FLASH tests</i>	64
4.1.5.1	Experimental conditions	64
4.1.5.2	Results	64
4.2	MULTI ROD TESTS.....	66
4.2.1	<i>MT tests</i>	66
4.2.1.1	Common characteristics	66
4.2.1.2	Main results	67
4.2.2	<i>The PHEBUS-LOCA tests</i>	70
4.2.2.1	Description of the test facility and test train	70
4.2.2.2	Test matrix.....	72
4.2.2.3	Results of the thermomechanical tests.....	73
4.2.2.3.1	Test 215 P	74
4.2.2.3.2	Test 215-R.....	78
4.2.2.3.3	Test 216.....	82

4.2.2.3.4	Test 218.....	83
4.2.2.3.5	Test 219.....	85
4.2.2.4	Main findings gained from the thermo-mechanics in the PHEBUS/LOCA tests	90
5	ANALYSIS OF THE RESULTS DATABASE	93
5.1	THE NUREG-630 DATABASE AND MODELS.....	93
5.1.1	<i>Database</i>	93
5.1.2	<i>Correlations in NUREG 630</i>	94
5.1.2.1	Rupture temperature.....	94
5.1.2.2	Burst strain.....	96
5.1.2.3	Assembly flow blockage.....	100
5.1.2.4	Conclusions relative to NUREG-630	101
5.2	INTERNATIONAL STANDARD PROBLEMS ISP-14 AND ISP-19.....	102
5.2.1	<i>ISP-14 (REBEKA-6 test)</i>	102
5.2.2	<i>ISP-19 (PHEBUS 218 test)</i>	107
5.3	SUMMARY OF PHEBUS-LOCA TEST INTERPRETATIONS.....	113
5.3.1	<i>Cladding failure</i>	114
5.3.2	<i>5.3.2 Strain rate</i>	115
5.3.3	<i>Complementary needs for the interpretation of thermomechanical aspects</i>	119
6	CONCLUSIONS	120
	REFERENCES	125

1 INTRODUCTION

Within the framework of cooperative links with EDF and Framatome-ANP, IRSN has been requested to provide a review of the past R&D programs devoted to loss-of-coolant accidents (LOCA), in view of updating knowledge that has been accumulated on the different phenomena occurring during such accidents, including conclusions from recent programs results. This update will make it possible to evaluate our current understanding and identify uncertainties and possible lacks in knowledge which, in turn, may lead to complementary needs in future R&D work.

This literature review has been divided into several parts corresponding to the main phenomena intervening in the successive phases of a hypothetical large break LOCA scenario:

1. Ballooning, cladding rupture, partial blockage of coolant flow in sub channels;
2. Coolability of a rod bundle containing a region with a high flow blockage ratio;
3. Cladding oxidation and embrittlement, capacity to withstand thermal shock quench loads and post quench loads.

Various literature reviews already exist ^[1,2,3,4,5,6,7], either covering the whole field of LOCA phenomenology or focusing more specifically on particular aspects. They have been largely consulted for the current study and readers may refer to these prior reviews for complementary information or analysis that has not been detailed here.

As this document does not claim to make a full and exhaustive review of the results related to the concerned topics, we have selected the programs recognized as major ones and disregarded results of partial programs of secondary interest generally with very little documentation.

The first section essentially deals with the phenomena of clad ballooning and resulting subchannel blockage that have been addressed in numerous experimental programs, both out-of-pile & in-pile, in single rod & bundle tests and with fresh as well as irradiated fuel rods.

After having briefly summarized the LOCA phenomenological aspects of clad ballooning and flow blockage in subchannels (Chapter 2), the main section of this report will be devoted to the review of the main experimental programs that have provided information on these topics.

Chapter 3 concerns out-of-pile tests programs; due to the considerable amount of data corresponding to the diversity of these programs, focus has been put on bundle test results.

Chapter 4 is devoted to both single rod and bundle in-pile tests. For single rod experiments, information will be given, beyond ballooning and rupture, on specific behavior observed with irradiated fuel. Among bundle test programs, only the PHEBUS-LOCA program can be qualified as integral, covering the whole LOCA LB transient scenario, starting from initial blowdown until final quenching of the fuel rods. Particular attention has thus been paid to this program and complementary indications will be given on some test results, beyond the aspects of clad ballooning and rupture.

Chapter 5 deals with the analysis of test results, within the limits of a selection of a few summary reports. We have chosen here to examine and comment on:

- The analysis of the results database and correlations recommended in the NUREG-630 report for clad rupture, burst strain and the flow blockage ratio;
- The comparative analysis of calculations performed within the framework of the International Standard Problems ISP-14 and ISP-19 ;
- The summary of interpretative work of thermomechanical results from the PHEBUS-LOCA tests.

Chapter 6 summarizes key knowledge gained from the review of experimental programs described in Chapters 3 and 4, as well as from the analysis of results discussed in Chapter 5.

2 THE PROBLEM OF CLAD BALLOONING AND FLOW BLOCKAGE IN A LOCA

We will be referring to large break LOCA scenarios in this chapter, which are considered as bounding for clad deformation and flow blockage aspects under consideration in this review.

During the primary circuit blowdown, an important pressure difference arises between the inside and outside of the fuel rod. During this time, the degraded rod-to-coolant heat transfers due to coolant flashing, combined with the release of energy stored in the fuel and the residual power, lead to a rapid rise in the clad temperature. Around 700°C, the mechanical resistance of Zircaloy is significantly reduced, with a plastic strain rate of about 1%/s. However, the clad ductility remains sufficient to allow for important hoop strain, even greater than 50% before clad burst, even though contact between neighboring rods is obtained with a strain value as low as 33% on both rods with the usual rod pitch. High strain values can thus be reached before cladding rupture that can induce local flow blockage in the rod assembly when these deformations are located at neighboring elevations (coplanar blockage).

The clad deformation during the so-called ballooning phase leads to a significant increase in the surface area of metal exposed to oxidation by steam during the quasi-adiabatic phase of the transient, during which the temperature can range between 1000 and 1200°C during a sufficiently long period. The oxidation area is thus almost doubled near the burst where the steam can reach the inside of the cladding on a more or less axial extent near the burst opening. Conversely, the deformation of the cladding leads to a wall thinning in proportion with the strain ratio. Therefore, at the elevation of the balloon, cladding of reduced thickness having been submitted to double-sided oxidation will have to withstand the quench thermal shock loads or post quench loads at low temperature. (The oxidation and embrittlement issues are reported in the third part of the IRSN literature review).

It is worth pointing out that, besides the well-known quantitative requirements limits on the Peak Cladding Temperature (<2200°F), Maximum Cladding Oxidation (ECR<17%) and Maximum Hydrogen Generation, the ECCS acceptance criteria (commonly considered as "LOCA criteria") prescribe two additional requirements to be fulfilled for the most severe postulated LOCA:

- The preservation of a coolable geometry, regardless of the changes in the core geometry (§50.46 (b)(4)),
- The maintaining of a long-term cooling capability (§50.46 (b)(5)),

The possibility to obtain large deformations and high blockage ratios within a reactor rod bundle under some thermal-hydraulic conditions typical of LOCA is one of the key questions in the LOCA-related studies and has given rise to numerous experimental programs, the most important of which will be reviewed in the following. The following tests help provide information on this question:

- Single rod analytical tests for the study of ballooning and rupture behavior under controlled thermal and mechanical loading conditions; these tests have made it possible to establish thermomechanical laws (creep velocity, rupture criteria,...) for cladding material under temperature and pressure conditions within LOCA domain ;
- Bundle tests of a more global character, which aimed to study the influence of bundle parameters such as the number of rod rows, the influence of a cold or heated shroud, of control rods, etc..., on the importance of strain, their axial extent, their coplanar character and thus on the resulting flow blockage ratio in the hydraulic subchannels of the rod bundle.

The associated question of the impact of high flow blockage ratios on the coolability of heated rods in the vicinity of the blocked regions has been studied in specific experiments which have been reviewed separately in the second part of the IRSN State-of-the-Art-Review.

3 REVIEW OF OUT-OF-PILE TEST PROGRAMS

3.1 Out-of-pile Single Rod Experiments

The characteristics and results of all of these experimental programs will not be described here in detail, the objective of which was to obtain the thermomechanical properties of Zircaloy-4 cladding material under LOCA conditions. For some of these programs, more particularly REBEKA, ORNL and JAERI, the single rod tests series were followed by bundle test series which will be reviewed in the next section. A brief review of three main programs (EDGAR, REBEKA, ORNL) will be provided, summarizing the test characteristics and the main lessons drawn from their results. Particular attention has been given to the French program EDGAR from which the physical models integrated in the CATHARE computer code were issued.

3.1.1 The EDGAR Experiments

The EDGAR experiments were separate effect tests on cladding mechanical behavior in the stress-temperature domain of a large break LOCA. The original Zy4 base tests were performed by the CEA in Saclay during the 1980s [8]. A new facility (EDGAR-2) is still currently in use for the testing of advanced clad material [9].

The tests were performed on cladding tube specimens obtained from different types of Zircaloy material: FRAMATOME, CEA or the specific alloy used in the PHEBUS experiments. The tube specimens, 50 cm long, were heated by direct resistance heating in a controlled atmosphere (steam, air or inert gas) and with internal pressure loading. The experimental system was regulated so as to impose any prescribed temperature or pressure transient.

The main objective of these tests was to provide a thermomechanical database for the development of physical models (strain rate and burst criterion) that were introduced in computer codes (the former code CUPIDON and later the fuel module of CATHARE).

3.1.1.1 Test Series

Around 500 tests were run under various conditions. The main test series worth mentioning are:

- 1) Creep tests at constant temperature (600 to 1000 °C) and pressure (10 or 25 bar)

These basic tests were used to derive the physical laws describing the thermomechanical behavior of the cladding material.

The analysis of creep tests has made it possible to correlate the secondary creep velocity with a Norton-type equation in each of the phase transformation domains (α , $\alpha+\beta$, β) of the Zircaloy material :

$$d\varepsilon_{\theta}^c / dt = A_i \exp(-Q_i / T) \sigma_{\theta}^{n_i}$$

where ε_{θ}^c is the circumferential creep strain, σ_{θ} the hoop stress and A_i, Q_i, n_i the coefficients of the Norton-type laws. A continuous strain homogenization model was used to evaluate the deformation rate in the domain transition ranges.

- 2) Temperature or Pressure Ramp Tests

These tests revealed that the strain rate under pressure or temperature ramp conditions can be correctly predicted by creep tests laws, while introducing a model for phase transformation kinetics.

- 3) Typical LOCA Transient Tests

Results of these tests revealed the influence on the strain rate of the thermal treatment associated with a transient temperature "first peak" within $\alpha+\beta$ domain (see Figure 1); this influence was taken into account in the modeling by evaluating the α -phase fraction that results, under non equilibrium, of the phase transformation during transient heat treatment.

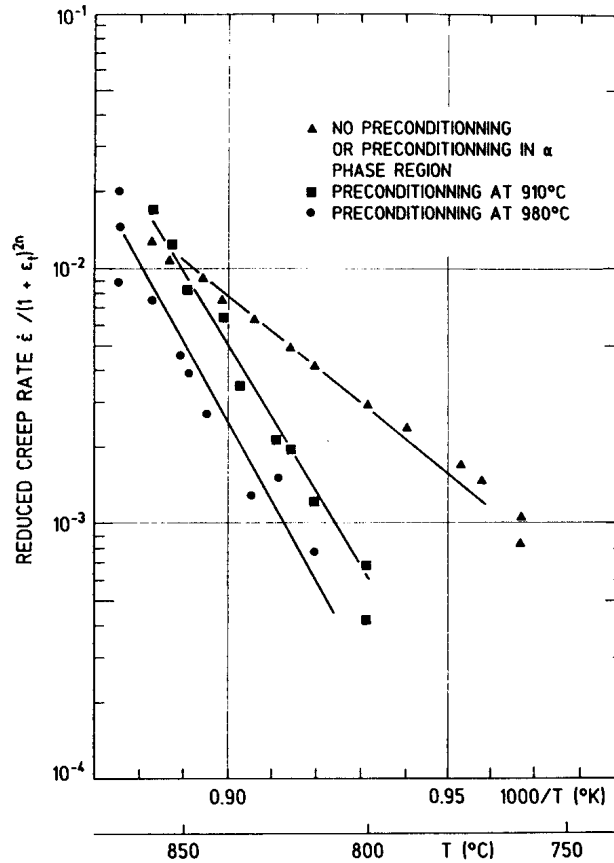


Figure 1: Effect of previous heat treatment of the cladding in the mixed phase domain on reduced creep rates.

3.1.1.2 Burst Strain and Burst Criterion

In the EDGAR tests, the deformation of burst specimens has been characterized by two parameters: the uniform elongation A_r and the total elongation A_t . The uniform elongation is highest value of the relative variations in tube circumference evaluated at two axial locations situated ± 20 mm apart of the burst opening tips, while the total elongation is equal to the maximum relative variation in tube circumference at burst opening. Figures 2 and 3 show the uniform and total elongations that were obtained in thermal ramp tests as function of the rupture temperature and ramp rate. The large deformations ($>100\%$) obtained in the high α domain reflect the uniformity of the temperature field, in axial and azimuthal directions, as a result of the heating method (direct heating) used in these tests.

A burst criterion was derived, with the stress condition corresponding to the onset of plastic instability that leads to burst:

$$\sigma_{\theta} = \sigma_B(f_{\alpha}, T)$$

where f_{α} is the α -phase volume fraction and $\sigma_B = k_i \exp(-q_i T)$, the coefficients k_i and q_i being fitted on the EDGAR creep test results in the i -phase domains ($i = \alpha$ or β). Plastic instability starts when the uniform elongation A_r is reached at the rupture level. The burst criterion may thus be used to derive the uniform elongation by:

$$\sigma_B = \sigma_{\theta}^0 (1 + A_r)^2$$

where σ_{θ}^0 is the initial hoop stress.

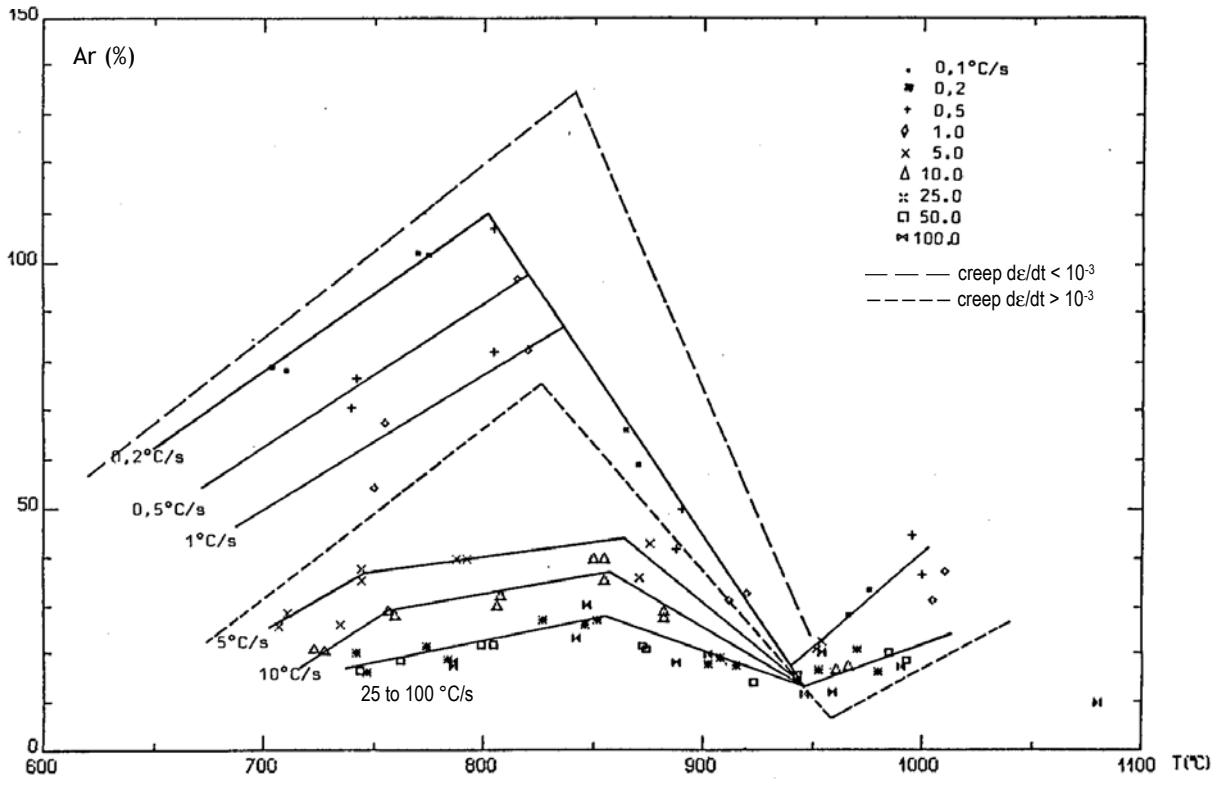


Figure 2: EDGAR thermal ramps tests - uniform elongation versus modified burst temperature.

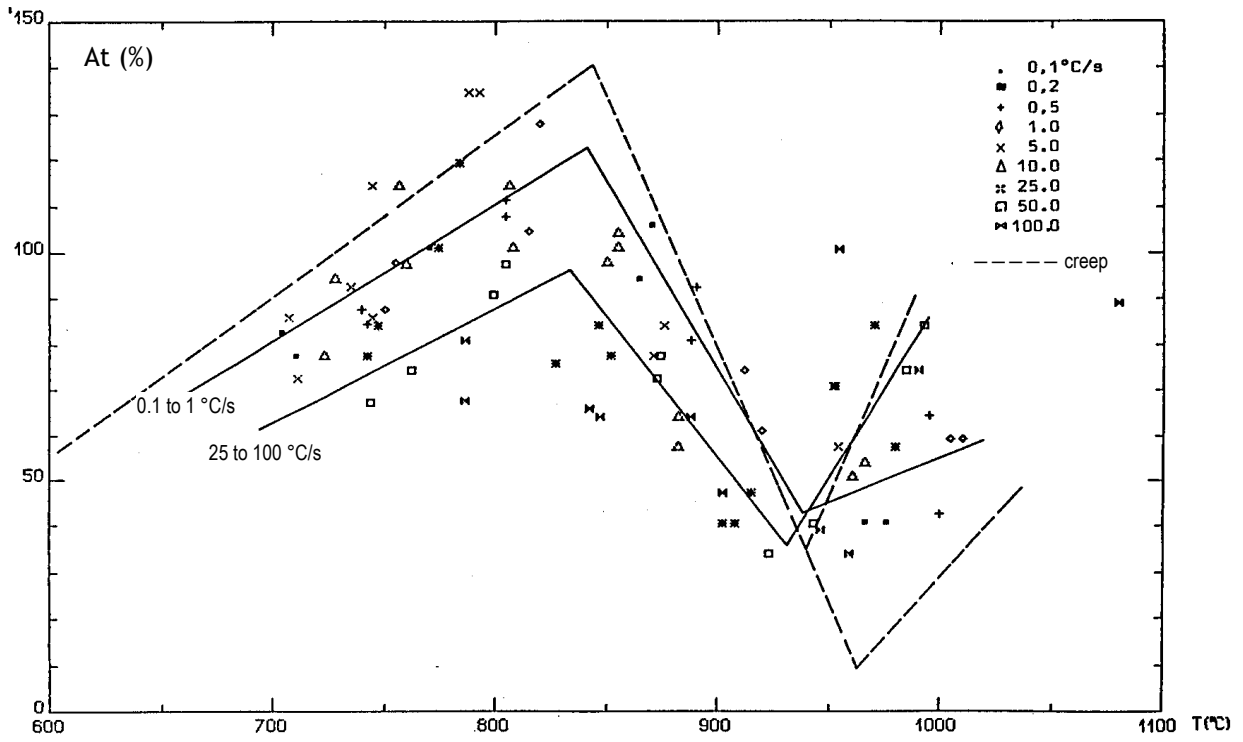


Figure 3: EDGAR thermal ramps tests - total elongation versus modified burst temperature.

Comparison between burst criterion predictions and experimental results leads to a ratio predicted/measured rupture times in the 0.7 to 1.7 range for creep tests and in the 0.9 to 1.1 range for thermal ramp tests. Figure 4 shows that the model allows a prediction of uniform elongation within $\pm 30\%$ uncertainty in most cases, but leads to a significant overestimation for long duration tests at low heating rates or low pressures: this deviation can be attributed to the effect of Zircaloy oxidation during such tests, which reduces the strain rate and burst stress, and thus the uniform elongation.

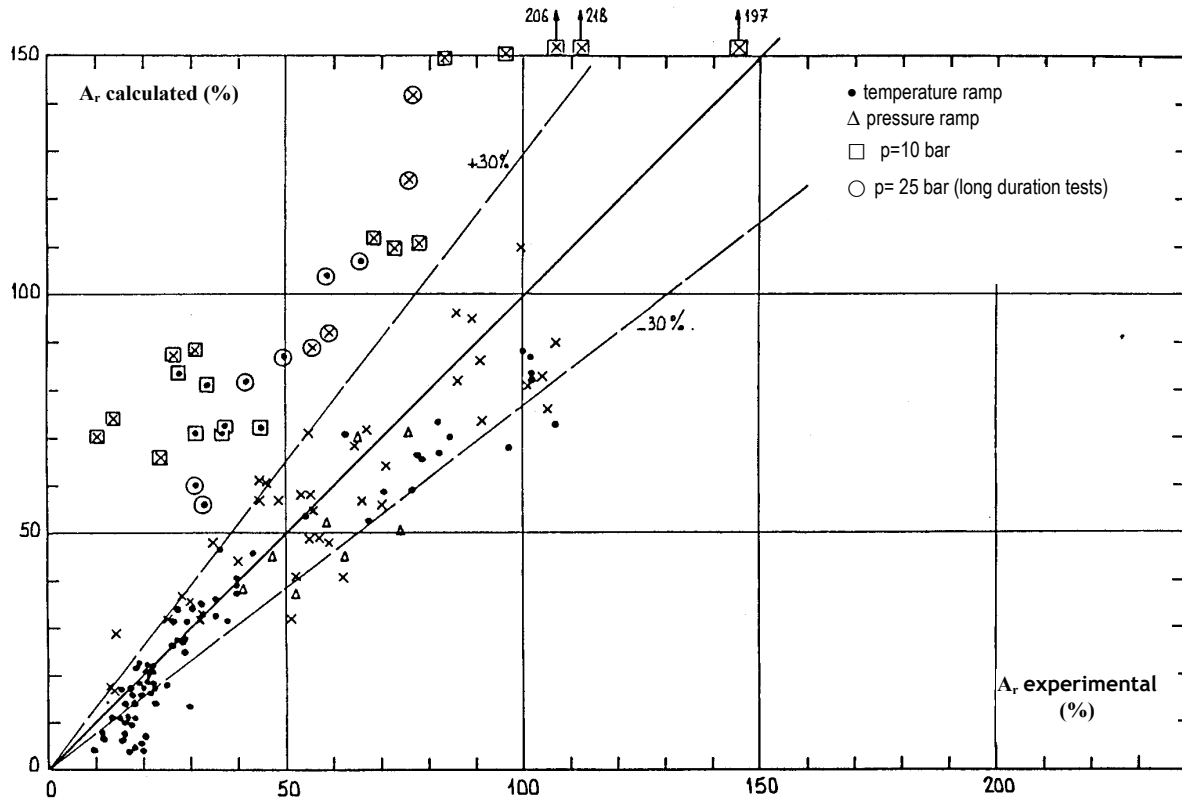


Figure 4: EDGAR tests - calculated versus experimental uniform elongations.

An additional model was also introduced to calculate the total elongation A_t (or rupture elongation), which is deduced from a "rupture" stress taking account of the average oxidation rate in the cladding.

It is worth mentioning that additional tests on irradiated cladding (the so-called EDGAR CHAUD tests) were undertaken to study the influence of irradiation on the clad thermomechanical behavior. However experimental difficulties, mainly related to the defueling of the irradiated rods, prevented the initially planned program from being completed.

3.1.2 The REBEKA Single-rod Experiments

The REBEKA single-rod tests were performed at the KfK in Karlsruhe in the late 1970s ^[10].

The test rod, 325 mm long, consisted of an inconel thermal heater, isolated from the zircalloy cladding by annular alumina pellets. It was heated in a steam or inert gas atmosphere and surrounded by a cylindrical shroud that could be heated or not in order to obtain a more or less uniform temperature field on the cladding circumference. The rod internal pressure and the heating rate were kept constant during the test transient, in the range 1 to 140 bar and 1 to 30 K/s respectively.

Figure 5 shows the rupture strain as a function of the rupture temperature for tests with low azimuthal temperature gradients ($\Delta T_{az} < 15K$); these results seem very consistent with the corresponding EDGAR results (see Fig. 3). The results indicate a decrease in rupture strain with

increasing temperature in the α and $\alpha+\beta$ domains; this trend reverses in the β domain beyond the maximum deformation, due to the oxidation of the clad material which reduces its ductility.

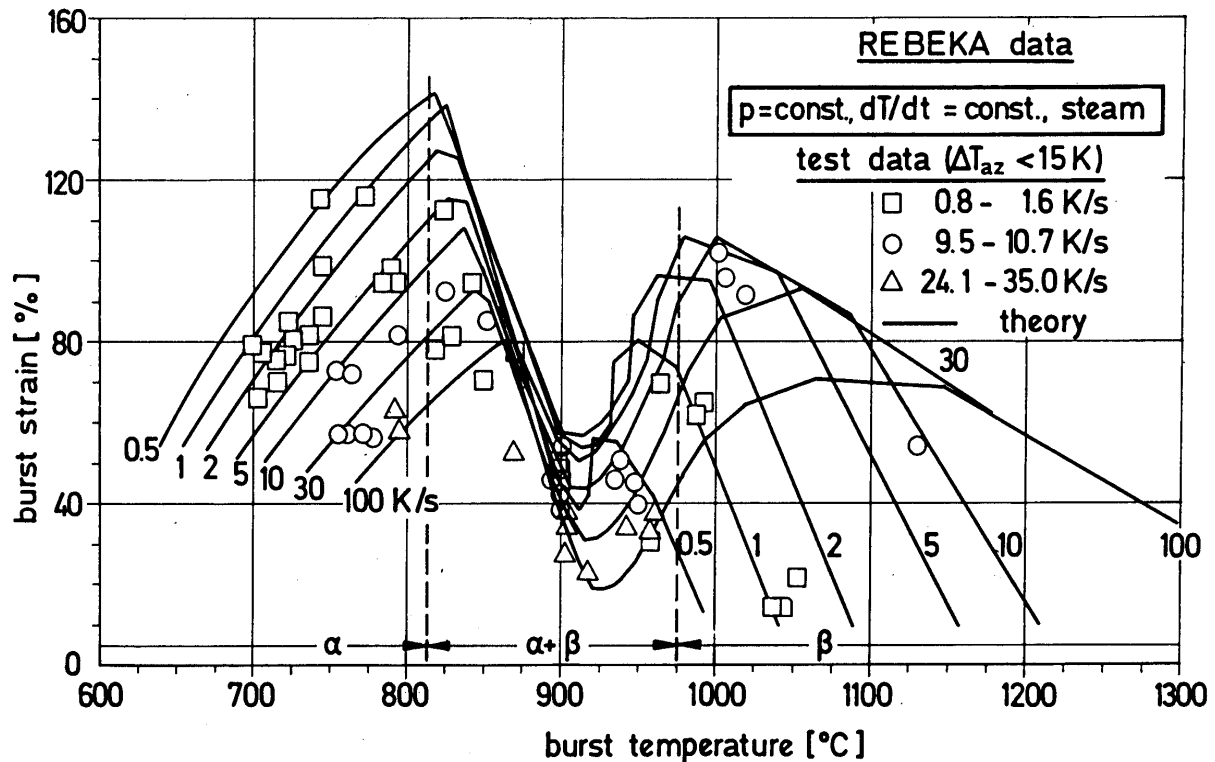


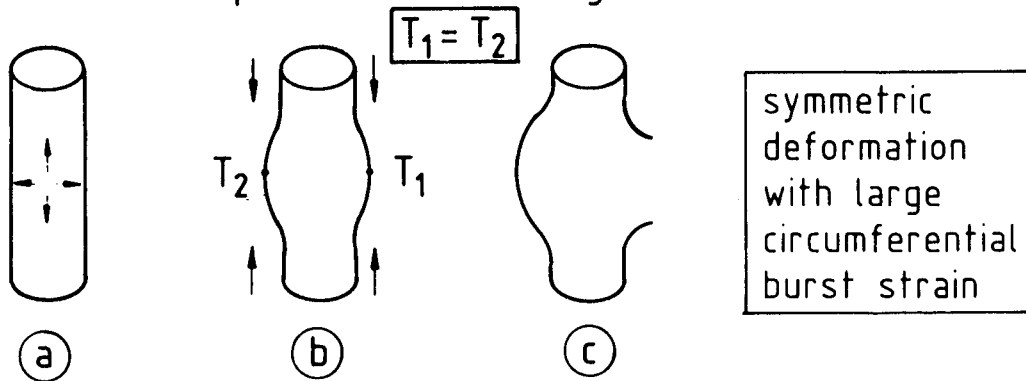
Figure 5: REBEKA tests - burst strain versus burst temperature of Zircaloy claddings.

The REBEKA single rod tests with a non heated shroud made it possible to reveal and quantify the essential influence of cladding temperature differences on the burst strain. This influence is related to the "hot straight effect" that results from the anisotropy of Zircaloy in α -phase and which can be explained as follows:

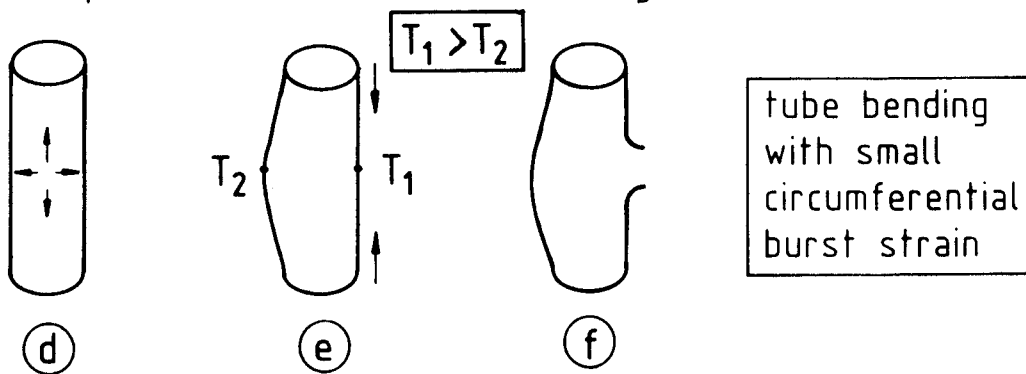
- In the high α domain and the $\alpha+\beta$ transition range, the strain velocity is very sensitive to the temperature; straining will occur first and concentrate near the hot side that results from unavoidable temperature differences;
- As a consequence of Zircaloy anisotropy, circumferential straining on the hot side will lead to an axial shortening, forcing the cladding into close contact with the heat source and lifting the opposite colder side of the cladding away from it (see Figure 6); this leads to an increase of the circumferential temperature difference on the cladding and an intensification of the phenomena that will result in an early rupture of the cladding with relatively low total circumferential strain (see Figure 7).

Figure 8 clearly illustrates the influence of the azimuthal temperature difference on the cladding circumferential burst strain. This temperature gradient ΔT_{az} is therefore a key parameter for the phenomena of burst deformation, flow blockage and related coolability in a LOCA transient.

uniform temperature on cladding circumference:



temperature difference on cladding circumference:



- (a) (d) tube under biaxial stress due to internal gas overpressure
- (b) axial material flow and tube shortening
- (e) hot side:
axial material flow, tube shortening, cladding contacts inner heat source
cold side:
tube bending, cladding moves apart from inner heat source
- (c) (f) burst cladding tube

Figure 6: Strain anisotropy and bending of Zircaloy cladding tubes in the α -phase

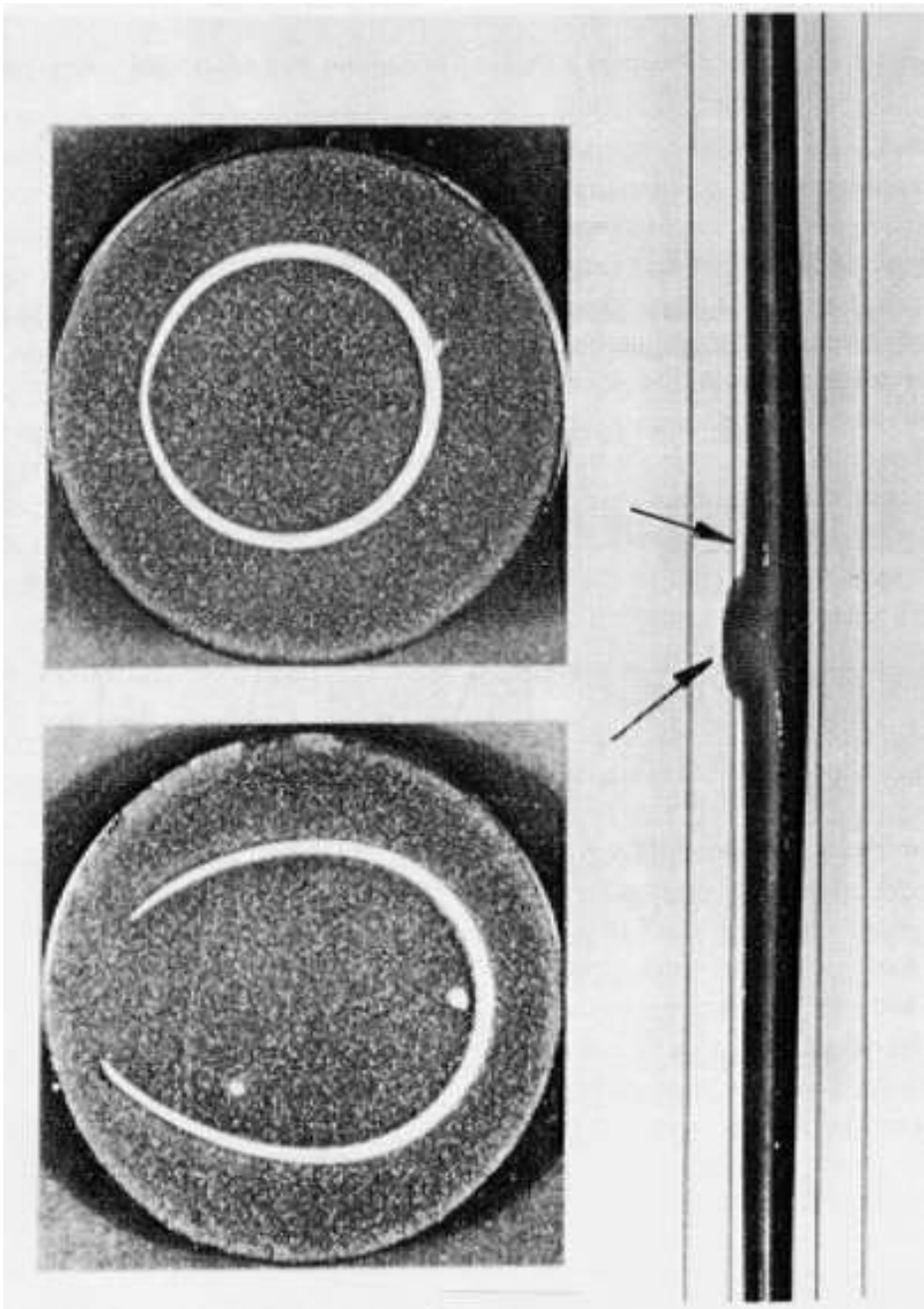


Figure 7: Bending of Zircaloy cladding tube deformed under azimuthal temperature difference cooling.

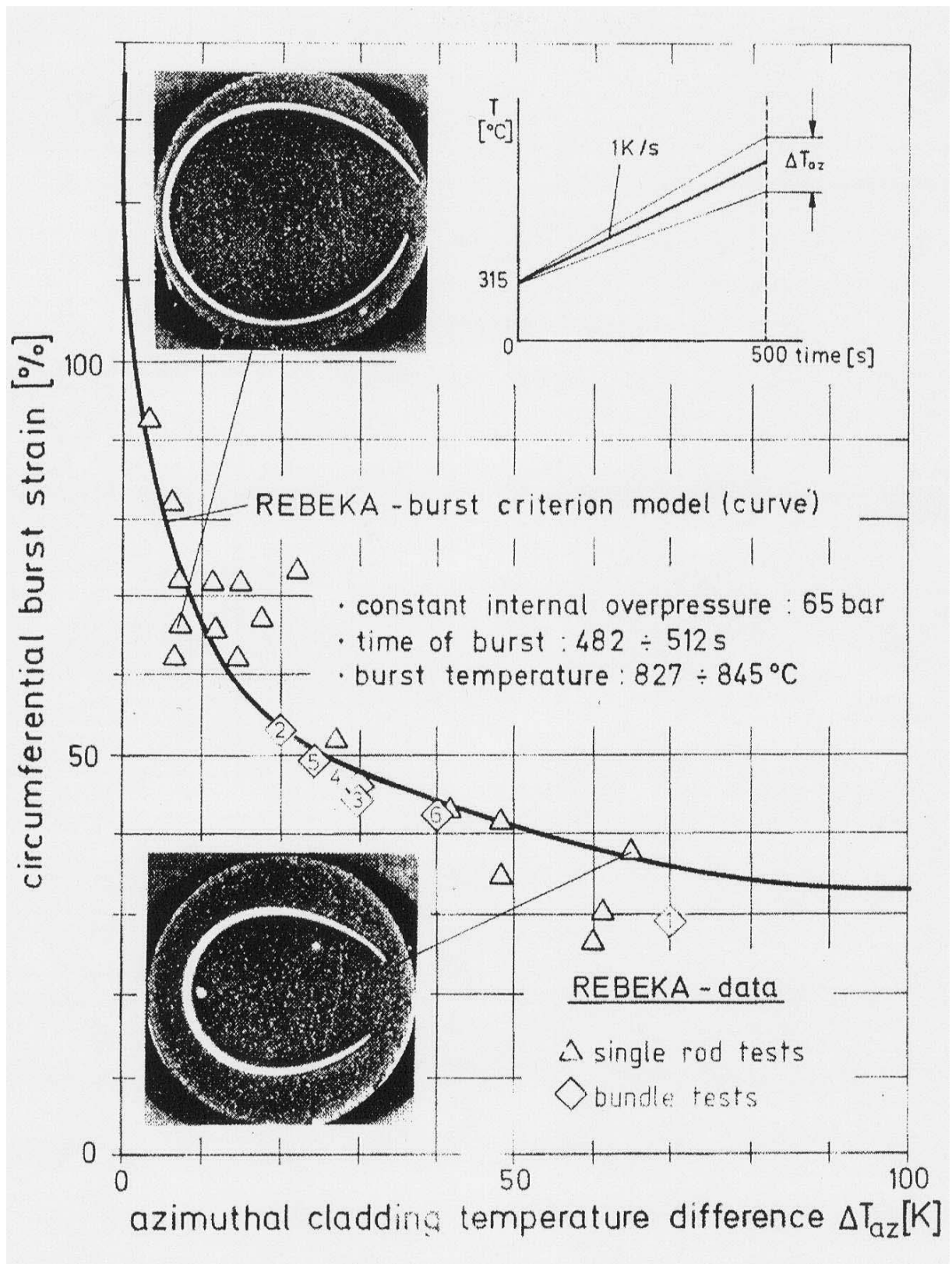


Figure 8: REBEKA tests - burst strain of Zircaloy-4 cladding tubes versus azimuthal temperature difference.

3.1.3 The ORNL Single-rod Experiments

Single-rod tests were performed in the MRBT program (test series PS and SR) at the Oak Ridge National Laboratory in the 1970s^[11].

The test rods, 915 mm in heated length, consisted of an electric heater inside a Zircaloy cladding tube made from the master lot purchased specifically for use in most NRC cladding research programs: 10.92 mm o.d., 0.635 mm wall thickness, intermediate between PWR and BWR designs. The internal electric heater had a spiral Kanthal heating element wound on a MgO core and isolated from its stainless steel sheath by boron nitride; the s.s. sheath was coated with a 0.05 mm zirconia plasma spray. The gas annulus between the heater and clad was filled with helium at a desired pressure value, this pressure being not controlled during the test transient. The nominal gap value was 0.23 mm in cold conditions. The test rod was placed inside a cylindrical shroud that could be heated or not and the gas atmosphere was steam or argon.

Most tests were run with a non heated shroud under a ramp heating rate of 28 K/s. Ramp tests with 5 and 10 K/s ramp rates were also performed, as well as some creep tests at a constant temperature around 760°C. The last SR series were performed with a heated shroud.

Circumferential elongation at rupture from 28 K/s ramp tests (the most numerous) are plotted on Figure 9A.

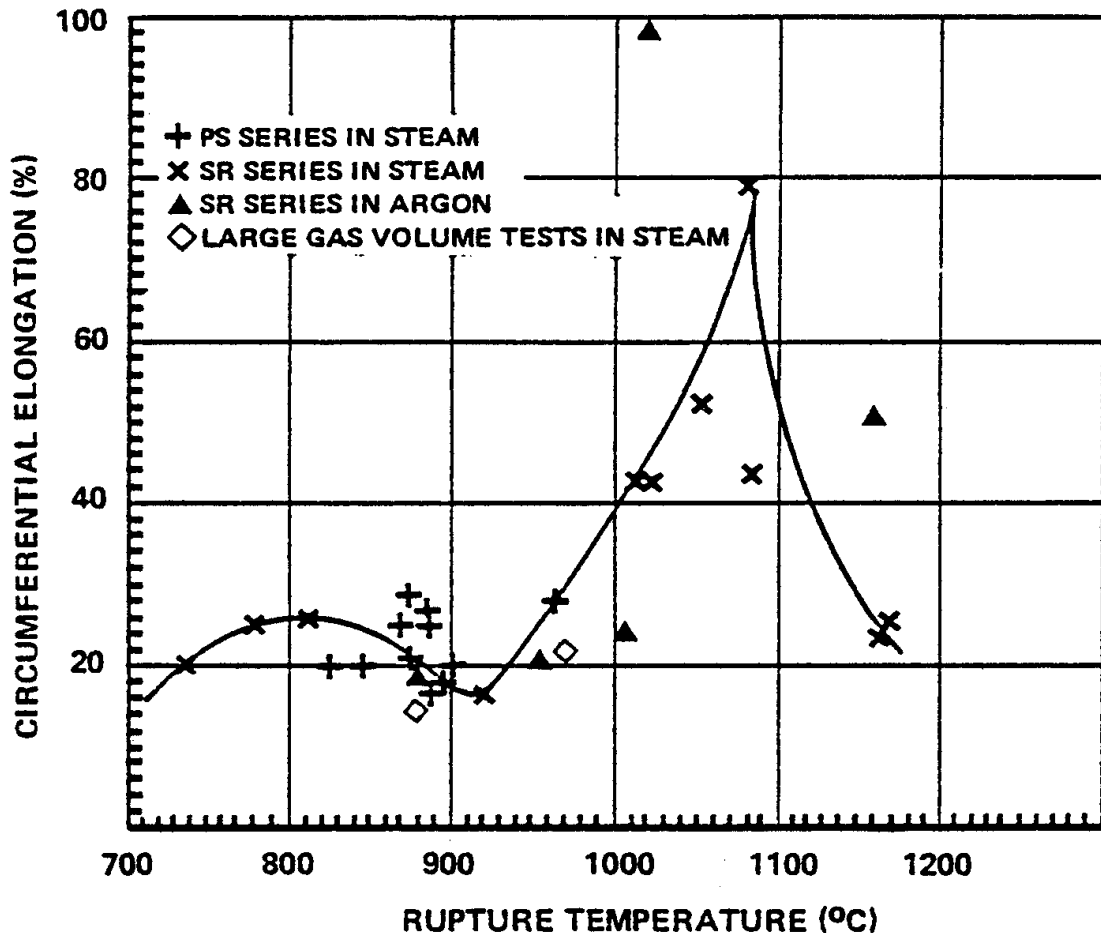


Figure 9B which gives the rupture elongations obtained in the high α -phase domain from creep or low ramp rate tests shows that the strain values in these tests are similar to those of 28 K/s ramp rate tests.

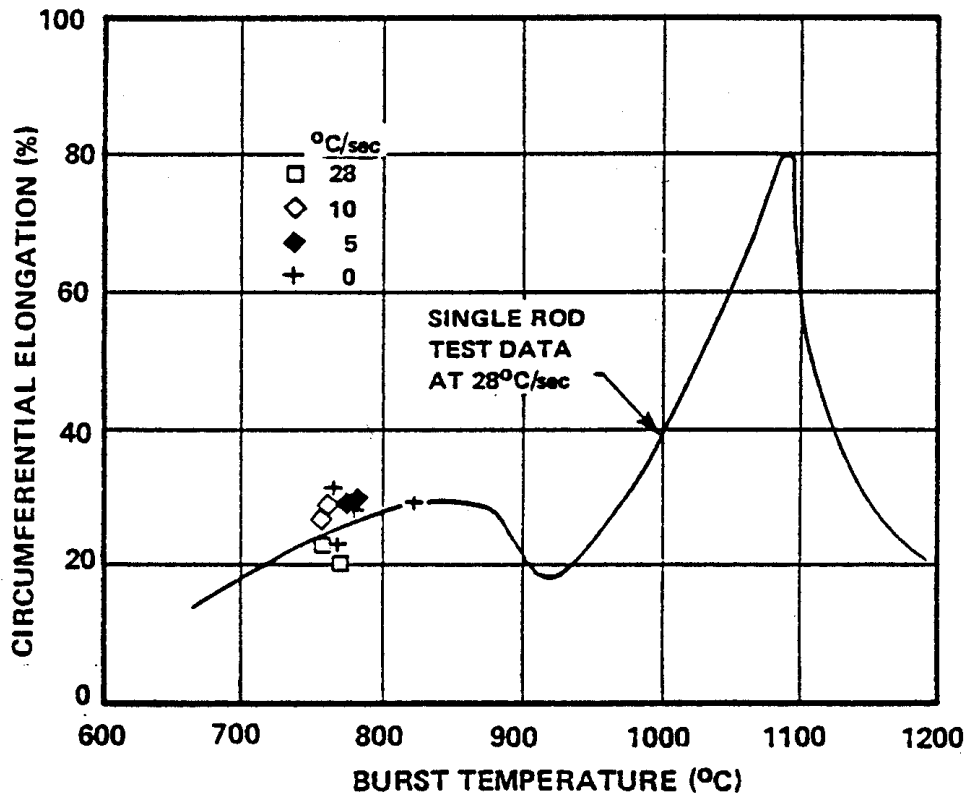


Figure 9B: ORNL tests - comparison of burst strain in creep rupture and low heating rate with data for 28 K/s tests.

The non heated shroud tests with bursting in the high α -phase or low $\alpha+\beta$ domains confirmed the "hot side straight effect" that results from the Zircaloy anisotropy and leads to non uniform circumferential straining and a burst elongation much lower than that obtained in tests with direct heating.

3.1.4 Main lessons from single-rod test results

The EDGAR tests, performed with the direct heating of cladding tube specimens, thus with a uniform azimuthal temperature distribution, led - as in the similar ANL tests by Chung and Kassner^[12] - to high values of burst elongation in the high α -phase domain. These testing conditions, which were considered as poorly representative of the actual conditions experienced in PWR by fuel rod cladding, nevertheless provide well-identified analytical conditions to establish the physical laws describing the material behavior (creep velocity, rupture criterion) in the LOCA domain.

The single-rod tests from the REBEKA and ORNL-MRBT programs, performed with internal indirect heating, thus with unavoidable azimuthal temperature differences (due in particular to the local offsetting of the heating rod) underlined the essential influence of the azimuthal temperature gradients on the clad straining until burst; the process involves a non uniform material weakening, combined with Zircaloy anisotropy, that leads to possibly high local rupture strain values, but with a moderate average circumferential elongation and limited axial extent.

3.2 Multi-rod out-of-pile tests

Once again, this review will focus on the three main programs (REBEKA, ORNL and JAERI) that have provided a consistent set of significant results.

3.2.1 The REBEKA multi-rod tests

The REBEKA multi-rod tests were carried out on different rods bundles: 5x5 rods in R-1 to R-4 and REBEKA-M, 7x7 rods in R-5 to R-7. They used internal electrically heated full-length simulators based on the German PWR fuel rod design (3.9 m heated length), maintained with 8 spacer grids at positions corresponding to those found in a fuel assembly. The test bundle was enclosed in a thin non-heated shroud.

In these tests, the thermohydraulic conditions were defined so as to simulate typical reflooding conditions common to German PWR of KWU design (water injection in both the hot and cold leg); thus, the temperature rise (~ 7 K/s) was carried out under a downward flowing steam (~ 2 m/s), until a desired temperature level was reached, followed by a reflooding phase under upward or downward flow depending on the case studied.

Table 1 summarizes the test conditions and results of the multi-rod REBEKA tests.

3.2.1.1 5x5 rods bundle tests

The multi-rod tests R-1 to R-4 were carried out using an inner 3x3 array of pressurized rods (70 bar internal pressure) surrounded by an outer row of 16 low-pressurized guard heater rods, with inconel cladding, the aim of which was to act as a non deforming thermal shield between the inner rods and the cold outer shroud. Therefore, the flow blockage values reported in these tests only concern the 9 inner rods.

Tests R-1, R-3 and R-4 were representative of a mean assembly, for which the temperature at the time of rod bottom reflooding reached 940 K; test R-2 was representative of a hot assembly for which the corresponding temperature reached 1120 K.

In test R-1, a slight malfunction led to the excessive cooling at the beginning of reflooding; clad temperature thus stabilized around 750°C during the reflooding phase, whereas the clad straining, which started under steam flow, continued over about 100 s during the reflooding phase before burst. The maximum strain was 32% and the maximum flow blockage ratio, 25%. In figure 10 showing the axial profile of clad deformations, a shift in the maximum strain locations towards the top of inter-grid spacing in the direction of flow can be observed: this shift results from the thermohydraulic effect of the grids which locally increases the exchanges between liquid and vapor, leading to a de-superheating of vapor and an increased cooling of the cladding downstream from the grids; the vapor superheating redevelops progressively towards the next grid, leading to a temperature difference of about 50 K on the cladding between to neighboring spacer grids at the time of burst.

In test R-2, reflooding was delayed until the 1120 K target temperature was reached and the clad straining developed entirely during the heat-up phase in superheated steam flowing down the test section; the maximum strain was 64% and the maximum flow blockage ratio, 60%. In figure 11 showing the axial profile of clad deformations, a shift in the maximum strain locations towards the bottom of grid-spans can be observed, therefore downstream from the steam flow, which can be explained much in the same way as test R-1. Deformations were much more coplanar than those observed in tests where the clad burst during the reflooding phase in two-phase flow, due to a more homogeneous azimuthal temperature distribution on the rods at a given axial level under steam flow.

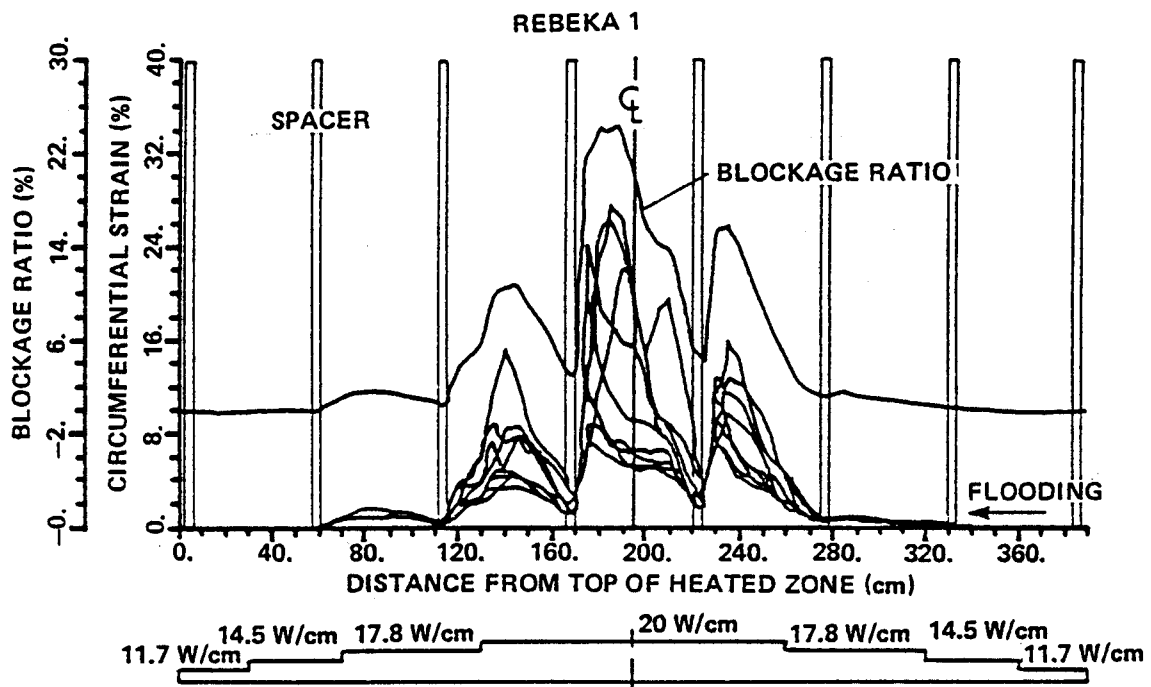
Test number	Bundle size	Thermal-hydraulics during cladding deformation				Burst data (averaged)						Max. flow blockage (%)	Remarks	Reference (c)
		Heating rate (K/s)	Coolant flow	Flow direction	Heat transfer coeff. (W/m ² /K)	Temperature measured nearest to burst at time of burst	Best-estimate burst temperature (°C)	Pressure (bar)	Circumferential strain (%)	Intergrid distribution of bursts (mm)				
1	5x5	7 ^a <1 ^b	- steam - reflood	reversed	30... 100	685	810	60	28		25	<ul style="list-style-type: none"> inner 3x3 pressurized only 2 rods burst high reflood rate at start of burst 	[72]	
2		7 ^a	steam	uni-directional	30	870	870	55	54	95	60	<ul style="list-style-type: none"> inner 3x3 pressurized 	[73]	
3		7 ^a <1 ^b	- steam	reversed	30... 100	808	830	51	44	203	52	<ul style="list-style-type: none"> inner 3x3 pressurized 	[74]	
4		7 ^a <1 ^b	- reflood	reversed	30... 100	795	830	53	46	242	55	<ul style="list-style-type: none"> inner 3x3 pressurized control rod guide tube in centre 	[75]	
M		0	quasi stagnant steam		<10	754	754	70	63	28	84	<ul style="list-style-type: none"> 1 W/cm inner 3x3 pressurized 2 rods leaked 	[76]	
5	7x7	7 ^a 0 ^b	- steam - reflood	reversed	30... 100	775	800	68	49	242	52	<ul style="list-style-type: none"> all pressurized 	[71]	
6		7 ^a -4 ^b		uni-directional	30... 100	765	790	62	42	140	60	<ul style="list-style-type: none"> 2 rods unpressurized instrument tube in centre 	[70]	
7		7 ^a -9 ^b		uni-directional	30... 100	755	790	57	55	200	66	<ul style="list-style-type: none"> all pressurized 		

Common tests conditions:

Heated length : 3900 mm ; decay heat at midpoint: 20 W/cm; axial peaking factor: 1.19; axial power profile: 7 axial steps (5x5 tests), cosine-shaped (7x7 tests); system pressure: 4 bar; coolant flow: ~2 m/s steam, ~3 cm/s forced flooding from bottom; Zircaloy-4 claddings: 10.75 x 0.72 mm, stress relieved

- a) During heatup
- b) During reflood at a time of high plastic deformation before burst
- c) In Erbacher, F.J. and Leistikow, S., "Zircalloy Fuel Cladding Behavior in a LOCA : A Review", Zirc. In the Nucl. Ind.: 7th Int; Symp.; ASTM STP P39, pp. 451-488.

Table 1: REBEKA Multi-Rod Burst Tests.



AXIAL DISTRIBUTION OF RATING IN FUEL SIMULATOR

Figure 10: REBEKA-1 - circumferential strain of the 9 inner rods and coolant channel blockage.

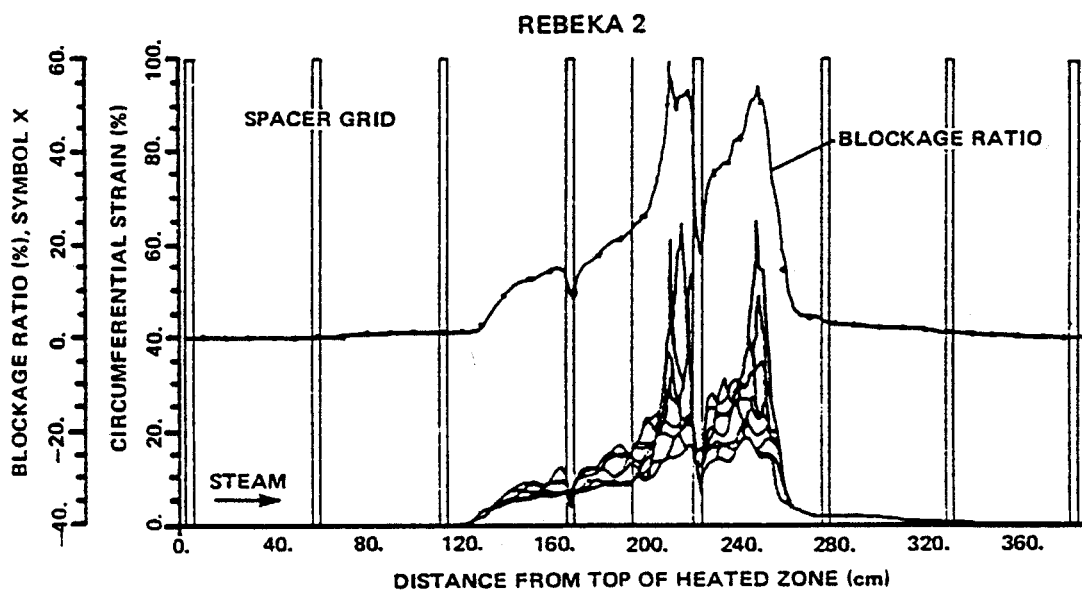


Figure 11: REBEKA-2 - circumferential strain of the 9 inner rods and coolant channel blockage.

Test R-3 was a repeat of test R-1, without malfunction, whereas R-4 was a test with conditions similar to those of R-3 but with a control rod guide tube replacing the central rod. The deformation and flow blockage profiles in R-3 and R-4 are compared in figures 12 and 13, which reveal a low coplanar character of the maximum strain locations on the different rods. For R-3, the maximum strain reached 64% and the flow blockage, 52%, whereas for R-4, despite the azimuthal temperature gradients resulting from the presence of the guide tube, the corresponding values were not reduced but increased: 79% for maximum strain, 55% for flow blockage.

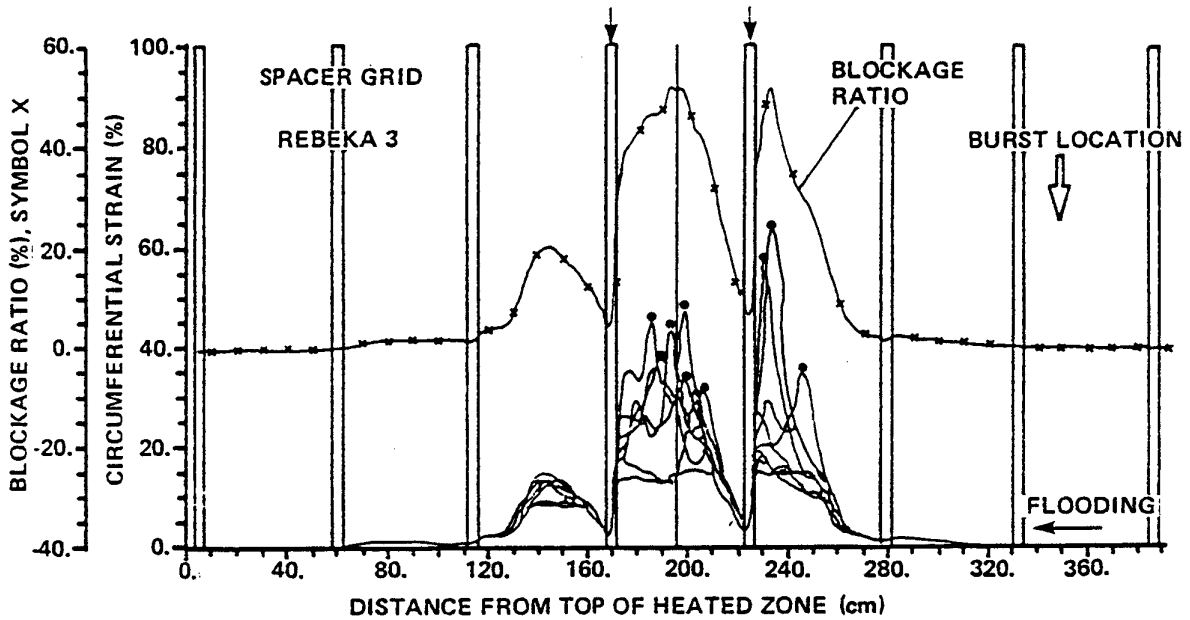


Figure 12: REBEKA-3 - circumferential strain of the 9 inner rods and coolant channel blockage.

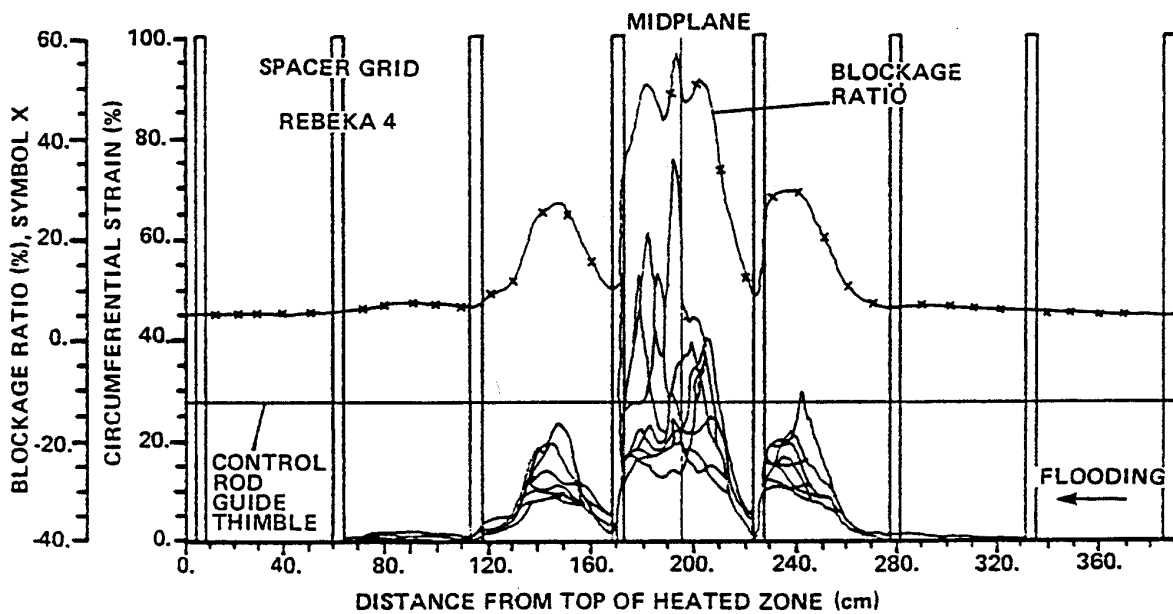


Figure 13: REBEKA-4. Circumferential strain of the 9 inner rods and coolant channel blockage.

This observation made during the REBEKA-4 test was unexpected in consideration of the single rod test results which had demonstrated the major influence of azimuthal temperature differences. This was analyzed by Wiehr et al. at KfK^[13] who proposed the explanation schematized in figure 14: the deformation of a rod near the guide tube, which starts on the cold side facing the guide tube (due to the "hot side straight effect"), is stopped at an early stage (at $\epsilon \sim 19\%$) when the deforming rod comes into contact with the guide tube. The straining is thus transferred to the opposite hot side, thereby increasing the gap size and hence reducing the temperature and then the azimuthal temperature gradient. Moreover, it was observed from the temperatures measured on the rods neighboring the guide tube a lower cooling at the start of reflooding on the side facing the guide tube than that measured on the opposite side. This thermohydraulic effect - attributed to the early blockage of the inner subchannels (where the rod straining started first) and the collapse of water droplets on the cold guide tube - emphasizes the cooling on the hot size and consequently the homogenizing of rod temperatures, which delays the time of burst and increases the circumferential burst strain.

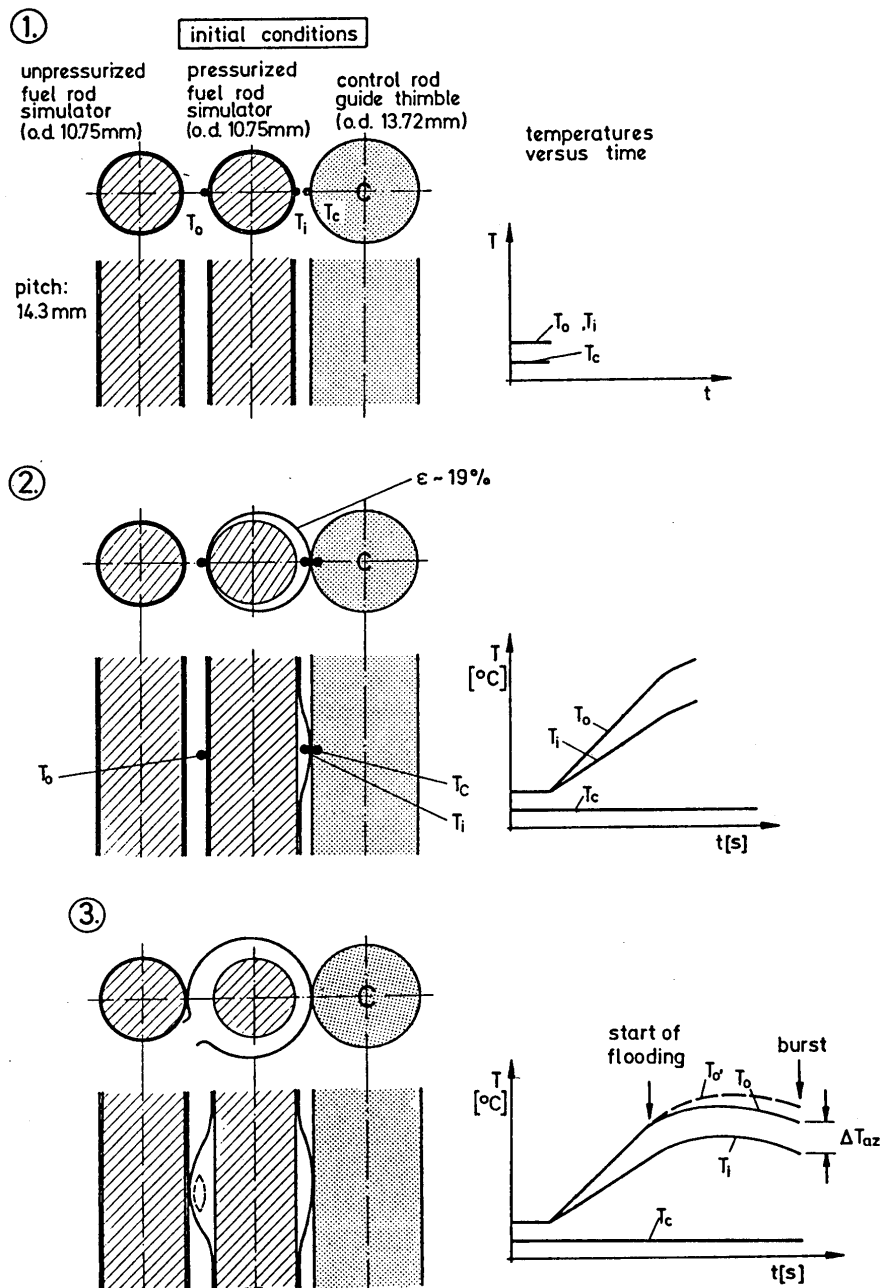


Figure 14: REBEKA-4 - cladding deformation mechanism under the influence of a cold control rod guide tube (schematic).

The REBEKA-M test was a 5x5 bundle test with all rods pressurized and run under very specific conditions: heat-up to 754°C, before reaching quasi-adiabatic and isothermal conditions (quasi stagnant steam, very low power of 1 W/cm to compensate heat losses). These atypical conditions for a LOCA were chosen so as to maximize rod deformations and the bundle blockage ratio. On the central rod, a maximum strain of 89% was reached, with an average strain of 63%, together with a maximum flow blockage of 84%.

3.2.1.2 7x7 rods bundle tests

In this test series, the 49 rods were all pressurized and the array was restrained by a non heated shroud placed at a half rod pitch from the center of the outer rods.

Test R-5 was run under conditions very similar to those of R-3 and exhibited strain profiles comparable to those found in R-3. The maximum strain was slightly higher (75%, for 64% in R-3), but the maximum flow blockage remained identical to 52%, due to the axial spread of the maximum strains, as shown in figure 15.

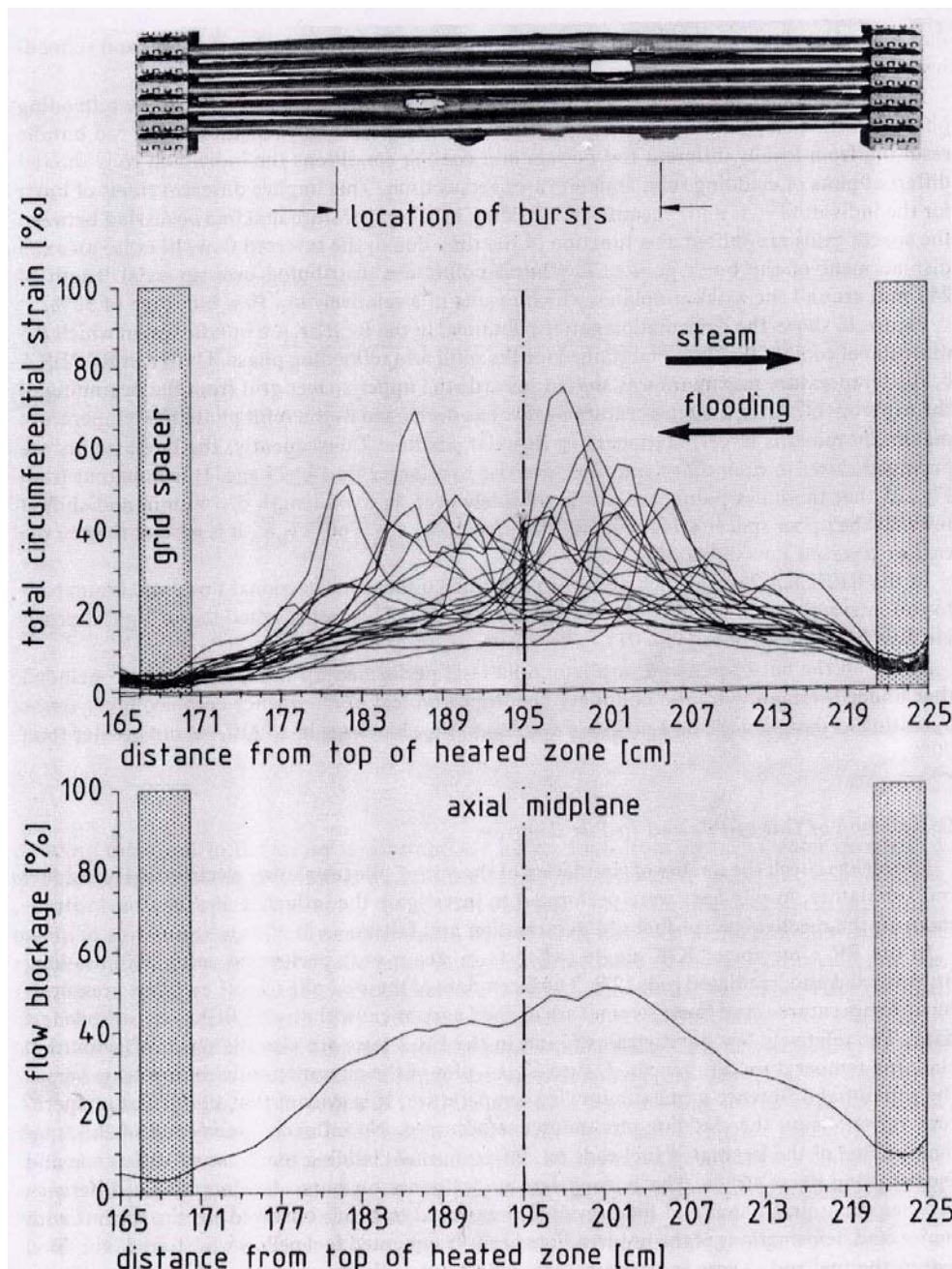


Figure 15: REBEKA-5 - circumferential cladding strain and flow blockage under reversed flow.

In test R-6, an instrumentation tube was placed in a central position and two rods were weakly pressurized in contrast to the remaining rods, pressurized to 60 bar. The steam flowed in the upward direction during the heating phase, as well as the reflooding phase; these thermohydraulic conditions led to a higher axial uniformity of the temperatures during ballooning, then to a lower axial spread of maximum strain than that in the case of countercurrent steam/flooding flows (R-5), as shown in figure 16 in comparison to the previous figure. In this test R-6, the maximum strain was 65% and the maximum flow blockage ratio, 60%.

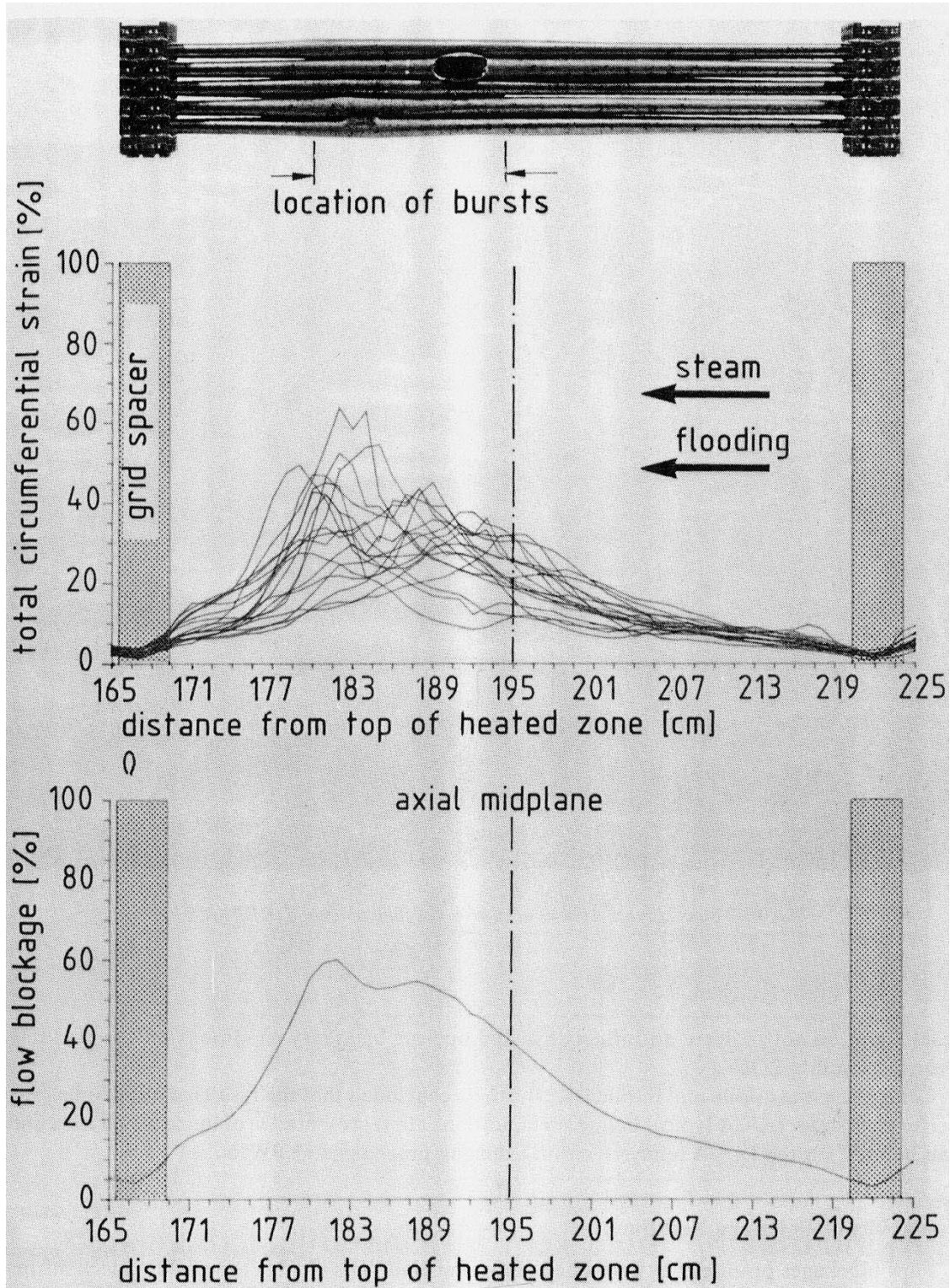


Figure 16: REBEKA-6 - circumferential cladding strain and flow blockage under unidirectional flow.

The final test R-7 was a repeat of R-6 with all 49 rods pressurized and exhibited the highest values of maximum strain and flow blockage ratio in the REBEKA multi-rod tests (test REBEKA-M excepted): 85% and 66% respectively.

3.2.1.3 Conclusions on REBEKA multi-rod tests

One main characteristics of the REBEKA multi-rod tests is the choice of thermohydraulic conditions representative of the refilling/reflooding specific conditions relating to the German KWU PWR design (safety injection in both the cold and hot legs). These conditions, with reversal of flow direction from vapor to the two-phase cooling, favor an axial non-uniformity of rod temperatures, hence an axial spread of the elevations of maximum strain that finally limits the extent of flow blockage. Under such conditions, the mechanical interactions between rods are sparse and weak (see figure 17) and the effect of the bundle size (R-5 results compared to those of R-3) is almost undetectable, which is not the case in the MRBT experiments discussed in the next section.

However, although the presence of a guide tube generates azimuthal temperature differences on adjacent rods, it does not necessarily lead to a reduction in the burst strain and blockage ratio, which can even be increased. The mechanical interaction between the guide tube and the neighboring deforming rods does indeed interrupt the asymmetrical straining of these rods ("hot side straight effect") and re-homogenize the azimuthal temperature field; this may further be emphasized by thermohydraulic differential effects, particularly in the two-phase flow conditions of the REBEKA tests. This conclusion on the influence of guide tubes will be confirmed by JAERI test results.

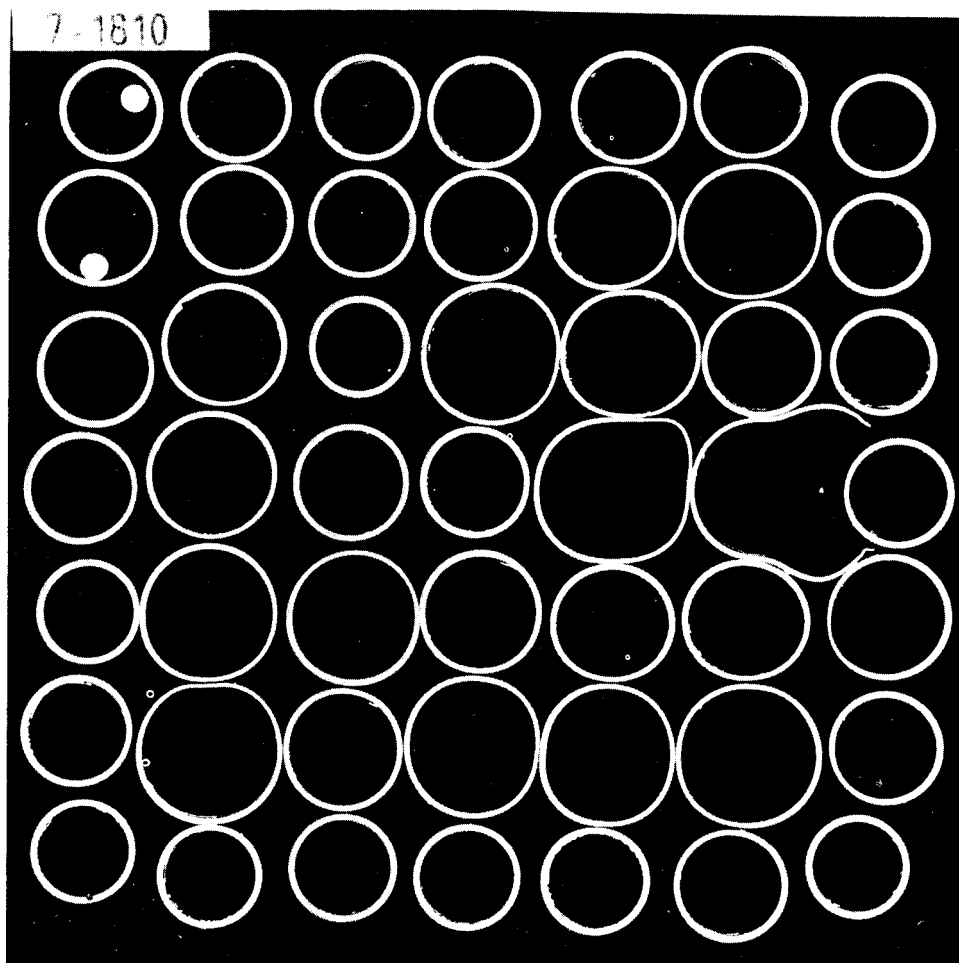


Figure 17: REBEKA-7 - bundle cross-section at maximum flow blockage.

3.2.2 The ORNL-MRBT multi-rod tests

The six MRBT (Multi-Rod Burst Tests) tests were carried out between 1977 and late 1981 on rod bundles of different sizes:

- 4x4 for tests B1, B2 and B3,
- 6x6 for test B4,
- 8x8 for tests B5 and B6.

All these tests were run under a steam atmosphere with very low downstream flow.

The test rods were electrical simulators with internal heating, identical to those used in the single rod tests and with the same heating length (0.915 m), pressurized and instrumented with 4 thermocouples welded onto the clad internal surface. The rod array was maintained by 3 spacer grids, with a 560 mm lower intergrid and a 345 mm upper intergrid.

3.2.2.1 4x4 rods bundle tests

In tests B1 to B4, the rod array was surrounded by a direct resistance heated shroud, located 13 mm apart from the external side of the outer rods so as to avoid electrical short-circuiting with them. Heating of the shroud at a temperature close to that of the test array provided a good radial temperature boundary. However, the large spacing between shroud and outer rod rows led to non restrained deformation and bowing of these outer rods without contact. Figure 18 provides a schematic view of the B1 test assembly.

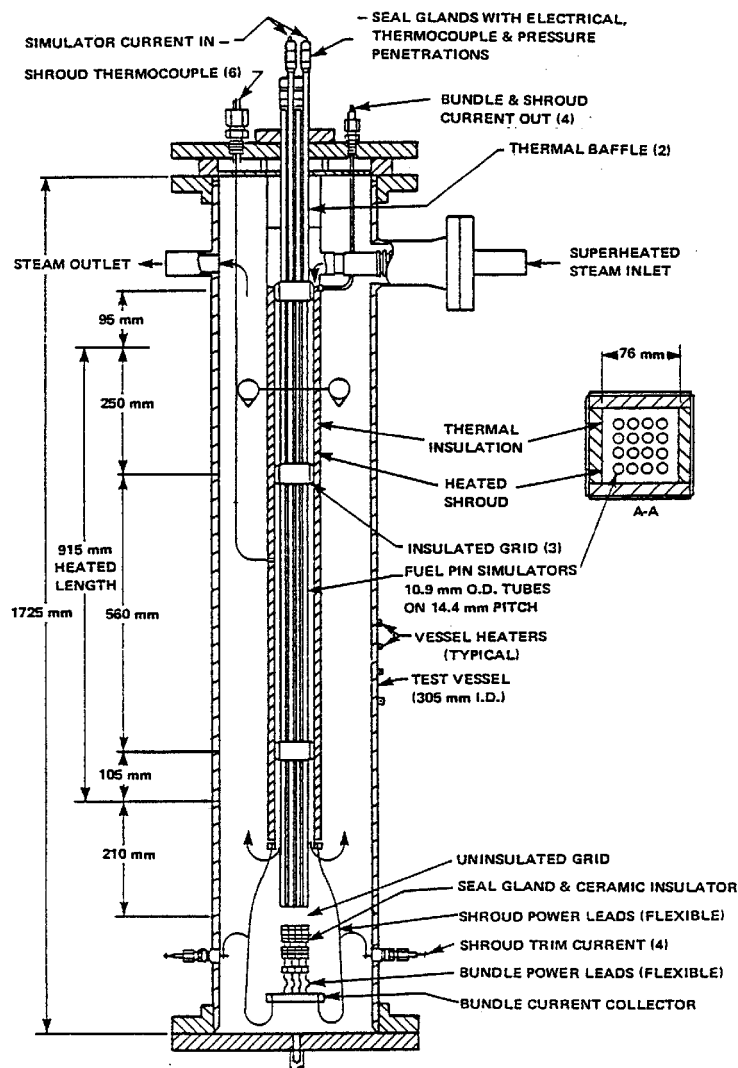


Figure 18: ORNL-MRBT - schematic of B1 test assembly.

In test B1, with the heated shroud, the temperature was ramped at ~ 30 K/s from 350°C until the rods burst, which occurred in the $850\text{-}880^\circ\text{C}$ temperature range. Burst strains range between 32 and 59% and the blockage ratio is 49%.

Test B2 was run under conditions very close to those of the B1 test, but without shroud heating. The burst strains were similar to those found in B1: 34 to 58%, with an even slightly higher blockage ratio: 54%. However, greater bowing of the peripheral rods could be observed due to the azimuthal temperature differences induced by the neighboring unheated shroud.

In test B3, with the heated shroud, the temperature ramp rate was lower (9.5 K/s) and the initial rod internal pressure was increased so as to cause rupture at about 760°C . All rods in B3 failed below 780°C , wholly in the α -phase region, with burst strain in the range 42 -77%; six rods had undergone strain greater than the maximum of both B1 (59%) and B2 (58%). The maximum flow blockage was at about 77%. Figure 19 shows that circumferential strain greater than 32% (corresponding to the contact with a neighboring rod bearing the same deformation) spreads axially over more than 10cm for a majority of the rods.

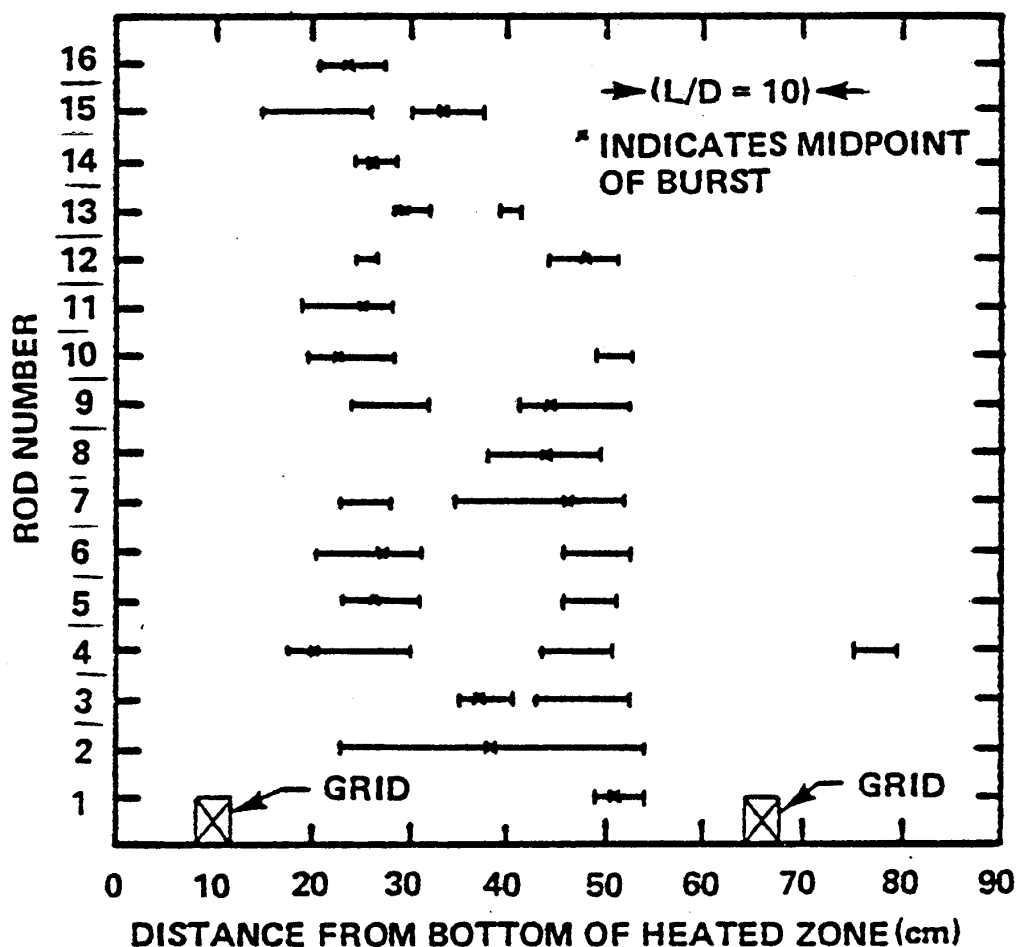


Figure 19: ORNL-MRBT - portions of tubes with greater than 32% strain in the B3 test.

Figure 20 shows the burst strains for B1 to B3 test rods as a function of the burst temperature and compared with the strain/temperature curve deduced from the single rod tests with an unheated shroud. The multi-rod tests, more particularly B3, exhibit significantly greater circumferential strains than those obtained in single rod tests with unheated shroud. However, the B3 deformation range is consistent with ORNL and REBEKA results from single rod tests with heated shroud, as shown in figure 21.

In the B4 test carried out on a 6x6 rod array, a dysfunction occurred leading to the test termination with a low level of strain on the rods ($<20\%$).

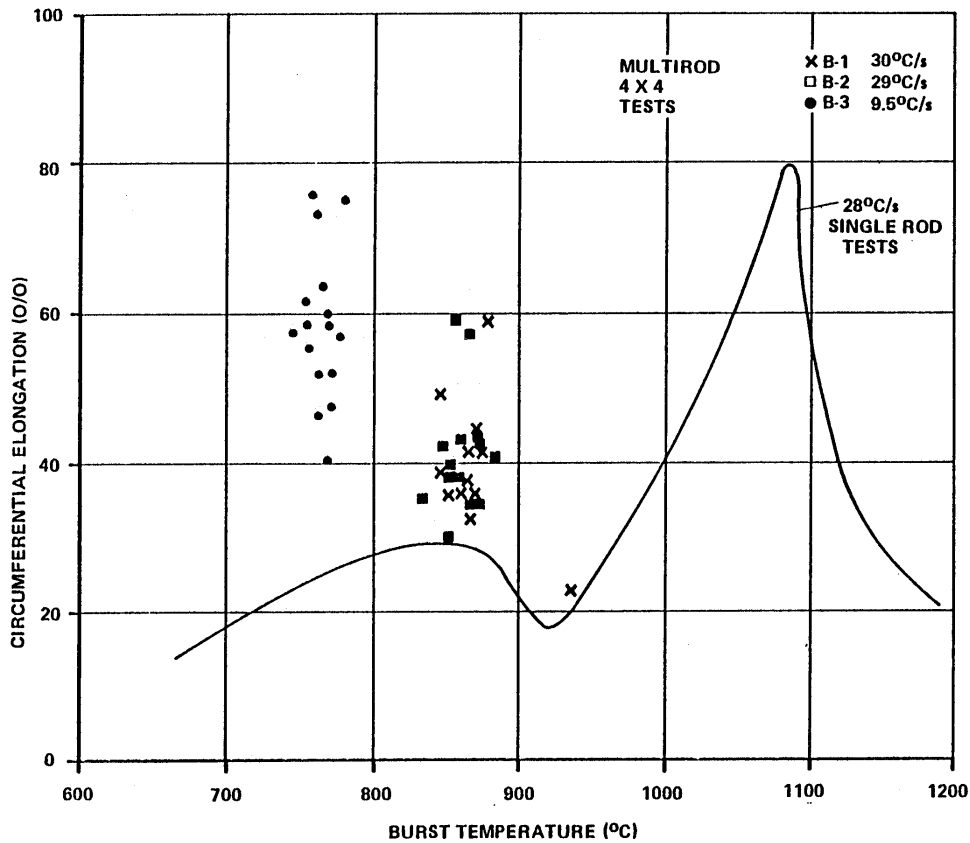


Figure 20: ORNL-MRBT - comparison of burst strain in the B1, B2 and B3 tests with single rod test data.

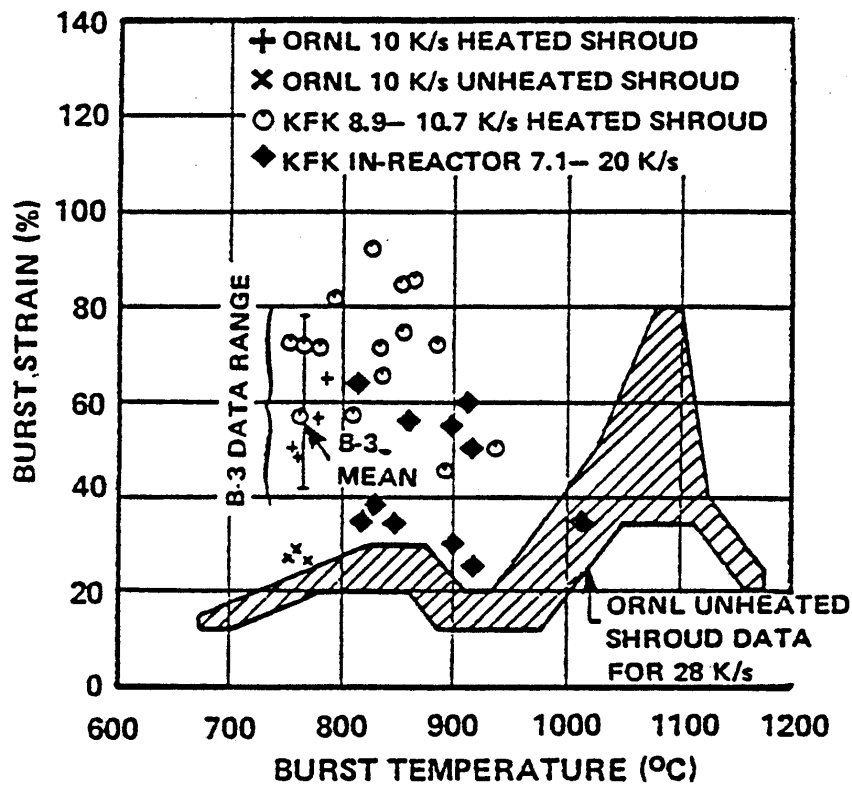


Figure 21: ORNL-MRBT - comparison of B3 bundle burst data with ORNL and KfK single-rod data for a heating rate of ~ 10 K/s.

3.2.2.2 8x8 rods bundle tests

The B5 and B6 tests were carried out on a 8x8 rod array surrounded by an unheated shroud spaced 1.8 mm from the outer surface of the row of outer rods (that is nearly half of the distance between the surfaces of two adjacent rods). This low spacing did not enable the direct resistance heating of the shroud as in tests B1 to B3. Therefore, the shroud was made of a thin (0.1 mm) stainless steel layer with a highly polished gold-plated inner surface to minimize thermal capacity and radiative losses; the stainless steel sheet was backed on the outside with a strong isolating supporting structure.

Test B5 was conducted under conditions very similar to those in the B3 test: 9.8 K/s temperature ramp and same steam mass velocity. All rods (except one that failed to hold its internal pressure at the start of the transient) ruptured at about 775° C within six seconds.

A comparative analysis of B3 and B5 test results was conducted by Chapman et al.^[14]. It can be considered that the 4x4 inner rods in B5 were submitted to similar thermal conditions as the rods in B3, in consideration of the two guard rows of heated rods in B5 and of the heated shroud in B3. Although all the rod simulators were pressurized at the same initial level, a significant reduction in the burst pressures of the B5 inner rods was observed in comparison to the B3 rods (10 to 20 bar), as shown in figure 22 plotting the burst temperature vs burst pressure in B3 and B5 compared to the prediction curve based on the ORNL single rod heated shroud test data. The scale magnification in the inset makes it possible to differentiate the B5 data for each of the three radial zones: the outer ring, next inner ring and the central 4x4 array, for comparison with B3 data. The plot shows that the B5 central 4x4 rods burst pressures were generally much lower than those for the outer rings and that the data for the B3 array corresponded well with those for the most outer ring of B5.

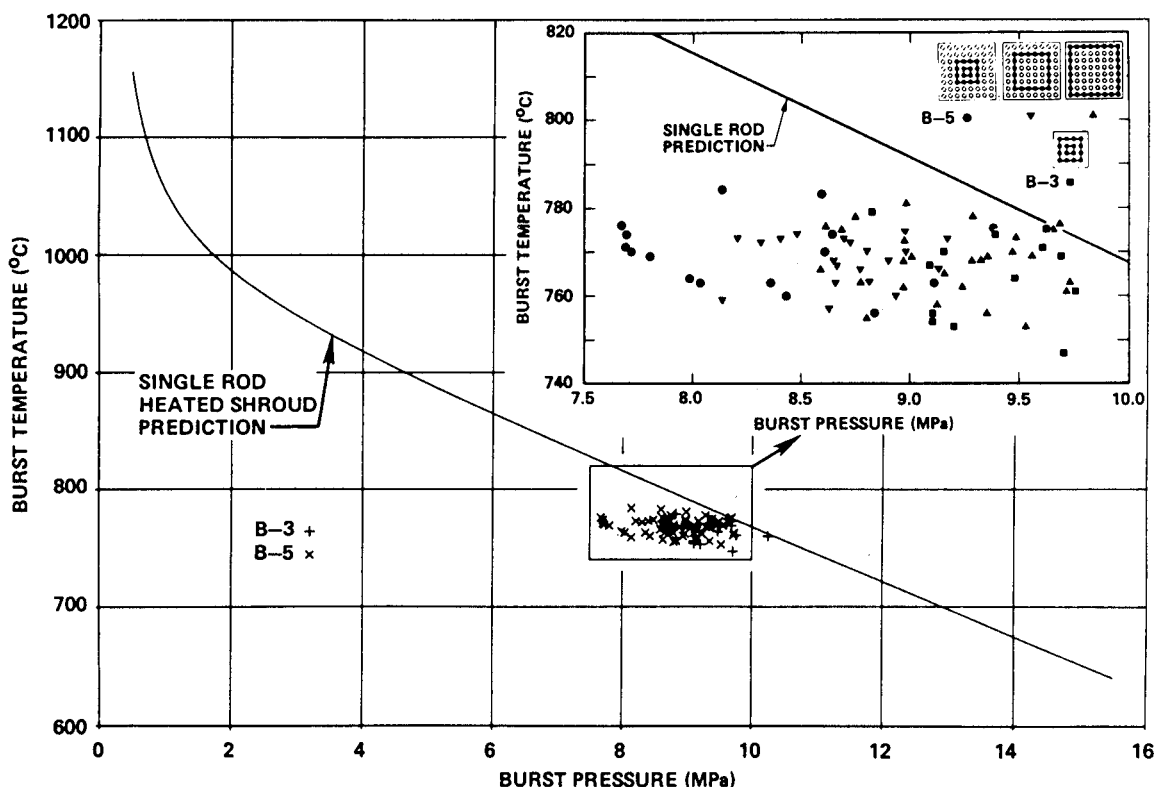


Figure 22: ORNL-MRBT - comparison of bundle burst data with predictions from single-rod heated shroud tests.

According to Chapman, this result is related to the influence of the mechanical interactions between rods during ballooning: as illustrated in figure 23, in test B3 the 13 mm distance between the shroud and the outer rods surface allowed an outward expansion of the rods without being constrained by the shroud; they behaved somewhat like single-rod heated shroud tests.

In the B5 test, however, the closely fitted shroud around the rod bundle limited the outward expansion throughout the array early in the transient, causing the tubes to touch each other and generate contact forces. With further straining after contact, the rods tended toward square cross sections. The contact forces, not being relieved by tube bowing, caused a redistribution of the straining pattern in both the azimuthal and axial directions in a dynamic process enhanced by the homogenizing of temperatures in the inside of the array. As a result, the volumetric expansion of the inner rods was increased and they burst at lower pressures than the outer ones.

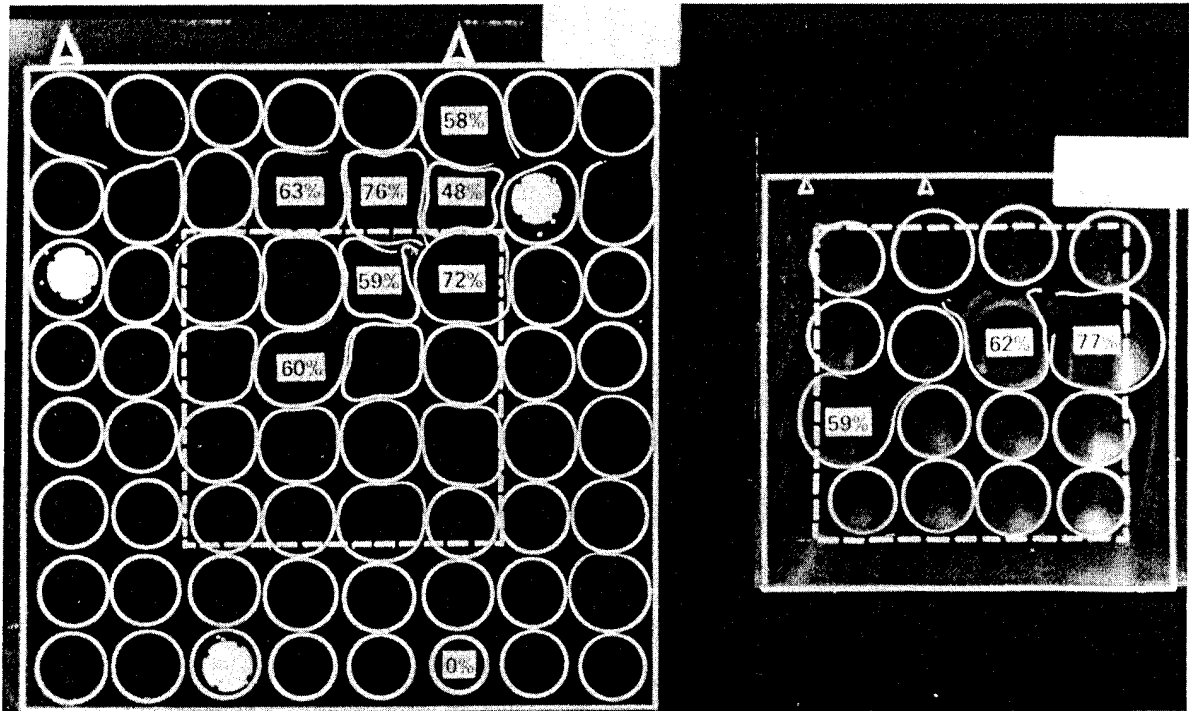


Figure 23: ORNL-MRBT - sections from highly deformed regions of B5 and B3 bundles showing effects of confinement.

Figure 24 plots the burst strain data in B3 and B5, displayed in the latter test in three subgroups corresponding to the two outer rings and the 4x4 inner rods; the B3 data were compared to the latter B5 subgroup. The average burst strains in the B5 subgroups and B3 do not appear very different, despite the large spread of burst strain values for rods in the outer rings of B5. Alternatively, figure 25, which illustrates the volumetric expansion data in a similar way as for burst strain data in the previous figure, clearly shows a greater volume expansion in the B5 central 4x4 array than in the outer rings and the B3 array for which the average volume expansion is close to the average value in the B5 outermost ring. The variation in volume expansion from the center to the outer regions of the B5 array confirms the burst pressure variation in Figure 22. The higher volumetric expansion in the B5 inner 4x4 array than in the B3 array leads to a flow blockage with a higher maximum value (90%) and a wider axial extent (> 70% over 23 cm), as shown in figure 26.

In test B6, the concluding test of the ORNL MRBT program, the conditions were chosen so as to obtain rod bursting at around 930°C, i.e. well into the $\alpha+\beta$ phase domain in order to ascertain the typically smaller strain level observed in single rod tests under similar conditions. The B6 results showed burst strain ranging from 22 to 56% with a 30% average value consistent with single rod test results (36% on average of the three tests under similar conditions). The corresponding flow blockage ratio was therefore rather modest: 39% for the whole 8x8 array to 46% for the inner 4x4 array.

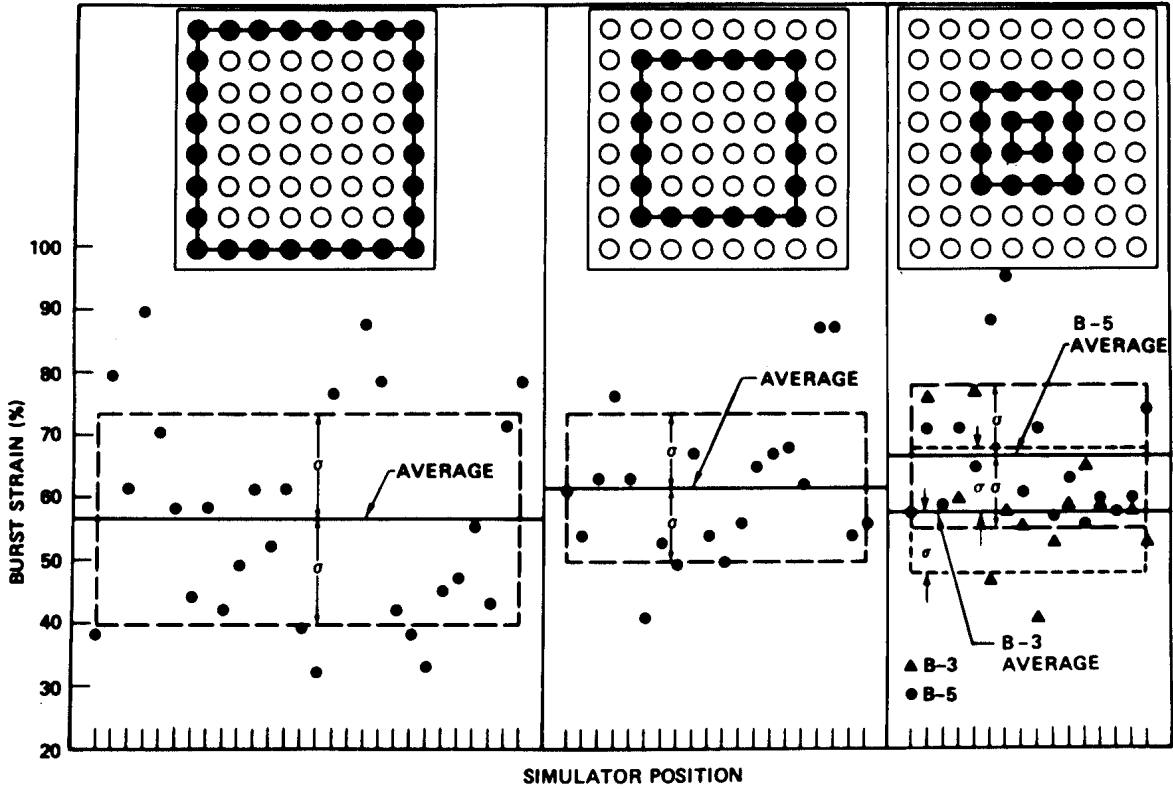


Figure 24: ORNL-MRBT - burst strain of B5 tubes.
 B3 (4x4) data shown for comparison with the inner 4x4 array of B5.

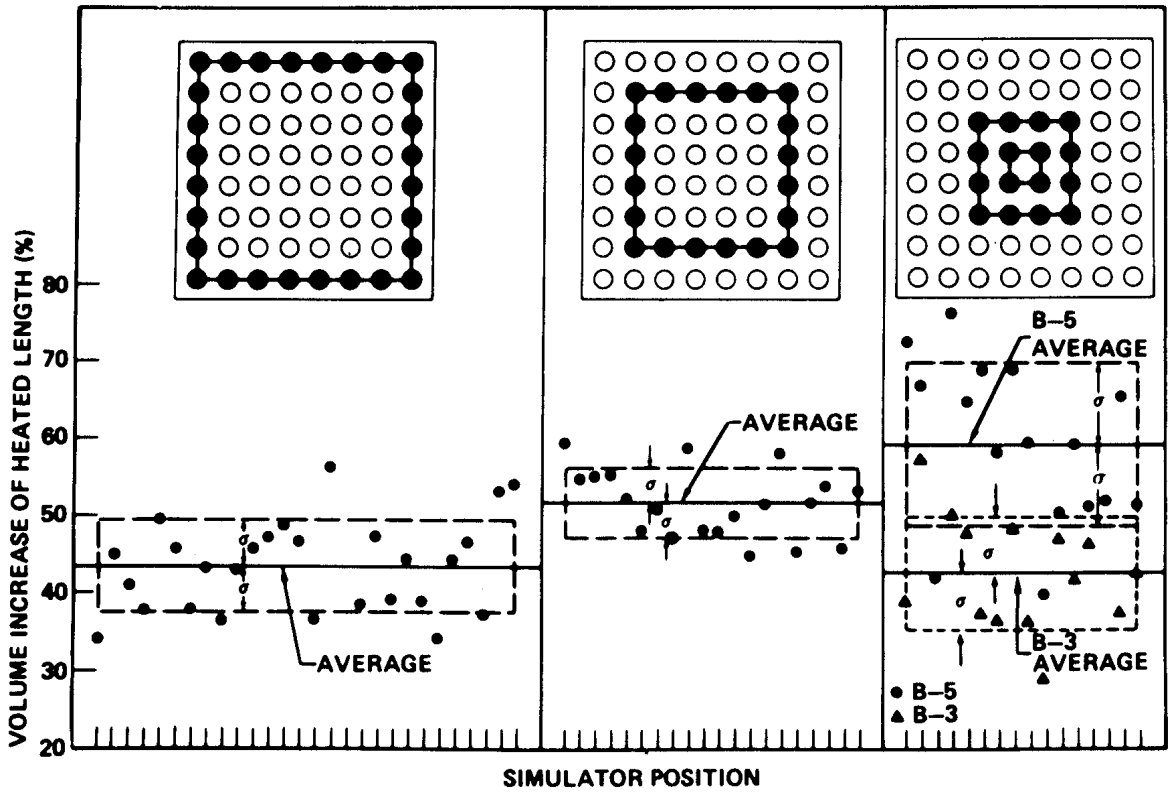


Figure 25: ORNL-MRBT - volumetric expansion of B5 tubes.
 B3 (4x4) data shown for comparison with the inner 4x4 array of B5.

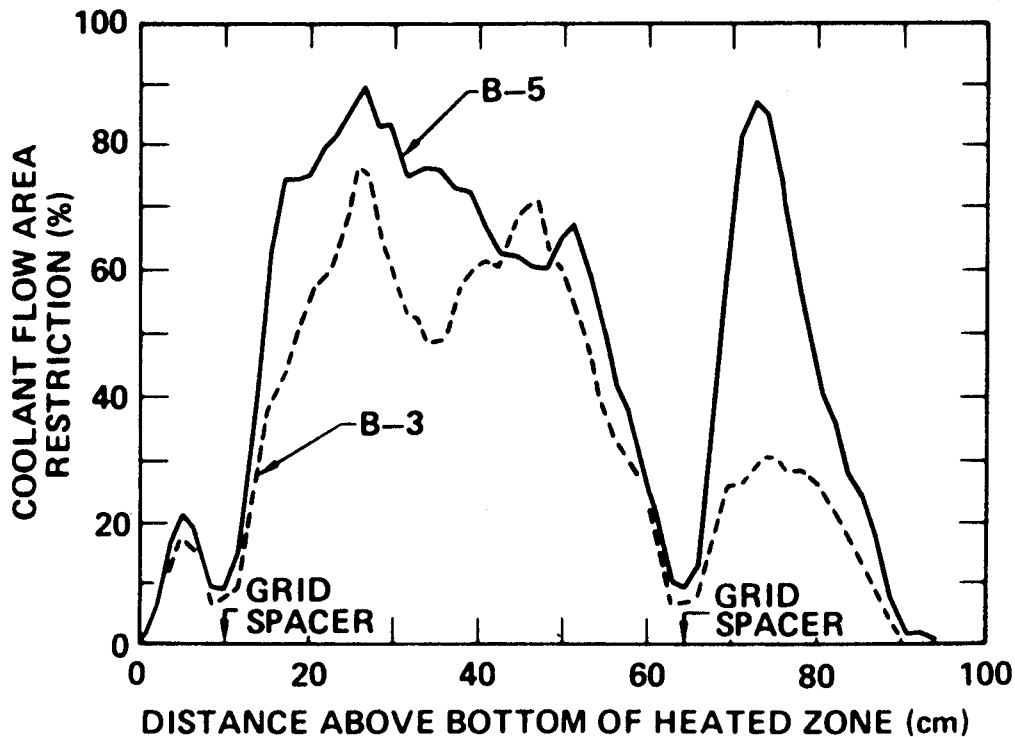


Figure 26: ORNL-MRBT - comparison of the B5 inner 4x4 flow area restriction with B3 array.

3.2.2.3 Conclusions on ORNL multi-rod tests

The main objective of the MRBT tests was to investigate the influence of the bundle size and the thermal & mechanical boundary conditions on the burst strain and flow blockage under thermal heat transfer conditions that did favor large deformations.

As provided by the comparison of the B3 and B5 data, the main results indicate that the straining of the inner rods in a large array leads to mechanical interactions between neighboring rods that modify significantly the spatial development of deformation until rupture, even if these interactions have a limited impact on burst temperature and elongation. Notably, the trapping of bulging rods appeared to cause the deformation to extend axially, resulting in a larger volume expansion and a larger axial extent of blocked regions. This also resulted in a deviation from the rupture temperature/pressure curve deduced from single rod heated shroud test data.

Thus the authors concluded that the flow area restriction in large arrays could be underestimated by test results on small unconstrained arrays and that two rows of deforming "guard" rods are necessary around the central deforming array to properly simulate representative conditions present in a reactor fuel assembly.

The presentation of these results, in particular at the 6th Symposium "Zirconium in the Nuclear Industry" by Chapman^[14], raised keen criticism from the authors of the REBEKA program who made rather different observations. F.J. Erbacher thus claimed that the thermohydraulic conditions in the MRBT tests (low steam cooling) were atypical of a LOCA and therefore the results were specific to these tests only; it was however replied that the two-phase cooling conditions used in REBEKA tests, under which the deformation did not appear sensitive to bundle size, were also specific of the German PWR and may not be applicable to US-designed PWR's.

Last of all, it is worth mentioning that only tests B1 to B3 were included in the database that was used to derive the clad swelling and rupture models described in the NUREG-630 report (see § 5.1). These three tests were used in particular to derive a coefficient linking the average burst strain to the average strain in the plane of maximum flow blockage, so as to derive the maximum flow blockage as a function of the burst temperature. Based on these three test results only, it may be thought that the proposed correlation remains rather uncertain.

3.2.3 The JAERI multi-rod tests

The multi-rod tests performed at JAERI in the late 70s to early 80s were carried out on bundles of 7x7 simulators of Japanese 15x15 PWR rods. These simulators had a heated length of 0.9 m, were internally pressurized in the range 20-70 bar and were maintained by two spacers.

Three test series were successively performed with three different configurations as outer boundary conditions for the 7x7 array, as shown in figure 27:

- Tests 5 to 8: close fitting unheated shroud,
- Tests 9 to 14: outer ring of 32 unpressurized heaters,
- Tests 15 to 24: unheated shroud backed by a ring of 32 guard heaters.

The tests were conducted under a steam atmosphere with very low flow, i.e. under thermohydraulic conditions favoring large deformations. The influence of a shroud heated by a guard ring can be deduced from comparing results of the 2nd and 3rd series. The influence of unheated rods simulating control rod guide tubes was also addressed by comparative tests, particularly in the last series. The primary objective of the last series of tests was to investigate a realistic upper bounding value of the flow channel restriction in the bundle.

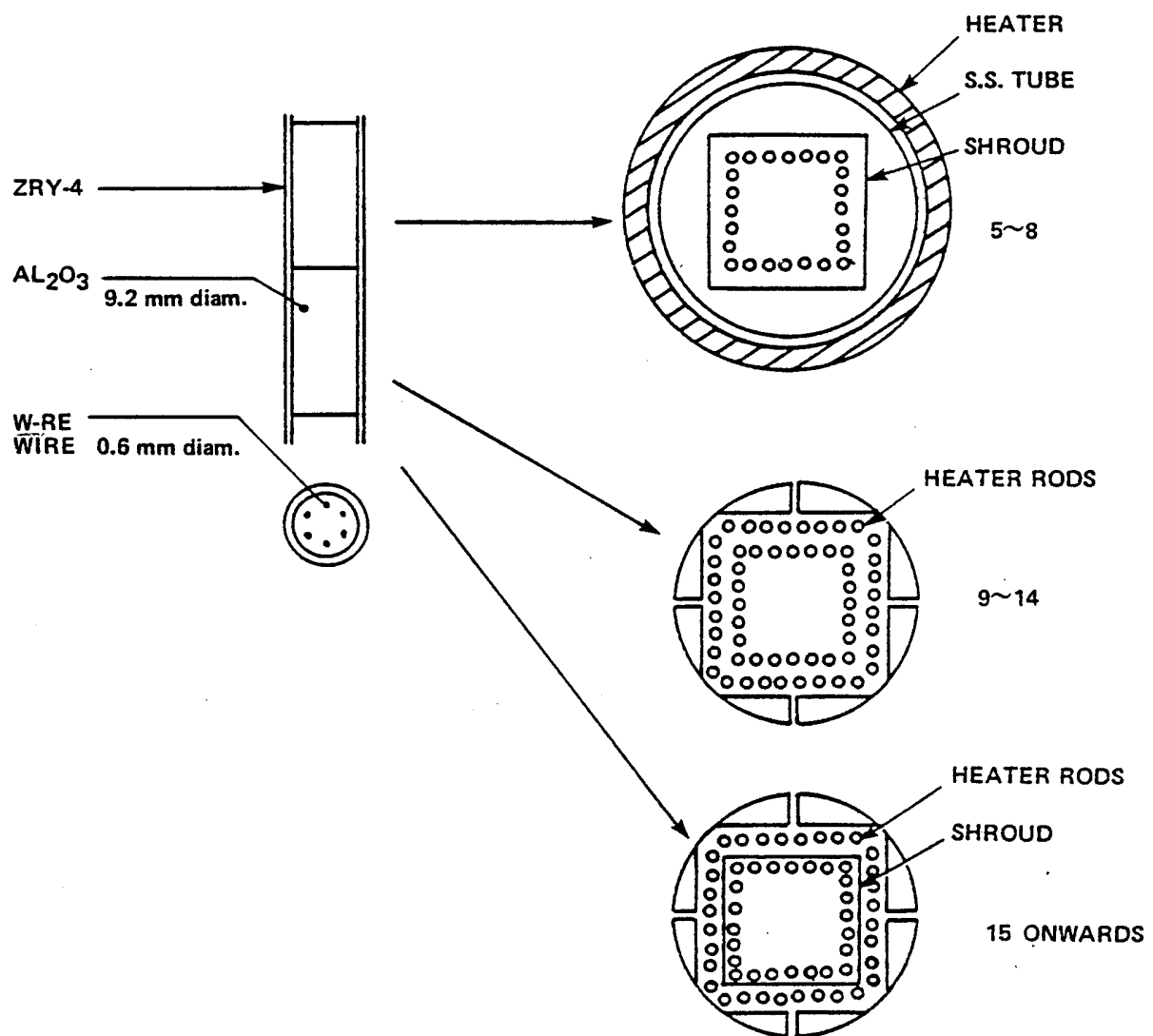


Figure 27: JAERI tests- schematic drawings of the fuel rods and heating systems.

3.2.3.1 Unheated shroud tests

This first series of tests, summarized in Table 2, examined the effect of the burst temperature in the high α and $\alpha+\beta$ phase regions, i.e. in the 740-920°C temperature range, on rod deformations with ramp rates of 6 to 9 K/s.

Bundle N°	Steam Flow Rate (g/cm ² xmin)	Heating Rate (°C/s) (500 – 860°C)	Initial Internal Pressure (kg/cm ²)	Maximum Internal Pressure (kg/cm ²)	Burst Temperature (°C)
7805	0.44	6.6 – 8.7 (500 – 860°C)	50	64 – 70	805 - 860
7806	0.40	7.3 – 9.0 (500 – 900°C)	20	26 – 29	870 - 920
7807	0.40	5.9 – 7.2 (430 – 830°C)	70	87 – 93	750 - 790
7808	0.44	5.9 – 7.9 (500 – 890°C)	35	45 - 48	870 - 880

Table 2: JAERI test matrix of bundle burst tests using W-Re wire heaters and a close fitting unheated shroud.

Figure 28 shows the axial profile of ballooning in the four tests, where the highest burst strains can be observed, as expected, for the tests that ruptured in the high α region (test 7, ass. n° 7807) or the low $\alpha+\beta$ region (test 5, ass. n° 7805).

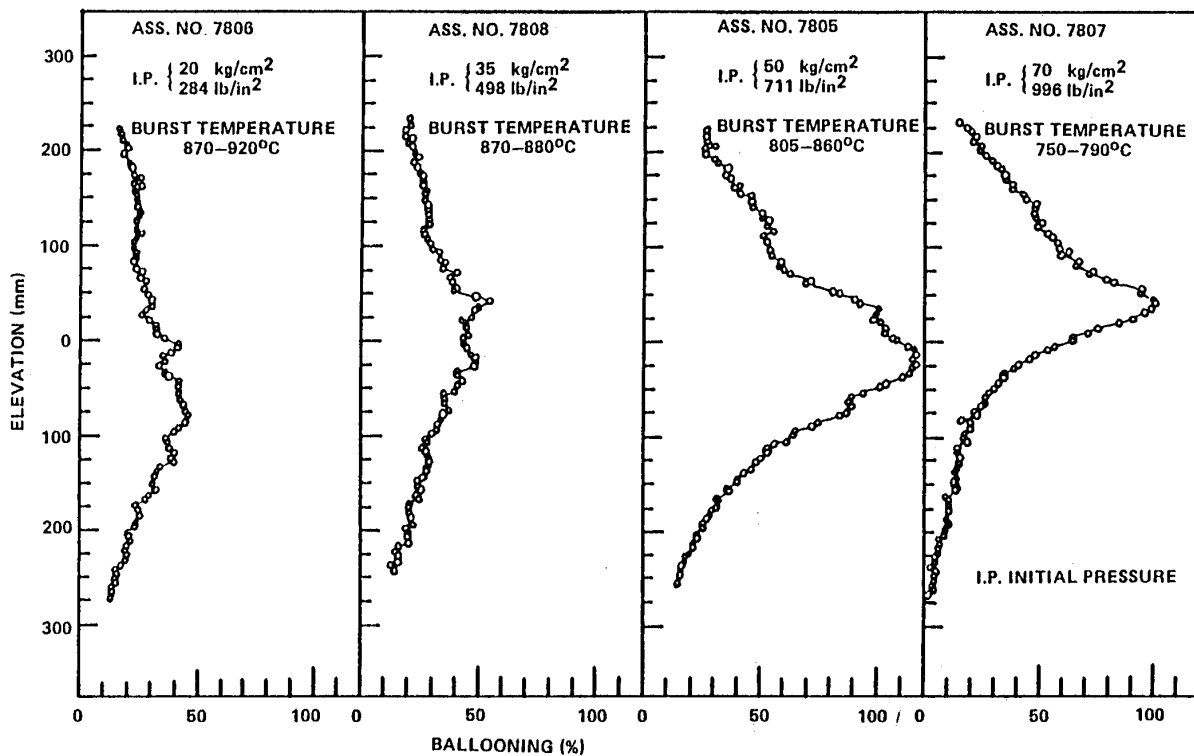


Figure 28: JAERI tests - axial distribution of ballooning in 7x7 multi-rod tests.

Figure 29 gives a failure map for test n°5, showing the axial position of bursts in relation to the axial temperature profile and the axial extent of circumferential strain greater than 34% (value corresponding to the contact between two similarly deformed neighboring rods): there appears to be a clear trend for a more axially extended deformation on the inner rods than on the peripheral ones, in agreement with the MRBT B5 test results.

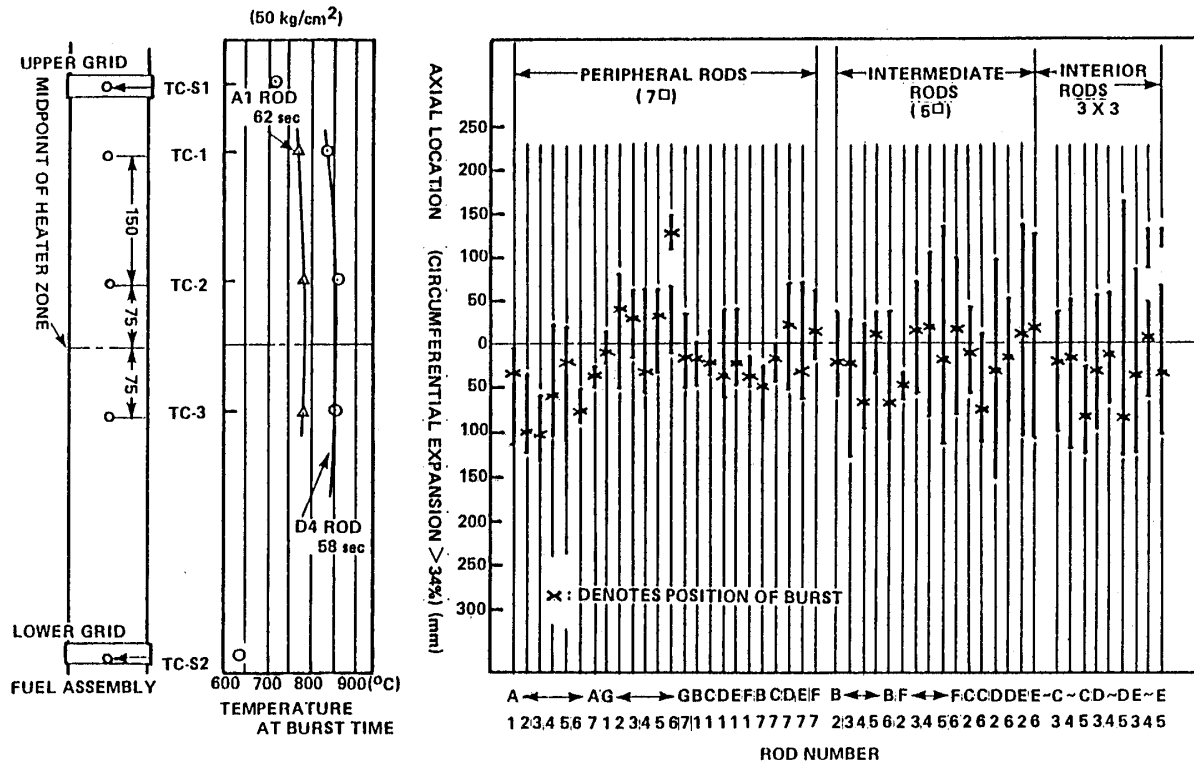


Figure 29: JAERI tests - axial locations of burst position and ballooned region in assembly N° 7805.

3.2.3.2 Tests with a guard ring of unpressurized heaters

In this series (9 - 14), the test conditions were similar to those of test n°5 which had led to the highest deformations: initial internal pressure = 50 bar, temperature ramp rate = 7 K/s (except in test n° 13). The presence of an outer guard ring of heaters reduced the temperature gradient between the center and periphery of the 7x7 array; this resulted in a greater axial extension of the deformations that also affected the peripheral rods (see Figure 30).

All 49 rods were heated in test n°10. The central rod was not heated in test n°11 so as to simulate a control rod guide tube; the deformations were not as axially extended as in test n°10, but remained mostly coplanar (see Figure 31). As previously mentioned, test 13 was run with a very low ramp rate (<1 K/s) and the rupture of rods in the 765-800°C temperature range (high α domain) led to extensive and significantly coplanar deformations, with maximum flow channel restriction reaching 87.6%.

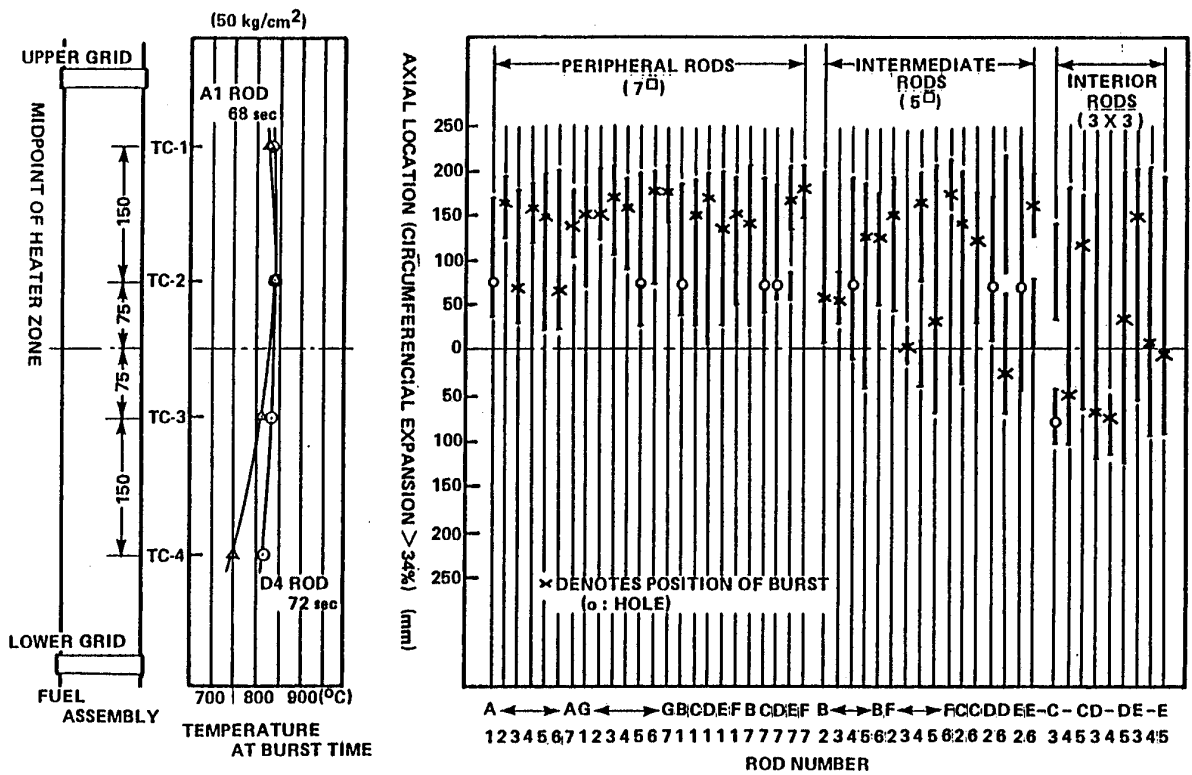


Figure 30: JAERI tests - axial locations of burst position and ballooned region in assembly N° 7910.

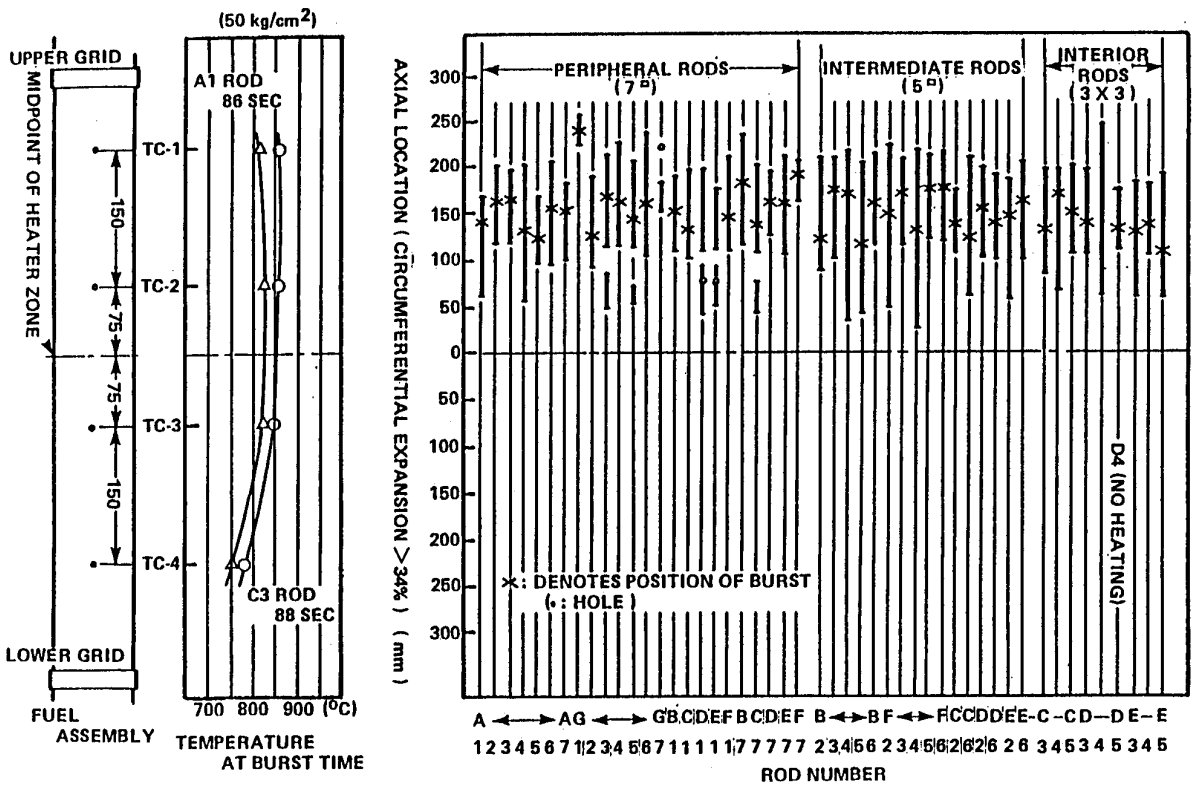


Figure 31: JAERI tests - axial locations of burst position and ballooned region in assembly N° 7911.

In the tests 12 and 14, four rods were unheated, simulating the presence of guide tubes to some extent. Despite the azimuthal temperature differences induced by these unheated rods, significant and axially extended deformations (> 34% over more than 20 cm) were observed in some rods adjacent to unheated rods (see figure 32). Although the conditions in tests 12 and 14 were quasi-identical, a detailed examination of the results in Figure 32 reveals different behavioral patterns for rods adjacent to unheated rods (except for the configuration with 2 heated rods aligned in between 2 unheated ones, as in positions C3, C4, D5 or E5), which resulted in longer balloons in test 14.

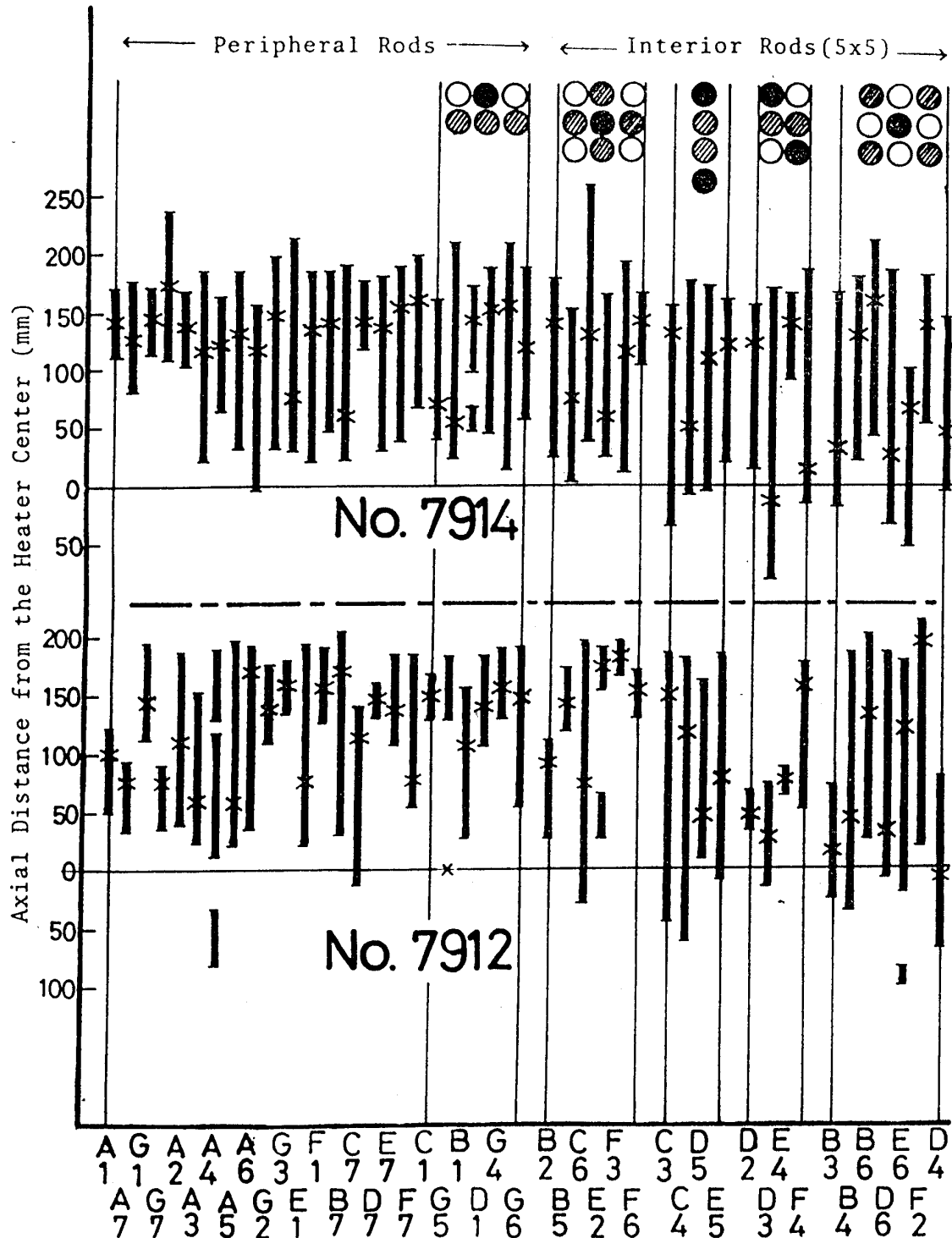


Figure 32: JAERI tests - portions of tubes with greater than 34% strain in assembly 7912.

● : non-heated rod ◐ : measured rod

In an in-depth analysis of these tests, Kawasaki^[15] suggested that the deformation on a heated rod adjacent to a non heated one was also highly influenced by the temperature difference with the neighboring rods. This hypothesis was supported by specific investigation in which analytical tests were performed on a 3x3 heated rods array, the central rod being pressurized and surrounded by 8 unpressurized rods^[16]. The results of these tests, schematized in figure 33, made it possible to draw the following conclusions:

- When the central rod temperature is lower than those of adjacent rods, deformation remains limited, the rupture occurring before or just at the instant of contact with a neighboring rod; a local hot spot where the strain begins does indeed become accentuated by the closeness of the hotter neighboring rod and leads to a localized burst.
- When the central rod temperature is greater than or equal to the temperature of adjacent rods, deformation starting on a local hot spot is counteracted and stopped by the closeness and possible contact of the deforming portion with the colder neighboring rod, thus resulting in radial, then axial, carry over and extension of the straining process ("long ballooning"). The higher the temperature difference with the cold neighboring rods, the greater the extension of the straining process. Ruptures are thus observed at the points of maximum stress where curvature reverses between concave portions contacting the neighboring rods and the bulging that develop in the interval between two adjacent rods. In one particular test with 2 unheated peripheral rods, it was observed that a 50 K azimuthal temperature difference was not sufficient to induce localized straining that could lead to early rupture before contact with neighboring rods.

This particular investigation made it possible to conclude that the deformation behavior of a rod cladding in a multi-rod array is not only influenced by the temperature gradients on the cladding but also by the temperature differences with the surrounding areas in adjacent rods.

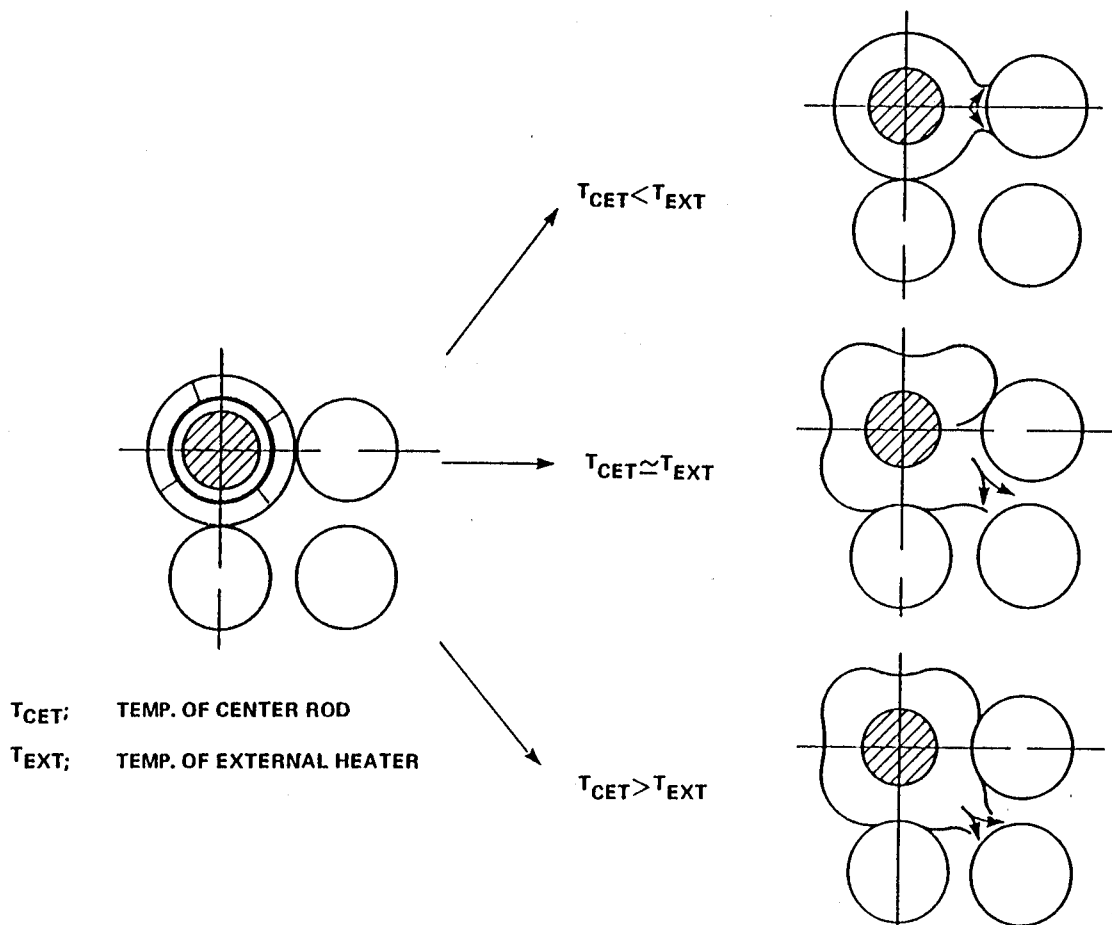


Figure 33: JAERI tests - illustrated deformation mechanism of a rod surrounded by external heaters.

3.2.3.3 Tests with a shroud backed by guard heaters

In this final test series (15-24), a shroud was introduced around the 7x7 central bundle and was backed by an outer ring of guard sub-heaters; the clearance with the bundle outer rods was 9 mm in tests 15 and 16 and at 3.7 mm thereafter. According to the shroud positioning in test 17 to 24 simulating the outer rods in a large assembly, the main objective of this part of the program was to investigate an upper bounding value of the flow restriction in the bundle with the differential impact of the presence of control rod guide tubes. To this end, in tests 21 to 24, four control rod guide tubes were substituted for pressurized rods and the test conditions were duplicated from tests 18-21. The initial pressure of the heated rods was 50 bar as in previous tests and two heating rates of 1 K/s and 7 K/s were used.

The results of this test series provided unexpected observations:

- In all tests with guide tubes, the ballooning behavior of rods neighboring a guide tube was not different from other rods, despite the larger azimuthal temperature gradient expected in these rods.
- The maximum flow blockage ratio in a bundle with control rod guide tubes was almost the same as that without guide tubes and the axial extent of the highly restricted portion was even higher in tests with guide tubes (see figure 34), in agreement with results from the REBEKA-4 test (see § 3.2.1.1).

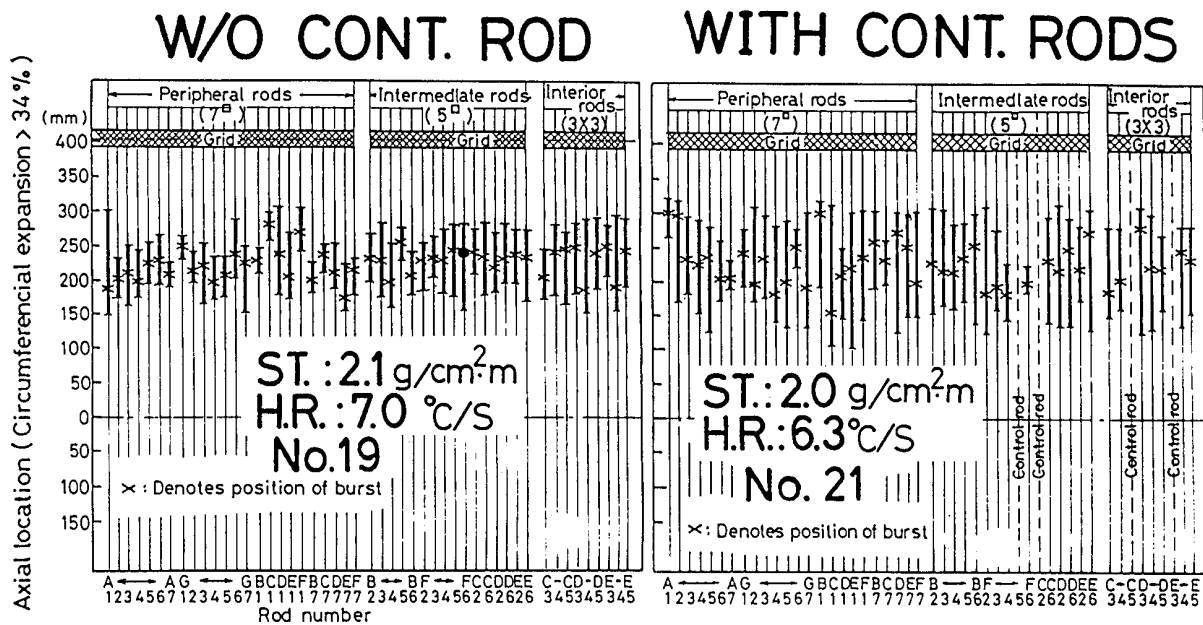


Figure 34: JAERI tests - axial locations of burst position and ballooned region in tests N° 20 and 21.

- There was little effect of the heating rate on the degree and extent of flow blockage: 91% maximum restriction for 1 K/s and 87% for 7 K/s (see figure 35).

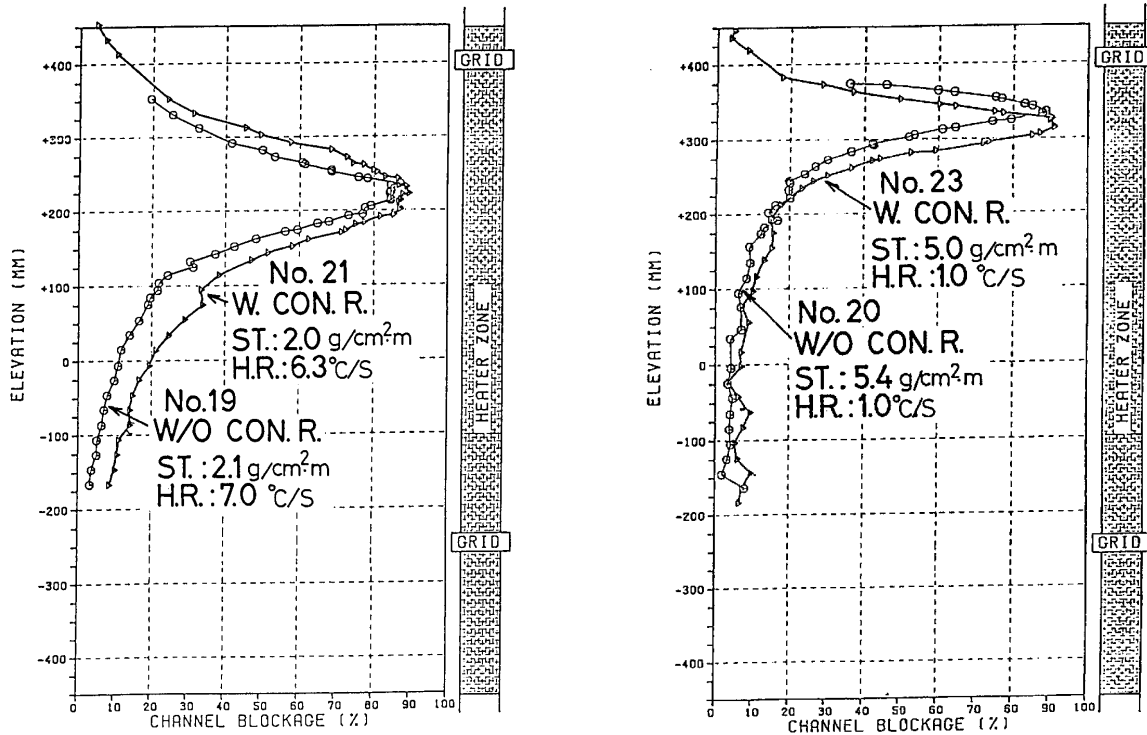


Figure 35: JAERI tests - axial locations of channel blockage in tests 19 and 21, 20 and 23.

In considering the 7 K/s ramp rate as more realistic and by limiting the cross-sectional area of a ruptured cladding to that of a circumference of the same length as the clad length at rupture, the authors evaluated a more realistic upper bound of flow restriction near 80%^[17]. However, it should be pointed out that local flow blockage ratios higher than 95% were determined in the area of maximum flow restriction in test 24 under a heating rate of 7 K/s (see figure 36).

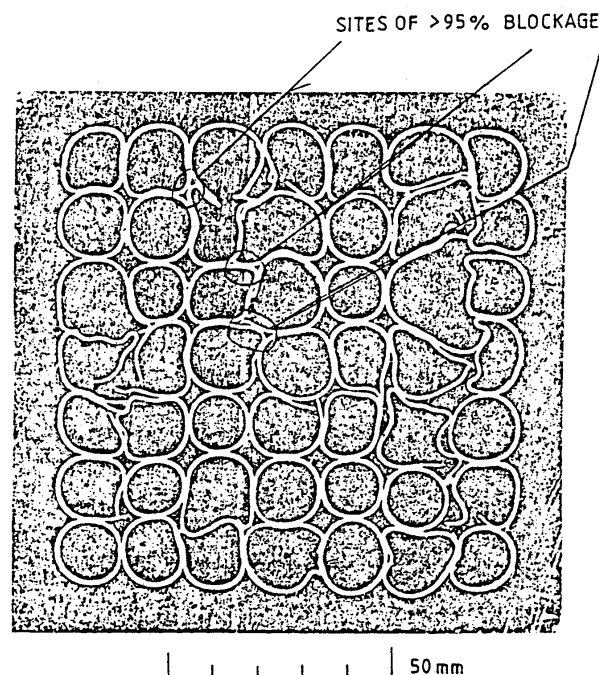


Figure 36: JAERI tests - cross-section of maximum blockage in test 24.

3.2.3.4 Conclusions on JAERI multi-rod tests

The JAERI multi-rod tests, carried out under thermohydraulic conditions similar to those in MRBT tests B3 and B5, show results consistent with those of the MRBT tests. The common feature of all these tests was the axial extension of the deformation that developed after contact without rupture between adjacent rods.

The important result provided by JAERI multi-rod tests concerns the influence of the presence of control rod guide tubes: in most cases, not only is the deformation on rods adjacent to a guide tube not lower than on other rods, despite the azimuthal temperature gradients induced by the cold guide tube, but the flow blockage ratio in the bundle section is even slightly increased and was axially more extended. This surprising result supports the REBEKA-4 test results (carried out however in more favorable thermohydraulic conditions) and can be explained by the effect of the mechanical interaction between a rod and an adjacent guide tube: due to the larger diameter of the latter, the contact of a deforming neighboring rod occurs with a moderate strain (~ 20%), before burst. This early contact leads to the transfer of straining onto other portions of the rod circumference, which homogenizes the azimuthal temperature field, then leading to the axial extension of the deformation.

To summarize, it appears that the mechanical interactions between rods in a rod bundle, more particularly with a guide tube, can lead to an increase in the burst strains and the flow blockage:

- On one hand as a result of a mechanical interruption of the "hot side straight effect" process (the effect of which on the limitation of burst strain was demonstrated in single rod tests),
- On the other hand, as a result of the re-homogenizing of the azimuthal temperature distribution.

It may thus be concluded that, under conditions conducive to significant mechanical interactions between rods, the spatial distribution of burst strains and the resulting flow blockage will not be realistically evaluated on the basis of single rod tests alone.

4 REVIEW OF IN-PILE TESTS PROGRAMS

4.1 Single rod tests

4.1.1 PBF-LOC tests

A series of four transient tests simulating a large break LOCA was carried out in the Power Burst Facility (PBF) reactor at INEL^[18,19]. The common objective of these tests was to investigate the effects of the rod internal pressure and the initial fuel burnup on clad deformation, as well as to provide data to be compared with existing out-of-pile test results, particularly ORNL experimental results discussed in § 3.1.3.

4.1.1.1 Common Characteristics

In each PBF LOC test, four 15x15 type PWR rods with an active length of 0.91 m, each contained in a separated unheated shroud, were simultaneously submitted to the same thermohydraulic conditions existing in the test section (see Fig. 37). Two rods were internally pressurized to values representative of PWR rods at start of life while the two others were pressurized to values representative of high burnup rods. One of each type of pressurized rods was a fresh fuel rod while the other rod had been previously irradiated in the Saxton reactor (PWR) to burnups ranging from 10 to 16 GWd/t. This moderate pre-irradiation did not cause the fuel-clad gap to close completely and resulted in a limited oxidation and hydriding of the cladding material.

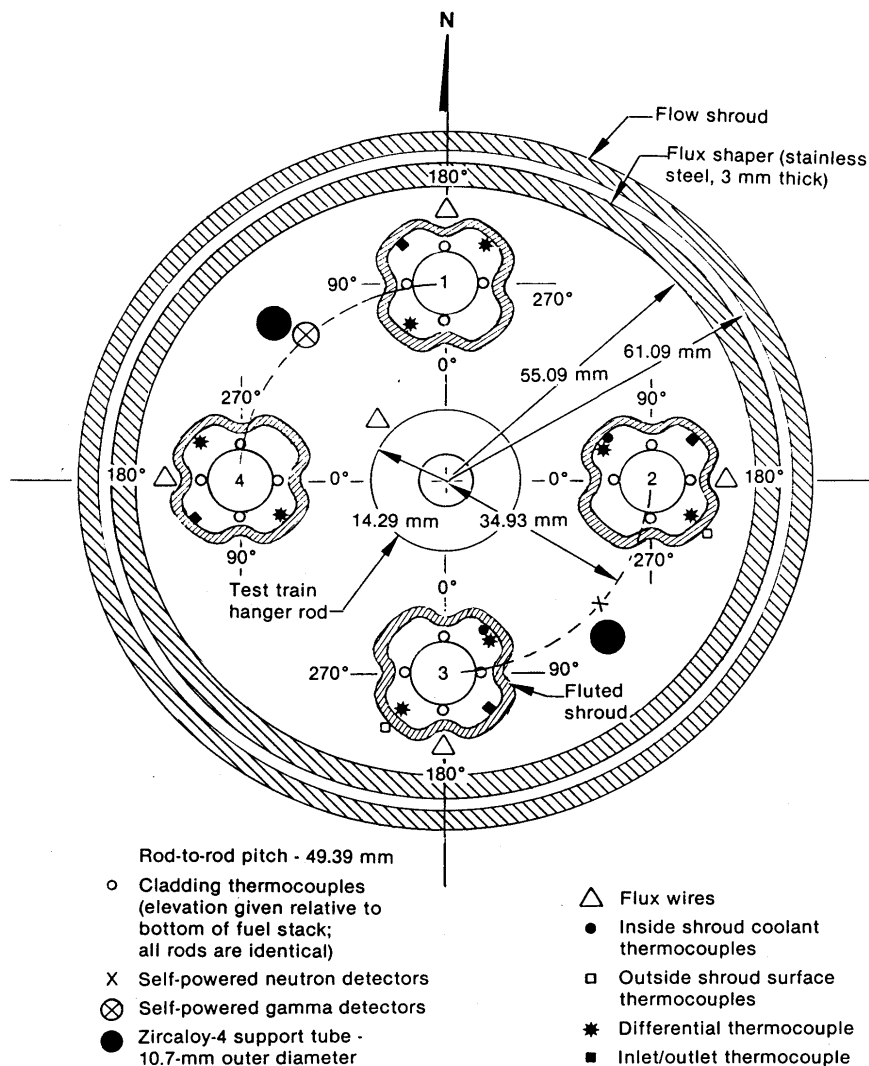


Figure 37: PBF LOCA fuel train orientation.

The test transient started from a steady-state regime under water at nominal conditions: 320°C, 15.2 Mpa, 450 W/cm lineic heat rate. After isolating the test section from the PBF circuit, a valve opening led to a blowdown representative of a cold leg large break LOCA. The nuclear power - with the axial profile flattened in the centre third of the active fuel length in order to simulate the conditions of a PWR rod at mid height - was monitored so as to reach and maintain the test's target temperature:

- Test LOC-6: 1070 K (800°C): maximum ductility in α phase,
- Test LOC-3: 1190 K (920°C): minimum ductility in $\alpha+\beta$ phase,
- Test LOC-5: 1350 K (1080°C): maximum ductility in β phase.

The heating rate of the different rods in a same test was variable, depending on the initial stored energy and the fuel/clad heat transfer. After having maintained the plateau temperature for a sufficient duration so as to reach rod rupture, the test was terminated by water quenching. As an example, figure 38 shows the variations in temperature, internal pressure and axial elongation on rod 11 from the LOC-6 test.

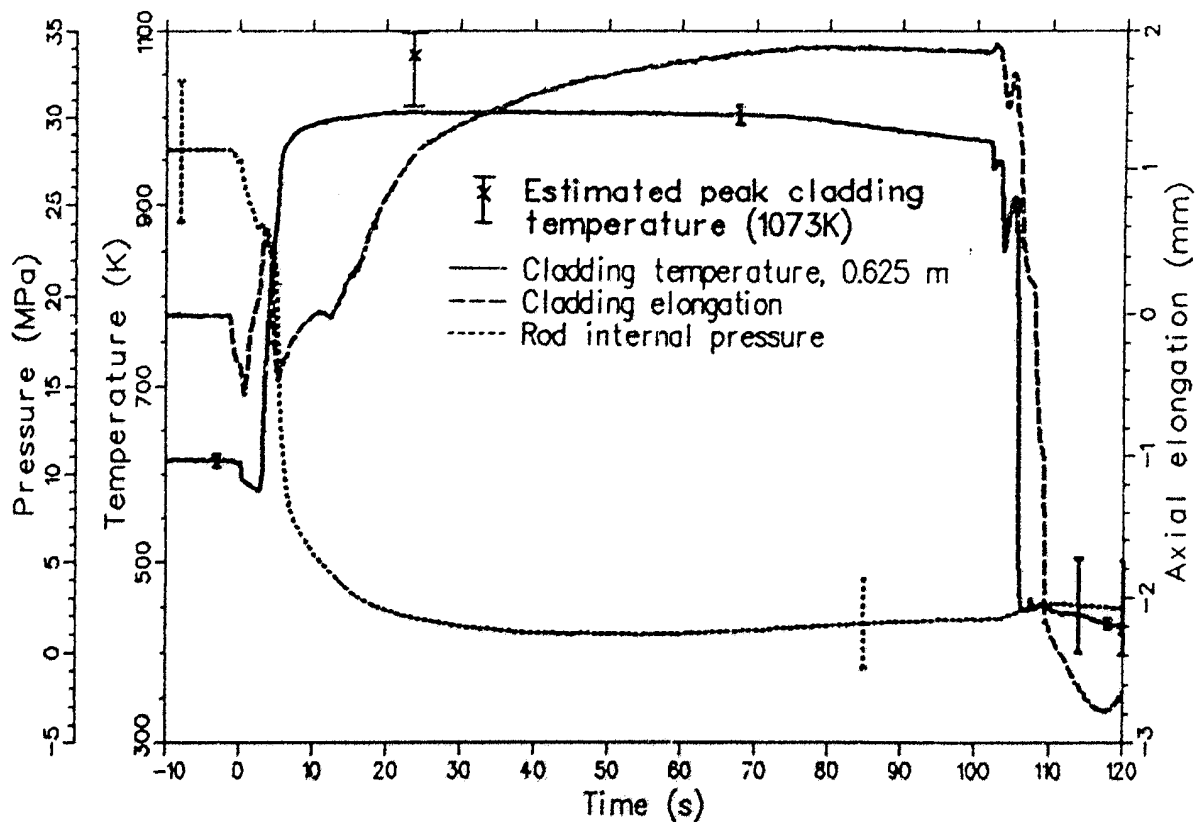


Figure 38: PBF LOC - thermal and mechanical response of Rod11 during test LOC-6.

From the 3 tests with usable results (LOC-3, LOC-5 and LOC-6), 13 rods were tested, with test LOC-5 having required two re-runs (5B defective, then 5C). Table 3 summarizes the initial conditions and cladding deformation results of the 11 usable rods, among which the 2 low pressure rods from LOC-6 test did not fail.

Test	Rod Number	Initial Pressure (Mpa)	Burnup (MWd/t)	Maximum Circumferential Elongation (%)	Axial Extent Of Deformation > 5% (m)	Location of Cladding Failure (m)	Failure Time (s)	Cladding Burst Temperature ^a (K)	Heating Rate ^b (K/s)	Burst Pressure (Mpa)
LOC-3	1	2.45	0	29	0.2 to 0.6	0.257	15.0	1140 to 1200 (1190)	4.3	1.6
	2	2.38	15960	40	0.5 to 0.6	0.543	7.9	1300 to 1350 (1300)	20.0	1.0
	3	4.92	0	20	0.15 to 0.6	0.244	10.1	1105 to 1130 (1110)	15.0	5.1
	4	4.75	16620	41.6	0.10 to 0.65	0.320	13.1	1110 to 1140 (1120)	15.0	4.8
LOC-5	6	2.41	17660	35	0.13 to 0.65	0.507	10.5	1300 to 1400 (1350)	0	0.6
	7A	4.83	0	19	0.10 to 0.60	0.258	2.75	1130 to 1230 (1160)	100.0	3.5
	7B	4.83	0	48	0.10 to 0.60	0.305	7.8	1300 to 1900 (1350)	70.0_	0.7
LOC-6	9	2.41	0	<1	— ^c	— ^c	—	—	—	—
	10	2.41	10800	13.6	0.25 to 0.56	— ^c	—	—	—	—
	11	4.74 ^d	0	31	0.25 to 0.43	0.374	5.2	1010 to 1105 (1098)	100.0	14.0
	12	4.83	10800	74	0.22 to 0.52	0.360	18.2	1010 to 1105 (1066)	0	5.3

- a. Temperatures in parentheses represent the best estimate within the range estimated from the cladding microstructure.
- b. This represents the heating rate from the cladding surface thermocouples at 0.625 m from the bottom of the fuel.
- c. Cladding did not fail.
- d. The initial internal pressure was probably about 12 Mpa, due to a coolant leak and subsequent formation of steam.

Table 3: summary of cladding deformation data from PBF tests LOC-3, LOC-5 and LOC-6.

4.1.1.2 Deformation and rupture behavior

4.1.1.2.1 Deformations of irradiated rods compared with deformations of fresh rods

One main feature of the PBF-LOC facility lies in the possibility to simultaneously test irradiated and fresh rods under identical conditions, with the comparison of deformation data of both types of rods being immediate.

Comparison of post-test data of rods with high initial pressure in LOC-6 and LOC-3 _with rupture occurring respectively in the high α phase and $\alpha+\beta$ phase domains_ reveals:

- A significantly larger maximum circumferential elongation on irradiated rods:
 - LOC3-4 (irradiated): 42% / LOC3-3 (unirradiated): 20%
 - LOC6-12 (irradiated): 74% / LOC6-11 (unirradiated): 31%
- Larger axial extent (see figures 39a and 39b) in the uniform temperature region,
- Wall thinning over the whole circumference of irradiated rods cladding, whereas it appears to mostly affect the azimuthal locations near rupture on fresh rods (see figures 40a and 40b).

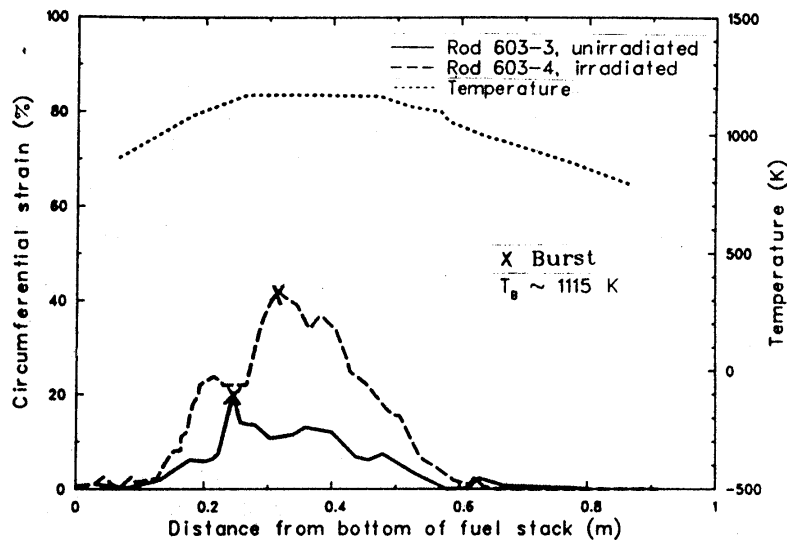


Figure 39a: PBF-LOC-3 - comparison of the axial profiles of cladding circumferential strain on the high pressure fresh and irradiated rods (Rods 3 and 4) that burst in the alpha-plus-beta transition.

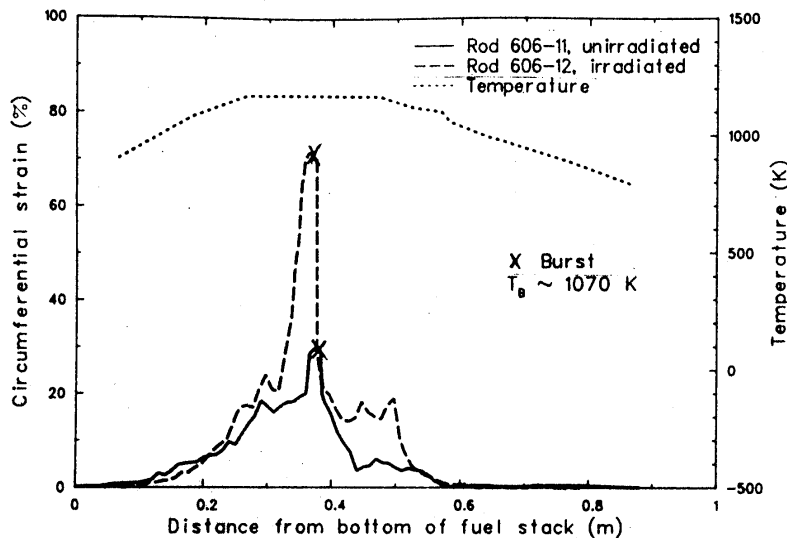


Figure 39b: PBF-LOC-6 - comparison of the axial profiles of cladding circumferential strain on the high pressure fresh and irradiated rods (Rods 11 and 12) that burst in the alpha phase.

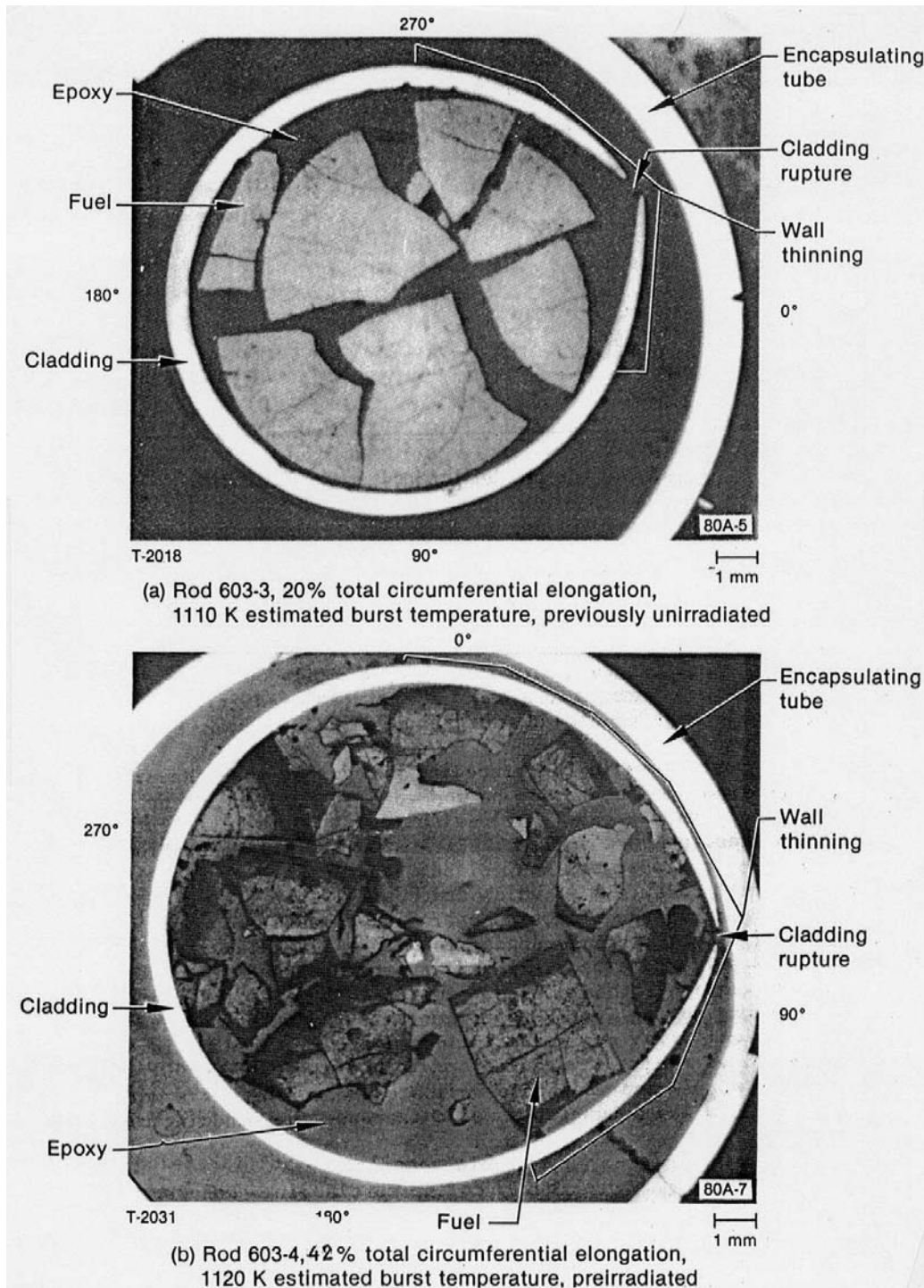


Figure 40: PBF-LOC-3 - cladding cross sections at the burst on the high pressure fresh and irradiated rods.

These differences may be attributed to the circumferential temperature distribution that was initially homogenized on irradiated rods due to the reduction in the pellet/clad gap as a result of the combined action of fuel growth & rearrangement and clad creepdown during irradiation. This effect was confirmed in test LOC-5 with the comparison of deformations on rods 7A and 7B: the former ballooned and ruptured during transient LOC-5A ($\epsilon = 19\%$), while the latter experienced clad collapse onto the fuel during the defective transient LOC-5B (reduced flow without depressurization) and underwent deformation during transient LOC-5C (almost identical to LOC-5A) under closed gap conditions until rupture with 48% circumferential elongation. Figure 41 gives the axial profile of the circumferential strain for these two rods, showing a narrow balloon near the 0.2 m elevation on the lower part of rod 7B, which was attributed to a local hot spot at the beginning of clad ballooning.

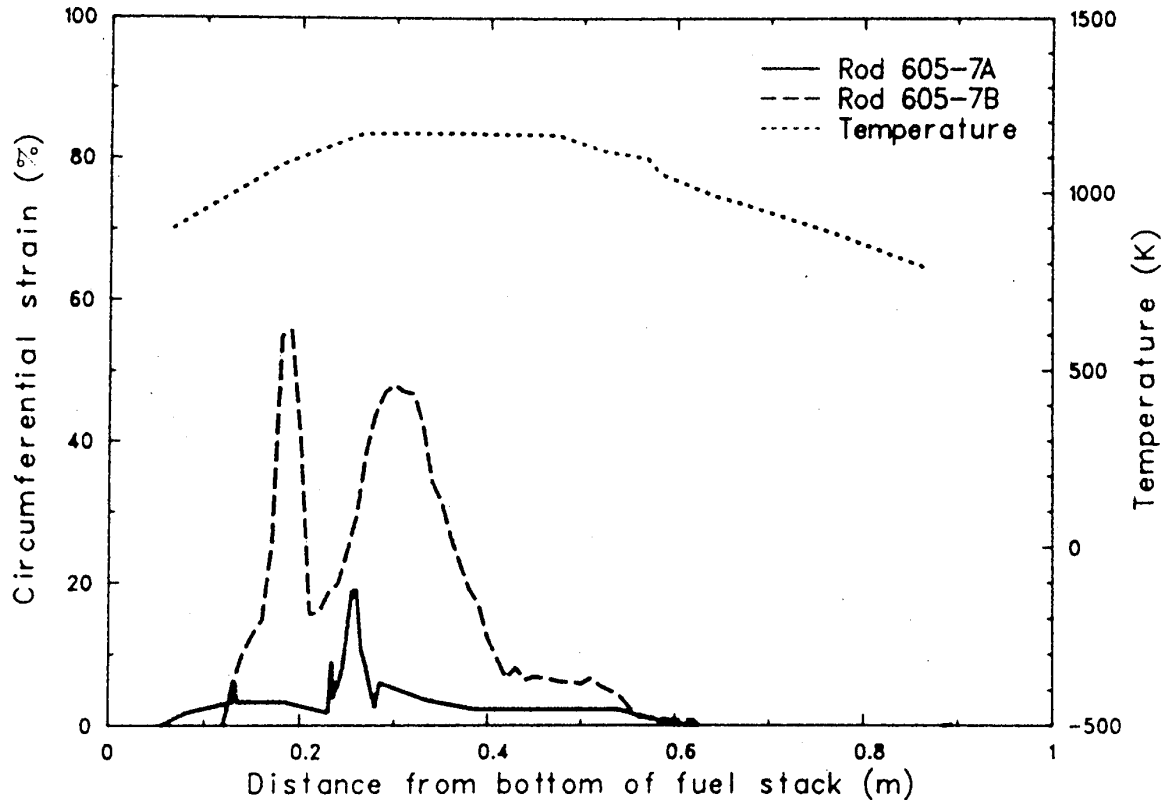


Figure 41: PBF-LOC-5 - comparison of the axial profiles of cladding circumferential strain on the unirradiated high pressure rods 7A and 7B with initially undeformed and collapsed cladding.

Direct comparison of irradiated/unirradiated strain data for deformations in the β phase domain was not possible for test LOC-5 because the available rods, 6 (irradiated) and 7A/7B were initially pressurized at very different levels (2.4 and 4.8 MPa respectively).

4.1.1.2.2 Analysis of deformation on rod LOC-6/11

Concerning the LOC-6/11 rod (unirradiated, high initial pressure = 4.74 MPa), the internal pressure during pre-transient phase should have been near 14 MPa but was in fact measured at 28 MPa. This overpressure was attributed to the flashing of a small quantity of liquid water that would have entered the rod through micro-fissures in the cladding wall.

Due to this high initial pressure, Rod 11 ruptured at 5.2 seconds, which was much earlier than the twin irradiated rod (Rod 12) at 18.2 seconds. This possibly calls into question the validity of a direct comparison of the deformations obtained on these two rods.

Analysis of the deformations on Rods 11 and 12 was carried out by EG&G with the FRAP-T6/BALLON-2 code in order to evaluate the influence of the initial internal pressure and azimuthal temperature gradients. Thus, for Rod 11, two calculations were performed with an internal pressure of 13.9 and 29.1 MPa respectively, associated with low initial ΔT_{az} (3 and 2.5 K respectively). The high pressure case led to early rupture at 4.4 seconds with 38.2% total elongation, corresponding well with the measured values. However, the low pressure case (pressure comparable to that of Rod 12) led to rupture at 22.5 seconds with 65.9% total elongation, which is somewhat comparable to the measured values for the irradiated Rod 12. It should not however be concluded that the LOC-6 test results were not reliable and that the behavior of the irradiated Rod 12 did not differ from that of the fresh Rod 11 just because the extrapolation at low pressure of the deformation of the latter was close to that of the former.

It must thus be pointed out that the LOC-3/3 rod (unirradiated, high initial pressure = 4.9 MPa) ruptured at a temperature close to that of LOC-6/11 rod (1100 K and 1098 K respectively, thus in the low $\alpha+\beta$ domain). However, despite both an initial pressure and temperature ramp during straining that were lower than that for the LOC-6/11 rod (see table 3), the LOC-3/3 rod showed low

elongation (20%) and a non-uniform clad thickness at rupture (see figure 40a), which indicates a large azimuthal temperature difference that developed during straining. It may thus be thought that, even with a low initial ΔT_{az} , the LOC-6/11 rod with its originally expected pressure (~ to the LOC-3/3 pressure) would have developed a sufficient ΔT_{az} during straining to limit its burst elongation to a moderate level, close to that obtained with the initial overpressure.

4.1.1.2.3 Comparison with ORNL-MRBT results

The PBF-LOC test results were compared by their authors with available out-of-pile test results, in particular ORNL single rod and multi-rod test results.

Figure 42 plots the burst strain versus burst temperature for the 9 ruptured PBF-LOC rods, in comparison with the trends derived from single rod ORNL tests:

- Dotted line: non heated shroud tests + heated shroud tests with heatup rate > 25 K/s, for $T_{burst} < 1250$ K;
- Dashed line: heated shroud tests with heatup rate from 5 to 15 K/s;
- Solid line: heated shroud tests with heatup rate from 0 to 5 K/s.

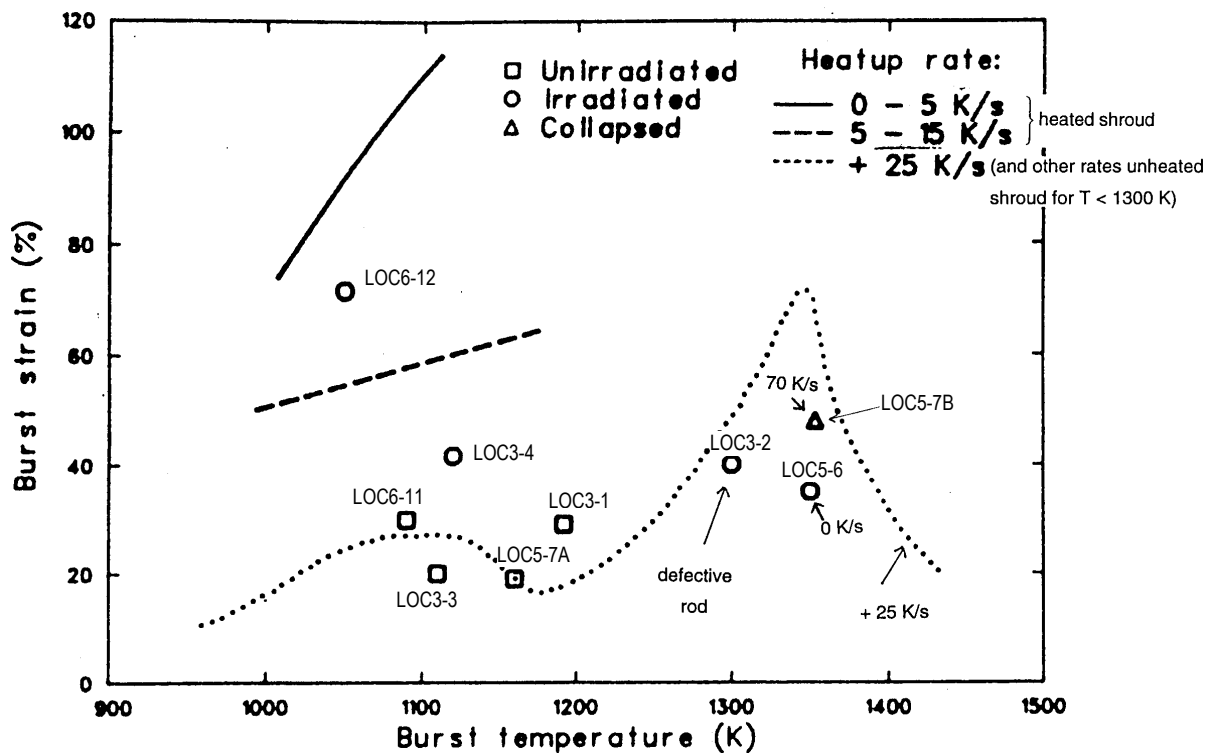


Figure 42: comparison of ORNL single-rod burst tests with PBF-LOC burst tests.

It appears that the deformations of the PBF unirradiated rods are consistent with ORNL unheated shroud test results. For irradiated rods, Rods 4 and 12 (high internal pressure) exhibit burst strain that are significantly higher than that for ORNL single rod unheated shroud tests, being more similar to that for single rod heated shroud tests with a low heatup rate. Results of the PBF irradiated rods LOC-3/2 & LOC-5/6 that ruptured in the β phase domain cannot be used for comparison with ORNL trends:

- LOC-3/2 experienced localized straining at 0.543 m level on a very hot spot resulting from an over-storage of energy during the pre-transient phase in a region where the fuel was fragmented and widely spaced from the cladding;
- LOC-5/6 ruptured during a temperature plateau and cannot be compared with the ORNL curve that shows a peak in burst strain at a neighboring temperature, since this curve results from ramp tests > 25 K/s; however, the deformation of the LOC-5/6 rod is higher than the value indicated at the same temperature by the "low ramp" curve in NUREG-630.

Comparison of the axial profiles of cladding circumferential strain in PBF-LOC and ORNL single rod tests proves that the behavior of PBF unirradiated rods is similar to that of ORNL single rods with an unheated shroud, whereas the behavior of PBF irradiated rods is more similar to that of ORNL single rods with a heated shroud, as shown in figures 43A and 43B.

In the same way figure 43A shows that, despite a high initial internal pressure, the unirradiated rod LOC-6/11 behaves similarly to the ORNL SR-5 rod ($P_{burst} = 9.6$ MPa, $T_{burst} = 1083$ K, $\epsilon_{burst} = 26\%$); the ORNL tests SR-28 and SR-29, under neighboring conditions exhibit identical burst strain. Under pressure and temperature conditions similar to those of rod LOC-6/12 ($P_{burst} = 5.3$ MPa, $T_{burst} = 1066$ K), the ORNL tests SR-33 to SR-36 (unheated shroud, very low temperature ramp) show burst strain in the 23% to 32% range: this is the burst strain level that could be expected for the LOC-6/11 rod with the initial pressure of the LOC-6/12 rod, thus coming close to the value measured (31%) with the initial overpressure. The comparison of results from LOC-6/11 and LOC-6/12 rods therefore remains possible.

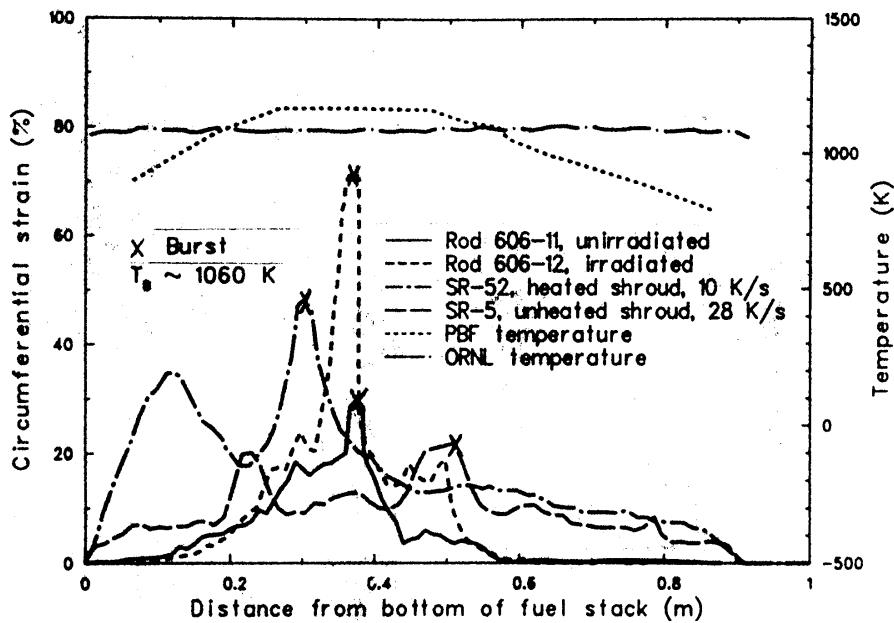


Figure 43A: PBF-LOC - comparison of the axial profiles of cladding circumferential strain between PBF and ORNL single-rod tests which burst in the alpha-phase.

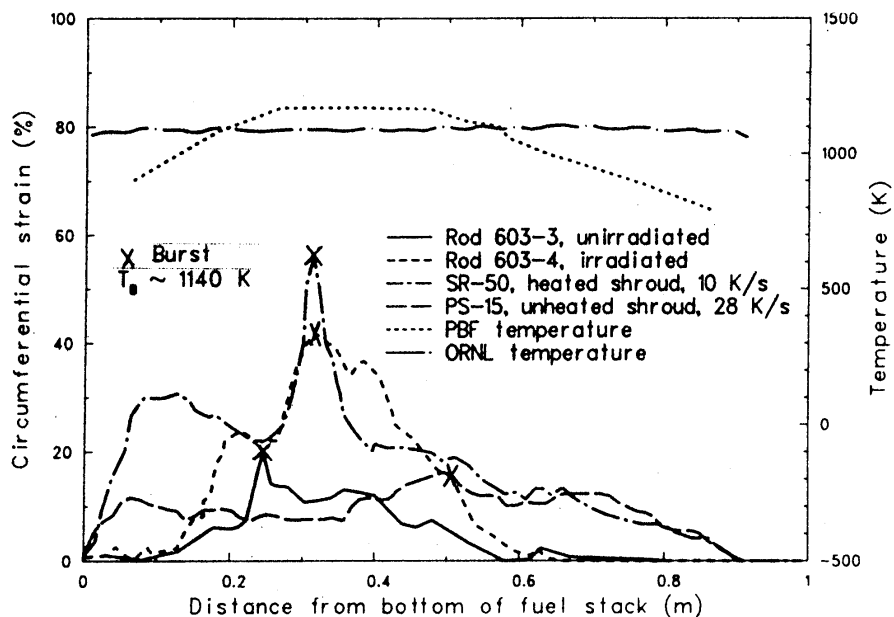


Figure 43B: PBF-LOC - comparison of the axial profiles of cladding circumferential strain between PBF and ORNL single-rod tests which burst in the alpha+beta transition.

4.1.1.3 Fuel behavior

Although the clad ballooning behavior and resulting flow blockage are not directly influenced by the fuel column behavior, it is interesting to report the observations relative to the fuel behavior in the PBF-LOC tests, insofar as this behavior can influence the subsequent evolution of the LOCA transient.

During the initial irradiation in the Saxton reactor, the fuel of the PBF-LOC pre-irradiated rods underwent an initial fragmentation and rearrangement, the latter resulting in an azimuthal homogenizing of the clad temperature. Thus, it was not surprising to observe significant fuel relocation in the balloons of the irradiated rods after the test, as shown in figure 44 by the neutron radiograph of the LOC-6/12 rod. In this figure, the visual aspect of the fuel segment located between the elevations 76 cm and 86 cm shows an irregular outer edge with some voids. It has been suggested by the PBF experimentalists that fuel displacement in this region would have occurred during the rod post-test handling and shipping.

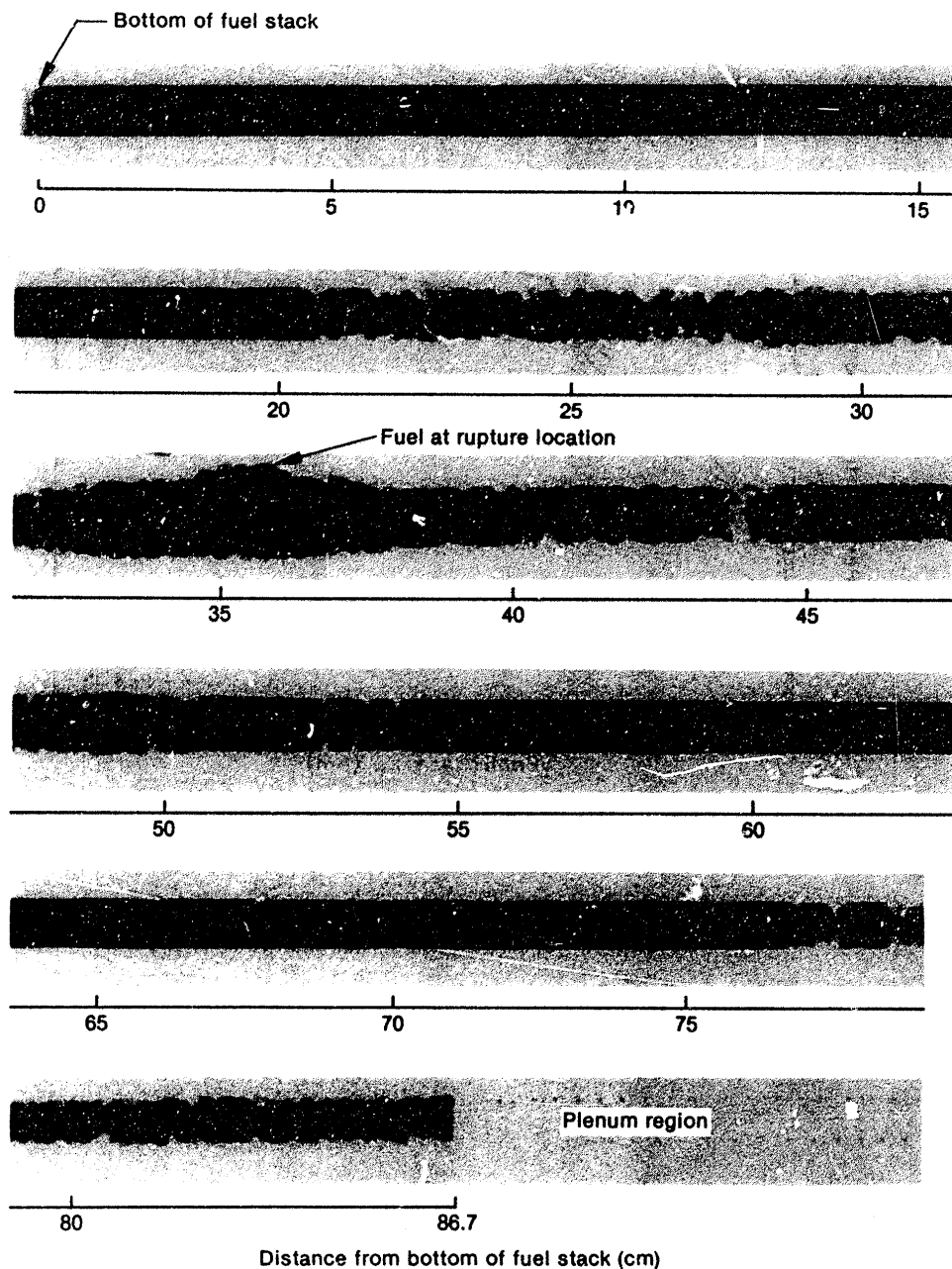


Figure 44: PBF-LOC - post-test neutron radiograph of Rod 12 (test LOC-6).

In the same way for the LOC-3/4 rod, the axial gamma scan (see figure 45) shows fuel relocation between two voided regions, with the lower voiding around the elevation 0.15 m having been attributed to fuel displacement during handling and shipping to hot cells; for the remaining, fuel relocation has been supposed to occur during the test transient, the instant of which was not specified with respect to rod bursting.

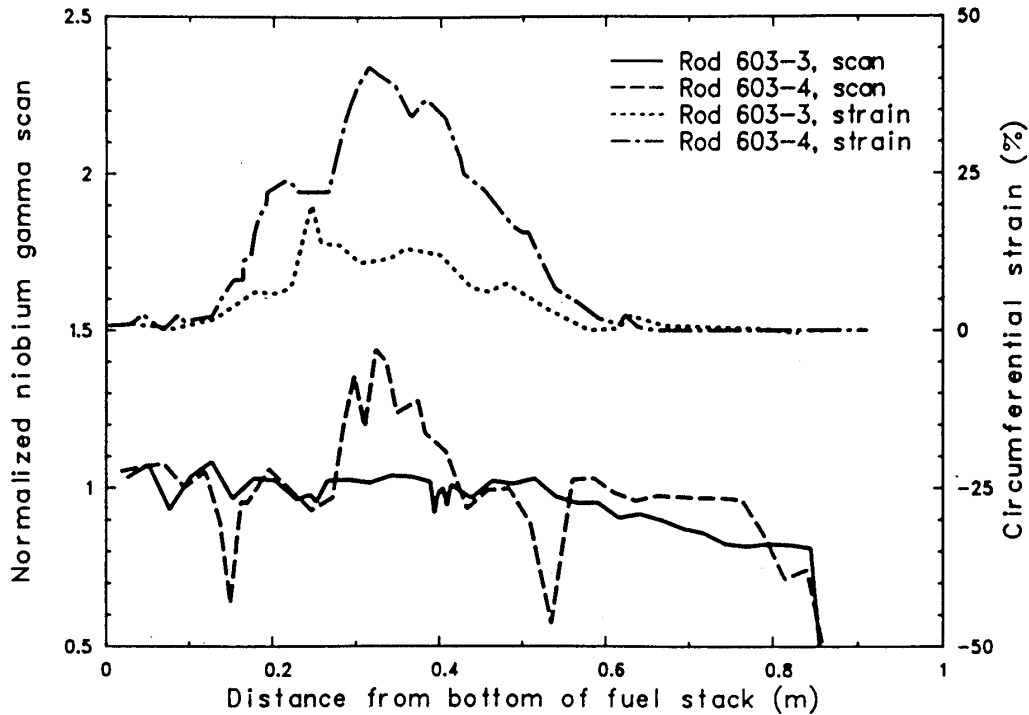


Figure 45: PBF-LOC - axial profiles of the normalized spectral gamma scans of Rods 3 and 4 (test LOC-3).

Fuel relocation with large fuel fragments also occurred on Rod 7B of the LOC-5 test (see figure 46), in the large balloon ($\epsilon_{burst} = 48\%$) that resulted from the particular conditions experienced by this rod (see § 4.1.1.2.1), demonstrating that the rod pre-conditioning (at 450 W/cm) before transient testing was sufficient to induce fuel fragmentation.

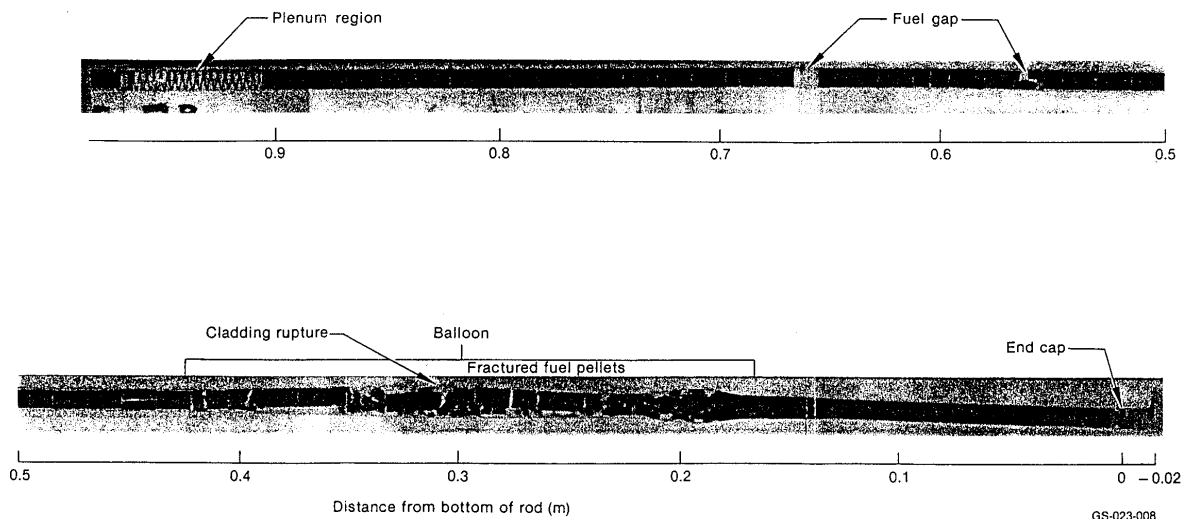


Figure 46: PBF-LOC - post-test neutron radiograph of Rod 7B (test LOC-5).

Based on the estimates of the volume of relocated fuel in the rods from tests LOC-3 and LOC-5, the PBF experimentalists evaluated the average relative fuel volume increase to 60% of the relative clad internal volume increase in the ballooned region.

4.1.2 FR2 tests

A total of 47 single rod tests were performed in the FR2 reactor at KfK^[20], aiming at providing a database of results to be compared with the REBEKA single rod tests, in view to evaluate the possible influence of a reactor environment on the behavior of a fuel rod with fresh and irradiated fuel under LOCA transient conditions.

These tests are grouped into several series using either fuel rods (fresh or irradiated fuel from 2.5 to 35 GWd/tU) or REBEKA electric simulators. The test matrix, summarized in Table 4, specifies the 25 tests performed with irradiated fuel, including 10 tests with 35 GWd/tU fuel.

Test Type	Test Series	Number of Irradiated Rods	Number of Tests	Target Burnup (GWd/tU)	Range of Internal Pressure at Steady State Temperature (bar)
Calibration, Scoping	A	-	5	-	25 - 100
Unirradiated Rods (main parameter: internal pressure)	B	-	9	0	55 - 90
Irradiated Rods (main parameter: burnup)	C	6	5	2.5	25 - 110
	E	6	5	8	25 - 120
	F	6	5	20	45 - 85
	G1	6	5	35	50 - 90
	G2/G3	6	5	35	60 - 125
Electrically-Heated Fuel Rod Simulators (main parameter: internal pressure)	BSS	-	8	-	20 - 110

Table 4: test matrix of the FR2 in-pile tests on fuel rod behavior.

4.1.2.1 Common Characteristics

The test rod with an active length of 50 cm was similar in type to the German PWR 1300 MWe fuel rod, but with only one plenum (instead of two in the standard German PWR). The pre-irradiation of the fuel rods was carried out in the FR2 reactor itself, but the particular conditions of such irradiation must be underlined here:

- Rod internal pressure: 3 bar at cold conditions,
- Coolant conditions: pressure = 2.4 bar, $T_{inlet} = 60^{\circ}\text{C}$.

These conditions led to low a level of clad corrosion & hydriding, and the weak migration of FP towards the fuel periphery. Moreover, the low coolant pressure prevented the creepdown of clad onto fuel for the most irradiated rods. Finally, it appears that the pre-irradiation consumed the fissile material in the lower part of the fuel column so that, under a nearly flat neutron flux, the axial power peak under transient has been shifted towards the top for the test series F and G with higher initial burnup.

Before the transient, the test rods were re-pressurized with helium, between 2.5 and 12.5 MPa (at 300°C); the internal pressure line made it possible to follow the pressure variations throughout the test transient. The fuel-clad gap, nominally at $190\ \mu\text{m}$, was reduced to $150\ \mu\text{m}$ for the rods both in the G3 series (35 GWd/tU) so as to partially compensate for the lack of irradiation creepdown and in the B3 series (fresh fuel) just for comparison with the G3 series.

The test rod was enclosed in a thin cylindrical unheated shroud with narrow spacing between them.

The experimental sequence that aimed to reproduce the quasi-adiabatic phase of a large break LOCA transient, typically consisted of:

- An initial steady-state under steam at 573 K, 6 MPa;
- The blowdown phase with stopping of the steam flow that led to a temperature rise at 12 K/s on average with neutronic power maintained around 40 W/cm;
- Near 1200 K, the reactor scram leading to the temperature turnover and followed in a given number of tests by a steam quench near 1000 K activated by the re-opening of the steam inlet flow valve.

Figure 47 shows a typical example of the variations in the clad temperatures, where the temperature drop indicated by the TC located in the balloon region corresponds to the rapid clad deformation just before rod burst.

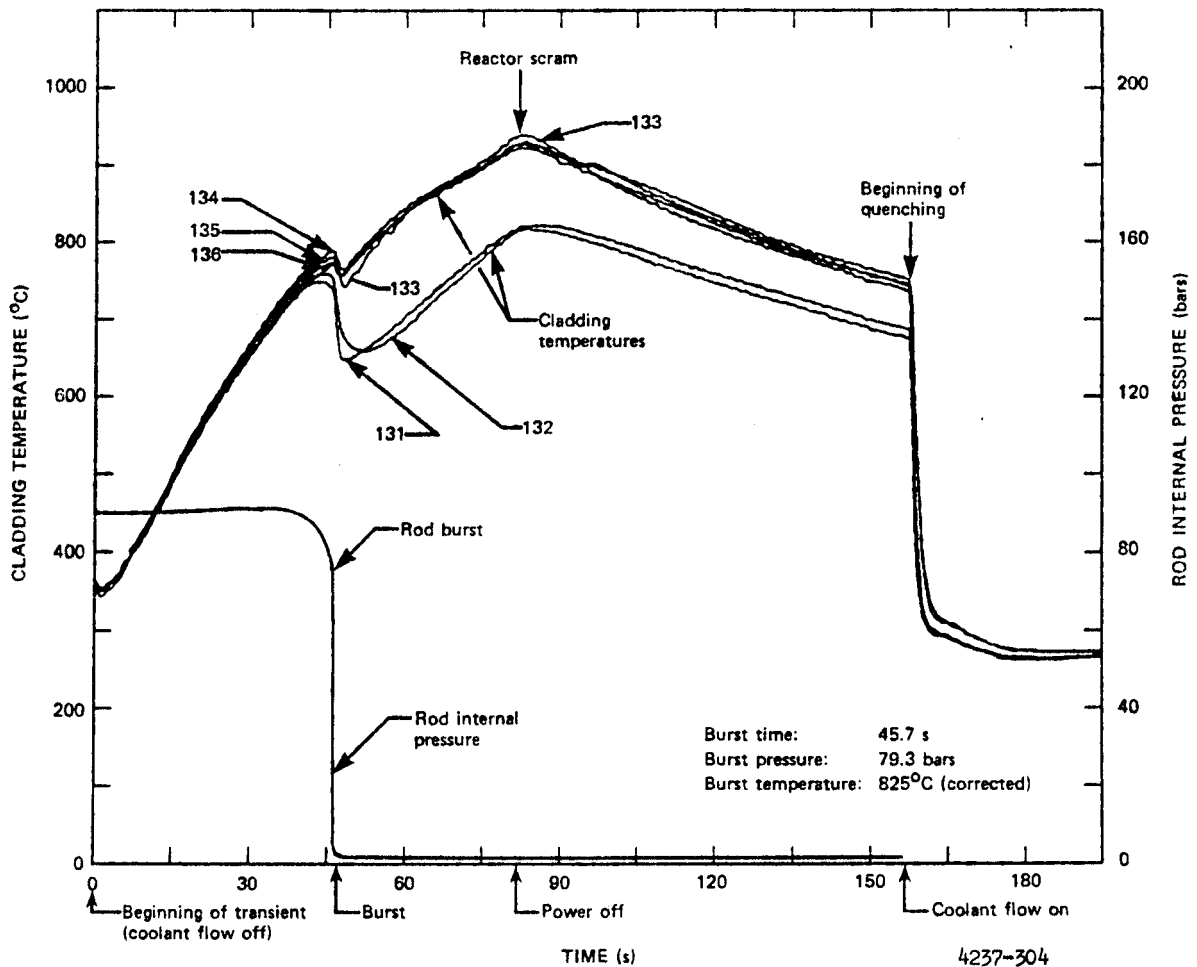


Figure 47: FR2 - typical temperature and pressure histories (measured data from test B3.1)

4.1.2.2 Deformation and rupture behavior

In terms of rupture conditions, the results of the FR2 tests do not reveal any appreciable differences between the behavior of irradiated rods, fresh rods and even of electric simulators. Variations in the burst temperature as a function of the burst pressure lie within the experimental data band obtained from most of the results of similar in-pile and out-of-pile experiments (see figure 48).

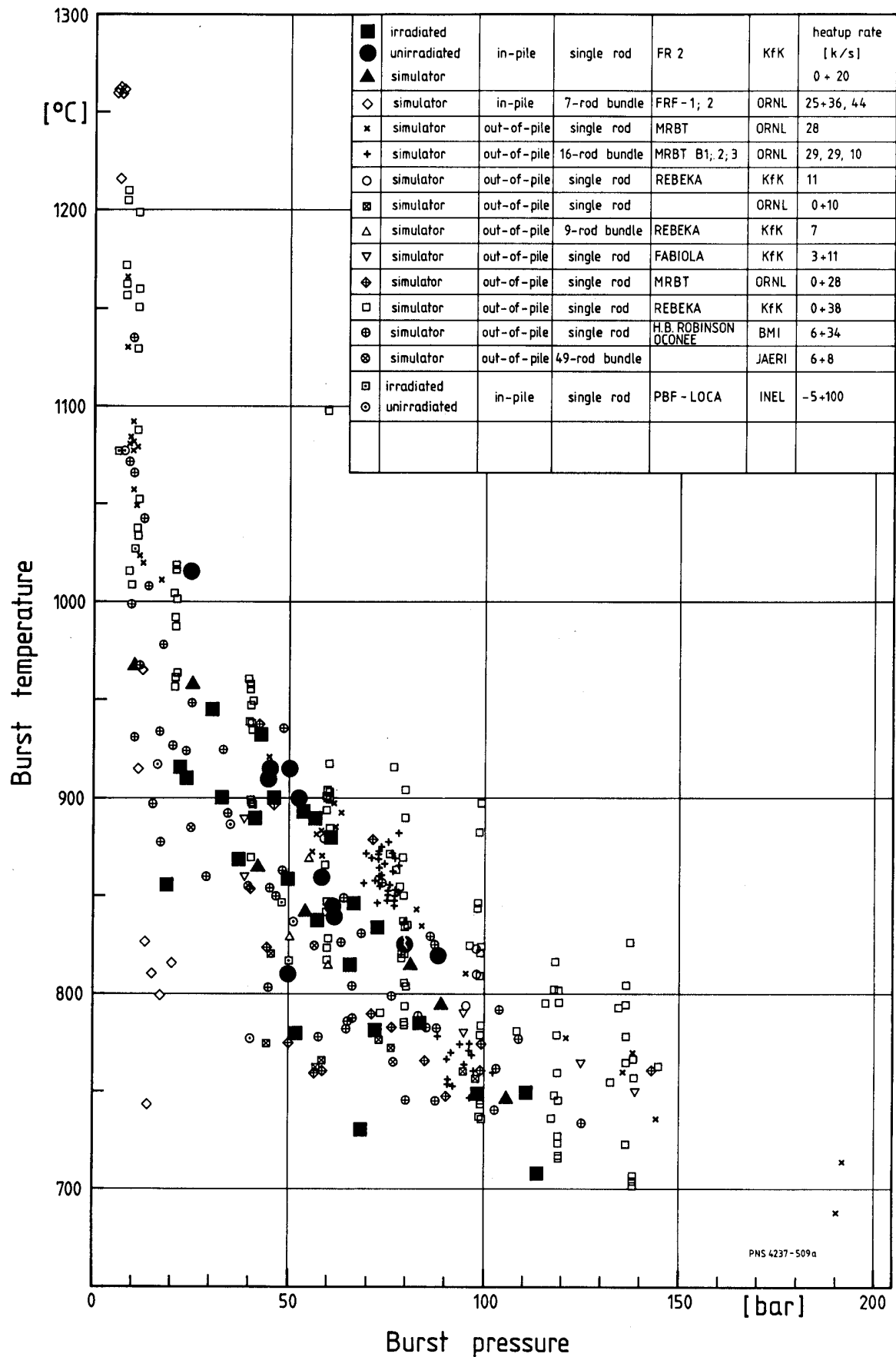


Figure 48: FR2 - burst temperature of Zircaloy tubes from various LOCA-type experiments.

In terms of burst strain, the FR2 results are rather scattered (25 to 67%), which does not highlight any influence of rod irradiation (see figure 49).

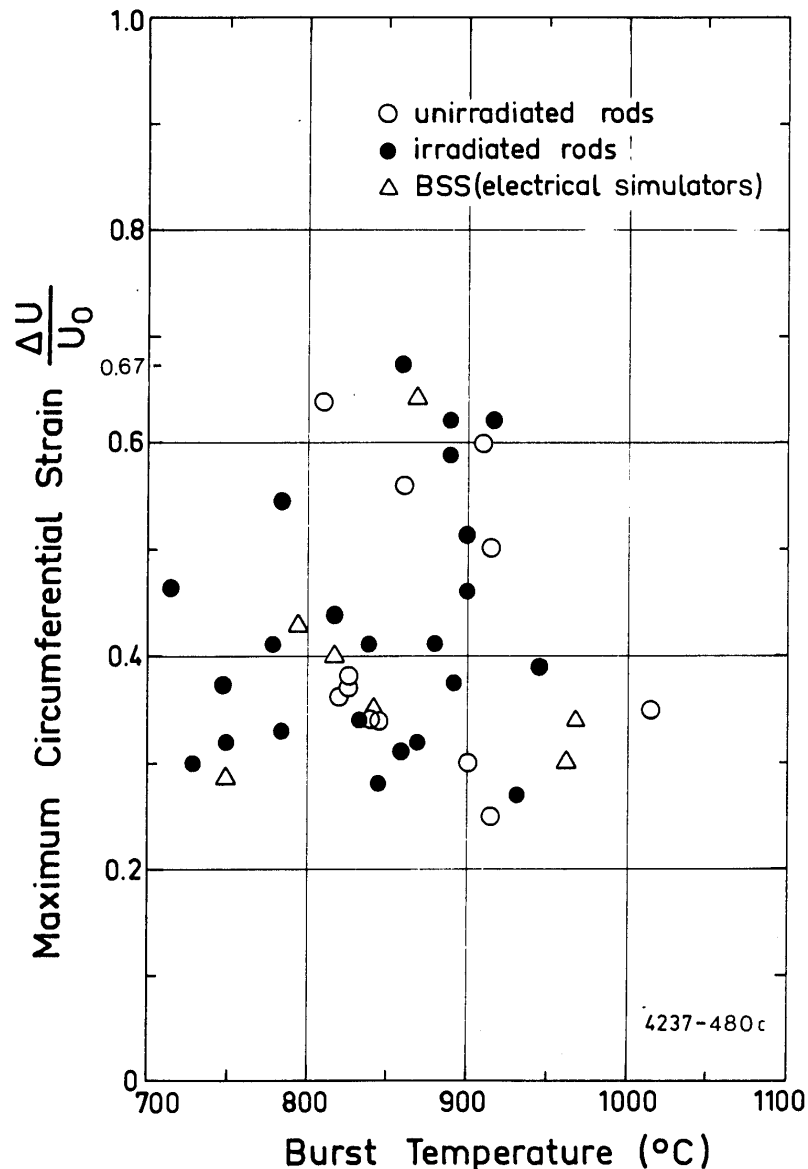


Figure 49: FR2 - maximum circumferential elongation versus burst temperature.

Moreover, in spite of the non heating of the shroud, figure 50 shows that the circumferential strain is quasi-insensitive to the azimuthal temperature difference (which was evaluated based on the microstructure observed in the post-test metallographic examinations), unlike in the REBEKA single rod tests. This behavior may be related to the observed variation in the cladding length during the tests: figure 51 shows an increase in the FR2 rods that ruptured between 750°C and 900°C, whereas the REBEKA and ORNL single rod tests exhibited a cladding shortening due to the anisotropy of Zircaloy in the α domain; this distinctive behavior can possibly be explained by the effect of the axial constraint from the spring, transmitted by the upper fuel pellets which are not bonded to the cladding due to the unclosed gap and the higher power in the upper part of the fuel column. The axial constraint would therefore limit the circumferential strain in tests with low azimuthal ΔT . It was also argued by the PBF-LOC authors [18, Appendix J] that the low inside diameter (18 mm) of the shroud would have caused the cladding to be in complete contact with the shroud's inside circumference, with only 67% total circumferential elongation (TCE) of the clad; thus, when the bubble (cold side) comes into contact with the shroud, the hot-side straight effect is halted, lifting the hot spot off the fuel column, leading to an atypical temperature distribution and stress, which could adversely affect the resultant cladding deformation and rupture.

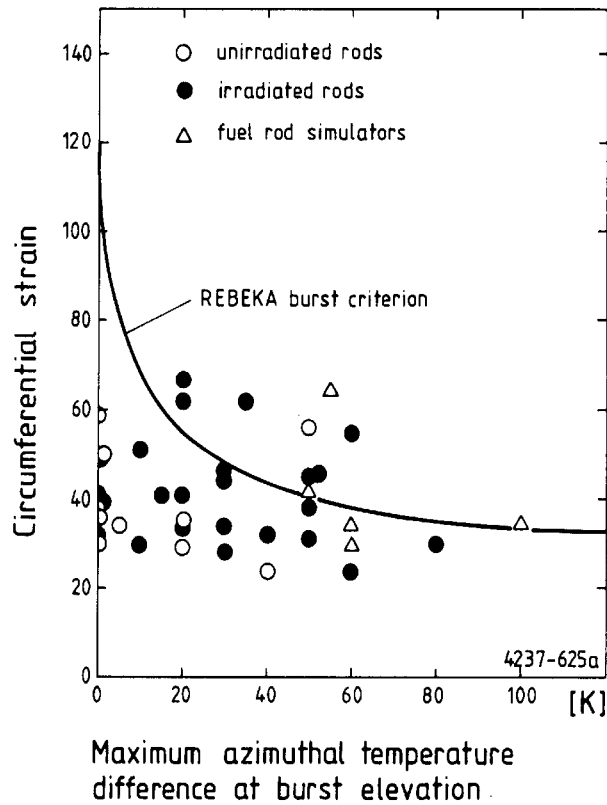


Figure 50: FR2 - local circumferential strain versus maximum azimuthal temperature differences in the rupture region.

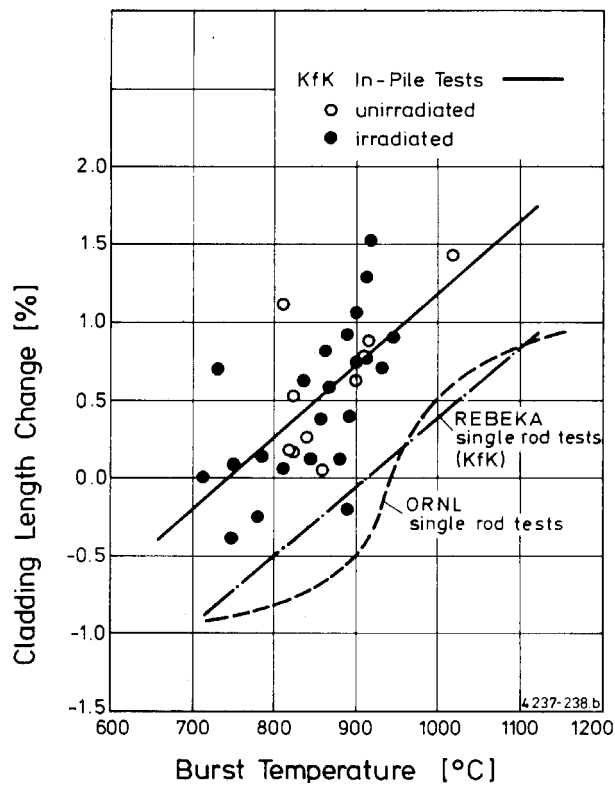


Figure 51: FR2 - cladding length change versus burst temperature.

Figure 52 plots the FR2 test results (burst strain versus burst temperature) in comparison with the database compiled from various other experiments; it appears that the burst strain in the FR2 tests is on average greater than that for single rod tests with an unheated shroud (ORNL: cross symbol, BMI: symbol + within circle), but remains lower than that for single rod tests with a heated shroud (KfK: symbol open square, ORNL: symbol + within diamond). However, on the basis of the preceding remarks about the effects of axial constraints and of the rod-shroud contact, it can be considered that the FR2 data are not representative of unconstrained single-rod deformation and do not provide reliable data on the effect of prior irradiation on clad deformation.

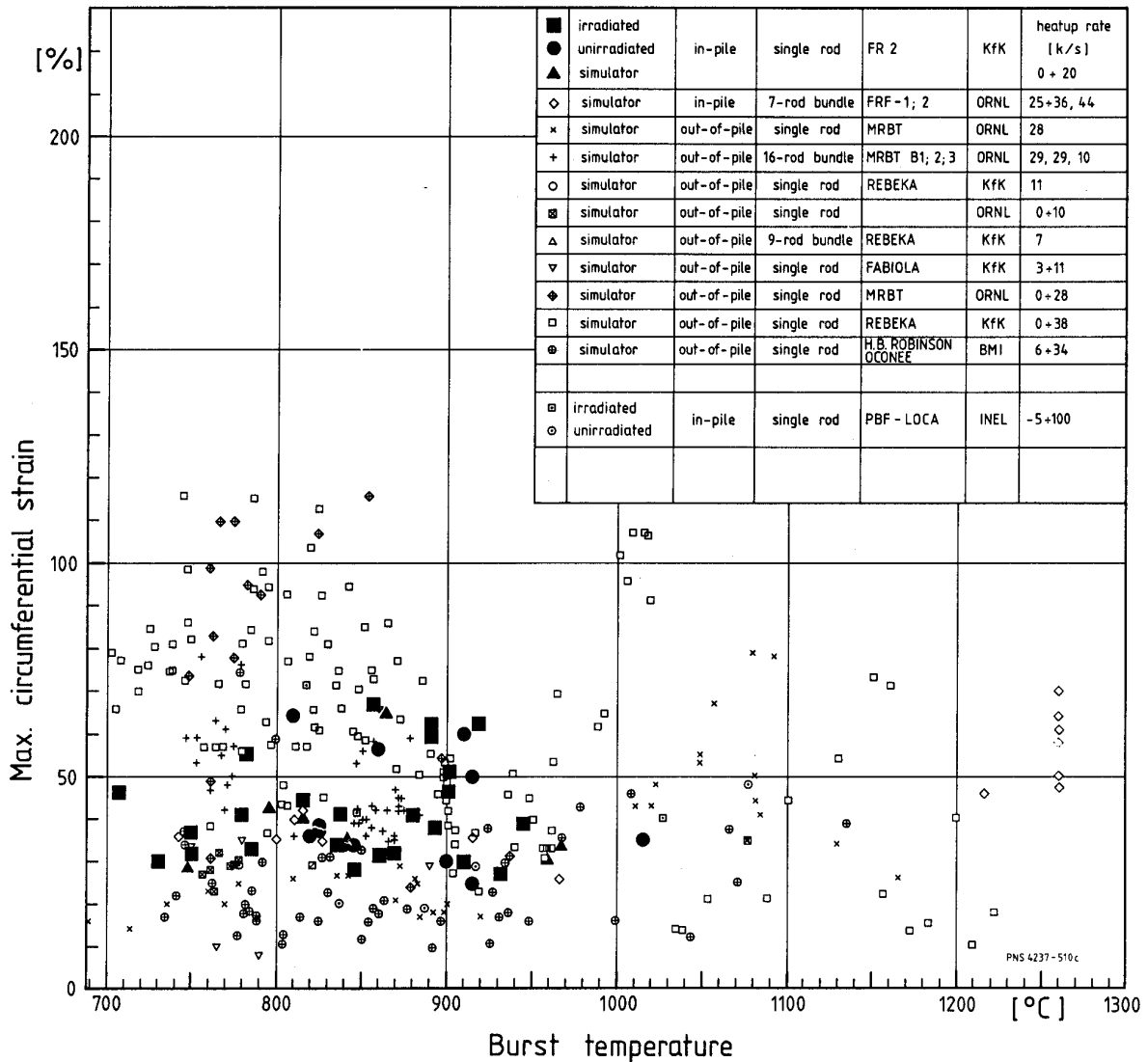


Figure 52: burst strain compiled from various LOCA experiments.

4.1.2.3 Fuel behavior

Actually, the main outcome from FR2 tests more addresses the behavior of the irradiated fuel rather than the cladding behavior, in consideration of the experimental particularities that have influenced the latter.

In a general way, the irradiated fuel appears fragmented after the pre-irradiation phase, regardless of the target burnup (2.5 to 35 GWd/tU). For the reference rods that were irradiated but not tested under a LOCA transient, the fuel fragments generally did not adhere to the cladding; moreover, after the transient, the fuel fragments do seem free to move with respect to each other and with respect to the cladding.

The major observation is that of fuel relocation after the transient for all irradiated rods (series C to G). This can be seen as a settling of the pellet stack, the reduction in height ranging from 3 to 83 mm (see figure 53). Unlike in the PBF-LOC tests, the higher power in the upper part and the unclosed fuel-clad gap during the pre-irradiation phase prevented fuel-clad bonding, so as fuel relocation in the clad balloon could propagate up to the top of the fuel column.

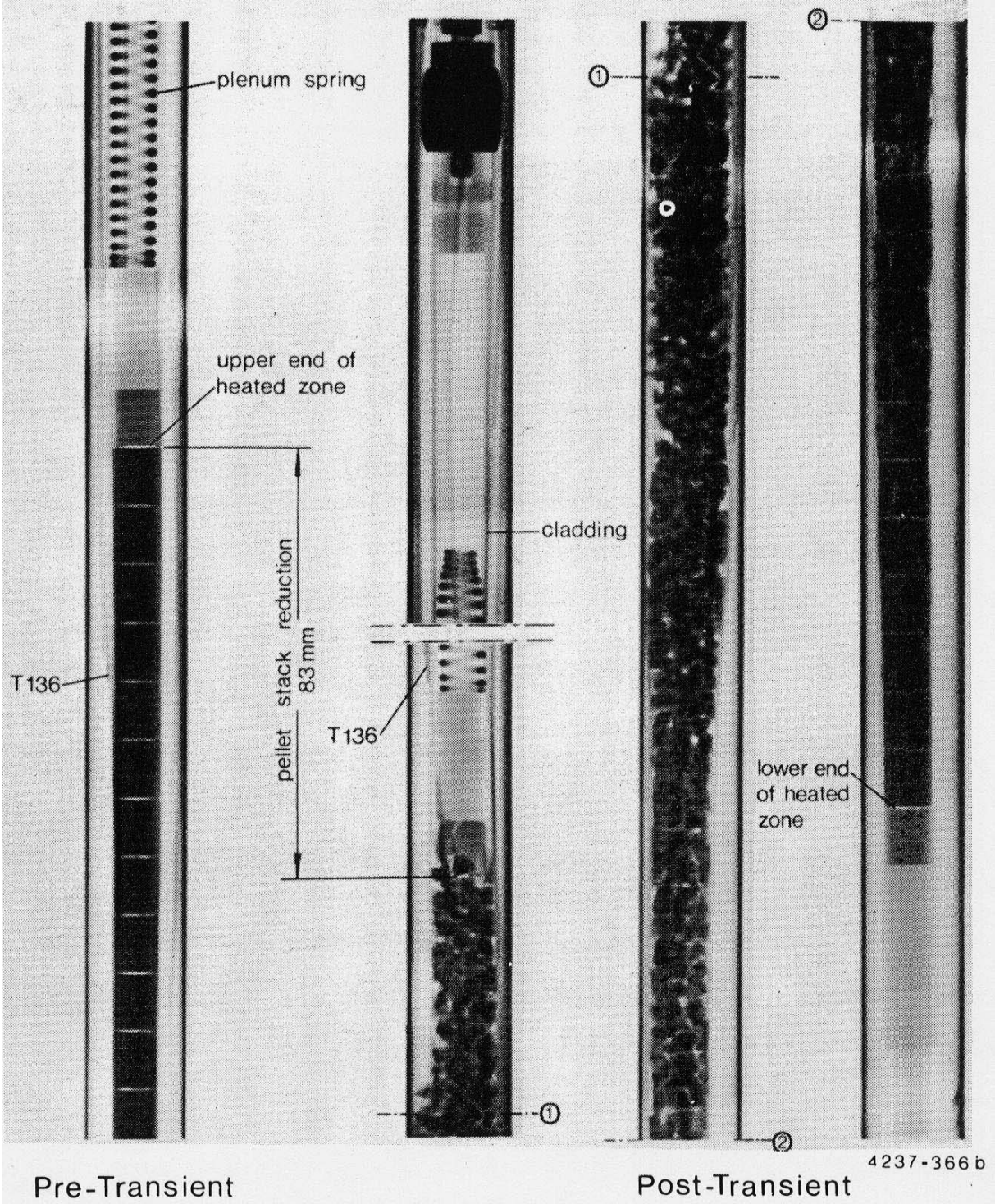


Figure 53: FR2 - neutron radiographs of Rod F1 (burnup 20 GWd/tU). Comparison between pre-transient and post-transient status.

An important issue was then to determine the instant fuel relocation was occurring, with respect to clad burst, in order to ascertain if the fuel relocation was affecting the cladding deformation and rupture. With this in mind, two tests (E3 and E4) were specially instrumented with 3 thermocouples near the top of the fuel stack, in order to detect a loss of fuel indicating the fuel relocation. Figure 54, which shows the temperature variations measured during test E4, clearly reveals a sharp drop in these 3 TC measurements at the time of burst, indicating the relocation of fuel when the cladding ruptured. The measurements for test E3 show a similar behavior. It may therefore be considered that the movement of fuel occurs only at or just after rupture, most likely activated by the push of the gases in the upper plenum, as far as a sufficient free space in the balloon allows the settling of fuel fragments in it. However, it is worth pointing out that in test E5, for which an atypical transient led to large circumferential elongation (67%) without bursting, producing only a flaw in the cladding leading to rod internal depressurization, significant fuel relocation occurred without requiring the driving effect of the plenum gases.

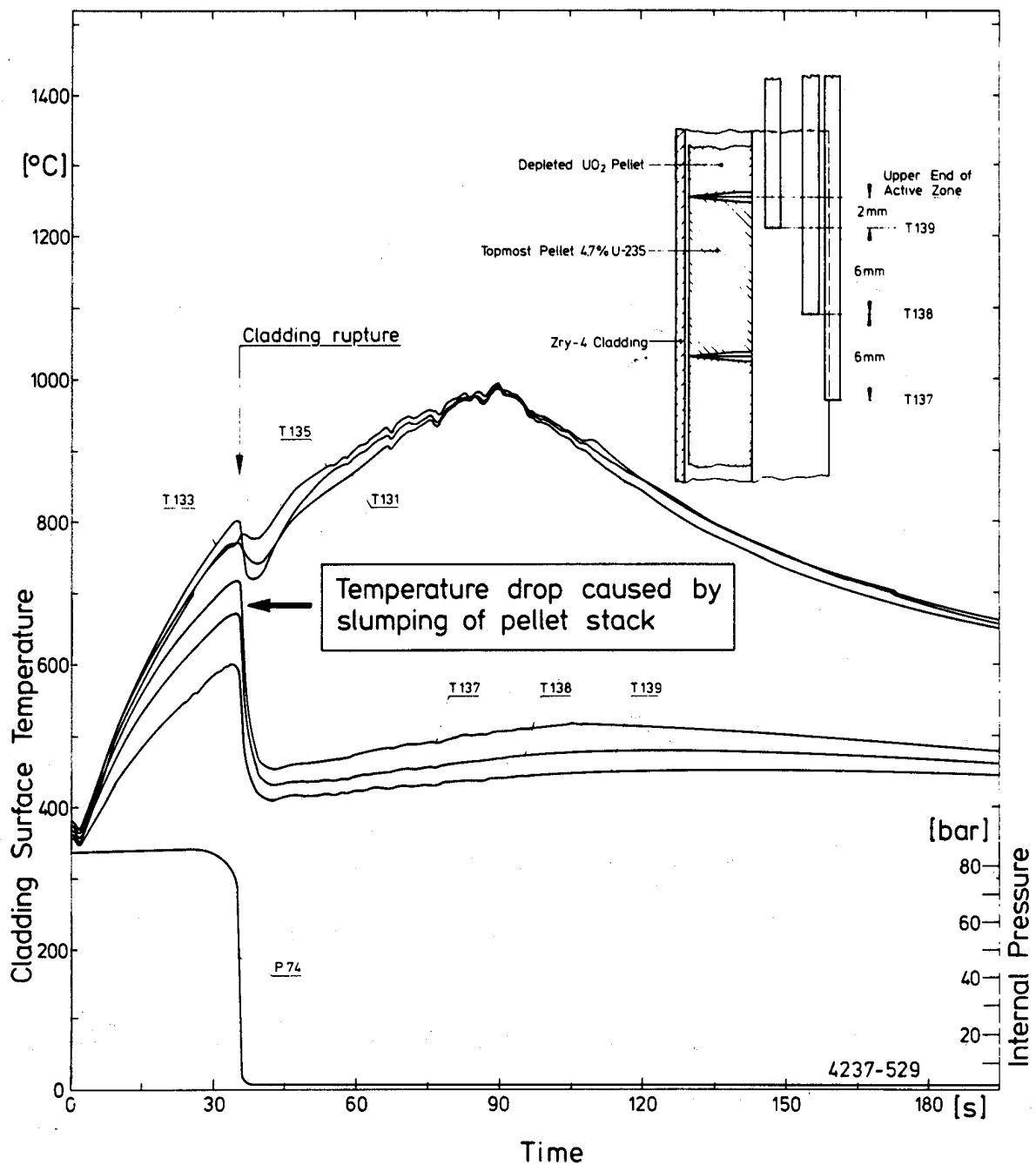


Figure 54: temperature and internal pressure histories in FR2 test E4.

The filling ratio of the free space resulting from the clad ballooning depends on the granulometry of the fuel fragments. Analysis of the fuel particle size distribution for the rods from each test series shows very similar distributions for the burnups in the 2.5 to 35 GWd/tU range, with 2 peaks near 2 mm and 3.15 mm in particle size; the average particle size, calculated over all the irradiated rods, is 2.78 mm. The measurement of the local fuel mass per unit rod internal volume in the samples used for the particle size analysis also provided an estimate of the filling ratio for these samples. Figure 55 shows a decrease in the fuel mass per unit rod volume for most of the samples, corresponding to the increase of volume without fuel relocation; in fact, this evaluation only concerns the samples with minor circumferential elongation (<30%); the two points that lie apart from the previous trend correspond to samples taken from test E5 with elongations of 48% and 67.5% respectively, where the measured fuel mass per unit volume corresponds to a filling ratio of 55.5% and 61.5% respectively.

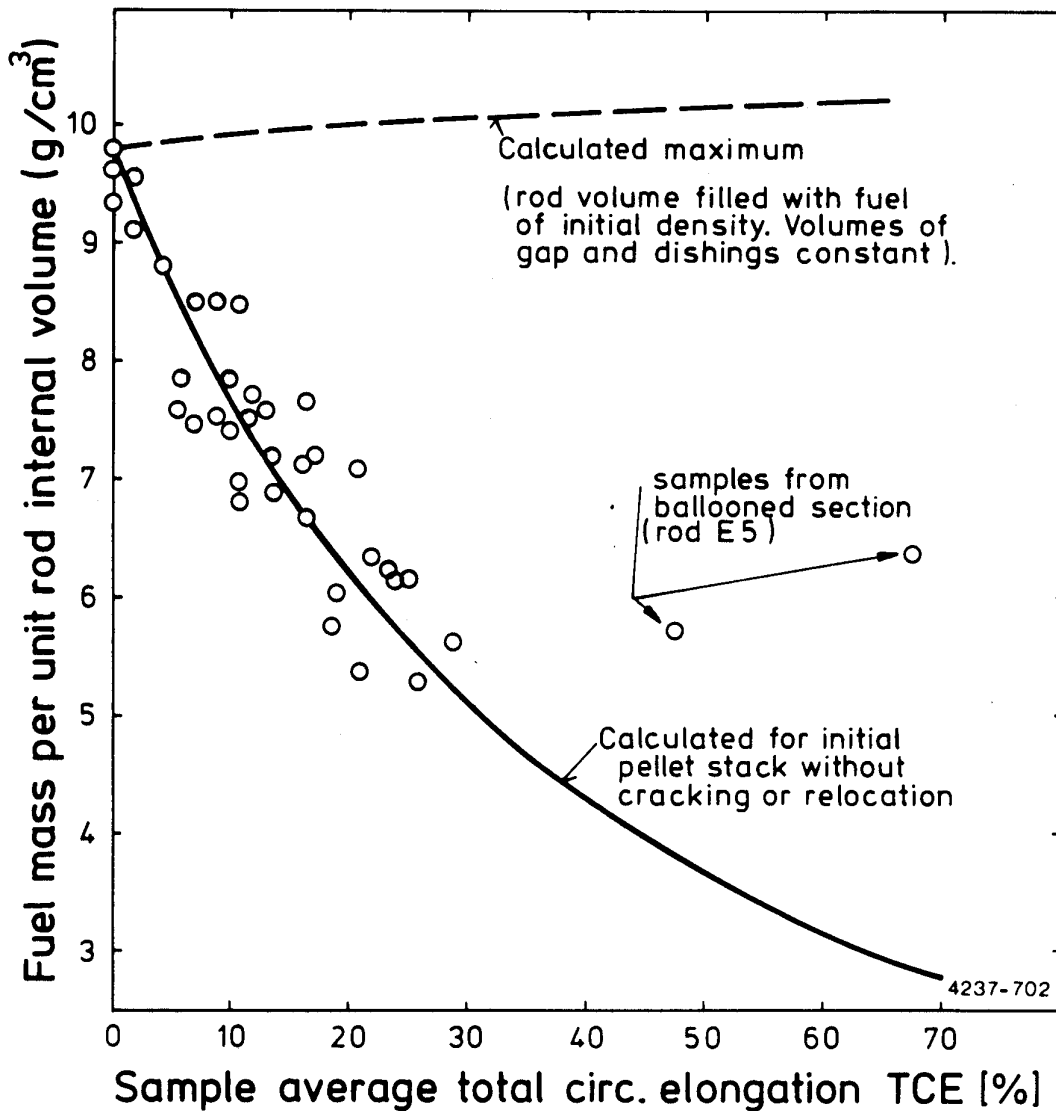


Figure 55: FR2 - fuel mass per unit volume of deformed cladding tube after relocation during LOCA burst test.

4.1.3 Main findings from the PBF-LOC and FR2 test results

The FR2 and PBF-LOC test results, which have already been widely detailed in a previous review by G. Hache^[7], provide the main elements needed to characterize the behavior of irradiated fuel at low to intermediate burnup during the ballooning and rupture phase of a LOCA transient.

The PBF-LOC and FR2 tests led to apparently contradictory observations relative to the influence of prior irradiation on the rod deformation:

- Significant increase in the burst strain of irradiated rods in comparison with that of twin unirradiated rods in the PBF tests;
- Insensitiveness to the prior irradiation in the FR2 tests.

Analysis of the experimental conditions in the FR2 tests showed that some particular features of these conditions (prior irradiation at low coolant temperature and pressure, axial constraint transmitted by the spring) may have occulted the effect observed on PBF-LOC, essentially related to the temperature azimuthal homogenizing, as a result of fuel rearrangement and clad creepdown. Thus, **it cannot not be considered**, as suggested in some reviews^[2,4], that the FR2 results "erase" to some extent the irradiation effect observed in the PBF-LOC results, and that in-pile data do not indicate an influence of the nuclear environment on cladding deformation.

As for the fuel behavior, the FR2 and PBF-LOC tests appear to be fairly consistent with respect to the relocation phenomena of fragmented fuel in the clad balloon. The impact of fuel relocation on the subsequent evolution of the LOCA transient, in particular on the histories of the local clad temperature and resulting oxidation rate, was not ascertained by FR2 and PBF-LOC test results. For the PBF-LOC case, only a simplified evaluation was performed on the clad and center fuel temperatures with fuel relocation in the balloon for two values of circumferential elongation^[18]. More recently, IRSN performed a series of simulation studies^[21,22] with the CATHARE code on a large break LOCA scenario both with and without fuel relocation at the clad rupture in the balloon formed on the hot rod; these calculations pointed out the possible importance of the fuel relocation in a ballooned cladding under LOCA transient for safety issues, with particular concern for high burnup MOX fuel and possibly with advanced ZrNb1 clad alloys.

4.1.4 ESSOR Tests

Six single rod tests with fresh fuel were performed in the EOLO-JR facility of the ESSOR research reactor in Ispra^[23], with the objective to study the clad ballooning behavior and rupture in the high alpha domain (970 - 1080 K) under a low temperature ramp.

4.1.4.1 Experimental conditions

The PWR KWU type test rod with an active length of 1 m was centered in an unheated shroud. The temperature was measured by 12 thermocouples on 4 axial levels (3 TC, 120° apart per level); a pressure line, connected to the rod plenum, allowed for the continuous monitoring of the internal pressure, the initial value being 4.8 MPa in cold conditions. The external coolant was a gaseous mixture of He + 5% O₂ at 0.5 MPa pressure.

Following a steady-state regime at 820 K for almost 2 hours, the test transient was started by a controlled reduction of the gaseous flow so as to induce a 3 K/s temperature increase until the target temperature T_f was reached (between 970 and 1080 K), which was maintained on this plateau during the time required to lead to clad ballooning and rupture, after which the test was terminated by a reactor scram.

Table 5 summarizes the main experimental characteristics of the 5 EOLO tests that were carried out after a preliminary calibration test.

Data	EOLO-1	EOLO-2	EOLO-3	EOLO-4	EOLO-5
Rod peak linear power (kW/m)	4.32	4.44	3.93	4.32	3.80
Fuel rod cold pressure P ₂ (MPa)	4.82	4.79	4.9	4.9 (I) ^b 4.0 (II)	5.0
P ₂ -P ₁ at t = 0 (MPa)	6.9	5.8	6.5 max. ^a 6.2	6.1	6.4
P ₂ -P ₁ at burst time (MPa)	6.2	5.5	5.7	5.6	5.0
Controlled clad temperature at t = 0 (K)	980	1056	1080	1010	970 ^c 990
Peak clad temperature at burst time (K)	1075	1044	1110	1030	995
Max. ΔT during ballooning (K)	101	92	38	55	48
Burst time (s)	200	130	10	372	3460 ^c 540

^a In test EOLO-3, the clad ballooning started during the temperature ramp (t = -20 s) when the peak clad temperature was 1070 K. Thus two values of P₂-P₁ corresponding to t = -20 s (ΔP max.) and t = 0 are shown.

^b In test EOLO-4, an unforeseen reactor scram occurred as soon as the required temperature was reached. The experiment was restarted but it was observed that the fuel rod cold pressure had decreased from 4.9 MPa to 4.0 MPa during the first phase, probably due to prior ballooning.

^c In test EOLO-5, the controlled PCT value T_f had been fixed at 970 K. After 2920 s without failure, the controlled clad temperature was raised to 990 K. Clad burst occurred 540 s after this change.

Table 5: summary of the main measurements in the EOLO tests.

4.1.4.2 Results

Based on test EOLO-2, figure 56 illustrates the history of the internal pressure and temperatures at level 0.65 m, close to the rupture level. The authors impute the decrease in the temperatures T8 and T9 at the beginning of deformation (t = 0) to rod bending which results from the anisotropic creep of Zircaloy ("hot side straight effect"). They also suggested that this effect may have been partially counteracted shortly before rupture by an adverse effect corresponding to a detachment of the clad on the hot side with subsequent enhanced cooling ("strain cooling effect"), which could also explain the unexpected axial extension of the clad deformation observed in tests EOLO-2 and EOLO-4.

Figure 57 illustrates the development of the azimuthal temperature gradients at the different levels of measurement in test EOLO-2. Figure 58 shows the axial profiles of diametral strain for the five EOLO tests, with the indication of the azimuthal temperatures before burst on the level nearest to rupture; ΔT values range from 30 to 90 K. The maximum elongation at burst is thus moderate, ranging between 20 and 38%, although rather axially extended and remains consistent, as a function of azimuthal temperature difference, with the results obtained at KfK (REBEKA) and KWU (see figure 59). However, the authors point out that the deformations in EOLO tests, which appear in the lower bound of the out-of-pile test results, might have been lowered by the influence of a welded thermocouple, four over the five rupture having occurred at a TC level.

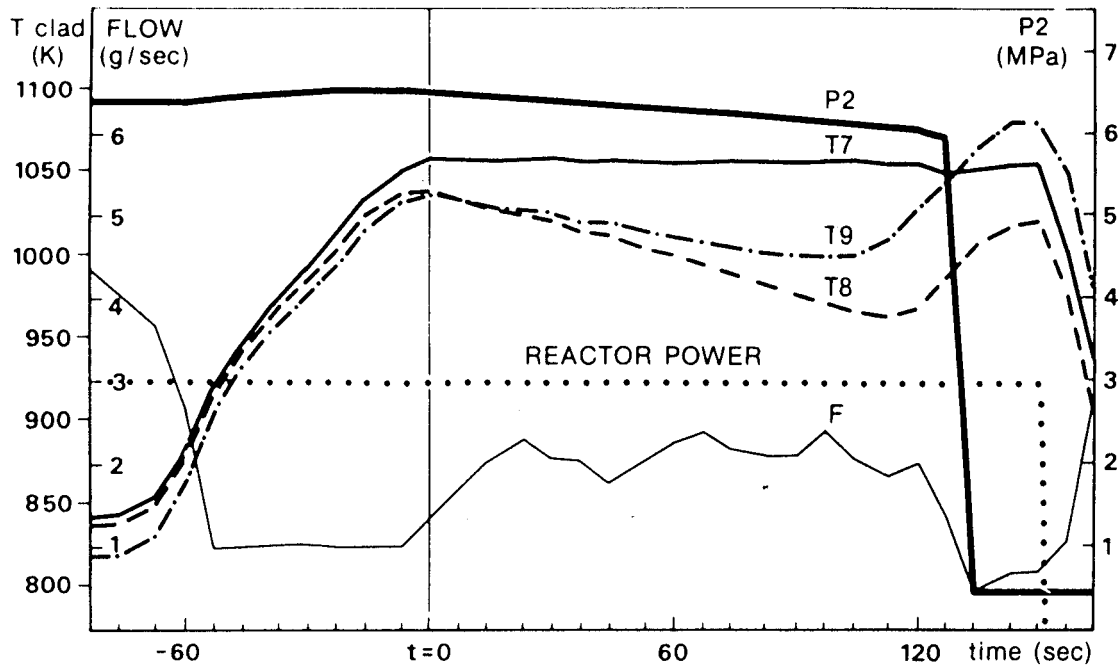


Figure 56: EOLO-2 - evolution of the cladding temperatures at the level 0.65 m, coolant flow and rod fill gas pressure during the test.

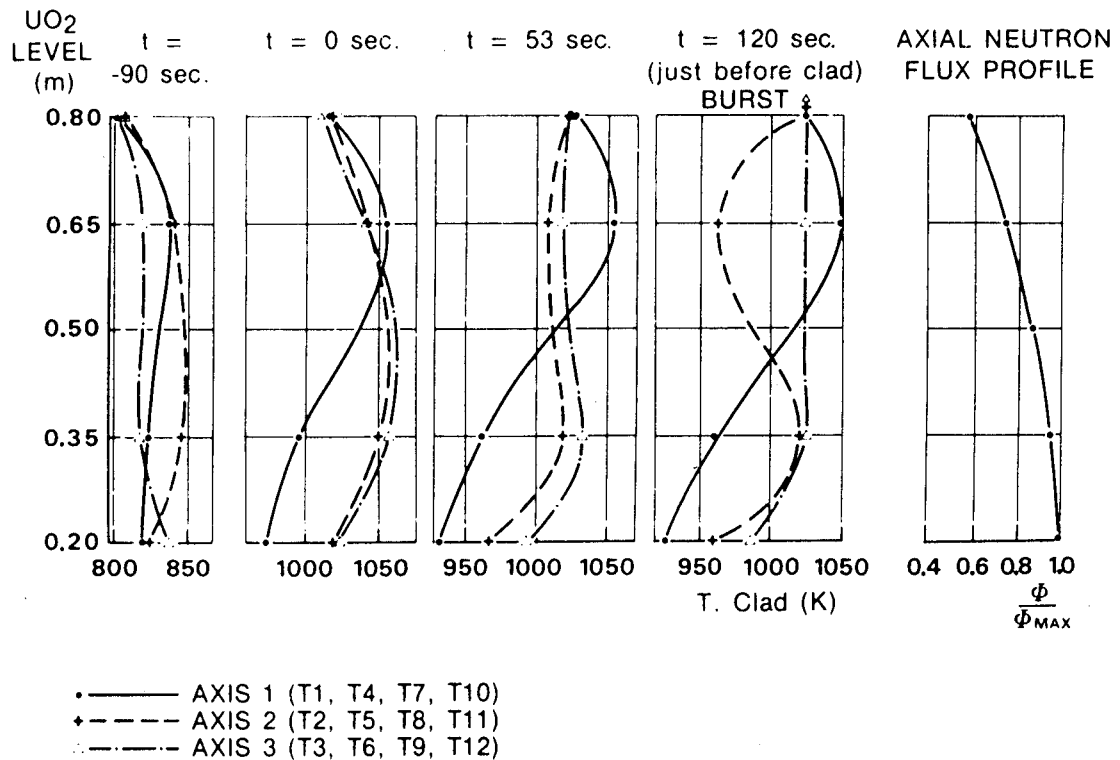


Figure 57: EOLO-2 - clad temperature and neutron flux axial profiles during the test.

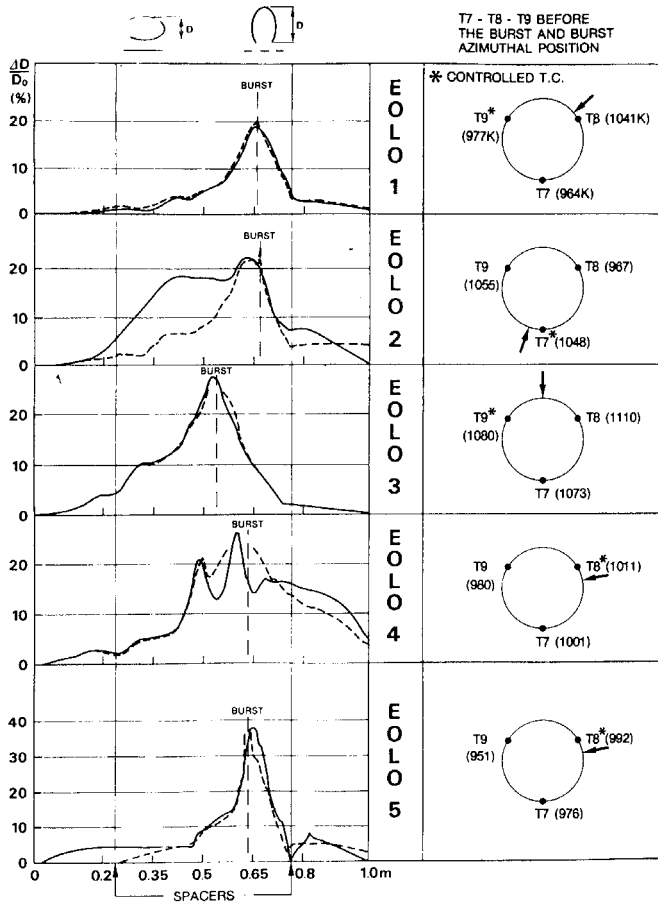
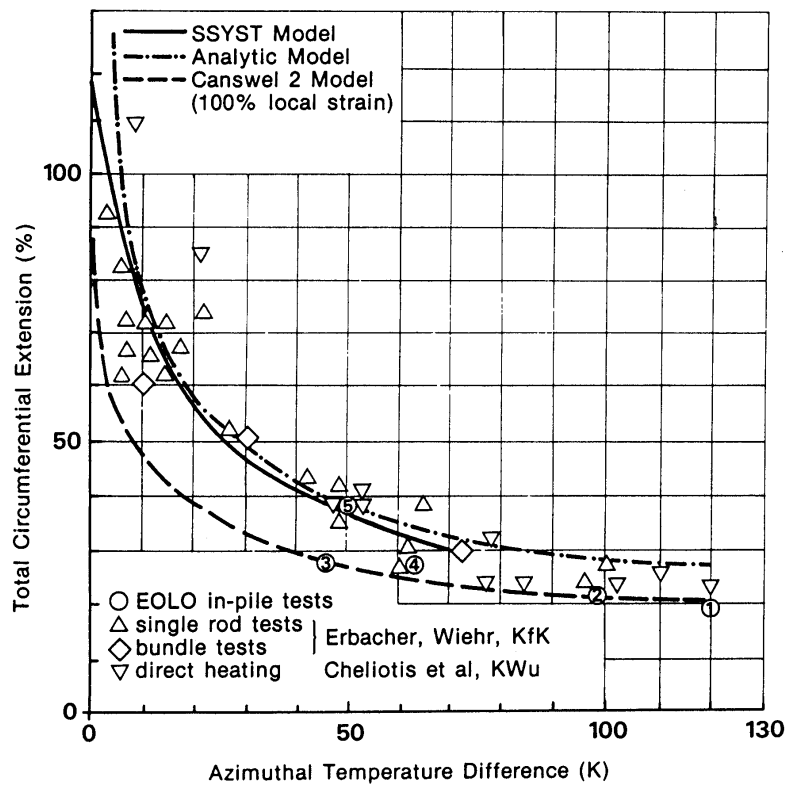


Figure 58: EOLO.
Post-irradiation diametral metrology of the five burst claddings.

Figure 59: EOLO.
Influence of azimuthal temperature gradient on burst strain.



4.1.5 FLASH tests

Five tests were carried out in the FLASH facility of the SILOE reactor at CEA/Grenoble, with the main objective to study the fission products release during a LOCA transient. These tests were performed on a pre-conditioned fresh fuel rod (FLASH-1 to FLASH-4)^[24] and a high burnup fuel rod (FLASH-5)^[25].

4.1.5.1 Experimental conditions

The PWR 17x17 type test rod with an active length of 30 cm was centered in an unheated shroud tube and cooled under a thermo-siphon regime within a finger-shaped irradiation device located on the reactor periphery, with this last particularity having induced large azimuthal temperature heterogeneities.

For the tests FLASH-1 to FLASH-4, a pre-irradiation phase at nominal PWR conditions (35 to 40 kW/m, 13 MPa), made it possible to produce a FP inventory at a burnup ranging from 1650 to 3320 MWd/tU. For the FLASH-5 test, the test rod was re-fabricated from a PWR 4 cycles rod (50300 MWd/tU burnup) and was also re-irradiated a few weeks in the SILOE reactor at about 17 kW/m in order to re-form short-lived FP species, thus adding 1412 MWd/tU to the initial burnup.

The experimental transient started with a power adjustment at about 7 kW/m, then the test train was depressurized to a residual pressure ranging from 0.5 to 2.1 MPa, associated with the injection of helium. This resulted in a clad temperature rise up to a target maximum temperature reaching:

- 1100°C in FLASH-1 and FLASH-2,
- 1270°C in FLASH-3 and FLASH-4,
- 1350°C in FLASH-5,

at which the test was terminated by reactor scram (FLASH-1 to 3) or quenching at hot conditions while maintaining the nuclear power for about ten minutes (FLASH-4 and 5).

4.1.5.2 Results

Figure 60 shows the clad temperature history in test FLASH-5, where the temperature rise rate at 28 K/s led to rupture at 995°C. In the tests FLASH-3 and 4, similar temperature ramps (~ 30 K/s) led to clad rupture at 930 and 940°C respectively. However, in FLASH-1 and 2, an untimely scram led to much lower temperature ramps (~ 1 to 2 K/s), resulting in axially extended strain with a slight opening in the clad that was undetected in these two tests due to the lack of internal pressure sensors.

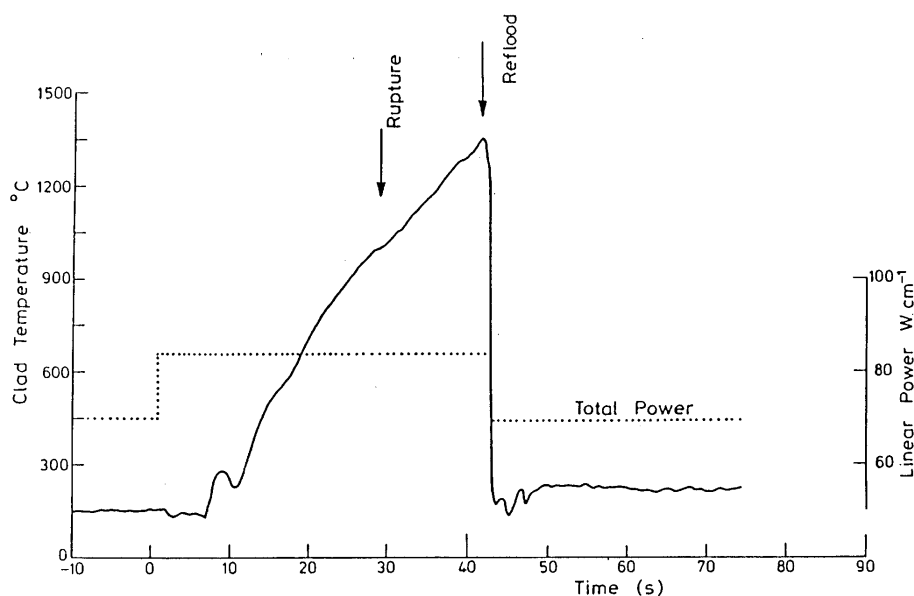


Figure 60: temperature history of the FLASH-5 test.

Rupture strain ranged from 16% in FLASH-5 to 62% in FLASH-2, the low strain values in FLASH-5 being explained by the occurrence of large azimuthal temperature differences, exceeding 110 K at burst time: this strain value was thus consistent with the results of out-of-pile single rod tests with an unheated shroud.

As for fuel behavior, it is interesting to point out the lack of fuel relocation during the transient in tests with pre-conditioned fresh fuel with however, the indication of some fuel relocation following handling (considered "severe") when removing the rod from the test device. In test FLASH-5 on an irradiated rod, fine fuel fragmentation in the central part near the maximum flux level was observed, as well as significant displacement of fuel fragments at the rupture level, in spite of the low clad strain (see figure 61).

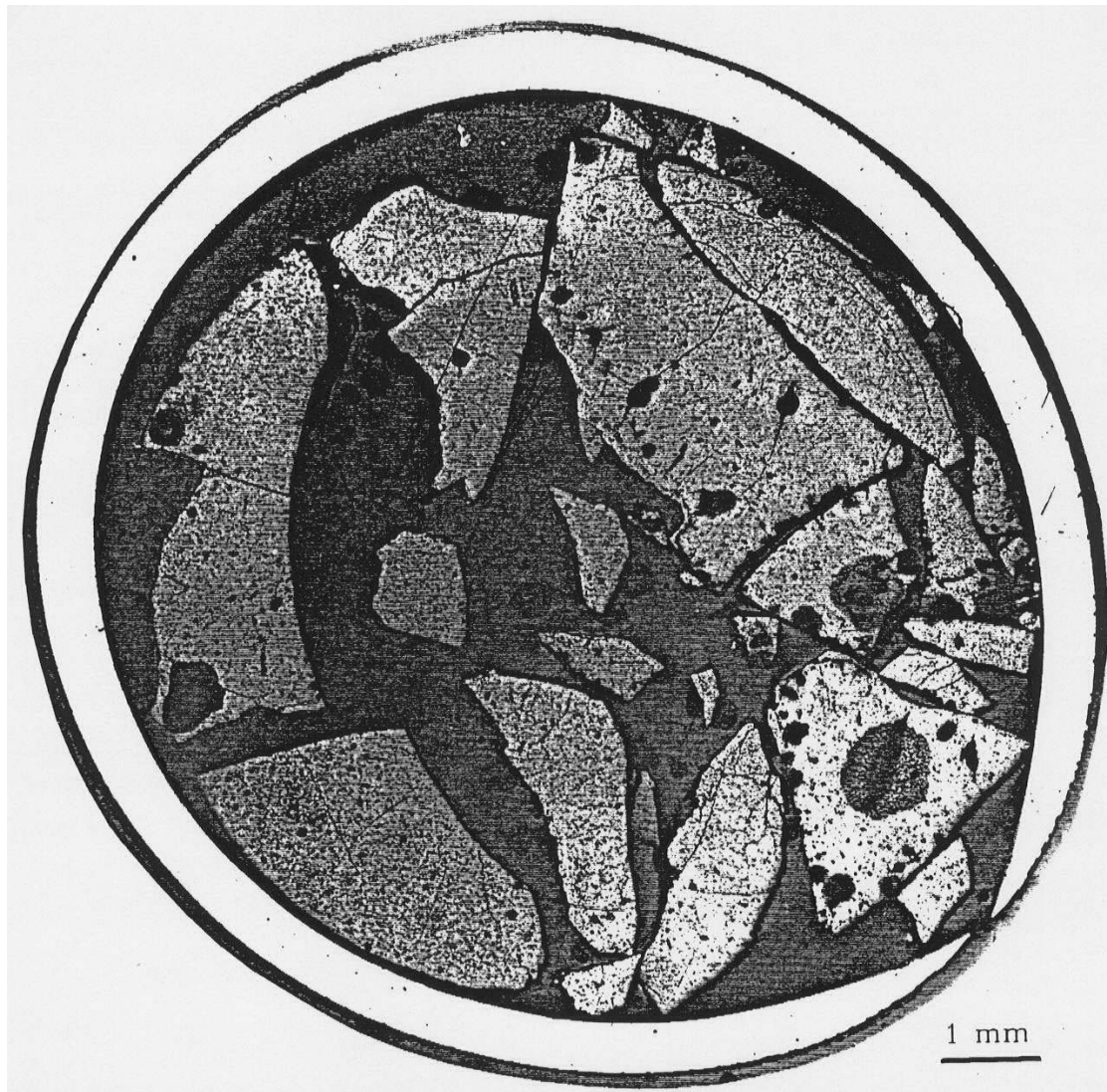


Figure 61: fuel aspect at rupture plane in the FLASH-5 test.

Since the main objective of the FLASH tests - FP releases - does not come under the scope of this review, only a brief summary of the main experimental observations will be provided:

- In FLASH-1 to 4, the amount of released gases roughly corresponded to the available gas inventory in the rod free volume and the FP release in the quench water was very low ;
- In FLASH-5, the release of gases was an order of magnitude greater than in the previous tests on fresh fuel rods, and even more so for the FP release in water; but this result was mostly attributed to the oxidation of fuel by steam after clad rupture while maintaining the nuclear power for 12 minutes after the start of quenching.

4.2 Multi rod tests

4.2.1 MT tests

A series of multi-rod tests simulating LOCA transients were carried out by PNL in the NRU reactor at Chalk River with the objective to study the thermohydraulic and thermomechanical behavior (deformation, flow blockage) within a bundle of 32 PWR full-length rods^[26].

4.2.1.1 Common characteristics

The test assembly consisted of a 6x6 array with the 4 corner rods removed, the 20 non-pressurized outer rods making a guard ring for the 12 inner pressurized rods. The test bundle was surrounded by a stainless steel shroud to protect the loop pressure tube (see figure 62). The fuel length of the test rods (3.66 m) was greater than the NRU core height (2.74 m), with the bottom and top ends of these rods thus being out of the neutron flux.

The test rods were fueled with fresh UO₂ pellets but were preconditioned prior to the LOCA transients by power cycling to full power which caused the fuel pellets to fracture.

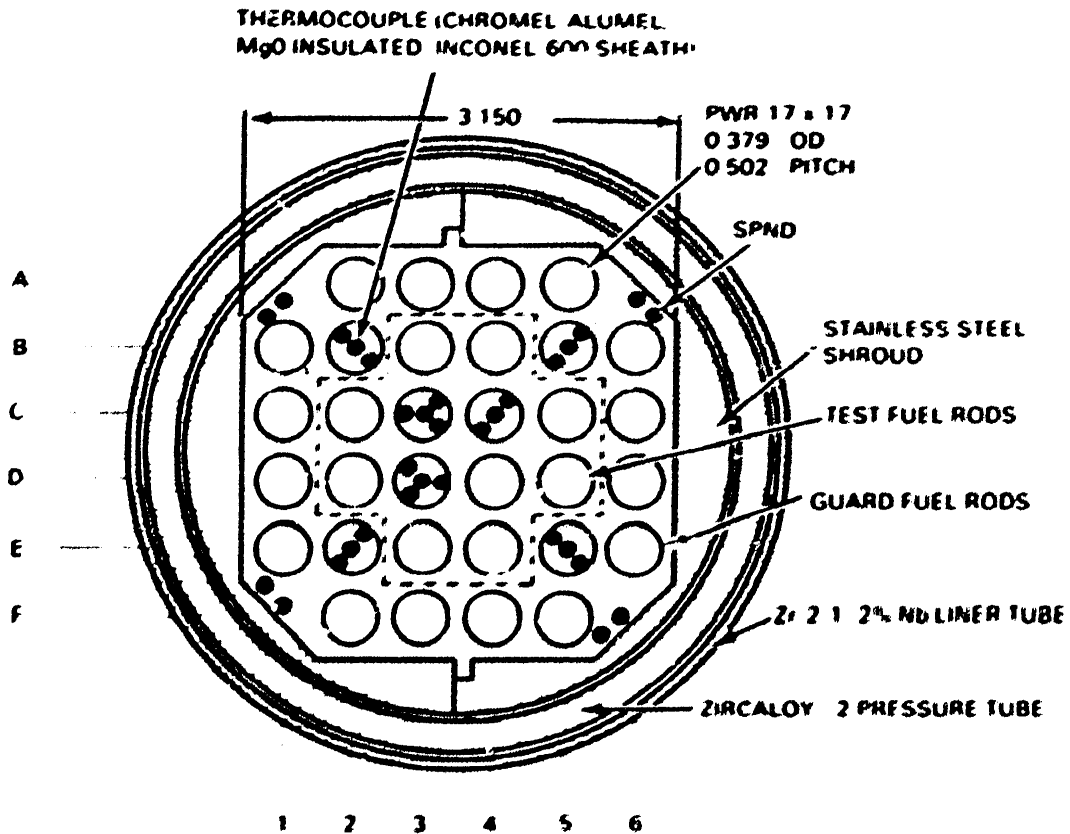


Figure 62: NRU-MT - cross section of the test assembly for the LOCA simulation program.

Seven LOCA-type tests were performed over the period from October 1980 to May 1982: 3 thermal hydraulic tests (TH) and 4 material tests (MT), the former having mainly been used for the adjustment of the thermal-hydraulic conditions of the MT tests, which will only be reported here.

Each test included several experimental preliminary phases before the final phase under the conditions defined for the target objective of the test. Schematically, the test transient was initialized by a temperature rise to ~ 650 K and stabilization under steam cooling. The transient was then started by stopping the steam flow that caused an adiabatic temperature rise during which a reflood was actuated at a given time so as to limit the peak clad temperature at a target value. The test was terminated by reactor scram.

4.2.1.2 Main results

In MT-1, where the inner array consisted of 11 pressurized rods and one "water rod", the target PCT of 1144 K (871°C) was reached. Six of the eleven pressurized rods ruptured, after almost 70 s on average, thus after the start of reflow (at 32 s), but sufficiently early for the ballooning phase to have occurred mostly during the quasi-adiabatic temperature rise under steam flow.

In MT-2, also with 11 pressurized rods + one "water rod", the target PCT was 1089 K (816°C). Due to a dysfunction, the PCT reached 1161 K, which was rather close to that of the MT-1 test, the results of which were approximately duplicated: rupture of 8 rods, 65 s on average after the start of the transient. Figure 63 gives the axial profile of the clad diametral strain in MT-1 and MT-2, showing a maximum deformation greater than 60% in MT-1 and greater than 70% in MT-2, although the average rupture strain for these two tests was reported at 43% in [26]. Reference [27] also reports a maximum "mean assembly deformation" (apparently defined as the axial maximum value of the average deformation at a given axial level) of 37.2% and 35.6% in MT-1 and MT-2 respectively, corresponding to flow blockage ratios of 70 and 67% respectively.

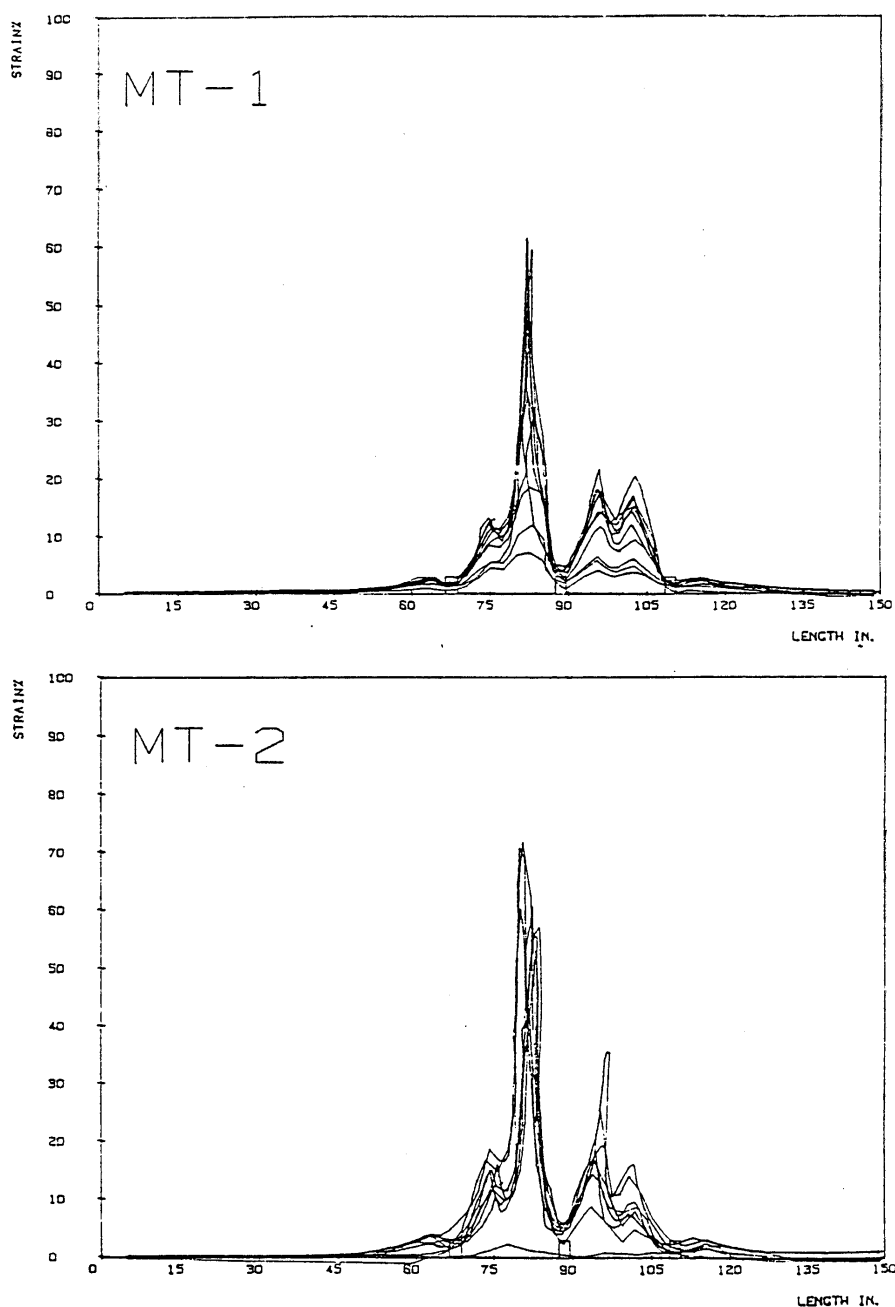


Figure 63: axial distribution of strain in NRU MT-1 and MT-2 tests.

In the MT-3 test with 12 pressurized rods, the reflood started at 9 s and the 12 rods ruptured on average close to 133 s, in the high α domain at an average quasi-stabilized temperature of 1067 K (794°C), under active two-phase flow cooling. Figure 64 gives the axial profile of clad diametral strain in MT-3 showing, as in the previous tests, the deformation concentrated in two grid-spans and, particularly for this test, the influence of grids on downstream cooling and the resulting shift of the deformations upstream from the next grid (effect also observed in the REBEKA tests). A maximum strain of 94% was observed on rod 5C; the average rupture strain was reported at 47% and the maximum "mean assembly deformation" at 36%, corresponding to a flow blockage ratio of 68%.

In the MT-4 test with 12 pressurized rods as in MT-3, the reflood started relatively late (at 57 s) and all 12 rods ruptured at 55 s(± 2 s) during the adiabatic heatup under steam, at an average temperature of 1094 K (821°C). The axial profile of the clad diametral strain, as plotted in Figure 64, shows a maximum strain of 96%, the average burst strain being reported at 72% in [26]. The higher cladding rupture strain in MT-4 was attributed to the cooling under a single phase steam flow which generated less temperature differences than under a two-phase flow. The maximum flow blockage ratio, which may locally be close to 100% in the subchannel adjacent to the maximum strain, does not exceed 25% in mean assembly value.

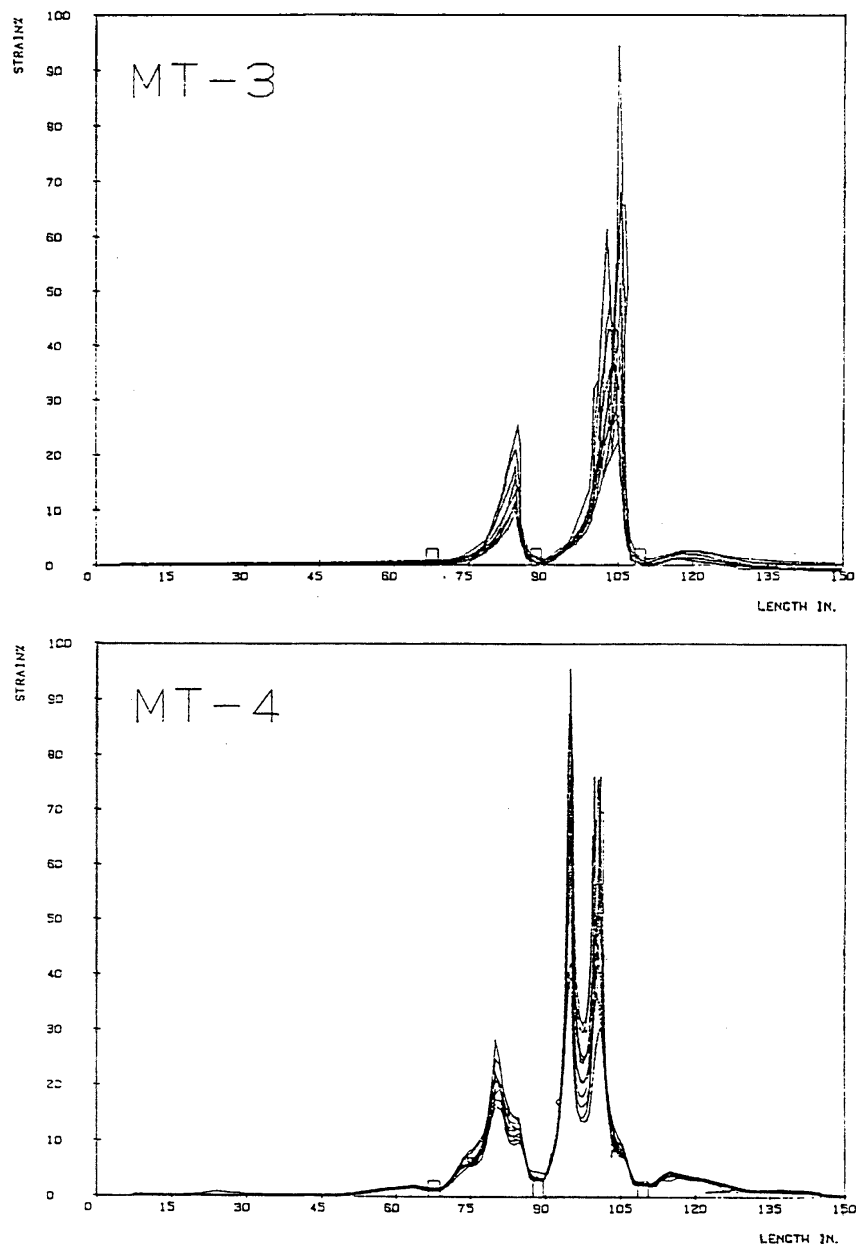


Figure 64: axial distribution of strain in NRU MT-3 and MT-4 tests.

From the experimental observations, the authors concluded that the rod deformations were significantly coplanar, as clearly shown in figure 64 for MT-3. These coplanar deformations seem to be favored in MT-3 by the influence of spacer grids under two-phase flow cooling, homogenizing the temperatures downstream from the grid before the development of rupture conditions towards the next grid. This observation thus contradicts Erbacher's conclusion (cf. § 3.2.1.2), based on REBEKA tests with countercurrent vapor and two-phase cooling flows, and particularly emphasizes the importance of the direction of flows as observed in the comparison of the REBEKA-5 and 6 test results.

In other respects, the particularly refined instrumentation of the MT-3 bundle at levels 13, 15 and 17 allowed for an overall estimate of the effect of a partial flow blockage on the compared temperature variations in deformed and undeformed rods. Figure 65, which plots the temperature histories of the MT-3 central and guard rods at level 15, close to the level of maximum flow reduction, does not reveal any significant difference between the two groups of rods. The influence of flow reduction on the heat transfers in the deformed region appears to be balanced by the increase in turbulence. The authors concluded that the coolability of a deformed bundle was relatively insensitive to the extent of average deformation, over the range of blockages obtained in these tests.

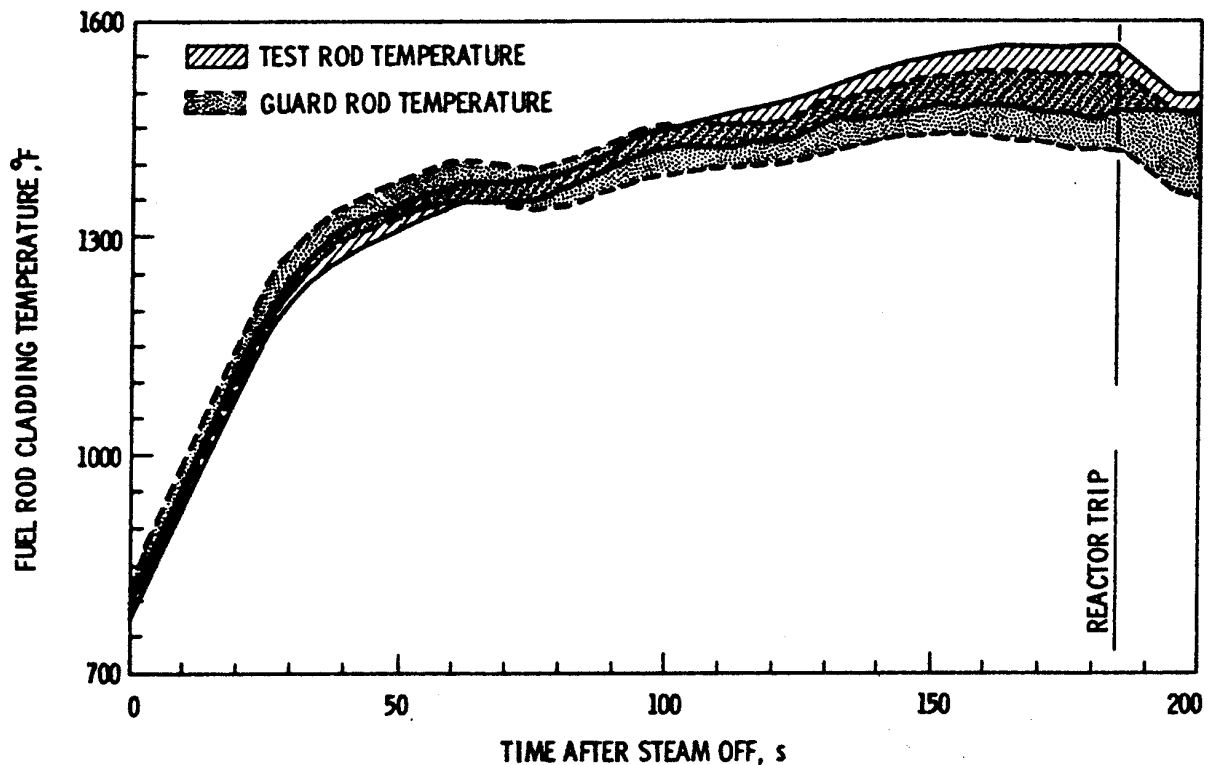


Figure 65: comparison of average test and guard rod temperatures at level 15 during MT-3.06.

Last of all, it is worth mentioning an additional test, MT-6A that was performed on a 21 rod bundle (5x5 array without corner rods), with all rods having ruptured in a quasi-adiabatic phase. This test, referred to in the review by Parson^[1], is not mentioned in the PNL summary reports^[26]. It may thus be thought that the validity of this test was deemed insufficient, which would explain why it was not included in the database of results.

4.2.2 The PHEBUS-LOCA tests

The PHEBUS-LOCA program performed by IRSN is still the only experimental in-pile LOCA program with integral tests on real fuel rods in a bundle configuration. Starting from an initial state representative of PWR nominal conditions, the test transient aimed at reproducing a hypothetical large break LOCA transient from initial blowdown until the final quench of the test device.

The PHEBUS-LOCA program was thus designed so as to allow the coupling of the main phenomena, with regards to thermal-hydraulics and thermo-mechanics under LOCA conditions in view of satisfying the following general objectives:

- Assessing the phenomenology of the fuel rod behavior under conservative LOCA conditions, including rod rupture and a subsequent temperature plateau for clad oxidation up to the acceptance limit, before a final representative quenching;
- Assessing the adequacy of safety criteria with respect to the coolability of fuel rods and clad embrittlement, with assessment of safety margins;
- Providing an experimental database for the validation of computer codes used in the simulation of the thermal-hydraulics and thermo-mechanics in LB LOCA, particularly the CATHACOMB module of the CATHARE system code.

A summary of the safety studies on LOCA conducted at CEA, mainly based on a comprehensive review of the PHEBUS-LOCA program, has been compiled by IPSN^[3].

The PHEBUS-LOCA experimental program was conducted from 1980 to 1984. It included 3 single rod tests and 22 tests with 25 rods bundles. Among the bundle tests, only 7 were performed with pressurized rods, while the remaining tests with all non pressurized rods were mostly used to study the thermohydraulic behavior from blowdown to reflood so as to adjust the conditions and procedure for the tests with pressurized rods.

With respect to the thermomechanical behavior, the above general objectives were specified as:

- Verification, under representative transient conditions and in a bundle geometry, of the cladding deformation and rupture models derived from out-of-pile single rod EDGAR tests;
- Evaluation of the maximum flow blockage ratio possibly reached during a LOCA transient, as well as of the coolability of the bundle containing such deformed rods.

4.2.2.1 Description of the test facility and test train

The test train was the central component of the experimental facility. It consisted of a bundle of 25 5x5 PWR type rods containing fresh UO₂ fuel, maintained by 4 Inconel spacer grids. The fuel pins were 1 m long (0.8 m active length) and could be internally pressurized. The fuel bundle was surrounded by a massive Zircaloy-2 shroud that linked the square section of the bundle to the circular section of the concentric outer structures: a zirconia insulation layer and the Zry2 test tube 114 mm in O.D. The test tube was itself placed in successive concentric outer tubes (pressure tube and safety tube) to ensure the confinement of the test train and the circulation of coolant around it.

The test device was included in a loop inserted in the PHEBUS driver core that provided the neutronic flux for the nuclear heating of the test rods. The test loop (see figure 66) was designed to reproduce the initial steady state conditions of the power plant before transient initiation. The transient was initiated by isolating the test section of the loop containing the fuel bundle, then rapid opening of valves on the upstream and downstream pipes to simulate breaks on the cold and hot legs. Simultaneously, the power of the driver core was decreased to simulate the nuclear power transient following plant shutdown.

The area of the breaks was adjusted in order to provide the desired system pressure history and flowrates in the hot and cold legs which make possible to control the position of the stagnation point (zero flow). Four injection lines, upstream and downstream from the test train, were used to refill the loop and the reflood of the bundle after the blowdown phase.

4.2.2.2 Test matrix

The PHEBUS-LOCA test matrix was defined to cover the main relevant phenomena that can occur in a PWR under LOCA conditions in order to satisfy previously identified objectives. With this in view, a typical test transient was defined (see figure 67) that consisted in:

- A first temperature peak near 920°C during the blowdown phase, inducing a temporary transus in the $\alpha+\beta$ metallurgical domain,
- Intermediate cooling towards 750°C followed by a second heatup phase after the blowdown phase up to a temperature plateau around 1200°C; the duration of the temperature plateau can be varied to cover oxidation rates up to the limit of the acceptance criteria (17% Baker-Just),
- Subsequent cooling at slow rate or by quenching.

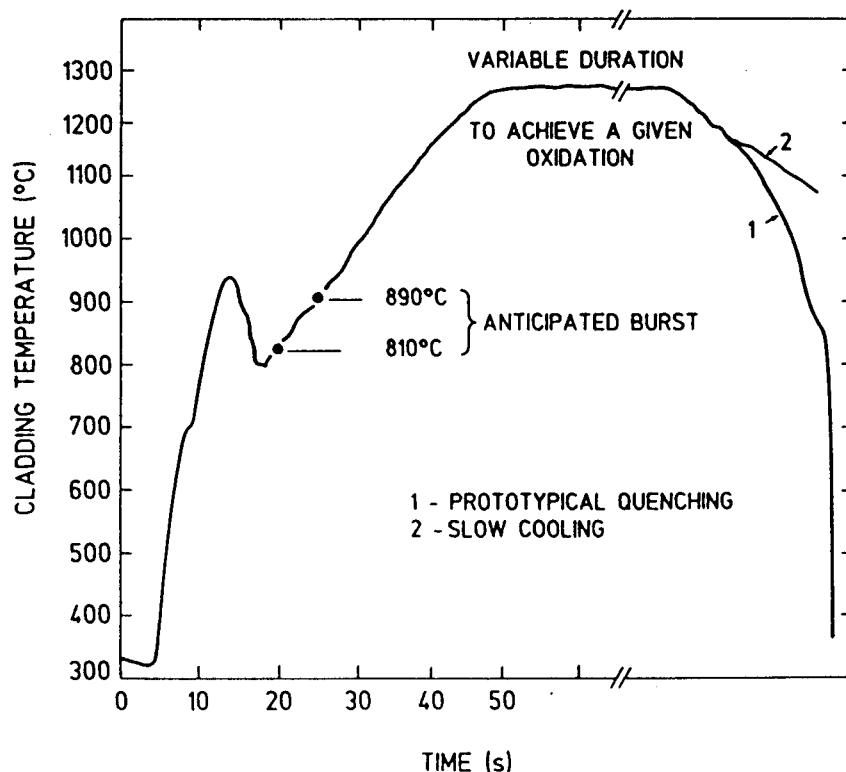


Figure 67: PHEBUS-LOCA typical test transient.

Table 6 summarizes the thermohydraulic characteristics of the 18 main tests. Tests numbers below 215 were carried out with non pressurized rods and were essentially devoted to adjusting experimental procedures to obtain the prescribed thermohydraulic conditions. Only the tests 215-P to 219, which were performed with nearly all rods pressurized in the bundle, provided information on the thermomechanical behavior under LOCA conditions and will thus be described hereafter.

As the scope of the present study focuses on ballooning and blockage aspects, only the results relative to rod thermomechanical behavior will be discussed here, disregarding the thermohydraulic aspects and only providing limited results on the oxidation and quench behavior of the rod claddings. Readers interested in such aspects shall find extensive information in the previously mentioned summary report^[3].

Test number	Date (DD/MM/YY)	DC SS power ⁽¹⁾ (MW)	DC BD power ⁽²⁾ (MW)	Liquid heating in S.S. ⁽³⁾ (°C)	Beak area ratio	Break second opening ⁽⁴⁾	DNB time (s)	Cladding temp. after		Events
								5 s	12 s	
210	04/06/81	0.0	0.0	0.0	1.3		13.0	Tsat	280	Rewet after 20s
211	09/09/81	19.5	2.5	6.6	1.3		1.8	600	650	Top rewet 13s
212	26/11/81	29.4	4.0	10.3	1.3		2.0	570	760	Top rewet 13s
213-A	27/06/82	29.1	4.0	10.0	1.3		2.5	640	500	Top rewet 12.5s
215-P	08/07/82	29.5	4.0	10.6	1.3		2.3	560	660	Top rewet 13s
213-B	21/10/82	32.4	4.5	12.5	1.1		2.8	620	780	
213-E	18/11/82	29.4	4.0	3.0	1.1		0.8	Tsat	250	Bot. rewet
213-C	25/11/82	29.1	4.0	2.0	1.2		0.8	Tsat	250	Bot. rewet
213-FB	10/02/83	34.2	4.0	11.7	1.1	HL 24 s	2.3	620	760	
213-G	14/04/83	34.0	8.5	11.0	1.1	HL 13 s	2.3	650	860	
215-R	06/05/83	33.7	11.0	9.7	1.1	HL 12 s	2.3	610	820	
216	01/12/83	33.7	8.5	10.0	1.2	CL 13.7s	2.3	660	900	
217	15/03/84	33.9	8.7	9.7	1.2		2.3	660	640	Bot. rewet 13s
213-GB	15/05/84	33.2	7.8	10.6	1.2		2.3	480	720	Bot. rewet 15.5s
213-GT	22/05/84	34.0	9.0	9.9	1.2	HL 14 s	2.5	680	850	
217-T	21/06/84	33.8	9.0	11.5	1.2	HL 12 s	2.2	650	680	
218	19/07/84	33.2	9.5	9.4	1.3	HL 12 s	2.2	700	980	
219	01/12/84	33.8	9.5	9.7	1.3	HL 11 s	2.5	700	930	

- (1) : driver core power in steady state
(2) : driver core power during blowdown
(3) : liquid heating across the core in steady state phase
(4) : HL = hot leg ; CL = cold leg

Table 6: thermohydraulic characteristics of the PHEBUS LOCA tests.

4.2.2.3 Results of the thermomechanical tests

Only five tests (215-P, 215-R, 216, 218 and 219) provided reliable information relative to thermo-mechanics; in test 217, experimental dysfunctions led to three successive transient runs, that made it impossible to provide a reliable analysis of the rod bundle thermomechanical behavior.

4.2.2.3.1 Test 215 P ^[28]

This test was the first test performed with 21 pressurized rods (4 MPa in cold conditions). As in the four previous tests, an early unexpected cladding rewet was experienced during the blowdown phase, from 4 to 13 s after the break opening, and which was attributed to the falling of water droplets onto the rod bundle. This rewet appeared to be anisotropic: early in the S-W half of the bundle (< 8 s) and a bit later in the N-E half (> 8 s). It limited the temperature at the 1st peak to less than 700°C at the hottest point, which did not lead to a phase transformation of Zircaloy during that temperature excursion. After a second dryout at the end of blowdown, the temperature was raised again to the level required for clad burst by delaying the quench beyond 200 s (see figure 68).

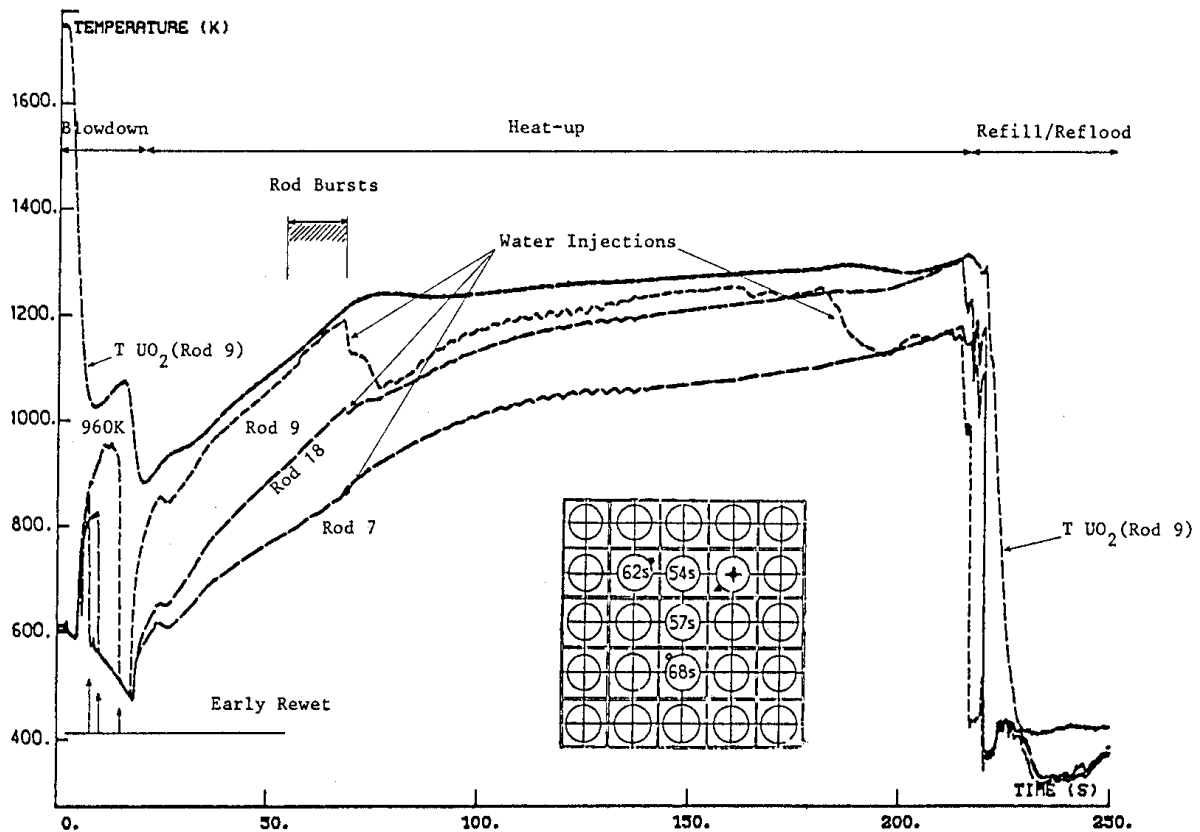


Figure 68: PHEBUS test 215-P - history of clad temperatures measured between two grid spacers.

During the heatup phase however, the thermal-hydraulics in the test was disturbed by several inflows of water in the test section (notably causing a flow reversal around 66 s: P2 event in figure 68), that resulted in a very irregular steam or two-phase flow; these disturbances tended to cool the upstream zone of the rods and move the hot spot downstream.

The early rewet combined with the hydraulic disturbances resulted in the development of large heterogeneities in the distribution of clad temperatures, which led to a spread in the clad rupture times: from 46 to 66 s on inner rods, up to about 150 s on outer rods.

The rod ruptures were oriented towards the bundle center and mainly located in the lower part of the bundle (see figures 69A and 69B).

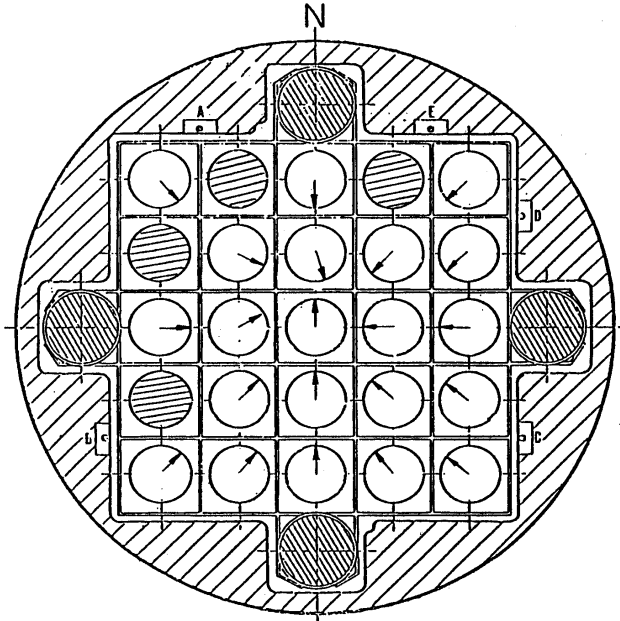


Figure 69A: PHEBUS Test 215-P.
Orientation of rod ruptures.

➤ **Inner rods:**

The clad ruptures for the 9 inner rods were axially grouped over 30 mm, 50 mm below the plane of maximum flux. They were even quasi-coplanar for 5 out of 6 of the hottest rods. The burst strain on inner rods ranged from 44 to 54% for the 6 rods in the "hot zone" and 18 to 25% for the 3 rods in the "cold zone". Cladding hoop strain greater than 34% (contact with neighboring rods with similar strain) spread over about 60 mm, indicating an axial extension of the clad ballooning through mechanical interaction between rods.

➤ **Outer rods:**

The clad ruptures were slightly more axially spread (50 mm) and located higher than that for the inner rods. The burst strain ranged from 15 to 38% depending on the rod position with respect to outer structures (shroud and braces). Cladding hoop strain greater than 34% (contact) did not spread over more than 15 mm.

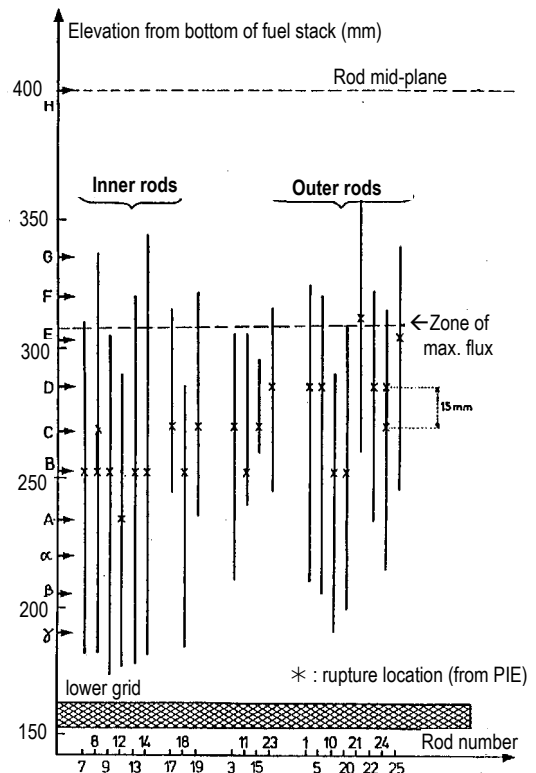


Figure 69B: axial distribution of deformed regions with >10% strain.

Figure 70 shows the axial profile of the clad hoop strain between the two lower grid spacers, where the coplanar feature and the typical "carrot" shape of the clad ballooning on inner rods can be observed. The shift of a few centimeters between rupture levels of inner and outer rods was most likely related to the flow reversal that occurred at 66 s between the rupture times on the two groups of rods: under ascending flow, the rupture levels shifted towards the bundle top.

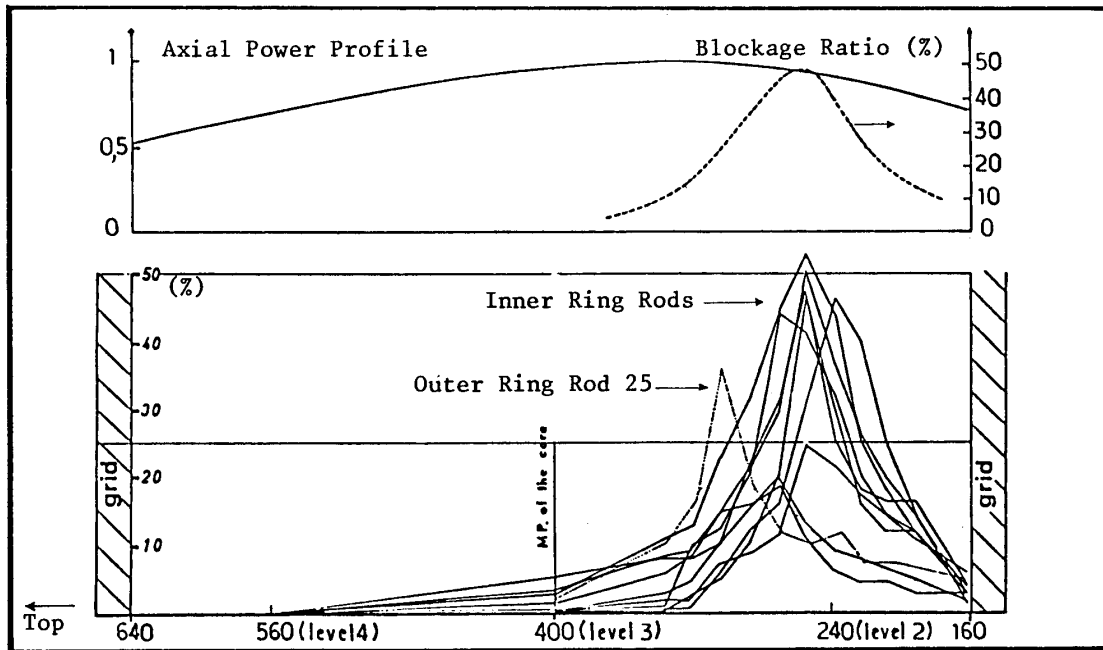


Figure 70: PHEBUS test 215-P - axial deformation profile between inner spacer grids and flow area restriction versus distance from bottom of fuel stack.

Figure 71 shows the distribution of the burst strain as a function of the rod position. The large difference between inner and outer rod burst strain reveals the variation in azimuthal temperature differences on the different rods of the bundle. These differences were due to the test device itself (cold peripheral structures and non uniformity of the neutronic power between inner and outer rods) and to the particular events that occurred in the experiment (very anisotropic early rewet and enhancement of convective exchanges following water inflows). An estimate of the azimuthal ΔT based on the strain versus ΔT curve derived from the REBEKA single rod experiments led to 30-50 K on inner rods of the "hot zone" and 70 K and above on inner rods of the "cold zone" and outer rods; the very heterogeneous thinning on ballooned claddings and the large variations in the oxide thickness support these azimuthal ΔT values.

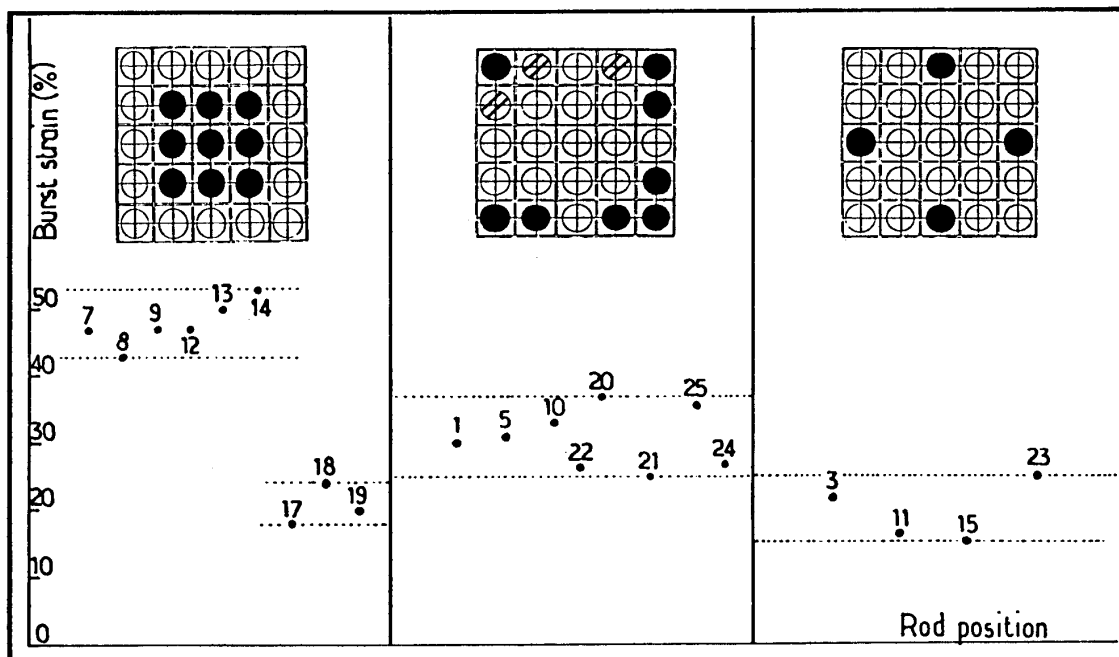


Figure 71: PHEBUS test 215-P - comparison of maximum burst strain with radial position.

In addition, the particular behavior of the inner rods 17, 18 and 19 from the “cold zone” that first experienced the early rewet, reasonably supports the explanation suggested by Kawasaki^[15] for the difference in behavior of rods neighboring a guide tube in JAERI tests:

- On the one hand, the temperature of the inner rods in the south row (17, 18, 19) is lower than that of the rods in the equatorial row (12, 13, 14); a local hot spot where deformation starts is enhanced by the bringing the hotter neighboring rod closer, thus leading to a localized rupture;
- On the other hand, the temperature of the inner rods in the north row (7, 8, 9) is higher than that of the rods in the equatorial row: local strain starting on a hot spot is counteracted, then stopped when the spot is brought closer and in contact with a colder neighboring rod, thus leading to circumferential then axial extension of the deformation process.

The maximum flow blockage ratio in the bundle section was 48%, but it reached 65% for the 9 inner rods and even 85% for the 6 rods in the central hot zone (see figure 72) where the mechanical interactions between rods mostly occurred. It is worth pointing out that the flow blockage in the bundle only resulted in a slight increase in pressure drop (+4%) and did not affect the final quench in comparison with test 213A without deformed rods.

Finally, it can be observed in figure 72 the low degree or absence of fuel pellet fragmentation, which is not representative of fuel having undergone a pre-conditioning phase, and which rules out any relocation of fuel in the balloons during the test transient.

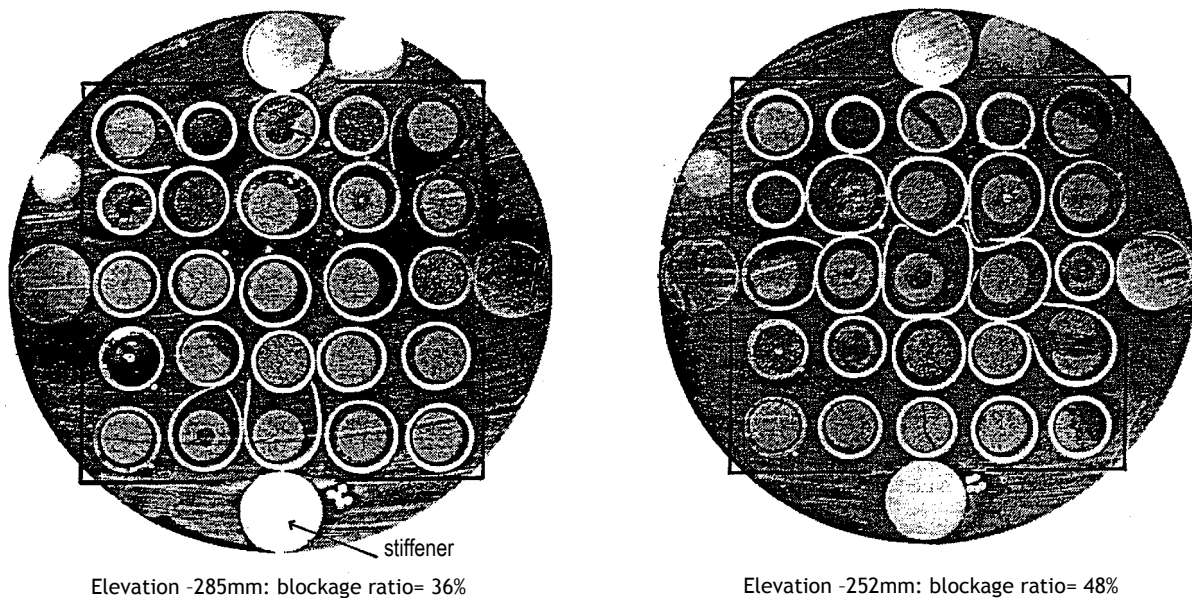


**Figure 72. PHEBUS test 215-P.
Metallographic cross sections at elevations 285 and 252 mm from fuel bottom.**

The particular conditions of the PHEBUS 215-P test make it possible for comparison with REBEKA 3 and 5 tests (see § 3.2.1) for which the maximum strain was slightly higher (64 and 75% respectively) but more axially spread, thus leading to a similar flow blockage ratio (52%). Compared with the NRU-MT3 test, disregarding the very large deformation of one rod in MT-3, the behavior of the inner rods in PHEBUS 215-P appears similar to that of the inner rods in NRU with respect to the coplanarity of the ruptures and the corresponding flow blockage ratio.

4.2.2.3.2 Test 215-R^[29]

Due to the disturbances to the thermal-hydraulics in the 215-P test, the transient characteristics of the test significantly deviated from those of the target transient as shown in figure 67. The 215-P test was thus followed by a series of tests that aimed at solving the problems encountered, particularly the early rewet of the bundle. This series was concluded by the 215-R test, which generally satisfied the features of the reference transient:

- First peak around 12 seconds, at 850 - 730 °C on the inner and outer rods respectively,
- Temperature drop of 150 to 250 °C after about 15 s,
- Heat-up ramp at 10 °C/s towards a plateau temperature of 1050 °C maintained for about 35 s,
- Progressive reflooding.

Figure 73 illustrates the temperature histories of fuel and cladding at mid-plane elevation for a non pressurized rod. In test 215-R, it should be noted that 3 rods (nr 2, 4 and 6) were unpressurized or slightly pressurized (1 or 5 bar in cold conditions) and that the rods 10, 15 and 18 appeared to have lost their initial pressurization. Finally, only 19 rods experienced a clad ballooning and rupture during the test transient.

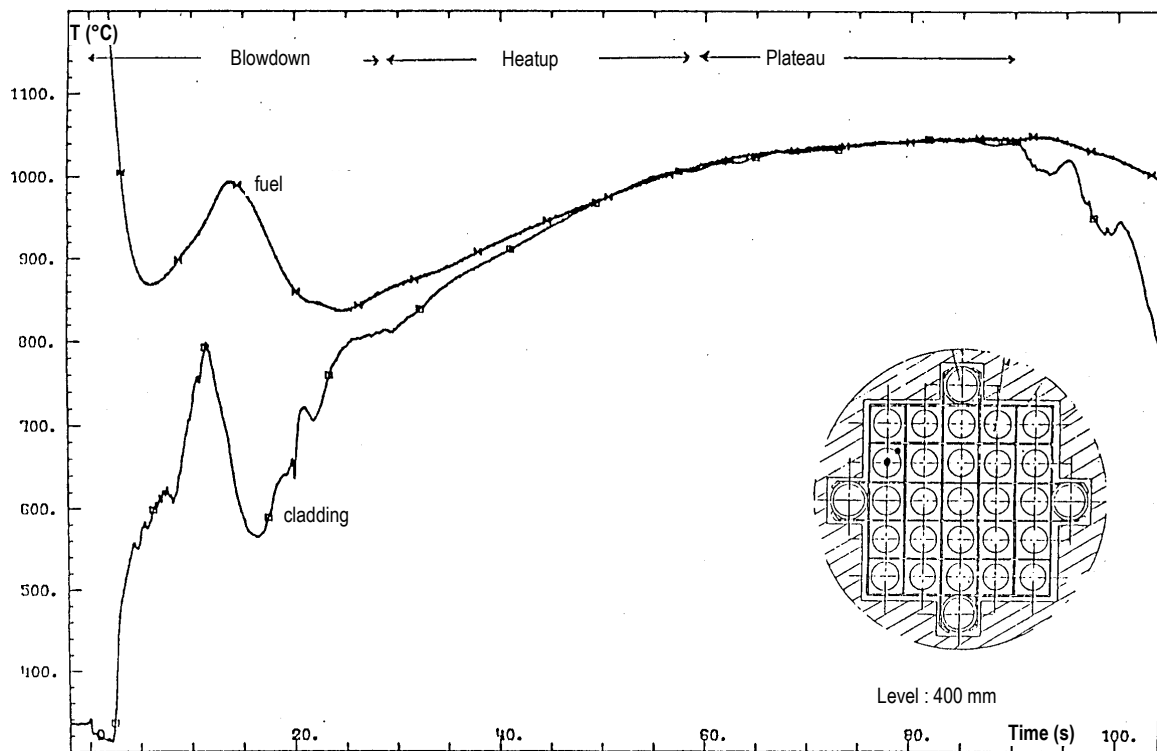


Figure 73: PHEBUS test 215-R - histories of clad and fuel temperatures on Rod 6.

Unfortunately, only a few direct temperature measurements in test 215-R were available on the pressurized inner rods, and the missing clad temperatures had to be evaluated from inverse thermomechanical calculations and cross-checking with available temperature measurements. Among those, the clad temperature on rod 18 exhibited a high level, 200 °C higher at the 1st peak than other measured temperatures; this temperature level can mostly be explained by the combined effects of the local power, the absence of a central hole in the fuel and the non deformation of the cladding (low internal pressure). It can be deduced from these analyses that the temperature at the 1st peak should have not exceeded 850 °C on the inner pressurized rods and about 800 °C on the outer pressurized rods, with about 50 °C uncertainty on these peak values. Under such conditions, it appears that even if the 1st peak temperature reached 900 °C for a few seconds, the fraction of transformed α phase should have remained very low and it can be considered that the 1st peak temperature excursion did not influence the thermomechanical behavior of the pressurized rods.

All ruptures of the pressurized rods occurred after 24 seconds in the adiabatic heat-up phase. Table 7 lists the burst strain and rupture time for the inner and outer rods. For inner rods, it should be pointed out that the lowest strain values correspond to the earliest ruptures, which indicates that the rupture conditions were met under a high temperature ramp rate (~ 25 K/s) without leaving much time for the development of large strain. For outer rods, the lower temperature level led to later ruptures, under a slightly slower ramp rate, which should have led to higher burst strain. The measured rupture strain, actually lower than that on inner rods, may be explained by the effect of the azimuthal temperature gradients around the cladding, which appeared to be more significant on outer rods, located between the hot inner rods and the cold shroud and peripheral structures.

Rod number	Level of rupture *	Burst strain (%)	Rupture time (s)	ΔP (MPa)	Comments
7	D	41	25.26		<u>Inner rods:</u> high dT/dt moderate ΔT_{az} high α -phase domain
8	C,D	49	25.8		
9	B,C	32	24.7		
12	C	40	25.2	6.2	
13	A	20	24.17	7.6	
14	C	42			
17	C	32	24.3		
19	D	44			
1	E	32			<u>Outer rods:</u> medium dT/dt large ΔT_{az} $\alpha+\beta$ two-phase domain
3	D	26			
5	C	30			
11	C	17			
16	E	32			
20	D	36			
21	D	30			
22	C	26			
23	F	30			
24	F	28			
25	D,E	39			

(*): A = 402 mm, B = 385 mm, C = 365 mm, D = 345mm, E = 322 mm, F = 302 mm from bottom of fuel

Table 7: rod burst conditions in the PHEBUS test 215-R.

Figure 74 provides a schematic map of the orientations of the ruptures, showing a clear trend in the rupture orientation towards the hot regions localized on the non pressurized rods 10 and 18. The map of axial positions of rod burst, provided in figure 75 together with that for test 215-P, shows that the ruptures in test 215-R occurred above the plane of maximum rod power, with the burst elevations spreading over 110 mm with 15 ruptures over less than 70 mm, thus with a slightly lower coplanar character than that in test 215-P. It is also worth pointing out that the axial extension of ballooned regions with more than 10% strain was slightly greater in 215-R, which corresponds to a flatter axial temperature profile in that test.

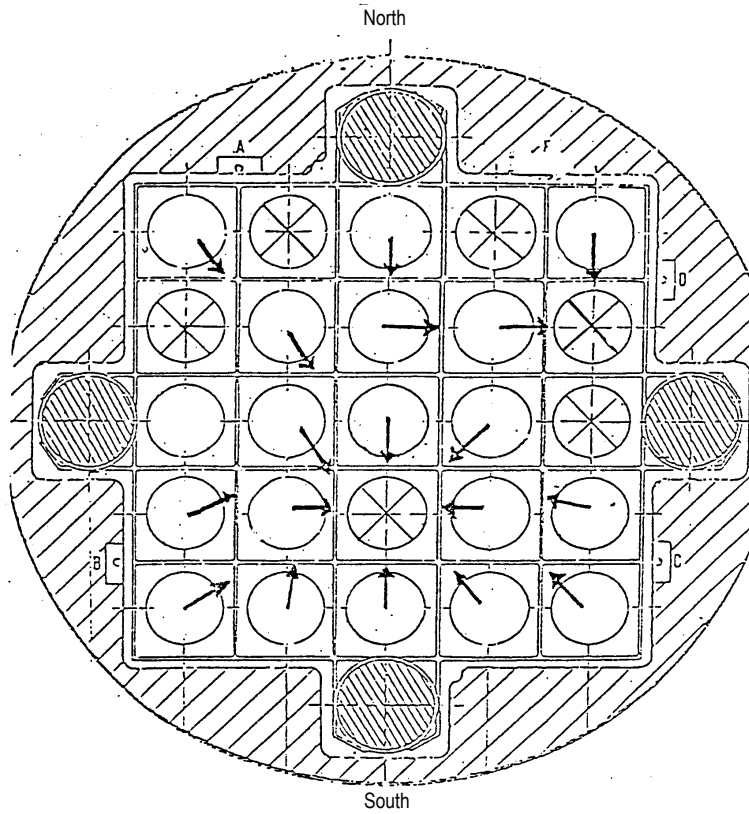


Figure 74: orientation of rod ruptures in PHEBUS test 215-R.

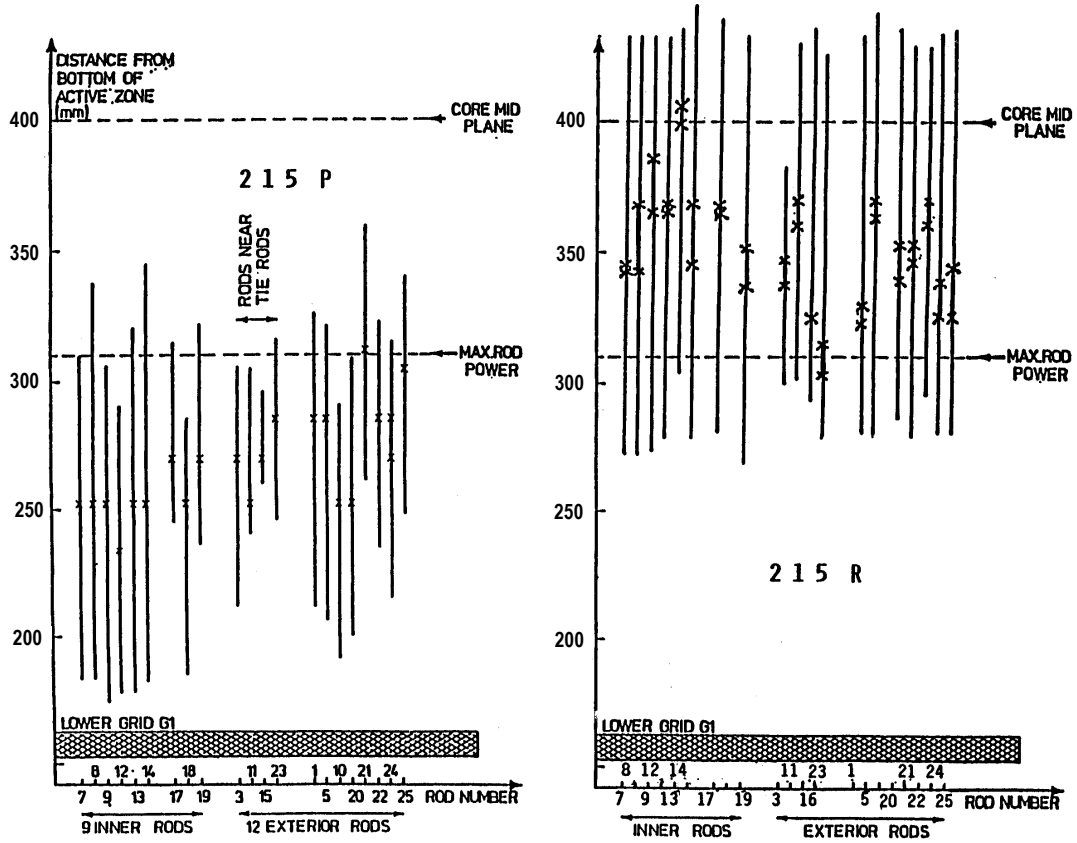
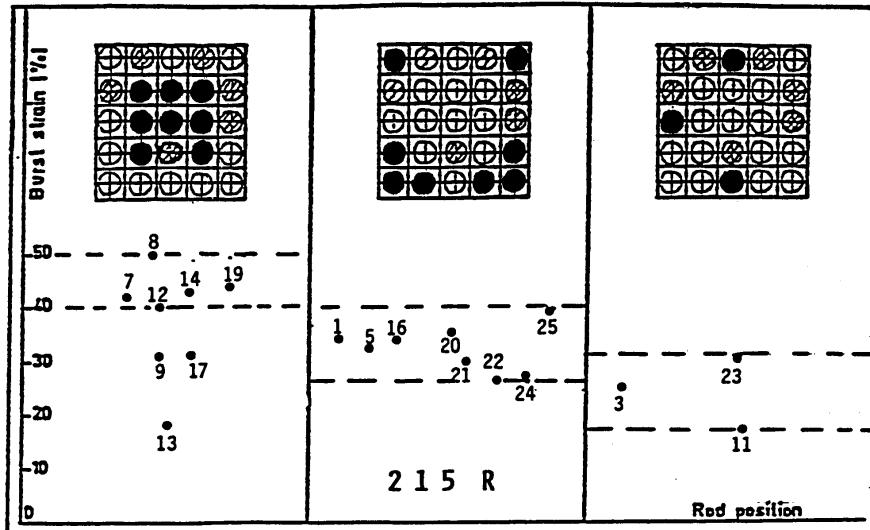


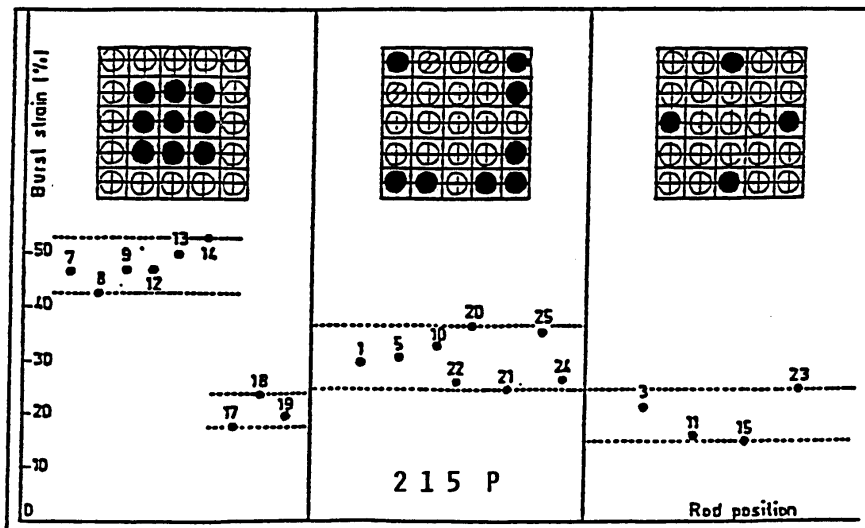
Figure 75: comparison of axial locations of ballooned regions (circumferential strain >10%) and burst positions in the PHEBUS tests 215-P and 215-R.

Comparison of burst strain, as done in figure 76, shows similar values for rods belonging to a same region:

- ◆ For outer rods, rod ruptures in tests 215-P and 215-R occurred under very similar conditions with regard to the temperature ramp rate and azimuthal temperature gradients.
- ◆ For inner rods, the most deformed ones ($40\% < \varepsilon < 54\%$) probably ruptured under similar conditions in both tests; ($\varepsilon < 30\%$). The rupture conditions were however different for the less deformed inner rods:
 - In test 215-P, the slightly deformed rods (nr 17,18, 19) are those in the south row that had been subjected to a large temperature gradient between the equatorial row and the outer rods (see explanation above);
 - In test 215-R, the least deformed rods (nr 9, 13, 17) are those that ruptured early (before 25 s), thus with a burst strain limited by the high temperature ramp rate.



(LOW INTERNAL PRESSURE FOR RODS 2, 4, 6, 10, 15, 18)



(LOW INTERNAL PRESSURE FOR RODS 2, 4, 6, 16)

Figure 76: comparison of burst strain according to rod position in the bundle for the PHEBUS tests 215-P and 215-R.

Remark:

In consideration of the 215-P and 215-R test results, it was decided to raise the 1st peak temperature at a higher value for the following tests in order to investigate the influence of a phase transformation of Zircaloy, during the temperature excursion, on the deformation and rupture behavior of the cladding.

4.2.2.3.3 Test 216

This test was characterized by temperature levels higher than those in the reference case: at 1st peak (920 to 1000°C on inner rods, 800 to 900°C on outer rods) as well as at the plateau temperature following adiabatic heat-up (1350°C).

The high ramp rate up to the 1st temperature peak resulted in early ruptures with limited burst strain, ranging from 15 to 30% for all of the inner or outer rods.

The high temperature at the plateau led to the significant oxidation of the Zircaloy cladding (75 and 62 μm oxide thickness on outer and inner surface respectively for Rod 9), leading to the considerable embrittlement of the cladding which experienced fracturing upon quenching.

4.2.2.3.4 Test 218 ^[30]

The temperature transient in test 218 more or less corresponded to target objectives with:

- A first temperature peak around 14 s, reaching 930 to 980 °C, thus slightly higher than the target temperature,
- A subsequent temperature drop, by 100 to 150 °C, thus slightly lower than expected,
- A subsequent rise of 12 K/s up to a plateau temperature around 1200 °C, overshoot on some TC measurements,
- A final slow cooling down to 700 °C followed by quenching.

Figure 77 shows the temperature histories over 30 s on the cladding of some inner rods at the hottest level.

The initial internal pressure of the rods was 3.35 MPa, except for rods 16 and 21 that were initially pressurized at 0.5 MPa, and rods 8 and 19 with low initial pressure.

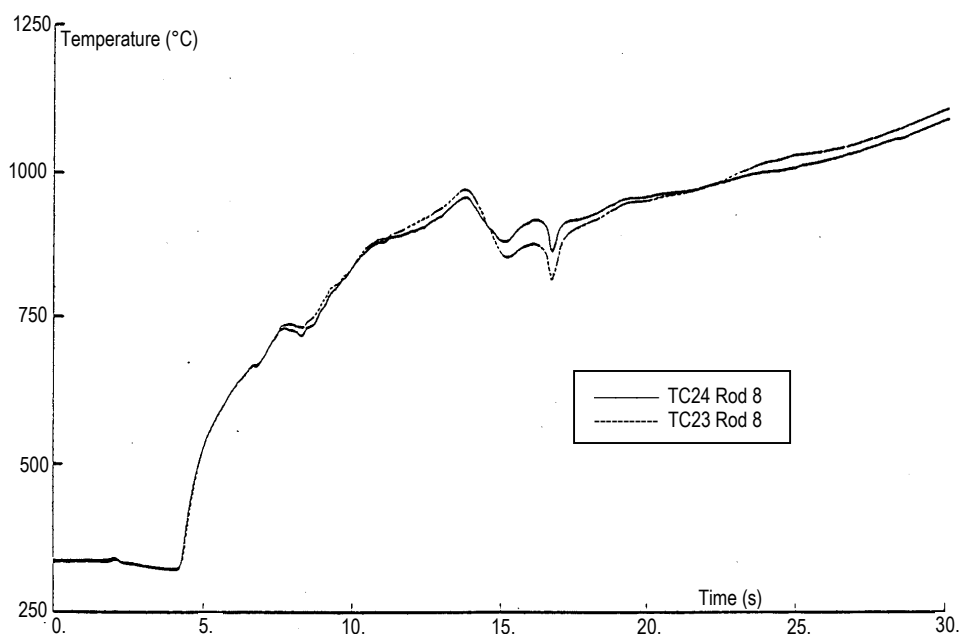
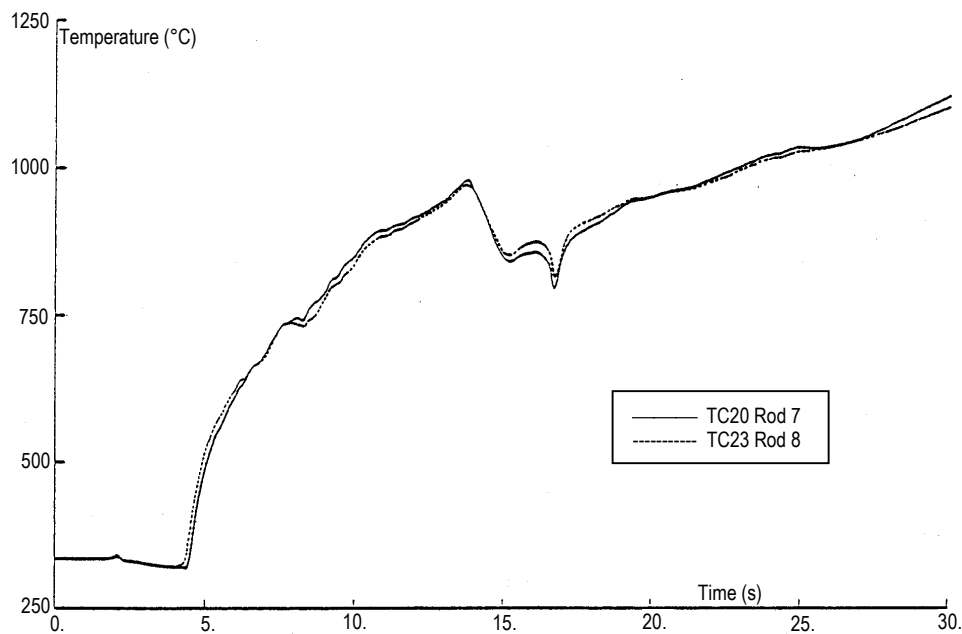


Figure 77: PHEBUS test 218 - history of clad temperatures measured at hottest level.

Cladding rupture and deformation and flow blockage ratio

For the pressurized inner rods, the cladding bursts occurred at the 1st temperature peak or during the subsequent drop, whereas most of outer rods burst later, around 23 s, during the so-called "adiabatic" heat-up. Thus, burst strain appeared rather low on inner rods (11 to 27%) and slightly greater on outer rods (12 to 36%) in spite of the azimuthal temperature gradients being greater on the latter. Burst elevations spread axially over 60 mm for the inner rods and over 80 mm for outer rods. Metallographic examinations performed after the test revealed an average orientation of bursts towards the bundle center, as displayed in figure 78.

The maximum flow blockage ratio, located at the experimental level + 316 mm from the fuel bottom, reached 24% for the inner rod subgroup and 38% for the outer rods ring.

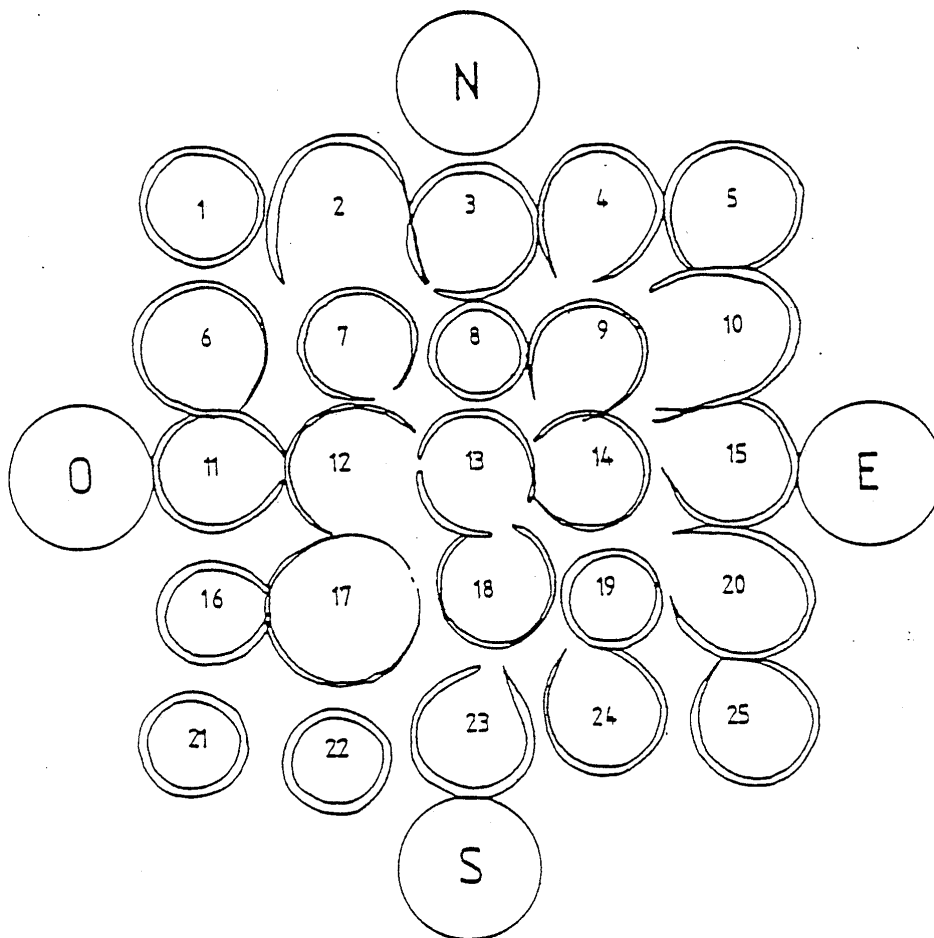


Figure 78: PHEBUS test 218 - view of burst strain of rods as projected in a same plane.

Oxidation

The post-test examination of the test bundle on 10 transversal cuts, concentrated over 214 mm and covering all the burst elevations, made it possible to determine the azimuthal distribution of the clad oxidation at different axial levels and to observe the oxidation microstructures obtained at different temperature levels. As a function of temperature, measured by available thermocouples, a fair consistency was observed in the measurements of zirconia thicknesses on rods in equivalent positions. On the undeformed Rod 8, the oxide thickness measured on the outer side reached 80 μm at the hot level (+ 314 mm), which is consistent with a plateau temperature having reached 1360°C. The development of a UO_2/Zr solid/solid interaction between fuel and clad was also observed on this rod at the same level, leading to the formation of an internal $\alpha\text{-Zr}$ layer. A spalling of the outer oxide layer was observed on several rods at different locations, which may indicate that the oxide layer formed on the inner Rod 13 at the hottest level should have exceeded 90 μm , the measured thickness of the inner oxide layer reaching 83 μm at this level.

Measurement of both microhardness radial profiles on some rod claddings and oxygen content profile by microprobe analysis on one rod cladding confirmed and complemented the visual microstructural observations obtained from metallographic examinations.

Last of all, it is worth mentioning that test 218 was chosen as the OECD International Standard Problem ISP-19, which will be discussed later in this document relative to the interpretation of LOCA test results.

4.2.2.3.5 Test 219 ^[31]

In order to avoid the early ruptures that occurred at the 1st temperature peak in test 218, test 219 differed from the previous test by a lower internal rod pressure (3 MPa versus 3.35 MPa in test 218). Among 25 rods, 21 were pressurized, with the 4 corner rods (Rod 1, 5, 20 and 25) unpressurized.

The test objective was to reproduce a temperature transient consistent with the reference scenario, with the following typical periods:

- A first temperature peak around 930 °C,
- A subsequent temperature drop to 800 °C,
- An "adiabatic" heat-up with clad ruptures around 890 °C in the $\alpha+\beta$ metallurgical state,
- A temperature plateau at 1200 °C maximum lasting long enough to reach an average oxidation of 17% on the inner rods,
- A prototypical reflooding phase: slow cooling down to 700 °C and final quenching.

The actual test scenario met the target objectives, with a 1st temperature peak at 930 ± 20 °C, followed by a temperature drop to 800 ± 30 °C and a subsequent heat-up towards the temperature plateau; this plateau phase was disturbed by an unexpected reactor scram, which induced a partial cooling; the maximum temperature during this phase reached 1330 °C. Figure 79 shows the temperature histories on an inner rod and outer rod at mid-plane. During the blowdown phase, the temperature histories show the same variations at all levels, except at the highest instrumented level (720 mm) where two successive early rewets occurred, as seen in figure 80.

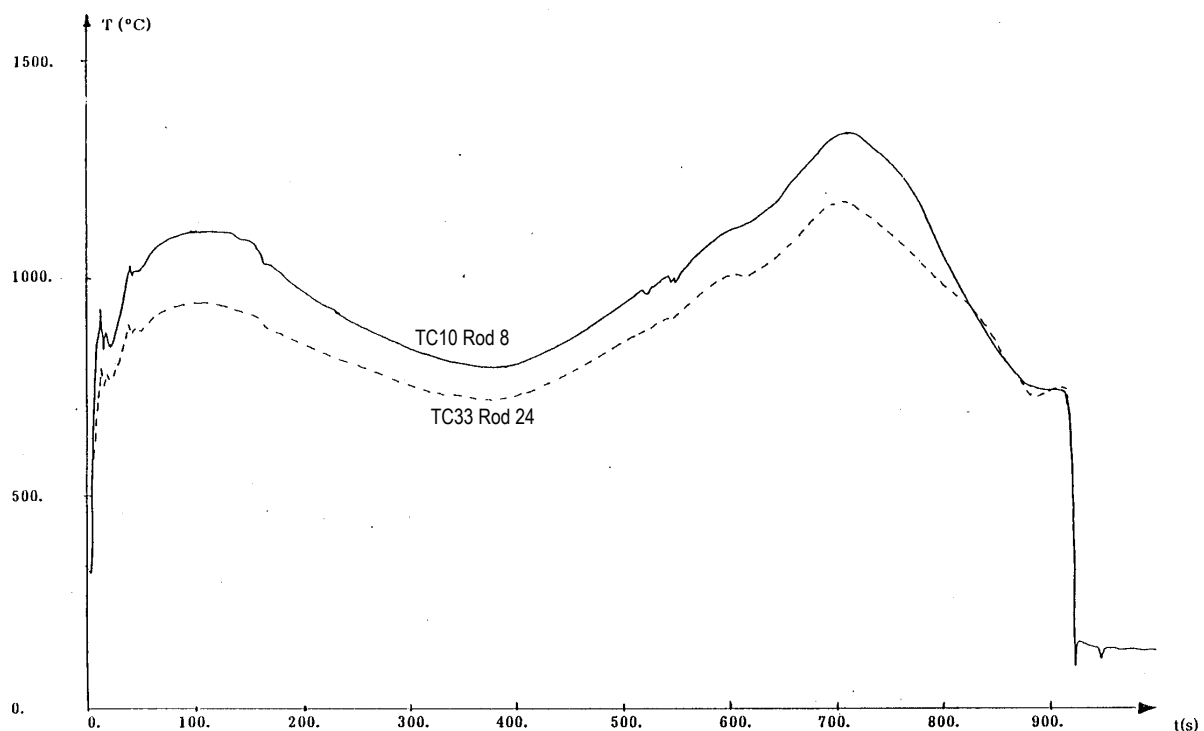


Figure 79: PHEBUS test 219 - history of clad temperatures measured at mid plane.

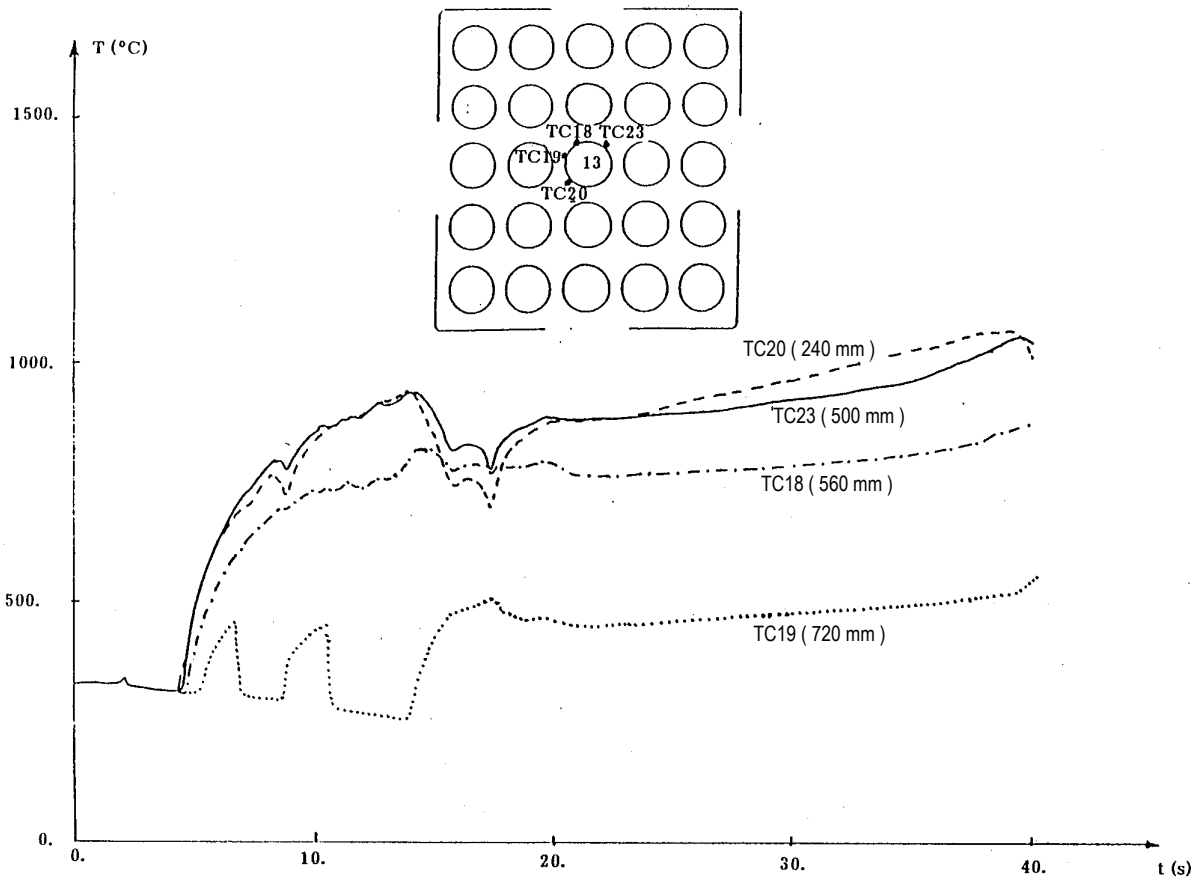


Figure 80: PHEBUS test 219 - history of clad temperatures measured on Rod 13 at different elevations.

Cladding rupture and deformation

The rupture time was directly determined only for rods instrumented with a pressure sensor and/or a TC in the plenum. Rupture was observed to occur between 23.8 and 25.4 s on the inner rods (except for Rod 19, at 35.8 s) and at 36.6 and 37.1 on the outer rods number 24 and 3. No rupture was thus detected at the 1st temperature peak (15 seconds).

The metallographic examinations that were carried out on a set of transversal cuts on the bundle show that the rupture elevations spread over 80 mm for the inner rods and only over 20 mm for the outer rods. The maximum strain measured in these examinations ranged between 18.6% and 46.2% for the inner rods and between 14.5% and 26.4% for the outer rods. This confirms the observation made in tests 215-P and 215-R pertaining to average strain that was lower on the outer rods than on inner ones, under the influence of greater azimuthal temperature gradients. The flow blockage ratio, which was not specified in the analysis report, should have remained limited seeing that the maximum value of the inner rod average strain did not exceed 25%.

Thanks to the high degree of available instrumentation in the test 219, it was possible to perform a refined study linking the rupture strain on inner rods with the azimuthal temperature differences as derived from different TC measurements. Over the 22-25 time interval, corresponding to the main phase of rod deformation, an average temperature difference ΔT was determined for the rods number 7, 9, 12, 14 and 19, then correlated with the maximum strain measured on these rods (see figure 81). The resulting correlation between rupture strain and azimuthal temperature difference was then successfully applied to different rods from tests 215-R and 218: for Rod 3 from test 218 (outer rod that ruptured during the adiabatic heat-up) the calculated rupture strain was thus 25% for a measured rupture strain of 27%.

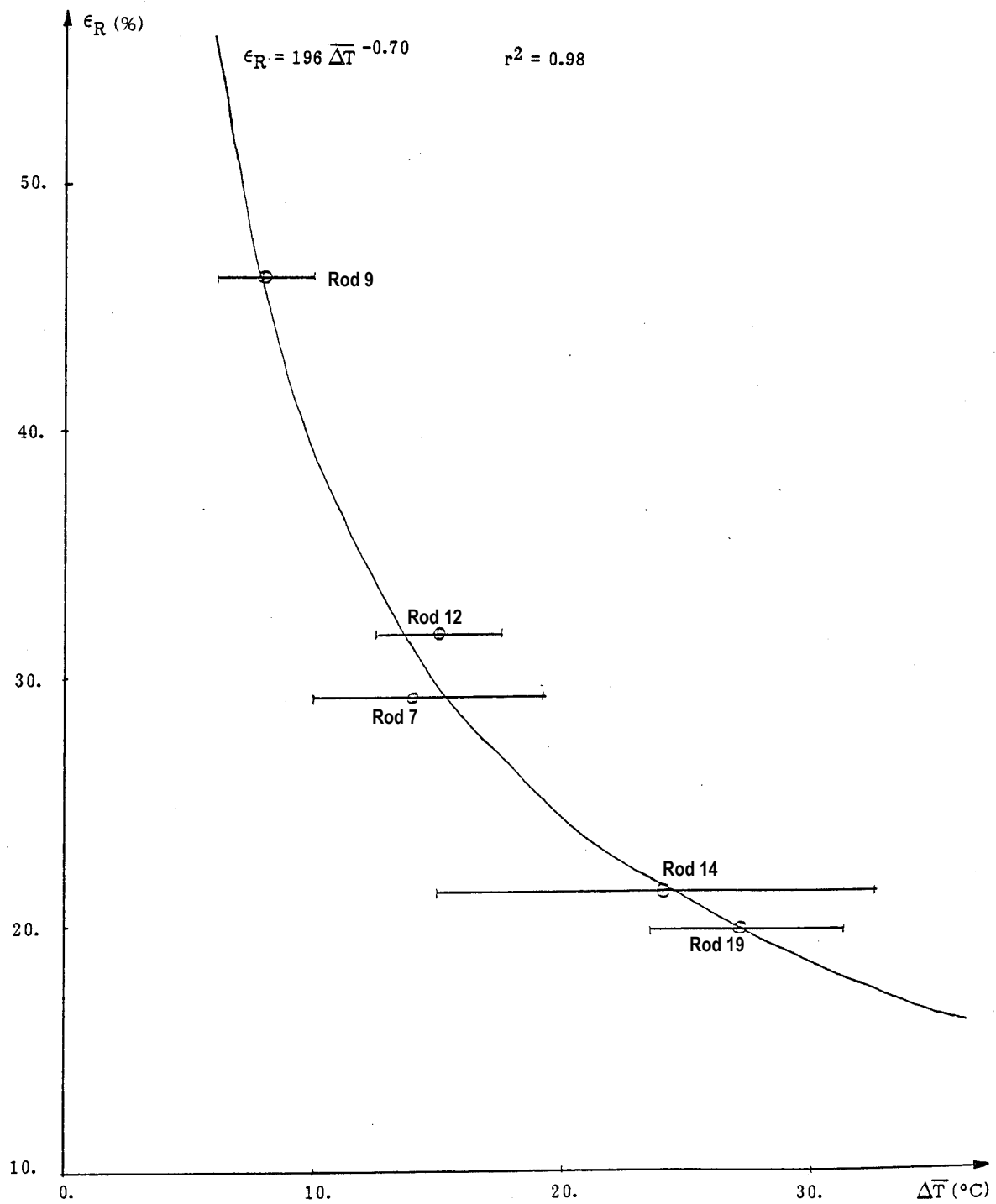


Figure 81: PEBUS test 219 - burst strain versus average azimuthal temperature difference in the 22-25 s time interval of the transient.

Oxidation

The metallographic examinations performed on a set of transversal cuts on the rod bundle revealed an unusual transversal displacement of the rods (see figure 82), as well as a loss of integrity on the clad of two rods (Rod 8 over about 80 mm and Rod 18 over 60 mm) which possibly occurred in regions embrittled by oxidation.

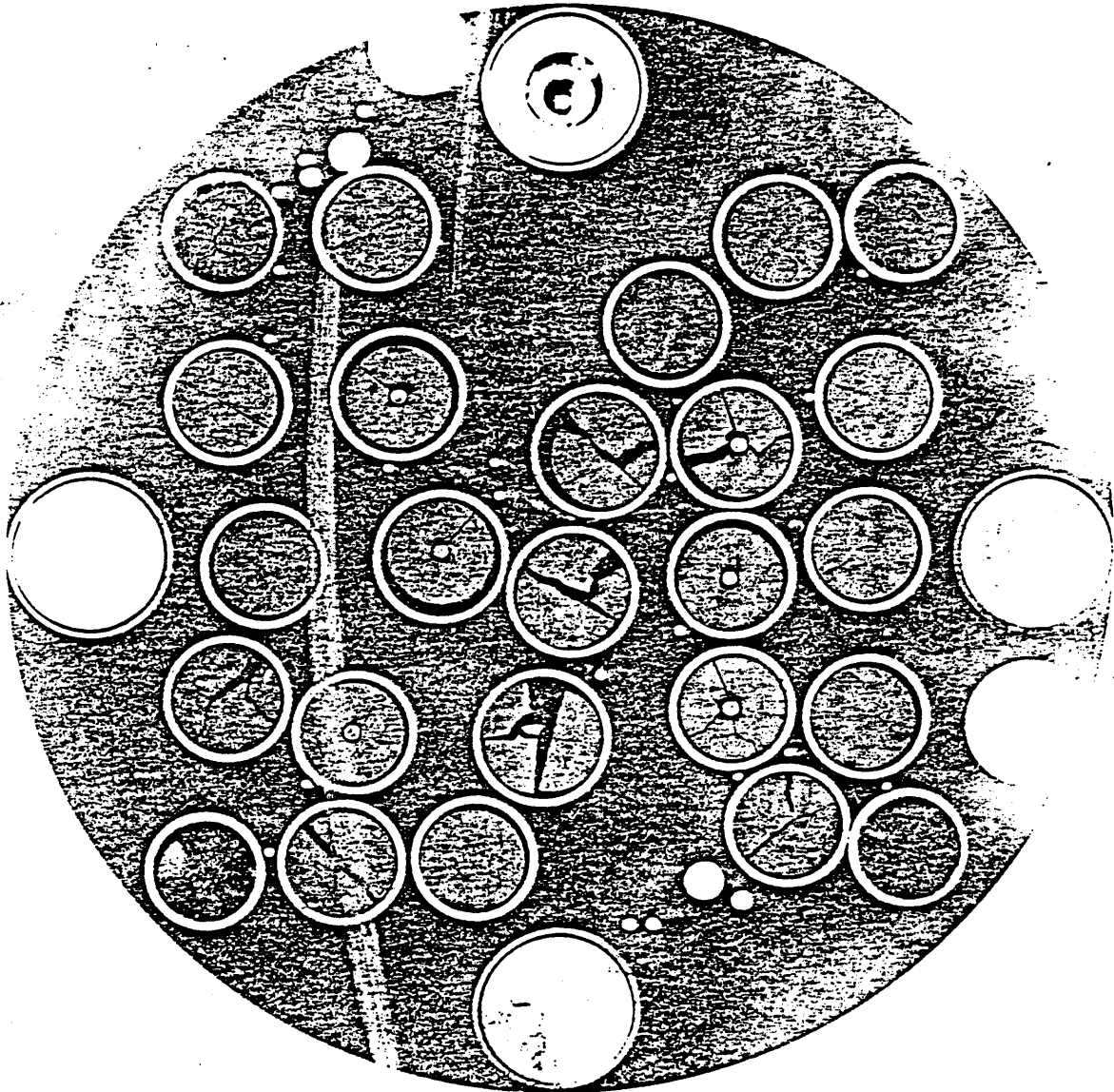


Figure 82: PHEBUS test 219 - metallographic cross section at elevation 437 mm from fuel bottom showing the radial displacement of rods

The measurements of oxide and alpha layer thicknesses at the hot level 322 mm (see Table 8), indicated values for the external oxide thickness ranging from 23 to 72 μm in bounding values for the inner rods, with average value per rod ranging from 31 to 55 μm ; the alpha layer thicknesses, were always slightly greater than the oxide thicknesses and followed the same distribution. It is worth remarking that the inner rods 12 and 13, which remained intact, were more oxidized than Rods 8 and 18: the evaluation of the oxidation rate with the average oxide thickness alone leads to values of 18 to 20% for Rods 12 and 13 and only 16 and 13% for Rods 8 and 18.

Level: 322 mm from bottom of fuel							Level: 402 mm from bottom of fuel					
Rod	Oxide ext. (µm)	Alpha ext. (µm)	Oxide/Alpha ext.	Oxide int. (µm)	Alpha int. (µm)	Oxide/Alpha int.	Oxide ext. (µm)	Alpha ext. (µm)	Oxide/Alpha ext.	Oxide int. (µm)	Alpha int. (µm)	Oxide/Alpha int.
3							32-38 35	33-50 40	0.8	9-11 10	35-41 37	0.27
7	23-51 36	26-67 47	0.77	24-50 37	27-79 47	0.78						
8	40-55 49	40-83 62	0.79	38-53 44	57-83 67	0.65	37-50 41	35-72 63	0.65	18-48 36	32-82 56	0.63
9							26-47 36	25-54 35	1.04	13-25 19	15-41 27	0.7
12	41-72 53	57-76 66	0.8	38-64 49	63-72 67	0.72						
13	55-56 55	78-88 82	0.67	58-63 60	70-87 79	0.75	51-70 57	43-52 47.5	1.2	12-20 17	28-36 31.5	0.5
14	35-46 42	40-50 46	0.92	38-41 39	47-56 51	0.76	34-48 41	23-50 38	1.07	13-24 19	23-40 32	0.6
18	39-45 39	33-51 41	0.95	30-41 35	29-52 40	0.87						
19	25-45 31	26-70 39	0.79	23-43 32	28-65 40	0.80	29-42 35	36-65 46	0.76	6-13 8	38-54 46	0.17
20							14-22 18	21-29 24	0.78	8-18 12	16-29 22	0.58
23	11-28 17	19-28 23	0.73	12-28 16	15-27 22	0.73						
24	10-17 12	12-24 20	0.60	11-16 14	13-27 19	0.68	15-19 16	18-41 28	0.57	6-15 10	21-37 29	0.34

Note: X-Y = range of measured values
Z = average value

Table 8: thicknesses of oxide and α -Zr layers measured on PHEBUS 219 test rods.

4.2.2.4 Main findings gained from the thermo-mechanics in the PHEBUS/LOCA tests

A summary of the temperature transients for the five PHEBUS tests described in the previous section is shown in figure 83. On each temperature curve, black dots indicate the time range during which the ruptures occurred.

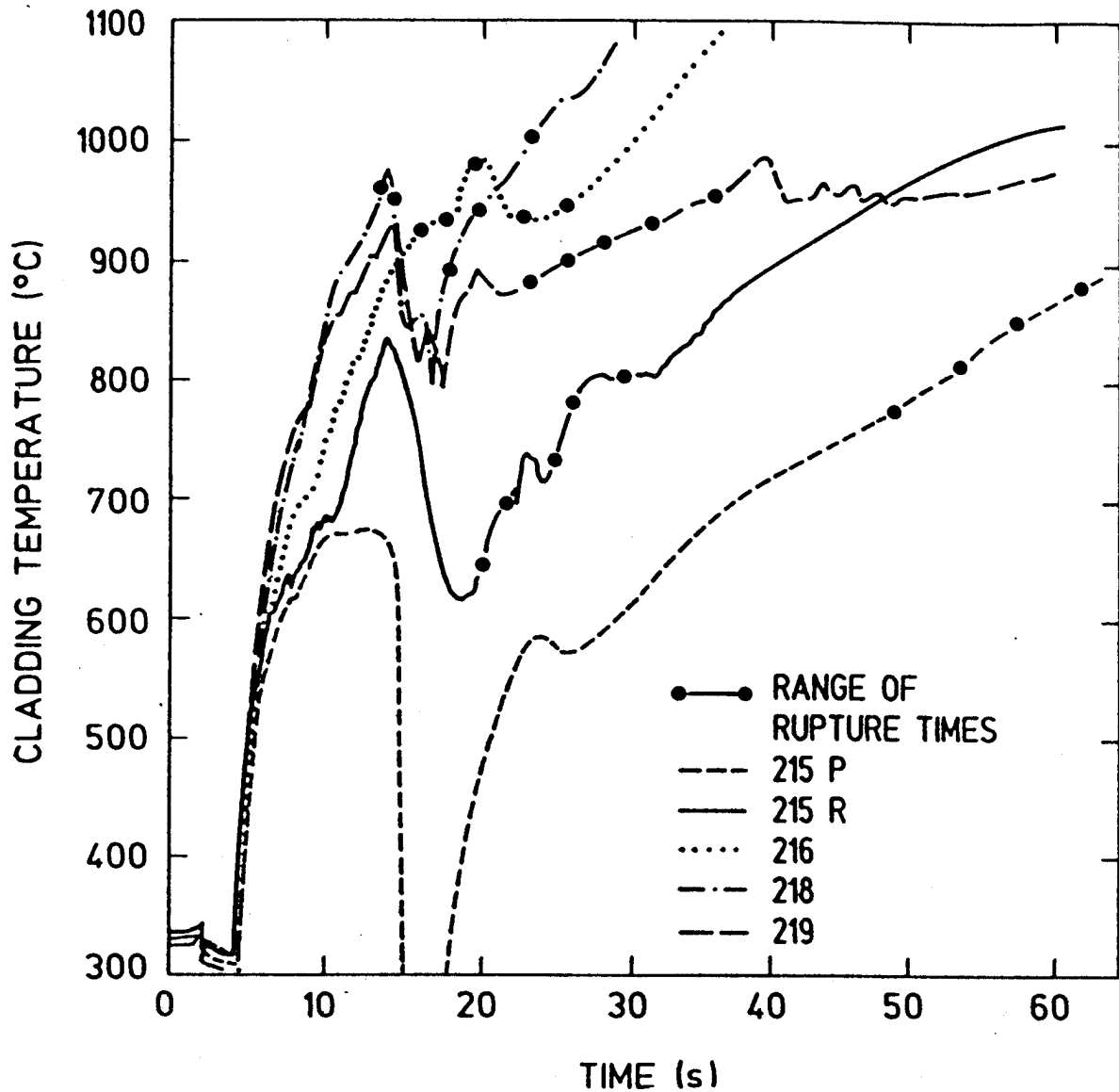


Figure 83: temperature histories in the PHEBUS LOCA tests.

Table 9 summarizes the main thermomechanical results regarding the rod ruptures and strains observed in these tests. From this table, the inner and outer rods exhibit a distinct overall behavior, which is reflected by the small standard deviation on the rupture strain for each group of rods.

Test number (rod pressure)	Rod group	Burst time (s)	Burst temperature (°C)	Orienta- tion of ruptures	Burst strain			T at first peak (°C)	Mechanical interaction
					Range (%)	Mean (%)	Std. Dev (%)		
215-P (40 bar)	inner	50 - 66	840	center	20 - 54	38	13	No	Yes
	outer	65 - 150	? - 830	center	15 - 38	26.6	6		
215-R (40 bar)	inner	20 - 25	800 - 860	center	20 - 50	38	9	800 - 860	Yes
	outer	25 - 30	760 - 830	hot pins	15 - 35	29.6	5.5	760 - 830	
216 (40 bar)	inner	14.6 - 17	920 - 1000	center	20 ? 30	-	-	930-1000	No
	outer	18.5 - 26.4	800 - 860	center	16 - 31	23.6	5	760 - 830	
218 (40 bar)	inner	11.5 - 13	900 - 1000	center	14 - 27	20	5	930 - 980	No
	outer	15 - 26	820 - 900	center	15 - 38	26	6	860 - 930	
219 (40 bar)	inner	21 - 34	850 - 950	center	19 - 46	28	9	910 - 950	No
	outer	33 ? 36	820 ? 880	?	14 - 27	20	4	850 - 910	

Table 9: thermo-mechanics of the PHEBUS LOCA tests.

For the *inner rods*, the ruptures occurred in the α -phase domain for tests 215-P and 215-R and in the mixed $\alpha+\beta$ phase domain for tests 216, 218 and 219. The rupture strain was thus significantly higher in tests 215-P and 215-R than in the other tests. They were however very close in these two tests despite the significant difference in temperature ramp rates in the ballooning phase (7 K/s compared to 20 K/s respectively). This can be explained by the fact that strain was limited by the large azimuthal temperature differences in test 215-P, whereas the limiting effect in 215-R was mainly the rapidity of the temperature ramp. For the three following tests, where bursting of the inner rods occurred in the mixed phase domain, different adverse effects acted simultaneously on the strain level:

- An increase in β -phase content limits the rupture strain,
- A rapid temperature rise also limits the rupture strain while delaying the $\alpha \rightarrow \beta$ phase transformation, thereby reducing the β -phase content which acts in opposite way.

The application of phase change kinetic models to the three tests 216, 218 and 219 showed that significant departure from equilibrium phase fractions was obtained in these tests, ranging from almost no $\alpha \rightarrow \beta$ transformation at rupture in test 216 and 218 to a maximum of 25% phase transformation in test 219. Owing to the effect of β phase fraction alone, lower strain could have been expected for the test 219 rods; observation of an opposite result led to the conclusion that the effect of the temperature ramp rate (lowest in test 219, compared to test 216 and 218) was the dominant factor.

For the *outer rods*, lower burst strain was generally observed with respect to that of the inner rods. This result was mainly attributed to the effect of azimuthal temperature difference, larger on outer rods owing to the influence of cold outer structures, particularly in tests 215-P and 215-R where these temperature differences were more pronounced. This effect is consistent with the orientations of the ruptures, which were found to be directed either towards the center of the bundle (215-P, 216, and 218) or towards some hotter non-pressurized rods (215-R and 219). These orientations underline the importance of radiative transfers between rods and structures on the appearance of "hot spots", which limit the deformation by the "hot side straight effect". In the particular case of test 218, the very rapid temperature ramp led to the rupture of the inner rods at the 1st temperature peak with low burst strain, whereas the outer rods, which ruptured later, exhibited a larger mean burst strain.

In summary, the rod thermomechanical behavior in the PHEBUS tests appeared to be influenced by different phenomena, which may be classified according to their relative order of importance:

- a) Temperature transient kinetics,
- b) Azimuthal temperature differences,
- c) $\alpha \rightarrow \beta$ phase change kinetics.

The accurateness of the prediction of such test results by computer codes thus highly depends on the capability of the codes to more or less accurately represent the above-mentioned phenomena.

5 ANALYSIS OF THE RESULTS DATABASE

Within the limited framework of this study, it was not possible to perform an exhaustive review of all the analytical work that has been carried out in relation to the different experimental programs described in the previous sections. Thus, the review of analytical work was limited to the examination and discussion of the main outcome from the following summary reports:

- The well-known NUREG-630 report which recommends a set of correlations for the evaluation of clad swelling and rupture and the resulting flow blockage based on a large database of results from several important experimental programs. The limitations of these correlations will be indicated, as well as the outcome of additional results obtained after the NUREG-630 report was issued.
- The final comparison reports of calculations performed within the framework of the international standard problems ISP-14 and ISP-19 that were conducted on the REBEKA-6 and PHEBUS-218 respectively.
- The summary report of interpretative work carried out at IPSN on the PHEBUS LOCA tests.

5.1 *The NUREG-630 database and models*

During the extensive 1972-73 ECCS Rulemaking Hearing, which led to the issuance of the ECCS acceptance criteria contained in 10 CFR 50.46 and Appendix K in late 1973, it was recognized that significant uncertainties did exist as to the prediction of the fuel rod behavior under LOCA conditions with the models used by U.S. fuel manufacturers. Therefore, the Commission directed the AEC's research office (now the NRC ONRR) to undertake a wide confirmatory research program on cladding behavior under LOCA conditions. This program mainly addressed the aspects of clad swelling/flow blockage, Zircaloy oxidation by steam and the resistance of oxidized claddings to quench and post quench loads.

Although not all research programs were completed, it was considered in 1980 by NRC that sufficient information had been collected, suggesting improvements be made to licensing models. In this respect, the NUREG-630 report^[32] was issued containing all relevant data and describing the evaluation of such data to obtain a set of correlations making it possible to calculate:

- The cladding rupture temperature,
- A bounding value for the circumferential burst strain,
- A bounding value for the maximum flow blockage ratio that can occur in a rod assembly after clad swelling and rupture.

It should be underlined that these correlations were developed within the perspective of Appendix K, in which requirements state that the models used for safety evaluation shall not underestimate the clad swelling and rupture. They were therefore intended to be somewhat conservative, particularly with respect to the maximum flow blockage.

A critical analysis of the NUREG-630 models has been carried out^[33] prior to the introduction of the total elongation correlation in the fuel behavior model of the CATHARE code.

5.1.1 Database

In terms of establishing the database used to derive correlations, the NUREG-630 authors were concerned about being sufficiently conservative while selecting "realistic" tests to provide data that were as representative as possible of the behavior of actual fuel rods in a reactor. In this respect, out-of-pile tests under direct or external heating, such as the EDGAR tests at CEA, were not considered prototypical in that they were characterized by low azimuthal temperature differences, consequently leading to unrealistically high burst strain. Only experiments under aqueous atmospheres and with either nuclear heating (in-reactor) or indirect internal electric heating (out-of-pile) were selected to be integrated into the reference database. The selected data thus came from the following test series:

- **FRF** in-pile tests (in the TREAT reactor) on 7-rod bundles under a steam atmosphere with a high temperature ramp (> 25 K/s) (data reference A in NUREG-630);
- **MRBT** out-of-pile tests on single rods with an unheated shroud under a steam atmosphere with a high temperature ramp (> 28 K/s) (data reference B in NUREG-630);
- **MRBT** out-of-pile tests B1 to B3 on 16-rod bundles with a heated shroud (except for B2) under a steam atmosphere with a 10 K/s or 29 K/s temperature ramp (data reference C in NUREG-630);
- **REBEKA** out-of-pile tests on single rods with an unheated shroud under an air or steam atmosphere with an intermediate temperature ramp (11 K/s) (data reference D in NUREG-630);
- In-pile tests in the **FR2** reactor on single rods under a steam atmosphere with temperature ramps ranging from 7 to 20 K/s (data reference E in NUREG-630);
- **MRBT** out-of-pile tests on single rods with an unheated shroud under a steam atmosphere with a low temperature ramp (< 10 K/s) (data reference F in NUREG-630);
- **REBEKA** out-of-pile tests R1 to R3 on 9-rod bundles with a ring of non pressurized rods and an unheated shroud under a steam or mist atmosphere with a low temperature ramp (7 K/s) (data reference G in NUREG-630);
- **FABIOLA** out-of-pile tests on single rods with a heated shroud under a steam atmosphere with a low temperature ramp (3 to 11 K/s) (data reference H in NUREG-630);
- **MRBT** out-of-pile tests on single rods with a heated shroud under a steam atmosphere with temperature ramps ranging from 0 to 28 K/s (data reference I in NUREG-630);
- **REBEKA** out-of-pile tests on single rods with a heated shroud under a steam atmosphere with temperature ramps ranging from 1 to 38 K/s (data reference J in NUREG-630);
- **BCL** (Battelle Columbus Laboratories) out-of-pile tests on fresh or irradiated single rods under a steam atmosphere with temperature ramps ranging from 6 to 34 K/s (data reference K in NUREG-630);
- **JAERI** out-of-pile tests on 49-rod bundles with a heated shroud under a steam atmosphere with a low temperature ramp (<8 K/s) (data reference L in NUREG-630).

5.1.2 Correlations in NUREG 630

5.1.2.1 Rupture temperature

The correlation was developed by Chapman at ORNL based on MRBT tests with an unheated shroud. It expresses the rupture temperature as:

$$T_R = 3960 - \frac{20.4 \sigma_c}{1+H} - \frac{8.51 \cdot 10^4 \sigma_c}{(1+H) + 27.9 \sigma_c}$$

with

T_R : rupture temperature (in °C)

σ_c : engineering hoop stress = $\Delta P r_0 / e_0$ (in kpsi)

H : ratio of the heating rate dT/dt to 28 °C/s with $0 < H < 1$ (saturation of the ramp-rate effects is assumed for $dT/dt > 28$ °C/s)

The clad rupture is supposed to occur at the time and location when the temperature first exceeds the value of T_R in the course of the transient.

The particular form of this correlation is worth remarking, with the use of the engineering hoop stress σ_c , which is a variable easily derived from experimental conditions, but which does not include the instantaneous strain unlike the true stress $\sigma_v = \Delta P r / e = \sigma_c (1+\epsilon)^2$ which is used, for instance, in the EDGAR rupture criterion.

Figure 84, which plots the points of the database along with the above correlation for the three most frequent ramp rates used in the experiments, shows that most of the data is found between the curves corresponding to low and high ramp rates. The data deviating the most from the major body are those from the FRF in-pile tests (up-right open triangles, low stress values), which is probably due to the large uncertainty in the temperature measurements. Data from the REBEKA tests with a heated shroud (closed squares) are also found above the 28 K/s correlation; for these data points, the difference has been attributed by NUREG-630 authors to the use of isobaric testing conditions rather than constant gas-inventory testing conditions as found in ORNL tests.

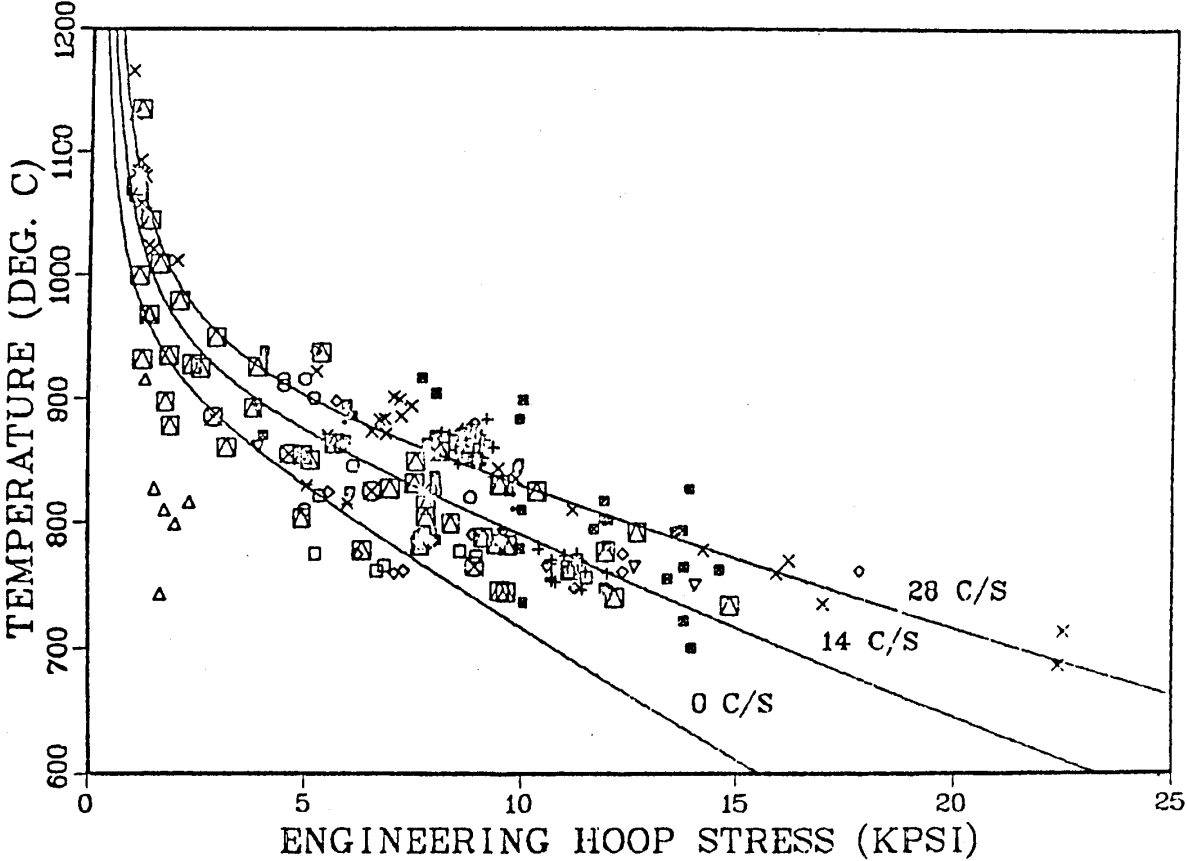


Figure 84: ORNL correlation of rupture temperature as a function of engineering hoop stress and temperature ramp rate from internally heated Zircaloy cladding in aqueous atmospheres.

5.1.2.2 Burst strain

The deformation at the rupture point (burst stain) depends in a complex way on different variables such as temperature, hoop stress, ramp rate and several other parameters including local temperature differences, the metallurgical state and the oxidation ratio of the clad material.

Figure 85 plots the burst strain as a function of the rupture temperature for the whole database selected in NUREG-630 and shows significant scattering of the data due to both experimental uncertainties - particularly temperature measurements - and the influence of other variables mentioned above.

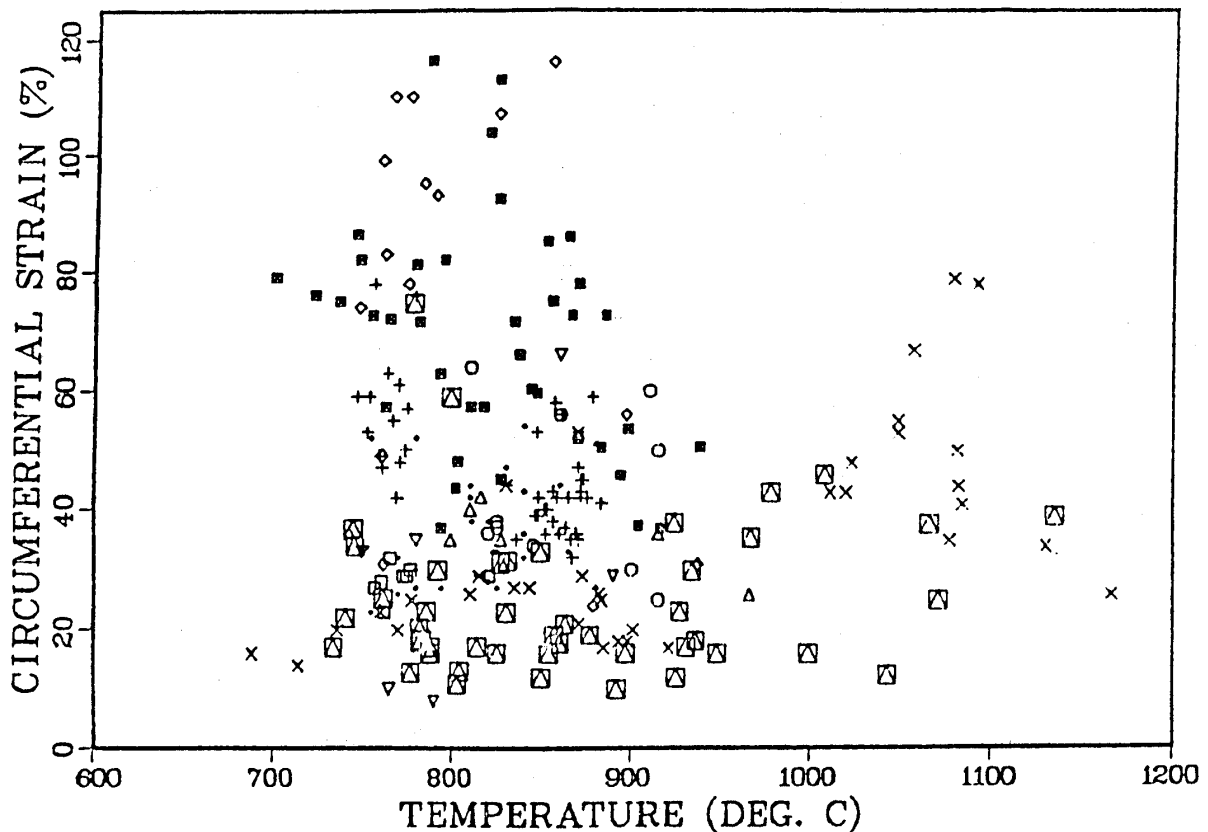


Figure 85: maximum circumferential strain as a function of rupture temperature for internally heated Zircaloy cladding in aqueous atmospheres.

Referring to the results of ANL deformation tests on short Zircaloy samples directly heated with different ramp rates under aqueous atmospheres^[34], the NUREG-630 authors chose to retain the shape of the ANL curves $\epsilon_{rup} = f(T_{rup})$, showing several deformation peaks, with one peak occurring in the alpha phase domain around 800°C and another in the high temperature beta phase around 1050°C, with an important deformation valley between these peaks around 925°C. Based on this shape, two correlations were recommended: one for the slow ramp rates (<10°C/s) (see figure 86) and the other for high ramp rates (> 25°C/s) (see figure 87).

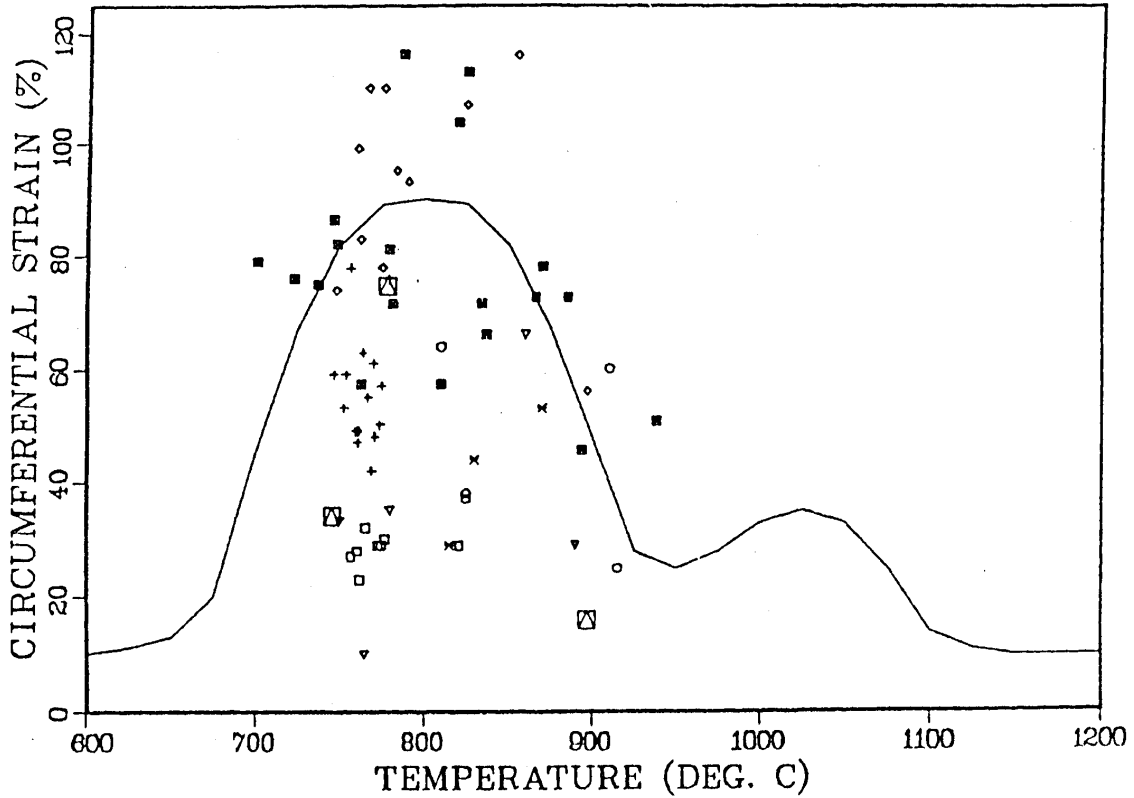


Figure 86: maximum circumferential strain as a function of rupture temperature for internally heated Zircaloy cladding in aqueous atmospheres at heating rates $\leq 10^\circ\text{C/s}$.

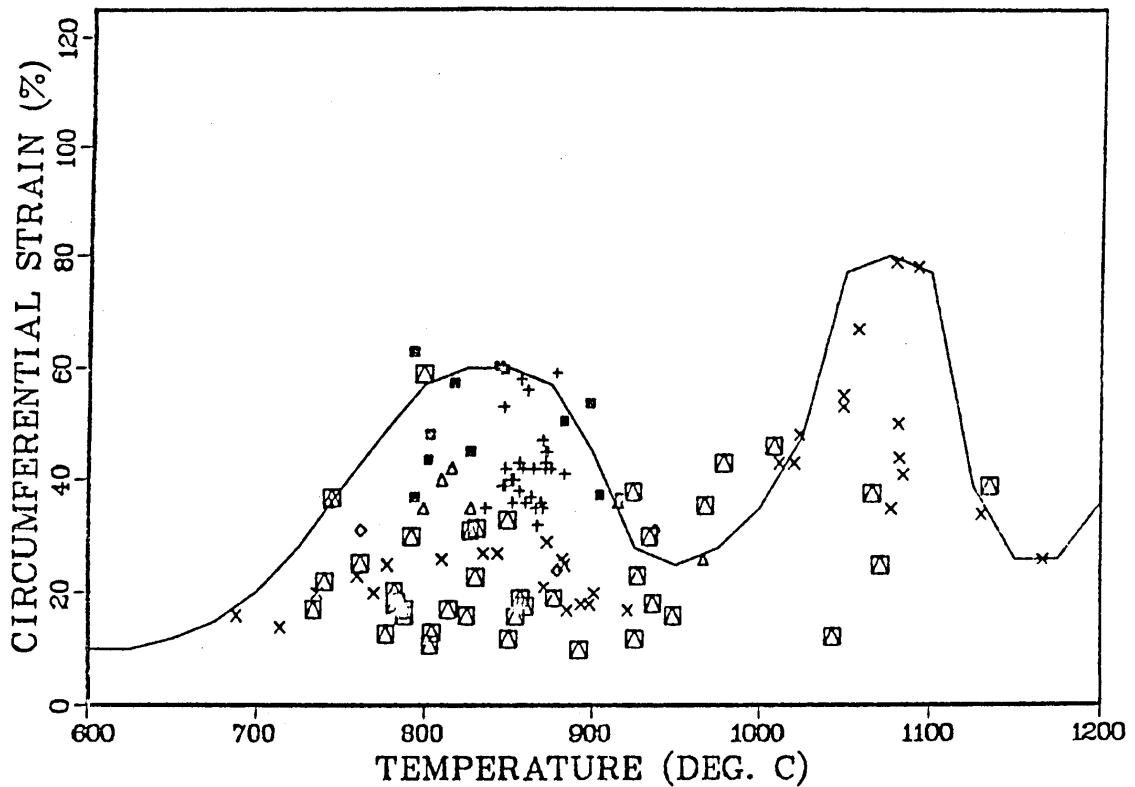


Figure 87: maximum circumferential strain as a function of rupture temperature for internally heated Zircaloy cladding in aqueous atmospheres at heating rates $\geq 25^\circ\text{C/s}$.

Examination of these figures led to the following comments:

Slow-ramp (figure 86)

The positioning of the alpha-phase peak at 800°C with an assigned value of 90% within the cluster of data may appear arbitrary; the authors justified it with the following considerations:

- Most of the low strain data (<30%), such the ORNL single-rod unheated-shroud data (□ symbol, ref. F in NUREG-630), were considered poorly representative due to the test features known to reduce the burst strain.
- Conversely, some of the high strain data (>90%) from the ORNL and REBEKA single-rod tests with a heated shroud (◇ and ■ symbols respectively, ref. I and J in NUREG-630) may have corresponded to test conditions equivalent to external heating (in furnace), exaggerating burst strain by maintaining small local temperature differences; thus, an average value was chosen among the results from these tests.

It is to be noticed that the alpha-phase peak bounds the burst strain of rods from the bundle test MRBT-B3 (+ symbol, ref. C in NUREG-630) and the average burst strain of the inner rods in the REBEKA bundle tests R1 to R3 (* symbol, ref. G in NUREG-630).

The highest temperature data point is located near 950°C and it appears that the beta-phase peak included in the slow-ramp curve was not supported by data from the NUREG-630 database. The authors indicated that this peak had been determined on the basis of the corresponding peak in the fast-ramp curve by evaluating the hardening effect of clad oxidation for a slow ramp, and by referring to the previously mentioned ANL work and other rod burst data. However, with the availability of new complementary data, the same authors did recognize^[35] as early as 1981 that the slow-ramp correlation in the NUREG-630 report was significantly non conservative above 950°C, as clearly shown in figure 88. The model derived from the single-rod heated-shroud REBEKA tests confirmed this non conservatism of the NUREG-630 slow-ramp curve (see figure 89) and provided an alternative for the evaluation of burst strain in that temperature domain.

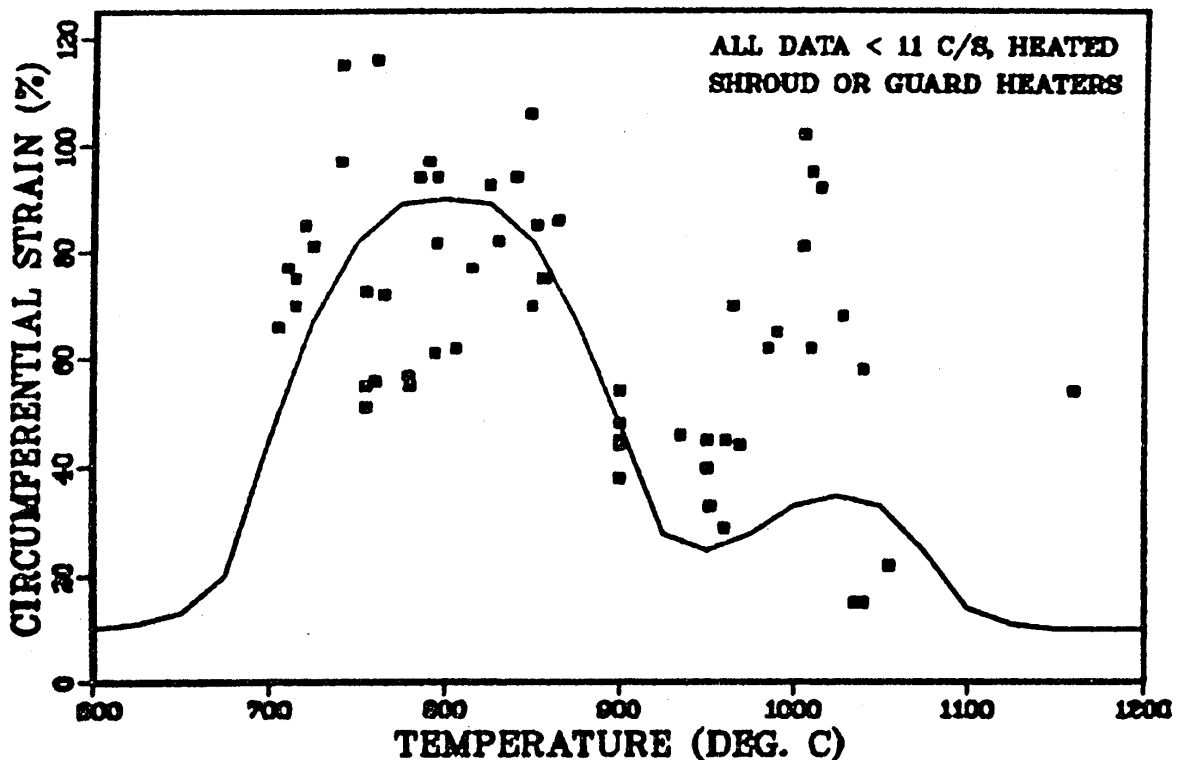


Figure 88: slow-ramp burst strain correlation from NUREG-630 and data reported after NUREG-630 was published.

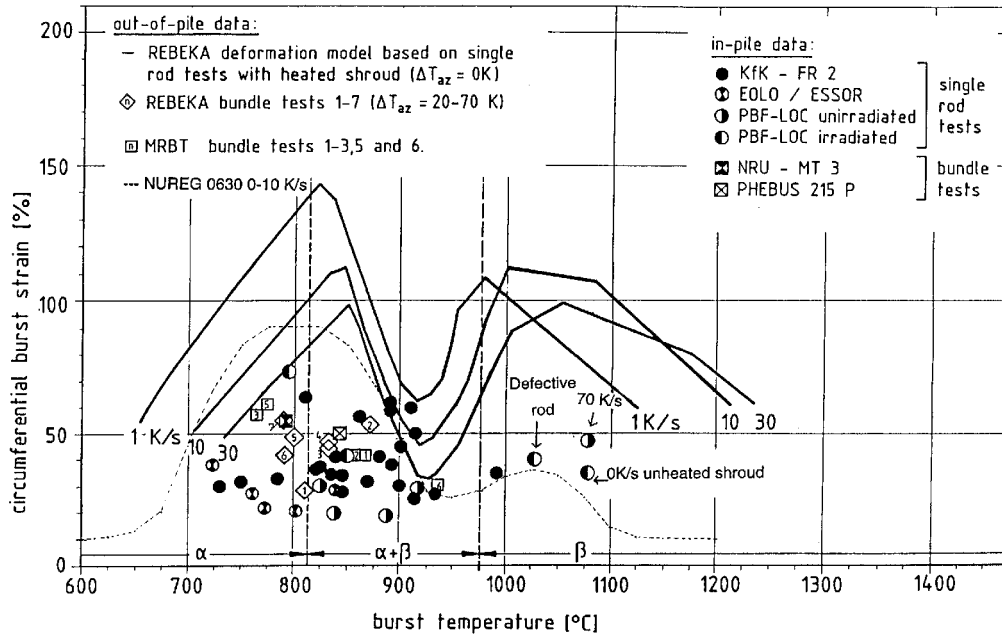


Figure 89: burst strain versus burst temperature of Zircaloy claddings. Comparison of out-of-pile and in-pile data. REBEKA model vs. NUREG-630 slow ramp.

Fast-ramp (figure 87)

The shape of the curve is the same as that for the slow-ramp, with a 60% strain peak set between 825 and 850°C and an 80% strain peak in beta-phase at 1075°C. Data from Battelle tests (⊠ symbol, ref. K in NUREG-630) look scattered with a tendency towards low strain. The detailed analysis carried out in [33] showed that the recommended curve bounds almost all data from single-rod and bundle tests, with a heated or unheated shroud, up to 950°C, but only the single-rod unheated-shroud data for higher temperatures. However, it should be noticed that the influence of an unheated shroud is less effective than in slow-ramp tests, as a high temperature ramp does not leave enough time for large azimuthal temperature differences to develop before burst. Comparison of the NUREG-630 fast-ramp curve with that derived from the REBEKA tests (see figure 90) still shows an underestimation by the former above 940°C.

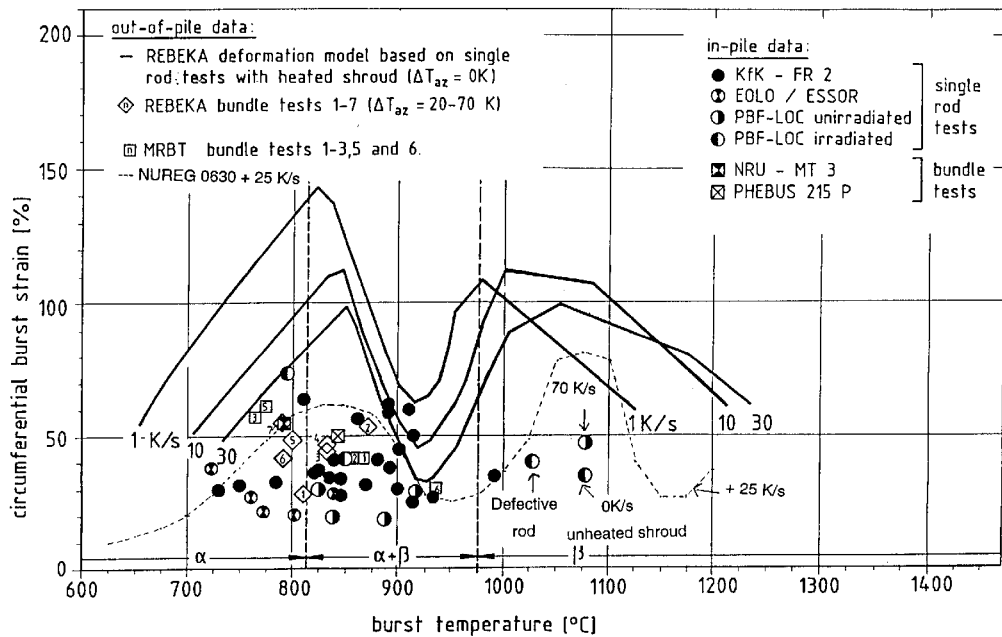


Figure 90: burst strain versus burst temperature of Zircaloy claddings. Comparison of out-of-pile and in-pile data. REBEKA model vs. NUREG-630 fast ramp.

Last of all, it is worth mentioning that a composite curve - envelope of the slow- and fast-ramp curves - was also provided in the NUREG-630 report, providing an estimate of the burst strain as a function of the rupture temperature for any ramp rate.

5.1.2.3 Assembly flow blockage

In addition to the burst strain correlations, the NUREG-630 report also provides correlations that give the maximum flow blockage in an assembly as a function of the average rupture temperature.

It was not possible to derive such a correlation directly from the bundle test results of the database for which a measure of flow blockage was available due to the limited amount (=11) of data.

It was thus necessary to derive bundle blockage from burst strain through a process defined by the following steps:

- 1) Derivation of an empirical factor linking the average burst strain to the average rod strain in the plane of maximum flow blockage. This factor was evaluated on the basis of the only three MRBT tests B1 to B3, at a value of 0.56, relevant for small bundles like those used in MRBT experiments. For large bundles, as in industrial-size fuel assemblies, a reduction factor was applied to take into account the averaging effect, of greater extent in large size bundles than in small size bundles. This factor was based on the ratio of maximum blockage to mean blockage in the axial height of significant blockage as observed in the MRBT B1 test; it reduces the previous factor from 0.56 to 0.46.
- 2) Derivation of the flow blockage as a function of the average rod strain in the plane of blockage, based on a simple geometric calculation.
- 3) Application of a final reduction of 5% to the flow blockage obtained in previous step to account for guide tubes and instrument tubes that do not balloon.

Figure 91 plots the two obtained correlations for slow- and fast-ramp respectively, giving the flow area reduction as a function of temperature applicable to PWR-size assemblies. The maximum blockage ratio appears at 71.5% for ruptures at 800°C under slow-ramp heating (90% maximum strain). The curves applicable to small assemblies without guide tubes, which show a maximum flow blockage of 91% under slow-ramp heating (see figure 92), bound all the available results from the NUREG-630 database, including the JAERI test 7805 with a 85.3% reduction in flow area.

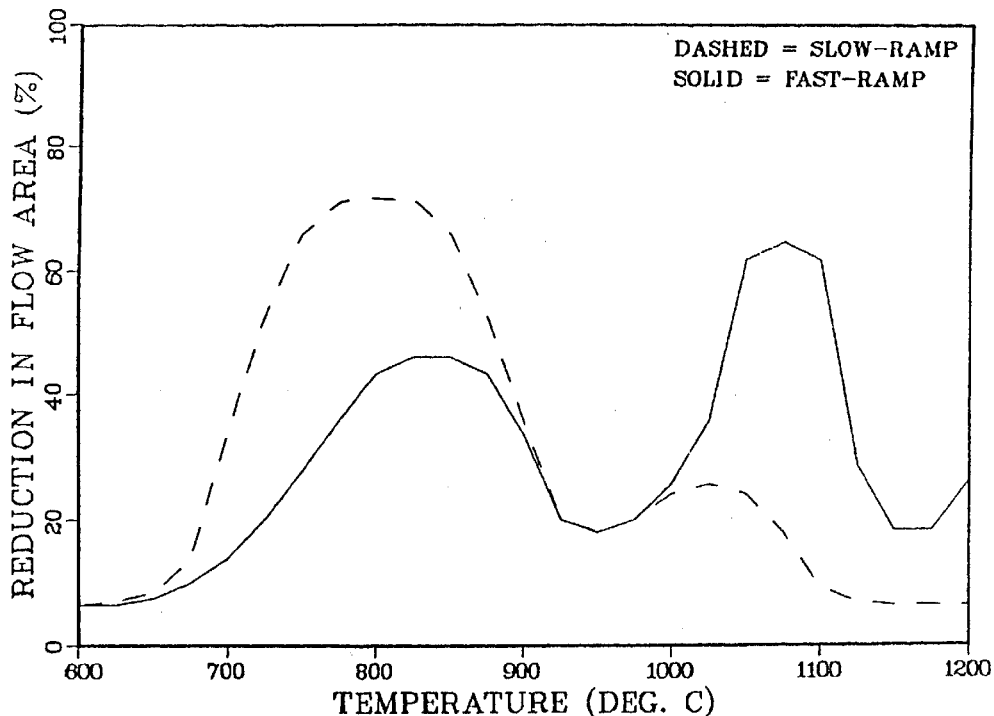


Figure 91: reduction in PWR assembly flow area as a function of rupture temperature and ramp rate.

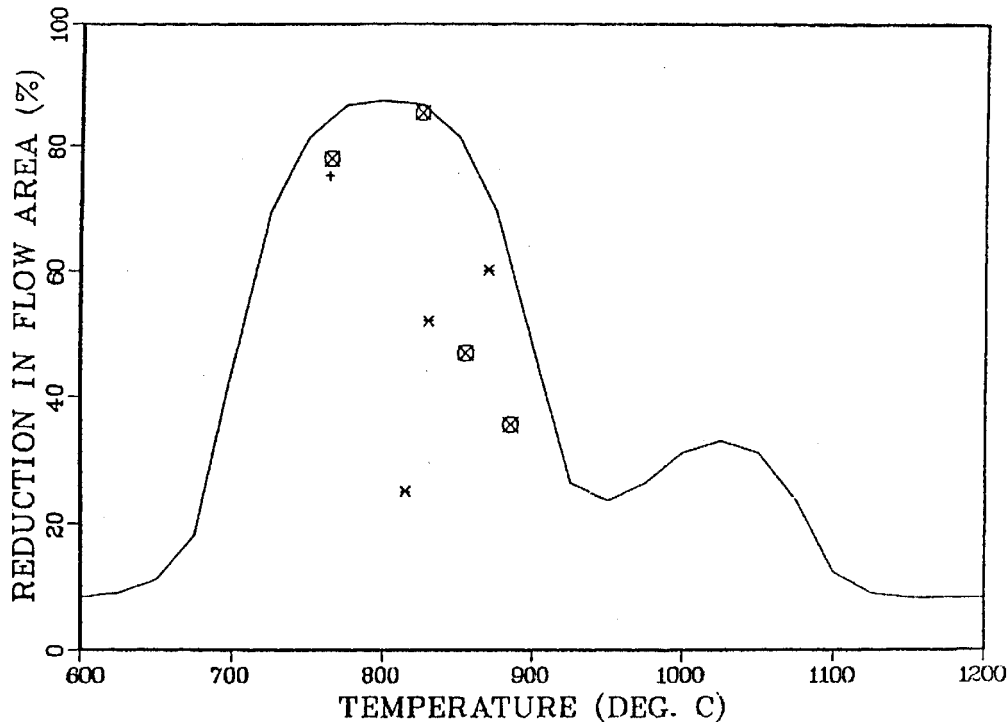


Figure 92: reduction in local flow area as a function of the rupture temperature for internally heated Zircaloy clad bundles in aqueous atmospheres at heating rates $\leq 10^\circ\text{C/s}$.

5.1.2.4 Conclusions relative to NUREG-630

The correlations provided in the NUREG-630 report for cladding rupture temperatures, burst strain and assembly flow blockage were established in 1980 on the basis of a large compilation of results from various tests carried out with electric simulators or actual fuel rods, in single-rod or bundle configurations, with a heated or unheated shroud and under various heating rates. The main characteristics of these correlations may be summarized as follows:

- For rupture temperatures, the ORNL correlation developed by Chapman was used, which suitably bounds most of the experimental results.
- For burst strain, two correlations were proposed for slow and fast temperature ramp rates. These two correlations virtually bound the bundle test results; however, in the alpha-domain, the slow-ramp correlation is only an average of the single-rod heated-shroud data. Above 900°C under slow-ramp and above 940°C under fast-ramp, the data for single-rod heated-shroud or bundle tests are scarce or lacking, which renders these correlations uncertain in the corresponding temperature domain.
- For flow blockage, two correlations were derived from the two former correlations by using the ratio between the average burst strain and average strain in the plane of maximum blockage, this ratio being the average value deduced from the three tests MRBT B1 to B3 only.

One may wonder that the burst strain and flow blockage correlations were not revised when new data became available, particularly in the temperature domain above 900°C , from the late bundle tests belonging to the REBEKA, ORNL and JAERI programs, as well as the in-pile tests with irradiated rods, notably the PBF-LOC test results.

More specifically, the flow blockage correlations appear insufficiently supported by experimental data and the 71% upper limit of the maximum flow blockage ratio in a PWR assembly should be revised in the light of the subsequent observations:

- No reduction, or increase, in the flow blockage in bundles containing guide tubes (REBEKA-4, JAERI 21 to 24 tests);
- Development of high blockage ratios in the inner sub-channels, due to the guard effect of the outer rods (MRBT-B5, JAERI 21 to 24 and NRU-MT4 tests), where values from 90 to 100% were obtained.

5.2 International standard problems ISP-14 and ISP-19

Two standard international problems, ISP-14 and ISP-19, were performed upon a REBEKA bundle test and a PHEBUS-LOCA test in 1984 and 1985 respectively. Participants of these problem exercises produced a set of calculations using several different computer codes. The main observations and conclusions of comparative analyses led respectively by GRS and IPSN shall be discussed in this document.

5.2.1 ISP-14 (REBEKA-6 test)

As a reminder, the REBEKA-6 test (cf. § 3.2.1.2) was an out-of-pile test performed on a 7×7 rod bundle composed of an unheated inner rod simulating an instrumentation tube and 48 heater rod simulators, two of which were slightly pressurized. The transient simulated a steam heating phase followed by a reflood phase, with ascending steam and reflood flows.

This test was performed in March 1983 and submitted to the CSNI for the open phase analysis of the ISP-14, which had been preceded by blind phase predictive analysis. The final comparison report^[36] only deals with open phase analytical results, for which a clad/ coolant heat transfer coefficient was provided to participants, associated with a reference coolant temperature derived from temperature histories measured on the slightly pressurized rods. These pseudo-thermal boundary conditions were provided in order to avoid hazardous predictions of rod thermomechanical behavior possibly resulting from excessive uncertainties in thermohydraulic calculations. Nevertheless, some participants involved in the exercise did not use this data and performed a personal calculation of the heat transfer coefficient.

Table 10 lists the five participants involved in the open phase analysis, as well as the computer codes used to calculate the behavior of rod No. 49 which was chosen for the comparison of experimental values with code calculations. At the end of the analysis of participant calculation results - carried out by GRS - a final workshop was held in November 1984 to discuss the different calculation results submitted by participants, as well as various other complementary studies that were conducted in parallel to the ISP problem or released out of the allotted time.

Participant	Identifier	Analyzed Rods	Model	Calculation Particularities
CEA	K	49, 29	CUPIDON 4.0	Heat transfer coefficient calculated with Dittus-Boelter during steam cooling
AEEW	L	"average rod"	MABEL-2D	Fluid dynamics calculated by TRAC-PD2
EG&G	M	49, 20, 29	FRAP-T6	Measured cladding temperatures as input
VTT	N	49	FRAP-T6	Fictive fuel material data
ÖFZ	P	49	BALO-2A	Separate empirical gas pressure model

Table 10: ISP-14 - survey of analyzed rods and calculation particularities

Thermal aspects

Figure 93 illustrates temperature variations in the cladding of Rod 49 at mid-height level, as measured and calculated by the different participants. Even though all calculations provide a correct estimation of cladding temperatures in the steam heating phase (except, rather strangely, EG&G FRAP-T6 code calculations where the measured temperature was taken as a boundary condition), this is no longer the case soon after the initiation of reflooding, where considerable differences appear. An advanced tool such as TRAC-PD2 proved to be no more effective than a simple heat transfer coefficient, as multiplicative factors had to be applied to both the reflood rate and the calculated heat transfer coefficients in order to obtain the measured temperatures. The dispersion between experimental and calculated values is to be related to the scattering of internal rod temperatures following the beginning of the reflood phase (see figure 94).

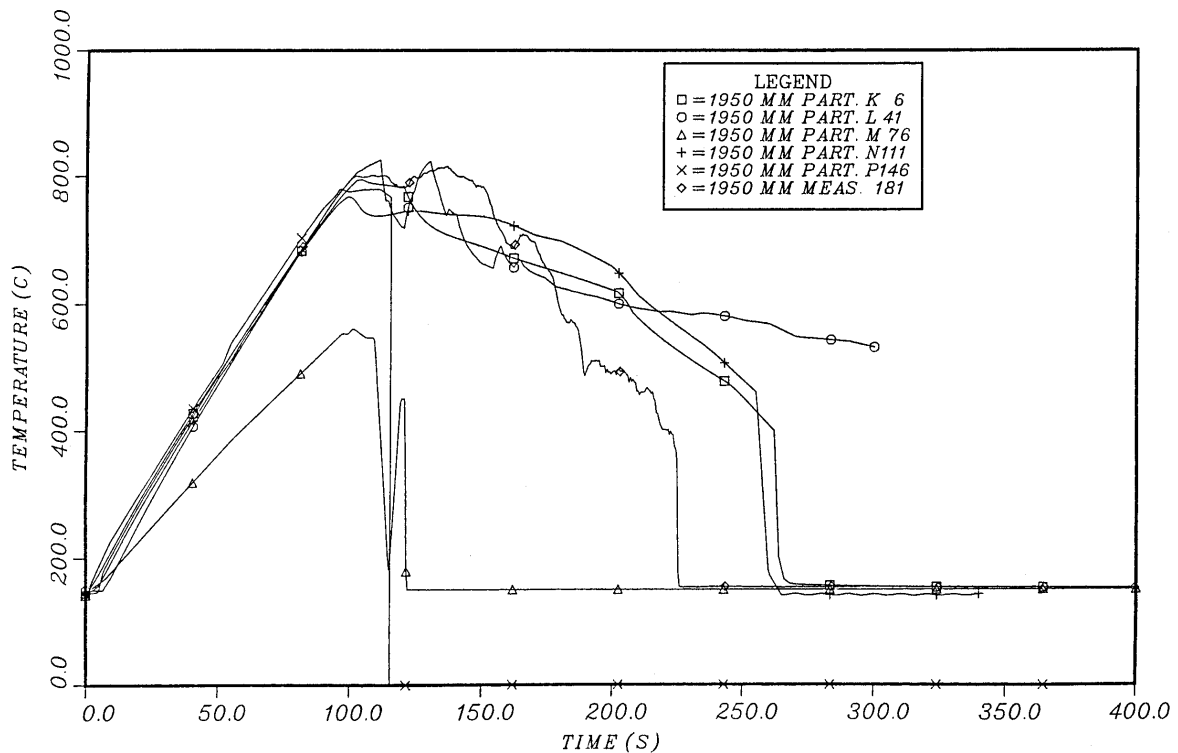


Figure 93: ISP 14 - comparison of calculated and measured temperature histories for rod 49.

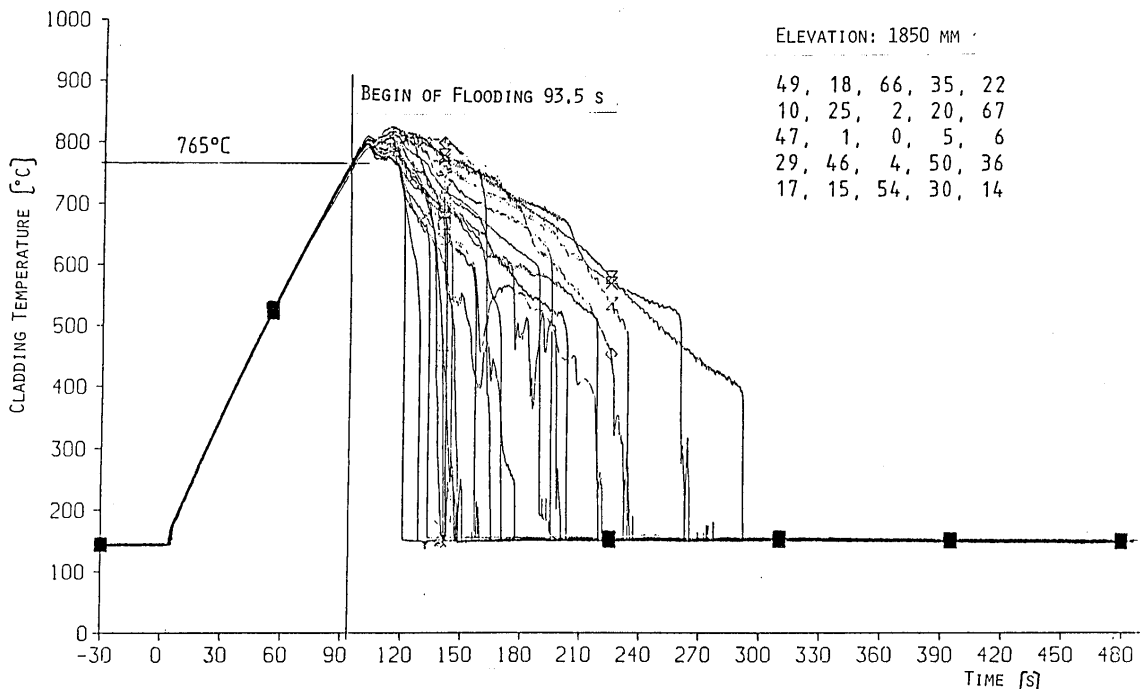


Figure 94: REBEKA-6 - cladding temperature sequence of the 24 inner rods for the 1850 mm elevation.

GRS - in charge of conducting the ISP-14 comparative analysis - came to the conclusion that the thermohydraulic codes (available at the time) had not the capability to calculate local cooling conditions in a bundle - particularly during a LOCA scenario - required to simulate the detailed thermomechanical behavior of bundle rods.

Thermomechanical aspects

Table 10 indicates the tools used to calculate the thermomechanical behavior. The computer codes CUPIDON, FRAP-T6 and BALO-2A (derived from BALON 2) dealt with fuel rod mechanics in 1D (in the plane perpendicular to the axis), even though a 2D representation of the balloon just before cladding failure was possible in FRAP. The MABEL-2D computer code allowed a 2D treatment (r,θ) of the rod thermo-mechanics.

Table 11 compares cladding failure parameters and maximum temperatures and internal pressures provided by the different calculations and experimental measurements. Cladding failure occurs between 104 s and 120 s, in comparison to 128 s recorded for Rod 49 and between 114 s and 132 s recorded for the other inner rods of the REBEKA-6 bundle. Burst strain was calculated between 52% and 104% in comparison to experimental values of 55% for Rod 49 and 31.7% to 63.7% for the other inner rods.

Participant	Identifier	Time of Burst (s)	Circum. Strain at burst (-)	Internal Pressure at burst (bar)	Max. Clad Temp. (1950 mm) (°C)	Max. Int. Pressure (bar)
CEA	K	120	95% (extrapolated)	69.5	795	76
AEEW	L	no burst (base case)	16%	-	834	74
EG&G	M	104	54%	40	815 (revised value)	81.7
VTT	N	108	104%	47.4	768	76.6
ÖFZ	P	115.3 (report)	52% (report)	58.9	785	77.5
Measured values	-	127	55%	59	814	74

Table 11: ISP-14 - comparison of various calculated parameters with the measured values for Rod 49

The axial profile of strain is provided in figure 95. It is important to point out here that the strain profile calculated using CUPIDON (participant K) represents uniform elongation, whereas the failure strain calculated by this participant (95%), as indicated in table 11, was extrapolated from the corresponding uniform elongation.

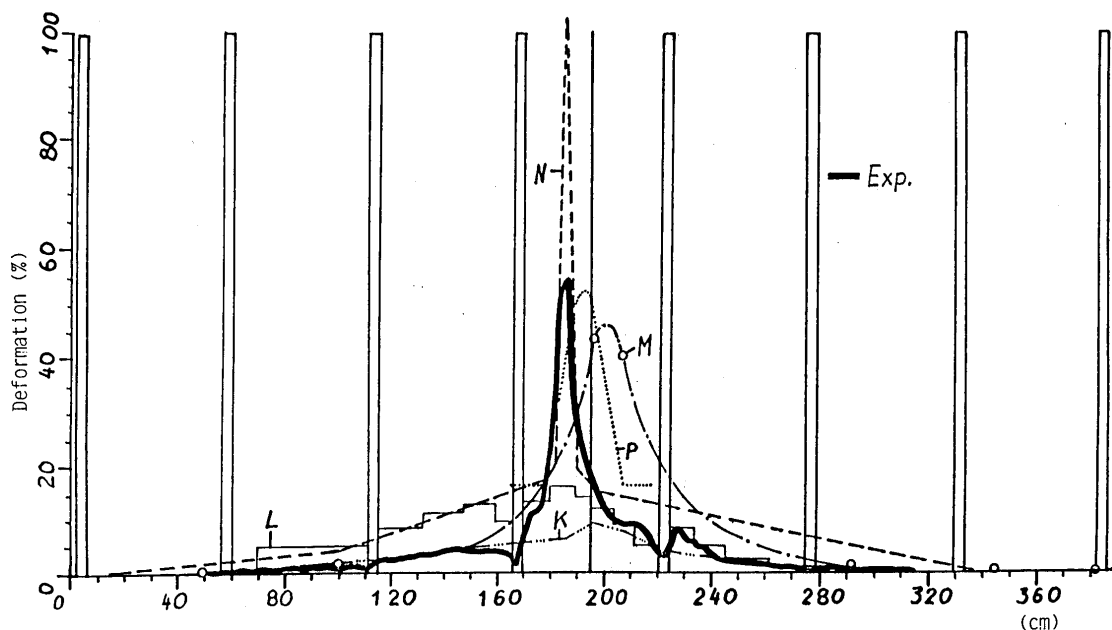


Figure 95: ISP-14 - comparison of calculated and measured distribution of circumferential strain for REBEKA-6.

The MABEL-2 calculation does not predict cladding failure in the basic case using creep laws provided by KfK, however AEEW did conduct a sensitivity study (presented at the final workshop) in which cladding failure occurred at 130 s, with an average strain of 31.7%, obtained by doubling the creep velocity. The question of correct creep laws for REBEKA-6 cladding was also dealt with in a sensitivity study carried out by the National Nuclear Corporation (NNC) in the UK, using the BART/TAPSWEL computer codes (cf. [36] Annex VII). This study suggested a factor of 2 for the creep velocity in relation to REBEKA-5 material. Table 12 provides a comparison of cladding failure parameters - both experimentally measured and calculated - using BART/ TAPSWEL with two creep laws. It is also worth pointing out that a RODSWELL (computer code very similar to MABEL) calculation was carried out by JRC/Ispra (cf. [36] Annex V), apparently using creep laws of a “weak” material: with a pellet/ cladding eccentricity of 1 (pellet contact with a cladding internal edge), the code predicted cladding failure at 132 s with 30% strain, more or less corresponding to the minimum experimental values for the internal rods; moreover, the cladding burst temperature and pressure were also similar to measured values.

Parameter	Data (central 18 rods + 3 specimen rods)	BART/TAPSWELL (standard creep)	BART/TAPSWELL (creep X 2)
Burst time (second)	114 - 131.5 Rod 20 ^a : 102 Rod 29 : 118 Rod 49 : 127	Average rod: 142	Average rod: 128
Burst pressure (bar)	59 - 63 Rod 20 ^a : 70 Rod 29 : 61 Rod 49 : 60	Average rod: 60	Average rod: 59.4
Burst temperature ^b (°C)	? Rod 20 ^a : 810 Rod 29 : 760 Rod 49 : 750	Average rod: 771	Average rod: 750
Burst strain (%)	32 - 64 Rod 20 ^a : 95 Rod 29 : 35 Rod 49 : 54	Average rod: 41.8 spread: 29-48% (for central 18 rods)	Average rod: 44.6 spread: 31-56% (for central 18 rods)

a: Rod 20 is rogue and should be ignored

b: burst temperatures are estimated

Table 12: ISP-14 - results of NNC post test analysis with BART/TAPSWELL

The relevance of considering a pellet/cladding eccentricity was also revealed by calculations carried out by KfK using SSYST-3 (cf. [36] Annex VI). In the basic case with no eccentricity (using material data and heat transfer coefficients provided in the specifications), the computer code does not predict cladding failure. However, with an eccentricity of 0.8 to 1, cladding failure occurs with strain of 42% to 45%. With an eccentricity of 1, the calculated azimuthal temperature difference reaches 83 K upon cladding failure, which is notably higher than the values of 40 K recorded during the experiment. According to KfK, the existence of large azimuthal gradients, associated with the uncertainty on the measurement of the burst temperature and its derivative, explains the apparent discrepancy between REBEKA bundle tests and single-rod tests, as shown in figure 96 providing the burst strain of bundle and single-rod tests, as well as model curves resulting from single-rod test results (with low or zero ΔT_{az}). Directly applying single-rod models to bundles, particularly the failure criterion, is therefore problematic. GRS thus concluded that the correct prediction of the thermomechanical behavior of a fuel rod in an assembly requires using a model that considers azimuthal gradients.

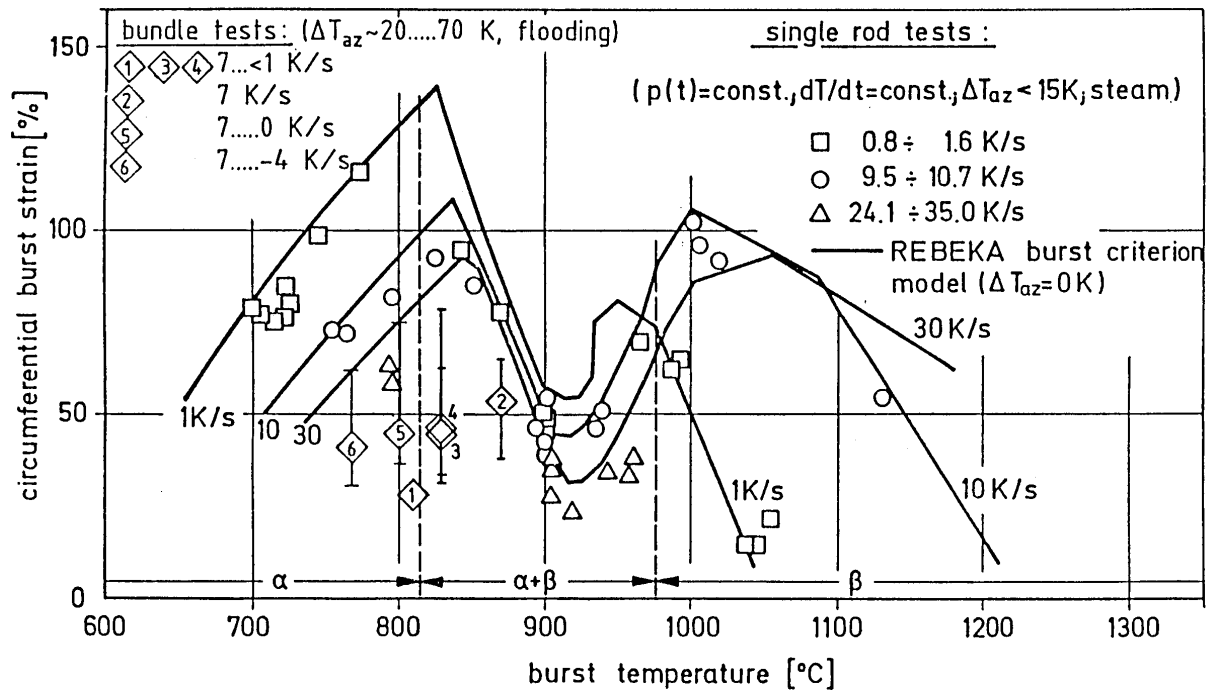


Figure 96: burst strain versus burst temperature of Zircaloy claddings in the REBEKA out-of-pile tests.

Summary

The ISP-14 exercise relying on the REBEKA-6 test, as well as various studies that were conducted in parallel, helped clarify several important points:

- ❑ Thermohydraulic codes do not produce sufficiently accurate predictions of the combined thermohydraulic/ thermomechanical behavior observed during a bundle test under LOCA conditions; this is due to the significant difference between the precision of temperatures - required for thermomechanical calculations (10 to 15 K) - and the precision available concerning local thermohydraulic conditions under two-phase flow conditions during reflow;
- ❑ A correct description of the material's mechanical properties is required to determine cladding failure conditions;
- ❑ Consideration of fuel distribution within the cladding (eccentricity, local fuel relocation), with a corresponding adaptation of the cladding failure criterion, is required to correctly determine cladding failure conditions during an asymmetrical swelling scenario.

5.2.2 ISP-19 (PHEBUS 218 test)

As a reminder, the PHEBUS 218 test chosen for this problem was an in-pile test on a 25 rod bundle, characterized by a rapid temperature increase having led to cladding failure of the inner fuel rods nearing the first temperature peak (cf. § 4.2.2.3.4). This test was conducted in July 1984 and submitted to the CSNI in May 1985 for the open phase analysis of the ISP-19. The comparative analysis of results was carried out by IPSN^[37].

Table 13 lists the 10 organizations that took part in the ISP-19 exercise, as well as the computer codes used for thermomechanical calculations. Four of the five participants involved in the ISP-14 exercise also took part in this problem, using practically the same computation tools.

Institution	Country	Corresponding Experts	Computer program	Identifier
Gesellschaft für Reaktorsicherheit (GRS), Köln	Germany	I.A. Keusenhoff	TESPA	A
Österreichisches Forschungszentrum (ÖFZ), Seibersdorf	Austria	G. Sdouz G. Sonnek	BALO-2A	B
Swedish Nuclear Power Inspectorate	Sweden	J. Mattson O. Sandervag	TOODEE-2 (Swedish version)	C
UKAEA, Springfields	United Kingdom	T.J. Haste	MABEL-2D	D
National Nuclear Corporation (NNC), Whestone	United Kingdom	R.E. Haigh, M.E. Shanawany	SWEM / BART	E
Swiss Federal Institute for Reactor Research, Wurenlingen	Switzerland	H. Gautier	FRAP-T6	F
Energy Research Foundation, ECN, Petten	Netherlands	Th. Van der Kaa	FRAP-T6	G
CEA / DMECN, Saclay	France	M. Fillatre	CATHACOMB	H
CEA / IPSN, Cadarache	France	I. Drosik	FRETA	I
VTT Technical Research Center, Helsinki	Finland	S. Kelppe	FRAP-T6	J

Table 13: participants of the International Standard Problem ISP-19.

Among the computer codes listed in table 13, the TESPA, SWEM, MABEL and FRETA codes had potential capabilities to perform 2D thermomechanical calculations, which were not used in the TESPA calculations carried out by GRS.

The various calculations were performed under boundary conditions selected from 3 levels:

- B.C.1: cladding temperature + internal pressure;
- B.C.2: power + heat transfer coefficient + coolant temperature;
- B.C.3: power + coolant characteristics at bundle inlet.

Table 14 indicates the boundary conditions for each calculation. For TESPA and SWEM calculations, with the cladding temperature used as boundary condition, comparison with other calculations and the experiment can only concern mechanical aspects, such as cladding burst times and strain. SWEM

calculations provided an interesting sensitivity study on creep laws with various pellet/cladding eccentricities. The MABEL code was used to calculate azimuthal temperature differences related to fuel pellet eccentricities. FRETA was the only code capable of producing a 2D calculation of the fuel rod bundle, with 4 azimuthal sectors per fuel rod (like in MABEL), and consideration of radiative exchanges between fuel rods and peripheral structures.

Identifier	Computer code	B.C.1 (clad temp.)	B.C.2 (fluid temp. + heat transf. coeff.)	B.C.3 (inlet fluid conditions)	Remarks
A	TESPA	each level			internal pressure
B	BALO-2A			used in RELAP4/Mod6 to derive H.T.C.	coupling of 2 computations
C	TOODEE-2			quality, flow rate and temperature	
D	MABEL-2D		based on supplied data, modified for vapor, axial average		
E	SWEM / BART	yes			internal pressure
F	FRAP-T6		supplied data HTC set 1 & 5		
G	FRAP-T6		HTC set 1 & 3 modified		modif. for Rod 3
H	CATHACOMB		HTC set 2 (Rod 12) set 6 (Rod 3) set 3 (Rod 8)		
I	FRETA			enthalpy and mass flow rate from exp. analysis	
J	FRAP-T6		HTC set 5 (Rod 3) set 3 (Rod 8) set 4 (Rod 12)		

Table 14: boundary conditions for ISP-19 computations.

Thermal aspects

The detailed comparison of temperature variations in the specified fuel rods was shared out among two groups, according to the choice of boundary conditions: FRAP-T6 and CATHACOMB codes on the one hand, and MABEL and other codes with the B.C.3 limit condition (BALO, TOODEE and FRETA) on the other hand.

Table 15 lists both measured and calculated temperatures at the hot level of Rod 12 (inner, pressurized rod) and Rod 8 (inner, non-pressurized rod) for times nearing cladding failure: the difference between calculated cladding temperatures and the measurement ranges between -65 K to +40 K for the pressurized fuel rod and -65 K to +155 K for the non-pressurized rod.

Experiment /Participant	Boundary condition	Rod 12, level 5 at 10 sec.				Rod 8, level 5 at 14 sec.			
		Clad T	Initial fuel T	Fuel T	ΔT fuel-clad	Clad T	Initial fuel T	Fuel T	ΔT fuel-clad
Experiment		850				960 940	1620	1115	155 175
B	3	785	1875	975	190	905	1995	1140	235
C	3	865	1875	1070	205	1070	1845	1150	80
D	2	855	1610	945	90	965	1595	1050	85
F	2	835	1740	910	75	950	1775	1065	115
G	2	890	1715	960	70	985	1780	1105	120
H	2	850	1610	935	85	885			
I	3	865	1615	960	95	1105	1730	1165	60
J	2	830	1580	895	65	945	1580	1040	95
Maximum deviation		105	295	175	140	220	415	125	175

Table 15: comparison of thermal results between the experiment and computations in ISP-19.

This dispersion observed in the calculated temperatures is possibly due to the combination of several factors:

- Uncertainties concerning experimental specifications provided to the participating organizations, particularly for the spatial power distribution and the TC temperature measurements;
- Variations in fabrication characteristics of the different fuel rods (gap, cladding thickness, dish and plenum volumes, ...);
- Modeling differences and options for some phenomena (fuel and gap conductivities, local fuel relocation, etc.);
- Choice of boundary conditions: the B.C.2 type boundary condition (heat transfer coefficient + coolant temperature) was based on measurements performed on non-pressurized fuel rods, which introduced uncertainties on both gap conductance (greater uncertainty at low pressures and smaller gaps) and thermal conditions during the swelling phase. The B.C.3 type limit condition (coolant characteristics at bundle inlet) is more problematic, as measurements of coolant thermohydraulic conditions at the bundle inlet were inaccurate, and implies an efficient thermohydraulic modeling in the computer code. Nevertheless, the quality of temperature predictions was rather similar for calculations using both types of boundary conditions.

Thermomechanical aspects

Variations in the calculated internal pressure of Rod 3 are illustrated in figure 97 for both calculations groups: FRAP + CATHACOMB on the one hand and all the other calculations on the other hand. Variations are very similar for calculations using the B.C.2 limit condition, with the only notable difference occurring upon cladding failure time (between 12.3 and 21 s). However, pressure variations were rather erratic for calculations C and I using the B.C.3 limit condition, due to the succession of coolant saturation and dry steam conditions which affected plenum temperatures and therefore the internal pressure. This illustrates the difficulty of correctly predicting the internal pressure using a combined thermohydraulic + mechanical calculation.

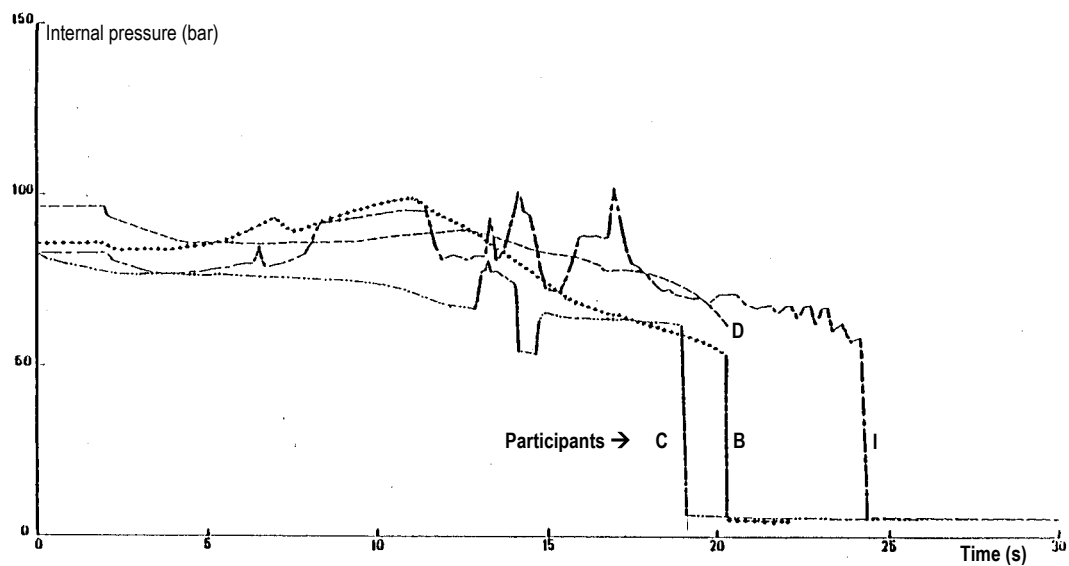
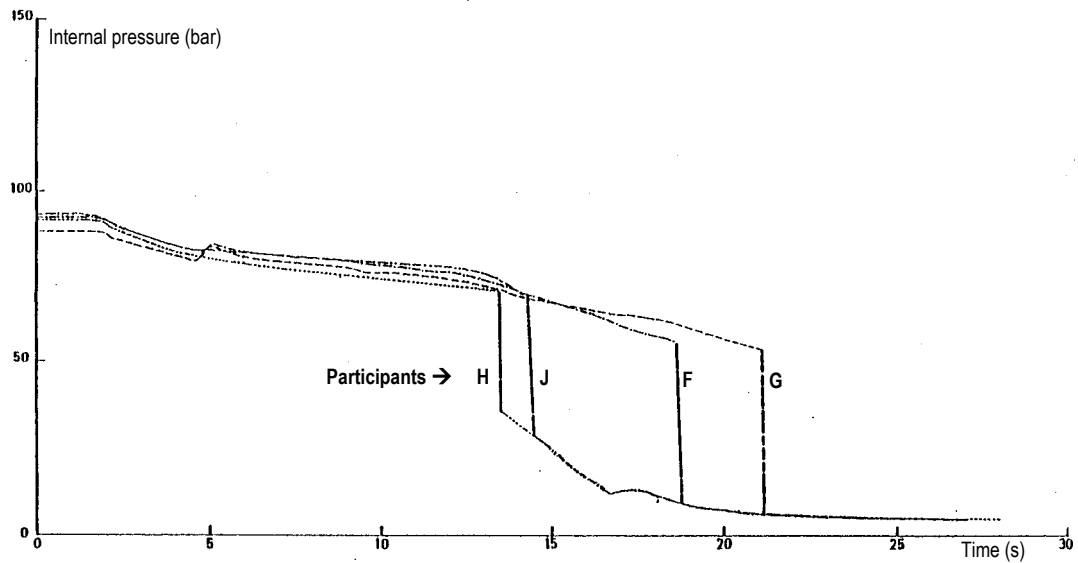


Figure 97: ISP19 - comparison of the variations in internal pressure for Rod 3 as given by different computations.

Figure 98 provides the hoop strain calculated histories for the peripheral Rod 3, showing a rather strong dispersion in the strain rate. This dispersion results from the sensitivity of the creep velocity on temperature and stress. However, the cladding failure characteristics (time and strain) of the inner rods remain correctly calculated by most of the calculations, as illustrated in table 16 (Rod 12 = inner, Rod 3 = peripheral). This is mainly due to the rapidity of the temperature increase where cladding failure is predicted to occur at relatively similar times, regardless of the model. It is nevertheless important to point out that the conservative TESPA and TOODEE calculations markedly overestimated cladding failure strain. Furthermore, the CATHACOMB calculation predicted minor strain for the two calculated fuel rods, associated with early failure for the peripheral Rod 3.

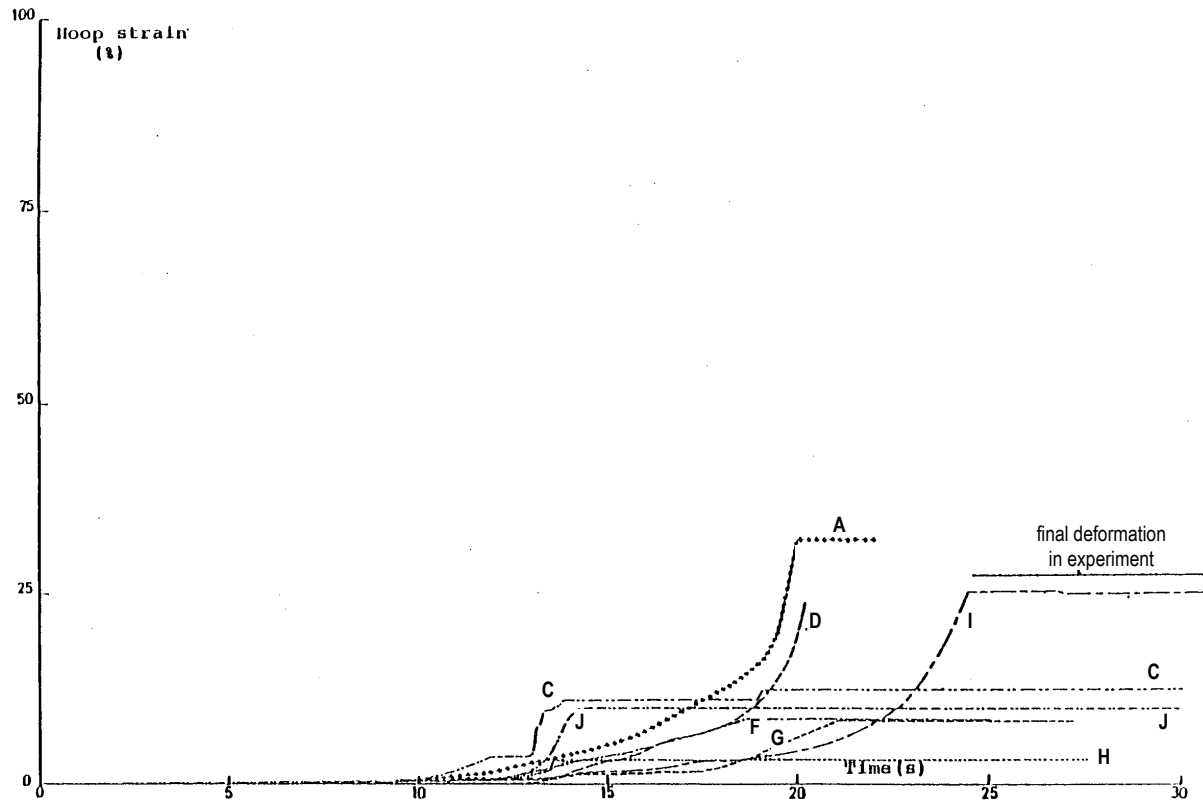


Figure 98: ISP19 - cladding deformation for Rod 3 at level 5. Comparison of computations with the final experimental value.

Participant	Rod 3			Rod 12		
	Time (s)	Level	Strain (%)	Time (s)	Level	Strain (%)
A	24.7	-7500	35	9.8	-7500	30.6
B	20.22	-7580	32	14.31	-7580	23.6
C	21.6	-7620	57	13.5	-7580	33
D	20.2	-7580	25	13.6	-7580	28
E	-	-	-	14.5	-7580	30.5
F	18.75	-7620	20	12.6	-7620	15
G	21.0	-7580	10.9	12.4	-7580	23.5
H	13.5	-7580	4	12.8	-7480	2
I	24.3	-7580	24	14.1	-7580	25
J	12.34	-7580	9.8	10.95	-7500	17.1
Experimental mean value	23.4		24.6	14		17.7
Standard deviation	3.16		6.8	0.5		6

Table 16: ISP-19 - comparison of experimental rupture conditions with computations.

Several sensitivity studies were conducted in parallel with calculations submitted by some participating organizations. IPSN studied the sensitivity of internal pressure to geometrical uncertainties (gap, dish and plenum volumes) using the CUPIDON computer code: the internal pressure seemed affected at the beginning of the transient, which disappeared before cladding failure occurred and did not affect burst time. Another sensitivity study of cladding failure on creep laws was carried out by NNC using the SWEM code, which revealed the necessity to take into consideration the phase change kinetics of Zircaloy for rapid transients such as the PHEBUS 218 test transient.

With reference to the contribution of 2D computer codes calculations, two aspects are worth mentioning:

1) Cladding failure criterion

For 1D codes, the cladding failure criterion is generally expressed in terms of failure stress that is a function of temperature; the cladding failure criterion for 2D codes is generally expressed in terms of a local strain criterion. No in-depth comparative studies concerning this aspect have been conducted, but it is worth considering the remarkable predictions of cladding failure times produced by a FRETA calculation, illustrated in figure 99.

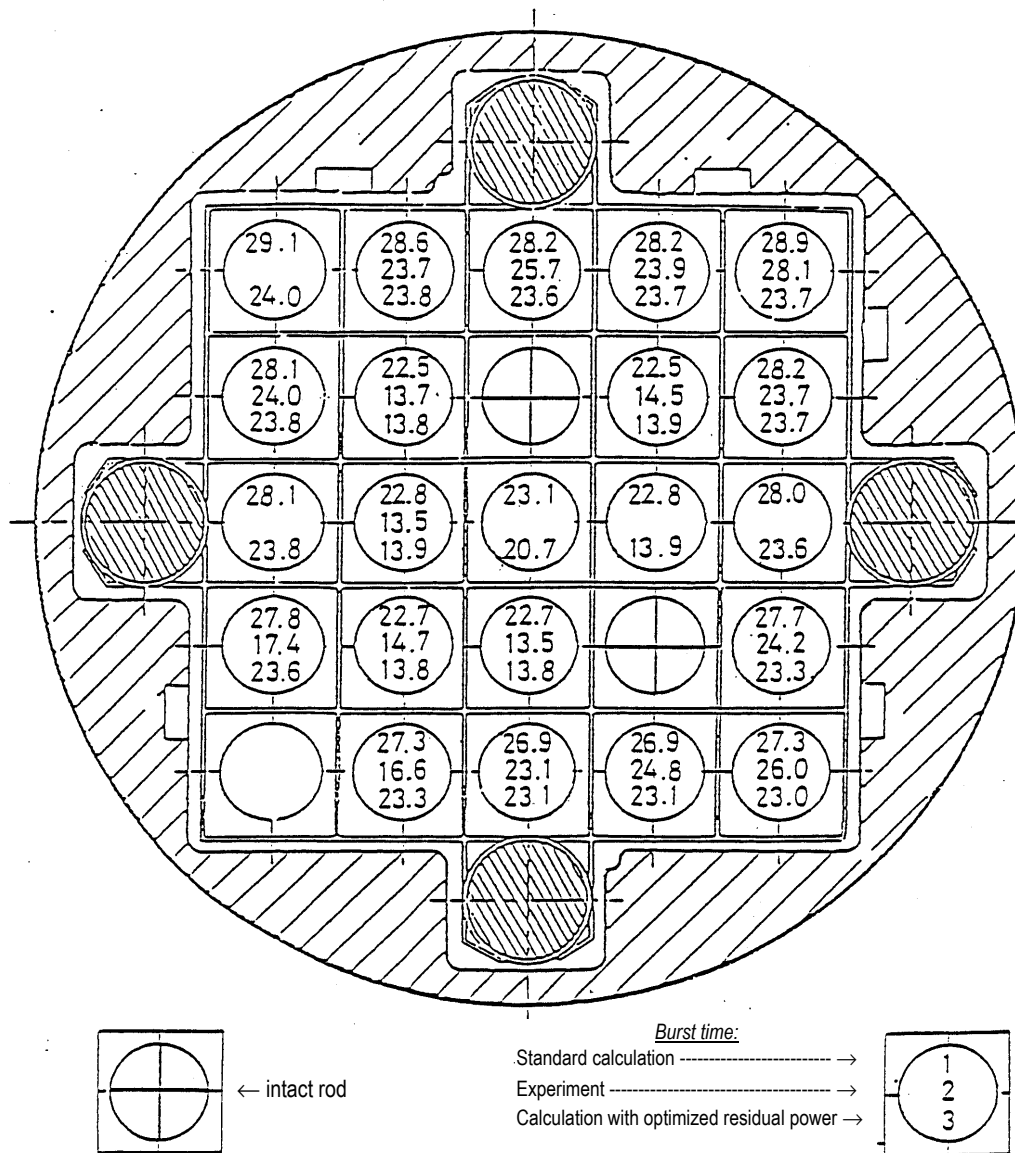


Figure 99: PHEBUS test 218 - comparison of burst times as calculated with FRETA to the experimental values.

2) Azimuthal temperature distribution

This parameter has a major effect upon cladding failure strain. At times nearing cladding failure of Rod 3 and 14, temperature differences of 50 K and 25 K respectively were measured for these two rods, which appear to be non-representative owing to the location of the TC that recorded these measurements. The MABEL calculation, which considers internal sources of azimuthal temperature heterogeneities (pellet/ cladding eccentricity), indicated a maximum ΔT_{az} of 10 K to 20 K. The FRETA calculation, which considers azimuthal heterogeneities resulting from radiative transfers with neighboring rods, indicated a maximum ΔT_{az} not exceeding 5 K for the inner rods and 10 K for the peripheral rods. The combination of internal and external causes therefore produced a ΔT_{az} of approximately 25 K, which is consistent with the experimental value recorded for Rod 14 but is still too low to significantly affect strain upon cladding failure. Analysis of test 218 led by IPSN came to the conclusion that transient kinetics had a preponderant effect upon cladding failure conditions for this test.

Summary

The ISP-19 exercise using the PHEBUS 218 test and parallel studies helped clarify several important points:

- The rapidity of the transient has a dominating effect upon azimuthal temperature differences with regard to failure conditions and hence strain;
- It is important to take into account phase change kinetics during the rapid transient.

As compared to the results of ISP-14, the thermomechanical predictions here appear more accurate and less scattered; however, it must be underlined that the rupture conditions under a rapid transient were less sensitive to experimental uncertainties and modeling than in the case of the REBEKA-6 test.

5.3 Summary of PHEBUS-LOCA test interpretations

A comprehensive summary of interpretations drawn from PHEBUS-LOCA test results is provided in [3], dealing with thermal-hydraulics, thermo-mechanics and cladding oxidation at high temperatures. In principle, it is possible to carry out a complete set of combined thermohydraulic/ thermomechanical calculations using tools such as RELAP4 or CATHARE. However, the accumulation of uncertainties related to thermohydraulic and thermomechanical aspects could produce a hazardous prediction of the mechanical performance. Due to the particularly complex thermal-hydraulics of PHEBUS tests, it was not possible to calculate the cladding temperature with better precision than $\pm 50^\circ\text{C}$. It was therefore necessary to carry out an analysis of test thermo-mechanics decoupled from thermohydraulic calculations. This approach required providing thermal boundary conditions, either in terms of temperatures (inferred from experimental measurements) or as heat transfer coefficients (obtained using inverse conduction calculations).

As discussions are limited to strain, cladding failure and blockage aspects in this part of the State-of-the-Art-Review, only work devoted to the interpretation of test thermo-mechanics shall be discussed below.

Various computer codes were used to analyse the thermo-mechanics of PHEBUS tests: RELAP, CUPIDON, FRAP-T4, RODSWELL, FRETA and CATHACOMB (mechanical model of CATHARE). They can be classified into two groups according to the level of representation of the rod in a transversal cross-section:

- ♦ 1D codes: RELAP, CUPIDON, CATHACOMB, FRAP-T4;
 - RELAP4/ MOD6 simply contains data tables providing cladding failure conditions, as a function of temperature, stress and strain;
 - CATHACOMB contains CUPIDON models with data from the EDGAR program results;
 - FRAP-T4 also includes a 2D treatment of straining that develops during the last moments of swelling;
- ♦ 2D codes: RODSWELL, FRETA;
 - RODSWELL uses the hypotheses of the CANSWEL/ MABEL codes developed by UKAEA and describes rod straining and contact with neighbors in a 3×3 rod array, with cladding/ coolant heat transfer coefficient and coolant temperature serving as limit conditions;

- FRETA is the only code that represents an entire bundle in two dimensions, including thermal and mechanical interactions between rods.

In terms of safety, rod strain and resulting flow blockage are the two main parameters to be taken into consideration. The final bundle geometry is a result of cladding strain and failure occurring in the bundle. Discussion in the following paragraph focuses on these two aspects.

5.3.1 Cladding failure

Cladding failure times were evaluated using different tools available at the time, which produced an analysis that indicated a strong dependence on the rapidity of the transient under consideration.

In test 215-P - characterized by a slow temperature rise - experimental results showed rather pronounced scattering in cladding failure times; the same applies for the different calculation predictions that were performed (cf. table 17). However, it is important to point out that even though the experimental scatter can be largely explained by the rather heterogeneous bundle thermics, differences in calculation tool predictions not only result from thermal differences, but also from differences between the various burst criteria. For such a slow transient, cladding failure conditions are progressively overstepped, which renders cladding failure times more sensitive to modeling differences.

	Experiment	FRAP-T4	CUPIDON	RELAP 4/Mod 6
Burst time (s)	54 < t < 68	48	64	57
Burst temperature (K)	~ 1110	1045	1160	1115
Burst pressure (MPa)	-	5.4	4.8	7.3
Burst strain (%)	50 ^a	85	65	35

a: average for inner rods

TABLE 17: PHEBUS LOCA - computed results for test 215-P.

This is no longer the case in test 215-R, where the prediction of the internal pressure for inner rod No.7, using different tools and with the measured temperature serving as the boundary condition (cf. figure100), showed that calculated failure times remain grouped over approximately 5 s nearing failure times measured on two inner rods, despite the different temperature variations after 12 s. This is a result of the rapid temperature increases (~ 25 K/s) during the time interval corresponding to the cladding failure of these fuel rods.

It proved to be more difficult to carry out calculation predictions for test 218, where the inner fuel rods ruptured during the first temperature peak and the peripheral rods ruptured later on. The comparison of previously discussed calculations performed during the ISP 19 exercise (cf. table 16) indicated greater scattering of calculation results in comparison to test results, when uncertainties induced by the temperature scattering are taken into account. In other respects, it is worth recalling the remarkably accurate prediction of the cladding failure times for all fuel rods in this test with the FRETA code (cf. figure 99), using the same thermohydraulic conditions for all fuel rods.

For tests with rapid transients, it can thus be concluded that most calculation tools correctly evaluate cladding failure times, with cladding thermal behavior having been evaluated with ± 50 °C uncertainty in the rupture region.

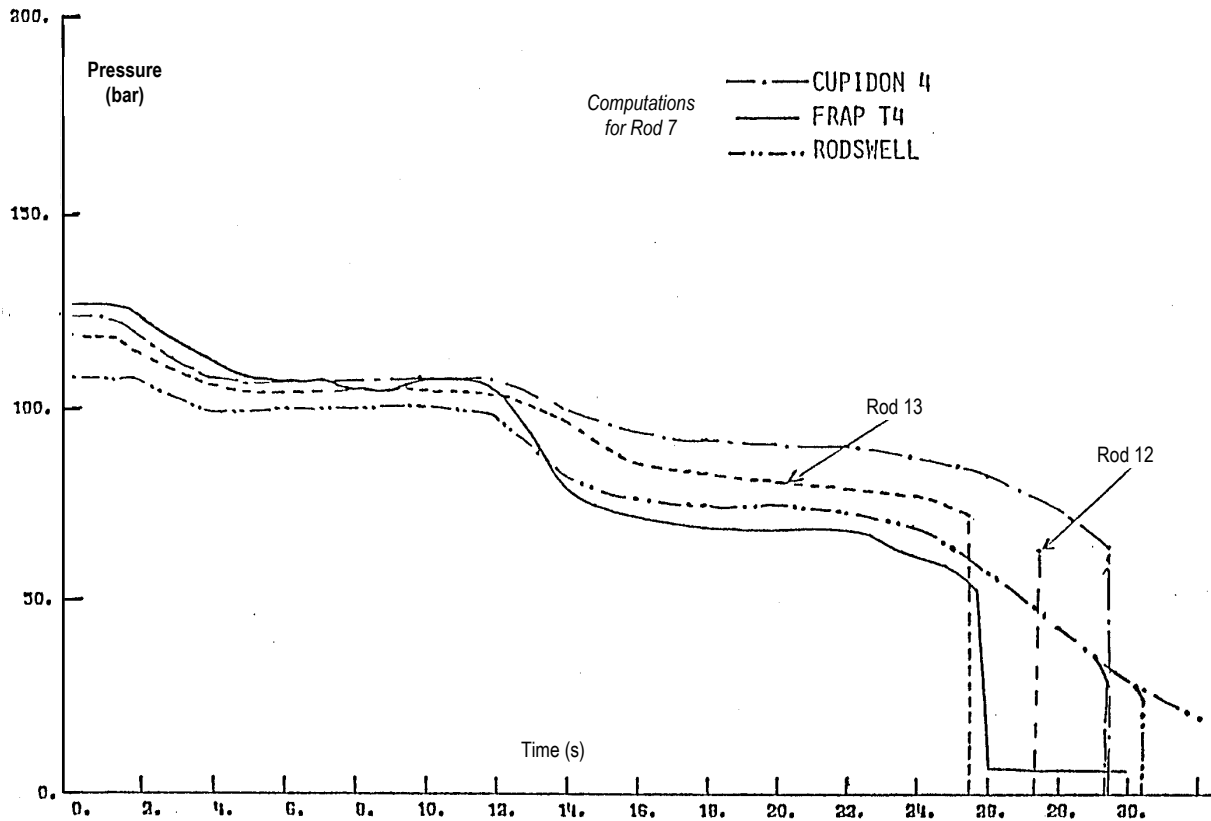


Figure 100: PHEBUS test 215-R - comparison of rod7 internal pressure as calculated from various computations with measured value on Rods 12 and 13.

5.3.2 5.3.2 Strain rate

Prediction of rod strain rates, particularly upon cladding failure, is a more difficult exercise and calculated values often overstep experimental margins. It is important to distinguish strain occurring in the cladding failure region from strain occurring in other regions of the rod.

Post-test metallographic examination only provides information on strain obtained at clad burst. Variations in average strain during the transient can be deduced from internal pressure variations, via the internal gas volume. Figure 100 shows how the internal pressure is underestimated after 12 s by FRAP-T4 and RODSWELL, which corresponds to an overestimation of the average strain whereas an inverse prediction is obtained with CUPIDON-4. It is possible to evaluate the validity of the creep laws implemented in computer codes on the condition that temperature variations have been correctly predicted. It can therefore be concluded that creep laws would correspond to a "weak" material in FRAP and RODSWELL, conversely to a "hard" material in CUPIDON. This explains why it was important to identify the creep laws specific to the PHEBUS material, which was made possible by conducting specific EDGAR tests.

As far as burst strain is concerned, it is necessary to distinguish the analysis of predictions with the different tools for tests 215-P and 215-R on the one hand and 216 and 219 on the other hand. As illustrated in table 10, rather pronounced dispersion (-15% to + 35% strain in comparison to the average experimental value of 50%) was observed for test 215-P. The amplitude of this dispersion can be compared with the dispersion obtained for previously discussed ISP-14 calculations (REBEKA-6), i.e.: calculated strain of 52% to 104% for a measured strain of 55% (cf. table 11). Similar dispersion was obtained in test 215-R predictions using 1D codes (cf. figure 101), even though cladding thermics were identical to experimental cladding thermics.

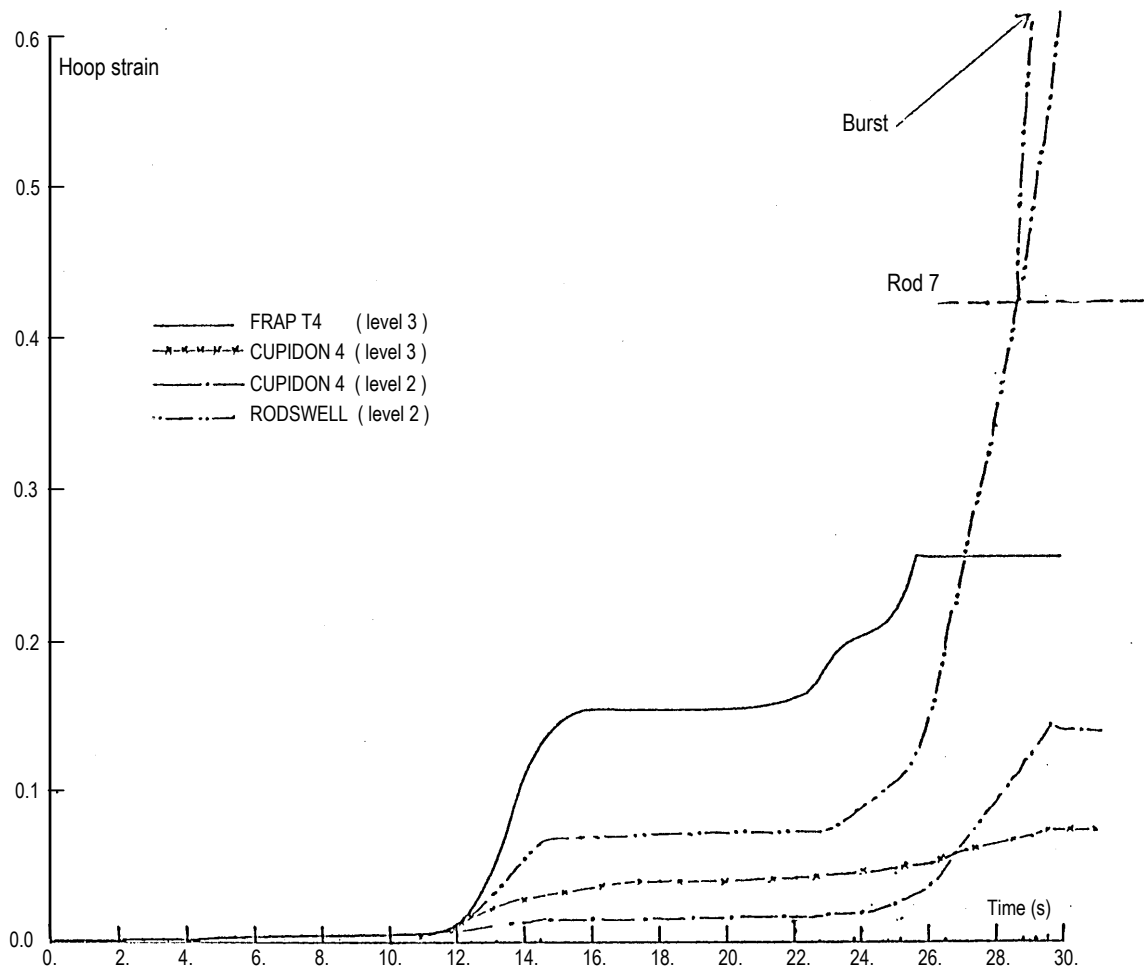


Figure 101: PHEBUS test 215-R - comparison of burst strain as calculated from various computations with measured value on Rod 7.

However, a notable improvement in the prediction was obtained in calculations taking into account the local temperature map, namely calculations performed using the FRETA code. One of the main advantages of this tool is that it takes into consideration the azimuthal temperature heterogeneities and their effect upon strain maps, with cladding failure being determined upon a local strain threshold. It was therefore possible to verify that the main source of heterogeneity in the PHEBUS rod bundle was related to the presence of the non-heated shroud. A FRETA calculation of test 215-R, carried out without radiative heat transfer (cf. figure 102A) produced an inversed strain map in comparison to the strain map obtained with a calculation considering radiative exchanges (cf. figure 102B) which is more representative of reality (cf. figure 103). In this test, the strain rate upon cladding failure was lower in comparison to the strain rate that could have been obtained without temperature heterogeneity (cf. figure 104), mainly on the peripheral rods that are most affected by radiative exchanges.

For tests 216 and 219 with more rapid transients, the overall quality of predictions proved to be much less sensitive to the description level (1D or 2D) used in the calculation. This was particularly highlighted through comparisons carried out within the framework of the previously discussed ISP-19 exercise. It appears that a precision of $\pm 20\%$ can be expected on calculated strain for this type of transient.

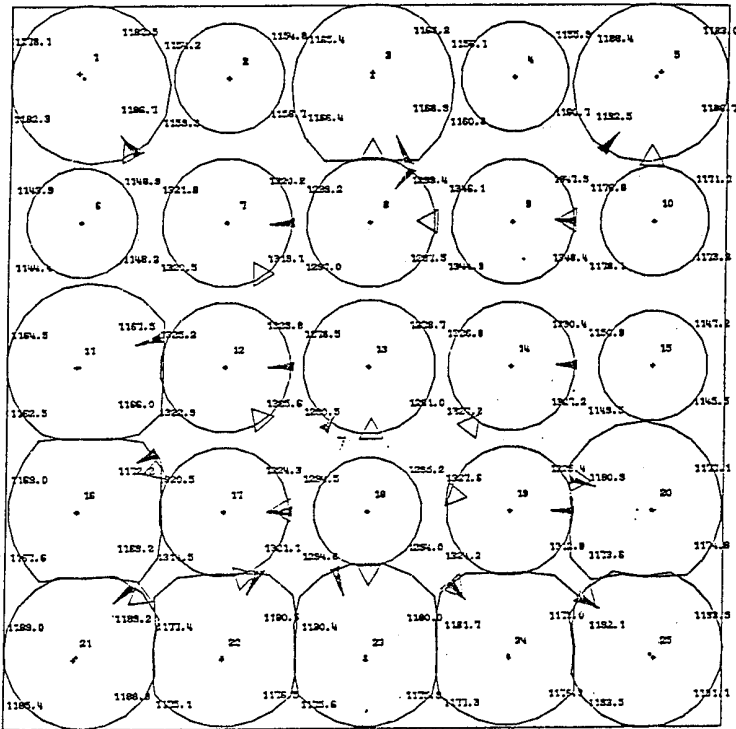
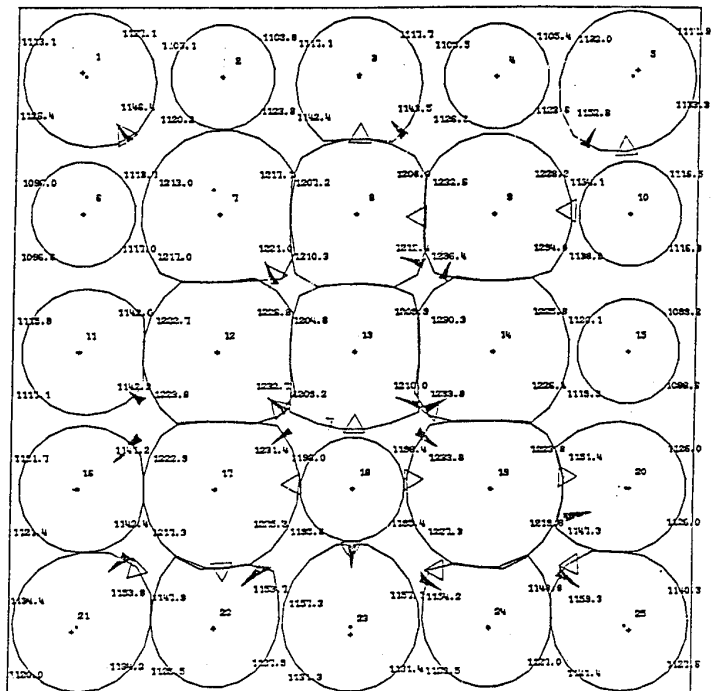


Figure 102 A: PHEBUS test 215 R. Strain and temperature map at 30 s, as calculated by FRETA-F without radiative exchanges. Comparison of the calculated burst locations (▽) with those observed in the experiment (▼).

Figure 102 B: PHEBUS test 215 R. Strain and temperature map at 30 s, as calculated by FRETA-F with radiative exchanges (default option). Comparison of the calculated burst locations (▽) with those observed in the experiment (▼).



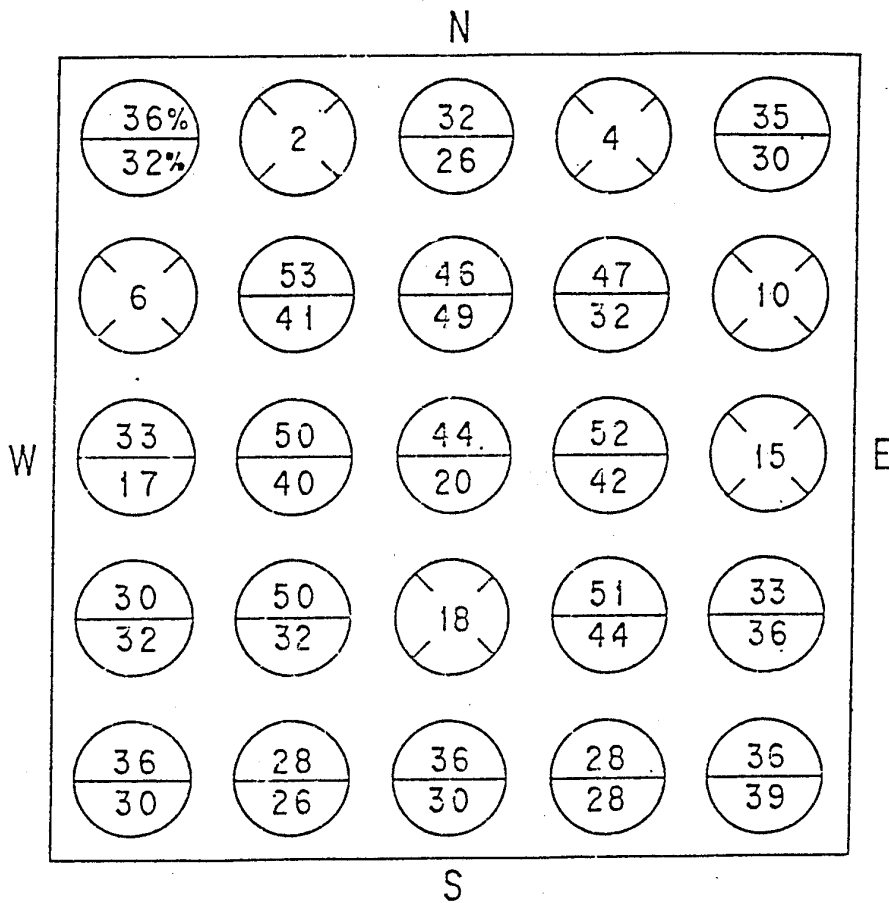


Figure 103: PHEBUS test 215 R - comparison of the burst strain as calculated by FRETAF in the standard option (upper number) with experimental values (lower number).

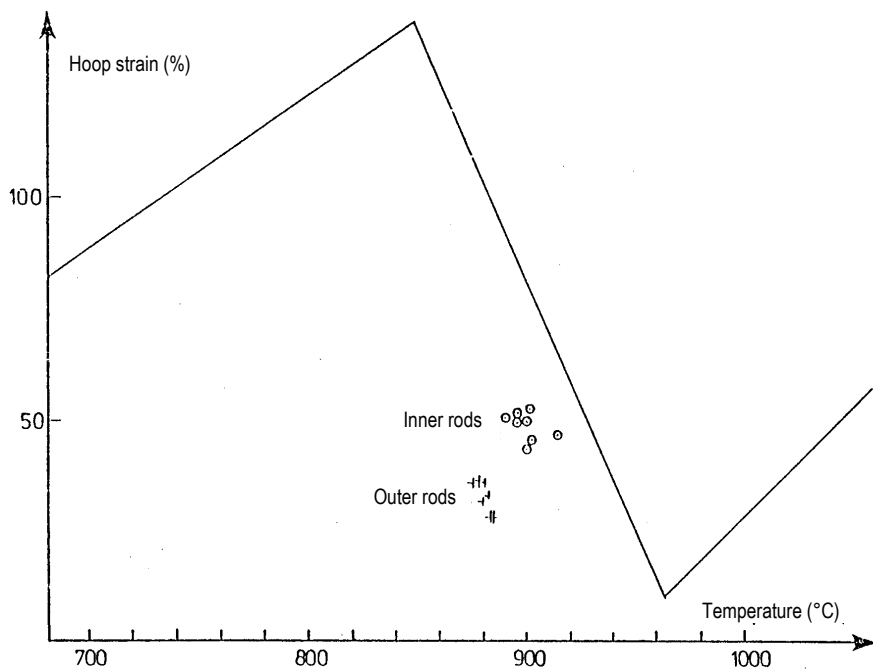


Figure 104: PHEBUS test 215 R - comparison of the average deformation at burst as calculated by FRETAF in the standard option with the burst criterion (maximum local strain).

Analysis of the different calculations performed indicated that the order of importance of parameters to be taken into consideration when calculating strain upon cladding failure is as follows:

- 1) Transient speed,
- 2) Local temperature map on the cladding,
- 3) Metallurgic phase of the material.

5.3.3 Complementary needs for the interpretation of thermomechanical aspects

In conclusion, analysis of the PHEBUS-LOCA test results has made it possible to identify a certain number of elements concerning the thermomechanical aspects of these tests.

- Evaluation of cladding failure times is related to the quality of the code's thermics, as well as to the integration of a creep law and cladding failure criterion adapted to the cladding material under consideration. Uncertainty on thermal behavior prediction has an impact on the dispersion of cladding failure times, but affects burst strain to a lesser degree. An accurate prediction of thermal behavior ($\pm 10^\circ\text{C}$) is therefore only useful in a limited number of cases where the cladding failure is the prime question. Furthermore, the physical basis of the retained failure criteria, in 1D and 2D descriptions, must be reinforced in order to better define their effect upon final strain, particularly in consideration of metallurgic disequilibrium that may occur under rapid transients.
- In addition to a correct prediction of the cladding temperature, the coupling of thermal-hydraulics and thermo-mechanics must provide a sufficiently accurate evaluation of the coolant temperature in the vicinity of the rod main gas volumes (plenum) in order to enable the correct calculation of internal pressure variations.
- The quality of burst strain predictions largely depends on the temperature transient speed: during a rapid transient, cladding failure conditions are overstepped during a rather narrow time interval, therefore minimizing the effect of the spatial description; during a slower transient, temperature heterogeneities have more time to affect the location of stress and strain. Correct treatment of temperature heterogeneities requires a 2D representation of rod thermics, making it possible in particular to take into account internal sources of heterogeneity related to pellet/cladding eccentricities, as well as external sources resulting from radiative exchanges between rods (and surrounding structures). Under the same development level, a 2D description of the cladding burst criterion is desirable, taking into account mechanical interactions via contact between neighboring rods.

6 CONCLUSIONS

A review of the main experimental programs devoted to the aspects of clad ballooning and burst and associated flow blockage, in both in-pile and out-of-pile tests in single rod or multi-rod configurations, has been carried out in this document. This review has made it possible to identify consistent knowledge, from which the main elements will be summarized below.

1) Single rod tests: influence of the azimuthal temperature gradients

The EDGAR tests involving the direct heating of cladding tube specimens, thus with a uniform azimuthal temperature distribution, produced high burst strain values in the high α -phase domain. Conversely, the single-rod tests from the REBEKA and ORNL programs involving internal indirect heating, thus with unavoidable azimuthal temperature differences (due in particular to the local offsetting of the heating rod) underlined the essential influence of the azimuthal temperature gradients on the clad straining until burst. The process involves the concentration of material weakening in a hot zone, combined with axial shortening resulting from the α -Zircaloy anisotropy (hot side straight effect), that lead to high values of local strain at burst but with a moderate average circumferential elongation and limited axial extent.

2) Bundle tests: influence of the thermal and mechanical interactions between neighboring rods

The results of bundle tests complicated the simplistic view gained from single rod tests where the leading phenomenon is the uniform character or not of the azimuthal temperature distribution.

The results of the ORNL-MRBT tests, provided in particular by the comparison of B3 and B5 data, indicated that the straining of inner rods led to mechanical interactions between neighboring rods in a large array; these interactions, although of limited impact on burst temperature and elongation, significantly modifying the spatial development of deformation until rupture. Notably, the trapping of bulging rods appeared to cause the deformation to extend axially, resulting in a larger volume expansion and a larger axial extent of the blocked regions.

ORNL experimentalists thus concluded that the flow area restriction in large arrays may be underestimated by tests on small unconstrained arrays and that two rows of deforming "guard" rods are necessary around the central deforming array to properly simulate representative conditions present in a reactor fuel assembly.

The JAERI multi-rod tests carried out under thermohydraulic conditions similar to those in MRBT tests B3 and B5 showed results consistent with those of MRBT tests. The common feature of all these tests is the axial extension of the deformation, which develops after contact without rupture between adjacent rods.

An important outcome provided by JAERI multi-rod tests concerns the influence of the presence of control rod guide tubes. In most cases, not only is the deformation on rods adjacent to a guide tube not lower than on other rods, despite the azimuthal temperature gradients induced by the cold guide tube, but the flow blockage ratio in the bundle section is even slightly increased and axially more extended. This surprising result supports the result from test REBEKA-4 (carried out in more favorable thermohydraulic conditions) and can be explained by the effect of the mechanical interaction between a rod and an adjacent guide tube: due to the larger diameter of the latter, the contact of a deforming neighboring rod occurs with moderate strain (~ 20%), before burst. This early contact leads to the transfer of strain onto other portions of the rod circumference, which homogenizes the azimuthal temperature field and ultimately results in the axial extension of the deformation.

To summarize, it appears that the mechanical interaction between rods in a rod bundle and more particularly with a guide tube, may lead to an increase in the burst strain and the flow blockage as a combined result of:

- A mechanical interruption of the "hot side straight effect" process (the influence of which on the limitation of burst strain was revealed in single rod tests),
- The re-homogenizing of the azimuthal temperature distribution.

It may thus be concluded that, under conditions conducive to significant mechanical interactions between rods, the spatial distribution of burst strain and the resulting flow blockage are not realistically evaluated on the basis of single rod tests alone.

3) PHEBUS-LOCA tests: influence of the transient characteristics

The PHEBUS-LOCA in-pile bundle tests, based on a reference scenario reproducing a hypothetical integral LOCA transient, provided fundamental results in relation to the characteristics of the thermohydraulic transient experienced by the rod bundle.

The analysis of clad ruptures and strain obtained in these tests made it possible to distinguish the overall behavior of inner and peripheral rods:

- For the inner rods, ruptures occurred in the α -phase domain for tests 215-P and 215-R and in the mixed $\alpha+\beta$ phase domain for tests 216, 218 and 219. The rupture strain was thus significantly higher in tests 215-P and 215-R than in the other tests. They were however very close in these two tests despite the significant difference in temperature ramp rates at the time of ballooning (7 K/s compared to 20 K/s respectively). This can be explained by the fact that strain was limited by the large azimuthal temperature differences in test 215-P, whereas the limiting effect in 215-R was mainly due to the rapidity of the temperature ramp. For the three following tests, where the ruptures of inner rods occurred in the mixed phase domain, different adverse effects acted simultaneously on the strain level:
 - An increase in β -phase content limits the rupture strain,
 - A rapid temperature rise also limits the rupture strain while delaying the $\alpha\rightarrow\beta$ phase transformation, thereby reducing the β -phase content which acts in opposite way.

The application of the phase change kinetic models to the tests 216, 218 and 219 showed that significant departure from equilibrium phase fractions was obtained in these tests, ranging from almost no $\alpha\rightarrow\beta$ transformation at rupture in test 216 and 218 to a maximum of 25% phase transformation in test 219. Owing to the effect of the β -phase fraction alone, lower strain was expected for the test 219 rods; observation of an opposite result led to the conclusion that the effect of the temperature ramp rate (lowest in test 219, compared to test 216 and 218) was the dominant factor.

- For the *outer rods*, lower burst strain was generally observed with respect to that of the inner rods. This result was mainly attributed to the effect of azimuthal temperature difference, larger on outer rods owing to the influence of cold outer structures, particularly in tests 215-P and 215-R where these temperature differences were more pronounced. This effect is consistent with the orientations of the ruptures, which were found to be directed either towards the center of the bundle (215-P, 216, and 218) or towards some hotter non-pressurized rods (215-R and 219). These orientations underline the importance of radiative heat transfers between rods and structures on the occurrence of "hot spots" that limit the deformation by the "hot side straight effect". In the particular case of test 218, the very rapid temperature ramp led to the rupture of the inner rods at the 1st temperature peak with low burst strain, whereas the outer rods, which ruptured later, exhibited a larger mean burst strain.

In summary, the rod thermomechanical behavior in the PHEBUS tests appeared to be influenced by different phenomena that may be classified according to their relative order of importance:

- a) Temperature transient kinetics,
- b) Azimuthal temperature differences,
- c) $\alpha\rightarrow\beta$ phase transformation kinetics.

4) Influence of the thermohydraulic conditions

The PHEBUS 215-P test, with its particularly complex thermohydraulic behavior (early rewetting, untimely water inflows in the test section) was not representative of an in-reactor LOCA and illustrated the fact that any hydraulic disturbance possibly affecting the rod thermal behavior increases the temperature heterogeneities (azimuthal gradients, temperature differences between rods), which in turn reduce the burst strain, spread the burst elevations and consequently minimize the flow blockage ratio.

Comparison of the REBEKA and ORNL-MRBT tests revealed that the choice of the thermohydraulic conditions can greatly influence the test results. Thus, the counter-current steam and two-phase reflood flows in the REBEKA tests - typical of the refill/reflooding conditions in KWU PWRs (safety injection in both the hot and cold legs) - favor a spatial heterogeneity of temperatures, therefore an axial spreading of elevations of maximum strain and a limitation in flow blockage. Under such conditions, the mechanical interactions between rods remain low and the effect of bundle size (R-5 results compared to those of R-3) is almost non-existent; which is not the case in MRBT tests.

While it looks obvious that two-phase cooling in comparison to single-phase cooling favors the thermal transfers and therefore the development of azimuthal and axial temperature differences, the influence of such cooling should however not be overestimated as fully prevailing over the effect of the bundle size, as claimed by Erbacher (see [14], discussion), who considered the MRBT tests conditions as atypical in comparison to the REBEKA tests conditions. Comparison of the NRU tests MT-3 and MT-4 - with ballooning/ruptures under two-phase cooling for the former and under single-phase steam for the latter - revealed the occurrence of very large strain (94%) in MT-3 that was possibly more significantly coplanar than for MT-4.

Moreover, it is almost obvious that the thermal transfers in the vicinity of a ballooned - and furthermore ruptured - cladding are significantly increased, due to 1) the larger spacing with the pellet that reduces the clad thermal inertia, 2) the possible penetration of coolant on the inside of the rod and 3) the increased turbulence and impact of droplets under two-phase cooling. These effects therefore contribute to favoring a rewetting of the deformed claddings. The influence on neighboring rods is more difficult to evaluate. According to Burman^[38], the hydraulic disturbance that results from a rod ballooning induces cross-flows that increase cooling on neighboring rods and therefore prevent the development of coplanar blockages. It would however not be wise to draw overly general conclusions from such partial qualitative considerations: the example of the REBEKA-4 test where, contrary to all expectations, the maximum strain (79%) occurred on a rod neighboring the central guide tube demonstrated that, in addition to mechanical interactions between rods, the thermohydraulic perturbations induced in the neighboring sub-channels can contribute to a re-homogenizing of the azimuthal temperature distribution in the neighboring rods and consequently increase their burst strain. Predicting these various interactions is complex and generally not taken into account in the current LOCA calculation tools.

5) In-pile tests on irradiated fuel rods

The PBF-LOC and FR2 tests led to apparently contradictory observations relative to the influence of prior irradiation on the rod deformation:

- Significant increase in the burst strain of irradiated rods in comparison to that of twin unirradiated rods in the PBF tests;
- Insensitiveness to the prior irradiation in the FR2 tests.

Analysis of the experimental conditions in the FR2 tests showed that some particular features of these conditions may have occulted the effect observed on PBF-LOC, essentially related to the temperature azimuthal homogenizing, as a result of fuel rearrangement and clad creepdown. Thus, it cannot not be considered that the FR2 results "erase" to some extent the irradiation effect observed in the PBF-LOC results.

As for the fuel behavior, the FR2 and PBF-LOC tests appear fairly consistent with respect to the relocation phenomena of fragmented fuel in the clad balloon. The impact of fuel relocation on the subsequent evolution of the LOCA transient, in particular on the histories of the local clad temperature and resulting oxidation rate, was not clarified by FR2 and PBF-LOC test results.

As an outcome of the comparison between the results of the PBF-LOC tests and those of the ORNL-MRBT tests, Broughton [19], considering that:

- The strain on fresh rods in PBF-LOC tests was consistent with that on single rod ORNL-MRBT tests with an unheated shroud,
- The strain in ORNL multi-rod tests was significantly higher than that in single-rod tests with an unheated shroud,
- The strain on irradiated rods in PBF-LOC was significantly higher than that on twin unirradiated rods,

recommended that in-pile bundle tests of sufficient size (8x8 rods) with irradiated rods be performed in order to study the cumulative effects of irradiation and the bundle size on burst strain so as to evaluate the likelihood to obtain a significant coplanar blockage. It should be noted that, since this 1983 recommendation, no bundle test with irradiated rods has been performed that could have provided information on this issue.

To complement the review of the main experimental programs, an overall review of the related analytical work was conducted, based on the examination and discussion of the main outcome from the following summary reports:

- 1) the NUREG-630 report,
- 2) 2) the international standard problems ISP-14 and ISP-19 final comparison reports,
- 3) 3) the summary report of the PHEBUS-LOCA test interpretative work.

The main conclusions of this complementary review will be recalled hereafter.

6) NUREG 630

The NUREG-630 report issued in 1980 by the USNRC aimed to define a set of correlations for cladding rupture temperatures, burst strain and assembly flow blockage that could be used for LOCA safety analysis within the perspective of Appendix K from 10 CFR 50.46. The requirement was therefore not underestimating the clad swelling and rupture occurring under LOCA conditions.

These correlations were established on the basis of the results from a set of selected tests under conditions that were considered realistic. These tests were chosen from a wide range of tests carried out with electric simulators or actual fuel rods, in single-rod or bundle configurations, with a heated or unheated shroud and under various heating rates. The main characteristics of these correlations may be summarized as follows:

- For rupture temperatures, the ORNL correlation developed by Chapman was used, which bounds most of the experimental results reasonably well.
- For burst strain, two correlations were recommended for slow and fast temperature ramp rates. These two correlations practically bound the bundle test results; however, in the alpha-domain, the slow-ramp correlation is only the average of the single-rod heated-shroud data. Above 900°C under slow-ramp and above 940°C under fast-ramp, data for single-rod heated-shroud or bundle tests are scarce or lacking, which makes these correlations uncertain in the corresponding temperature domains.
- For flow blockage, two correlations were derived from the two former ones by using the ratio between average burst strain and average strain in the plane of maximum blockage, with this ratio being the average ratio deduced from the only three tests MRBT B1 to B3.

One may wonder that the burst strain and flow blockage correlations were not revised when new data became available, particularly in the temperature domain above 900°C, from the late bundle tests belonging to the REBEKA, ORNL and JAERI programs, as well as the in-pile tests with irradiated rods, notably the PBF-LOC test results.

More specifically, the flow blockage correlations appear insufficiently supported by experimental data and the upper limit of 71% of the maximum flow blockage ratio in a PWR assembly should be revised, in the light of the subsequent following observations:

- No reduction, or increase, in the flow blockage in bundles containing guide tubes (REBEKA-4, JAERI 21 to 24 tests);
- Development of high blockage ratios in the central sub-channels due to the guard effect of the outer rods (MRBT-B5, JAERI 21 to 24 and NRU-MT4 tests), where values from 90 to 100% were obtained.

7) The International Standard Problems ISP-14 and ISP19

The ISP-14 exercise relying on the REBEKA-6 test and various other studies that were conducted in parallel helped clarify several important points:

- Thermohydraulic codes do not produce sufficiently accurate predictions of the combined thermohydraulic/ thermomechanical behavior observed during a bundle test under LOCA

conditions; this is due to the significant difference between the precision of temperatures - required for thermomechanical calculations (10 to 15 K) - and the precision available concerning local thermohydraulic conditions under two-phase flow conditions during reflood;

- A correct description of the material's mechanical properties is required to determine cladding failure conditions;
- Consideration of fuel distribution within the cladding (eccentricity, local fuel relocation), with a corresponding adaptation of the cladding failure criterion, is required to correctly determine cladding failure conditions during an asymmetrical swelling scenario.

Moreover, the ISP-19 exercise using the PHEBUS 218 test helped identify several important influences:

- The rapidity of the transient has a dominating effect upon azimuthal temperature differences with regard to failure conditions and hence strain;
- It is important to take into account phase change kinetics during the rapid transient.

As compared to the results of ISP-14, the thermomechanical predictions here appear more accurate and less scattered; however, it must be underlined that the rupture conditions under a rapid transient were less sensitive to experimental uncertainties and modeling than in the case of the REBEKA-6 test.

8) Summary of the PHEBUS-LOCA test analysis

In conclusion, analysis of the PHEBUS-LOCA test results has made it possible to identify a certain number of elements concerning the thermomechanical aspects of these tests.

- Evaluation of cladding failure times is related to the quality of the code's thermics, as well as to the integration of a creep law and cladding failure criterion adapted to the cladding material under consideration. Uncertainty on thermal behavior prediction has an impact on the dispersion of cladding failure times, but affects burst strain to a lesser degree. An accurate prediction of thermal behavior ($\pm 10^\circ\text{C}$) is therefore only useful in a limited number of cases where the cladding failure is the prime question. Furthermore, the physical basis of the retained failure criteria, in 1D and 2D descriptions, must be reinforced in order to better define their effect upon final strain, particularly in consideration of metallurgic disequilibrium that may occur under rapid transients.
- In addition to a correct prediction of the cladding temperature, the coupling of thermal-hydraulics and thermo-mechanics must provide a sufficiently accurate evaluation of the coolant temperature in the vicinity of the rod main gas volumes (plenum) in order to enable a correct calculation of internal pressure variations.
- The quality of burst strain predictions largely depends on the temperature transient speed: during a rapid transient, cladding failure conditions are overstepped during a rather narrow time interval, therefore minimizing the effect of the spatial description; during a slower transient, temperature heterogeneities have more time to affect the location of stress and strain. Correct treatment of temperature heterogeneities requires a 2D representation of rod thermics, making it possible in particular to take into account internal sources of heterogeneity related to pellet/cladding eccentricities, as well as external sources resulting from radiative exchanges between rods (and surrounding structures). Under the same development level, a 2D description of the cladding burst criterion is desirable, taking into account mechanical interactions via contact between neighboring rods.

It is important to point out that this first part of the State-of-the Art Review is accompanied by the second part of the review covering the impact of a flow blockage in a rod assembly upon the rod coolability in the vicinity of the blockage; this aspect was studied in specific experiments of a very different nature from that of the ballooning/rupture experiments which were reviewed in this present report.

The aspects of cladding oxidation and resistance to thermal shock quench loads and post-quench loads are reviewed in the third part of the S.O.A.R.

REFERENCES

- [1] P.D. PARSONS, E.D. HINDLE and C.A. MANN,
The Deformation, Oxidation and Embrittlement of PWR Fuel Cladding in a Loss-of-Coolant Accident. A State-of-the-Art Report.
NEA/OECD-CSNI Report 129, December 1986
- [2] F.J. ERBACHER and S. LEISTIKOW,
Zircaloy Fuel Cladding Behavior in a a Loss-of-Coolant Accident : A Review.
Zirconium in the Nuclear Industry : 7th Int. Symp., ASTM STP 939, 1987.
- [3] E. SCOTT DE MARTINVILLE,
Comportement du combustible REP en cas de grosse brèche dans le circuit primaire : Synthèse des études de sûreté au CEA.
Note technique DERS/SEMAR Mars 1989
- [4] F. IFFENECKER,
APRP : Impact du gonflement du gainage combustible sur le refroidissement du cœur. Etude bibliographique.
Note ENT/TH/91.094 Juillet 1992
- [5] C. GRANDJEAN,
Programme TAGCIS. Synthèse bibliographique. Les critères de fragilisation d'une gaine Zircaloy en conditions APRP. Base expérimentale, inter-comparaison, marges.
Note technique DRS/SEA/LERES 2/92 Février 1992
- [6] C. GRANDJEAN,
Le critère APRP réglementaire. Revue critique : base physique, formulation, application au cas de gaines irradiées.
Note technique DRS/SEA/LERES 3/94 Février 1994
- [7] G. HACHE,
Besoin en études et essais concernant le comportement du combustible irradié en cas de brèches primaires.
Rapport DRS/ADJ/96/859 Juillet 1996
- [8] M. REOCREUX and E.F. SCOTT DE MARTINVILLE,
A Study of Fuel Behavior in PWR Design Basis Accident : An Analysis of Results from the PHEBUS and EDGAR Experiments.
Nuclear Engineering and Design 124 (1990), 363-378.
- [9] T. FORGERON,, J.C. BRACHET, F. BARCELO, A. CASTAING, J. HIVROZ, J.P. MARDON and C. BERNAUDAT,
Experiment and Modeling of Advanced Fuel Rod Cladding Behavior Under LOCA Conditions : Alpha-Beta Phase Transformation Kinetics and EDGAR Methodology.
Zirconium in the Nuclear Industry : 12th International Symposium, ASTM STP 1354 (2000), pp. 256-278.
- [10] F.J. ERBACHER,
LWR Fuel Cladding Deformation in a LOCA and its Interaction with the Emergency Core Cooling.
ANS/ENS Topical Meeting on Reactor Safety Aspects of Fuel Behaviour,
Sun Valley, Idaho, USA, 2-6 August 1981.
- [11] R.H. CHAPMAN, J. L. CROWLEY, A.W. LONGEST and G. HOFMANN,
Zirconium Cladding Deformation in a Steam Environment with Transient Heating.
Zirconium in the Nuclear Industry (Fourth conference), ASTM STP 681 (1979), pp. 393-408.
- [12] H.M. CHUNG, A.M. GARDE, and T.F. KASSNER,
Deformation and Rupture Behavior of Zircaloy Cladding under Simulated Loss-of-Coolant Accident Conditions
Zirconium in the Nuclear Industry, 3rd Int. Conference, ASTM/STP 633, 1977, pp. 82-97.
- [13] K. WIEHR, F.J. ERBACHER, and H.J. NEITZEL,
Influence of a Cold Control Rod Guide Tube on the Ballooning Behaviour of Zircaloy Claddings in a LOCA.
CSNI Specialist Meeting Safety Aspects of Fuel Behaviour in Off-normal and Accident Conditions, Espoo, Finland, 1-4 September 1980.

- [14] R.H. CHAPMAN, J.L. CROWLEY and A.W. LONGEST,
Effect of Bundle Size on Cladding Deformation In LOCA simulation Tests
Zirconium in the Nuclear Industry, 6th Int. Symposium, ASTM/STP 824, 1984, pp. 693-708.
- [15] S. KAWASAKI et al.,
Effect of Non-heated Rods on the Ballooning Behavior in a Fuel Assembly under Loss-of-Coolant Condition
ANS/ENS Topical Meeting "Reactor Safety Aspects of Fuel Behavior", Sun Valley, Idaho, August 2-6, 1981.
- [16] M. SUZUKI,
Simulation Test on Interactions of Zircaloy Claddings Deforming in Fuel Assembly under LOCA Conditions
J. Nucl. Sci. Technol., 20(6), pp. 475-490 (June 1983)
- [17] S. KAWASAKI, H. UETSUKA and T. FURUTA,
Multirod Burst Tests under Loss-of-Coolant Conditions.
OECD-CSNI/IAEA Specialists' Meeting on Water Reactor Fuel Safety and Fission Product Release in Off-normal and Accident Conditions
Riso, Denmark, 16-20 May 1983.
- [18] J.M. BROUGHTON et al.,
PBF LOCA Test Series. Tests LOC-3 and LOC-5. Fuel Behavior Report
NUREG/CR-2073, EGG-2094, June 1981.
- [19] J.M. BROUGHTON et al.,
PBF LOCA Tests LOC-6. Fuel Behavior Report
NUREG/CR-3184, EGG-2244, April 1983.
- [20] E.H. KARB et al.,
LWR Fuel Rod Behavior in the FR2 In-pile Tests Simulating the Heatup Phase of a LOCA. Final Report.
KfK 3346, March 1983.
- [21] C. GRANDJEAN, et al.,
High Burnup UO₂ Fuel LOCA Calculations to Evaluate the Possible Impact of Fuel Relocation After Burst.
SEGFSM Topical Meeting on LOCA Fuel Safety Criteria, Aix-en-Provence, France, March 22-23, 2001.
- [22] V. GUILLARD et al.,
Use of CATHARE2 Reactor Calculations to Anticipate Research Needs
SEGFSM Topical Meeting on LOCA Issues, Argonne National Laboratory, USA, May 25-26 2004.
- [23] P. JONES et al.,
EOL-JR : A Single Rod Burst Test Programme in the ESSOR Reactor.
ANS/ENS Topical Meeting "Reactor Safety Aspects of Fuel Behavior", Sun Valley, Idaho, August 2-6, 1981.
- [24] M. BRUET, J.C. JANVIER,
FLASH Experiments in SILOE Reactor. Fuel Rod Behaviour during LOCA Tests.
OECD-CSNI/IAEA Specialists' Meeting on Water Reactor Fuel Safety and Fission Product Release in Off-normal and Accident Conditions
Riso, Denmark, 16-20 May 1983.
- [25] M. BRUET et al.,
High Burnup Fuel Behavior During a LOCA type Accident : the FLASH 5 Experiment.
IAEA Technical Committee Meeting on Behavior of Core Material and Fission Products Release in Accident Conditions in LWR's
Cadarache, France, 16-20 March 1992.
- [26] M.D. FRESHLEY, G.M. HESSON,
Summary Results of the LOCA Simulation Program Conducted in NRU.
PNL-SA-11536, October 1983.
- [27] C.L. MOHR, G.M. HESSON,
Ballooning and Flow Blockage for High Alpha LOCA Conditions.
IAEA Specialists' Meeting on Water Reactor Fuel Performance Computer Modelling
Preston, UK, 14-19 March 1982.
- [28] B. ADROGUER,
Synthèse de l'essai PHEBUS 215 P.
Rapport technique IPSN/DERS/SEAREL n° 2/84, Juillet 1984.

- [29] E. SCOTT DE MARTINVILLE, H. RIGAT, J. POUBLAN, M. PIGNARD,
Interprétation de l'essai 215 R.
Note Technique SEAREL 176/87, Note PHEBUS 77/87, Octobre 1987.
- [30] I. DROSIK, H. RIGAT, M. PIGNARD,
Interprétation de l'essai PHEBUS 218.
Note Technique SEAREL 154/87, Note PHEBUS 86/88, Juin 1988.
- [31] H. RIGAT, M. PIGNARD,
Interprétation de l'essai PHEBUS 219.
Note Technique SEMAR 04/88, Note PHEBUS 87/88, Mai 1988.
- [32] D.A. OWERS, R.O. MEYER,
Cladding Swelling and Rupture Models for LOCA Analysis.
NUREG-0630, April 1980.
- [33] A. de CRECY,
CATHARE. Analyse critique de NUREG 630. Etude de la rupture des crayons combustibles et de ses conséquences.
Note technique STR/LML/EM/92-98, Juin 1992.
- [34] H.M. CHUNG, and T.F. KASSNER,
Deformation Characteristics of Zircaloy Cladding in Vacuum and Steam Under Transient Heating Conditions : Summary Report.
USNRC Report NUREG/CR-0344, July 1978.
- [35] R.O. MEYER, et al.,
Licensing Requirements for Fuel Behavior During DBAs.
ANS/ENS Topical Meeting "Reactor Safety Aspects of Fuel Behavior", Sun Valley, Idaho, August 2-6, 1981.
- [36] H. KARWAT,
International Standard Problem ISP 14.
Behaviour of a Fuel Bundle Simulator During a Specified Heatup and Flooding Period (REBEKA Experiment). (Results of Post-Test Analyses). Final Comparison Report.
OECD/NEA CSNI Report n°98, February 1985.
- [37] E. SCOTT DE MARTINVILLE, M. PIGNARD,
International Standard Problem ISP 19.
Behavior of a Fuel Rod Bundle During a Large Break LOCA Transient with a Two Peaks Temperature History (PHEBUS Experiment). Final Comparison Report.
OECD/NEA CSNI Report n°131, 1987.
- [38] D. L. BURMAN, et al.
Inhibition of Coplanar Rod Bundle Blockage by Cross-Flow Cooling.
ANS/ENS Topical Meeting "Reactor Safety Aspects of Fuel Behavior", Sun Valley, Idaho, August 2-6, 1981.